USGS
science for a changing world

Prepared in cooperation with the U.S. Department of Energy, National Nuclear Security Administration Nevada Site Office, Office of Environmental Management under Interagency Agreement, DE-EM0004969

Groundwater Flow Conceptualization of the Pahute Mesa–Oasis Valley Groundwater Basin, Nevada: A Synthesis of Geologic, Hydrologic, Hydraulic-Property, and Tritium Data

Scientific Investigations Report 2020–5134

U.S. Department of the Interior
U.S. Geological Survey

Cover: Photograph of Colson Pond in northern Oasis Valley, looking south toward Beatty, Nevada. Photograph by Steven R. Reiner, U.S. Geological Survey, 2020.

Groundwater Flow Conceptualization of the Pahute Mesa–Oasis Valley Groundwater Basin, Nevada: A Synthesis of Geologic, Hydrologic, Hydraulic-Property, and Tritium Data

By Tracie R. Jackson, Joseph M. Fenelon, and Randall L. Paylor

Prepared in cooperation with the U.S. Department of Energy, National Nuclear Security Administration Nevada Site Office, Office of Environmental Management under Interagency Agreement, DE-EM0004969

Scientific Investigations Report 2020–5134

U.S. Department of the Interior
U.S. Geological Survey

U.S. Geological Survey, Reston, Virginia: 2021

For more information on the USGS—the Federal source for science about the Earth, its natural and living resources, natural hazards, and the environment—visit https://www.usgs.gov or call 1–888–ASK–USGS.

For an overview of USGS information products, including maps, imagery, and publications, visit https://store.usgs.gov/.

Suggested citation:
Jackson, T.R., Fenelon, J.M., and Paylor, R.L., 2021, Groundwater flow conceptualization of the Pahute Mesa–Oasis Valley Groundwater Basin, Nevada—A synthesis of geologic, hydrologic, hydraulic-property, and tritium data: U.S. Geological Survey Scientific Investigations Report 2020–5134, 100 p., https://doi.org/10.3133/sir20205134.

ISSN 2328-0328 (online)

Contents

Figures

Tables

Plate

Conversion Factors

U.S. customary units to International System of Units

Multiply	By	To obtain
	Length	
inch (in.)	25.4	millimeter (mm)
foot (ft)	0.3048	meter (m)
mile (mi)	1.609	kilometer (km)
	Area	
Acre	0.0015625	square mile (mi^2)
Acre	4,047	square meter (m^2)
	Volume	
acre-foot (acre-ft)	1,233	cubic meter (m^3)
	Flow rate	
acre-foot per year (acre-ft/yr)	1,233	cubic meter per year (m^3/yr)
inch per year (in/yr)	25.4	millimeter per year (mm/yr)
	Velocity	
foot per day (ft/d)	0.3048	meter per day (m/d)
	Hydraulic gradient	
foot per foot (ft/ft)	1	meter per meter (m/m)
foot per mile (ft/mi)	0.000189	foot per foot (ft/ft)
	Mass	
kiloton (kt)	0.001	megaton (Mt)
	Hydraulic conductivity	
foot per day (ft/d)	0.3048	meter per day (m/d)
	Radioactivity	
picocuries per liter (pCi/L)	0.037	becquerel per liter (Bq/L)
	Transmissivity*	
foot squared per day (ft^2/d)	0.09290	meter squared per day (m^2/d)

*Transmissivity: The standard unit for transmissivity is cubic foot per day per square foot times foot of aquifer thickness [(ft^3/d)/ft^2]ft. In this report, the mathematically reduced form, foot squared per day (ft^2/d), is used for convenience.

Datum

Vertical coordinate information is referenced to the National Geodetic Vertical Datum of 1929 (NGVD29).

Horizontal coordinate information is referenced to the North American Datum of 1983 (NAD 83).

Altitude, as used in this report, refers to distance above the vertical datum.

Groundwater Flow Conceptualization of the Pahute Mesa–Oasis Valley Groundwater Basin, Nevada: A Synthesis of Geologic, Hydrologic, Hydraulic-Property, and Tritium Data

By Tracie R. Jackson, Joseph M. Fenelon, and Randall L. Paylor

Abstract

This report provides a groundwater-flow conceptualization that integrates geologic, hydrologic, hydraulic-property, and radionuclide data in the Pahute Mesa–Oasis Valley (PMOV) groundwater basin, southern Nevada. Groundwater flow in the PMOV basin is of interest because 82 underground nuclear tests were detonated, most near or below the water table. A potentiometric map and nine sets of hydrostratigraphic and hydrologic cross sections supplement the conceptualization.

Potentiometric contours indicate that groundwater in the PMOV basin generally flows south-southwest and discharges at Oasis Valley. Groundwater encounters an alternating sequence of low- and high-transmissivity rocks, referred to as dams and pools, respectively, as it moves from east to west across eastern Pahute Mesa. Flow from all Pahute Mesa nuclear tests is to Oasis Valley and is well-constrained by water-level data. Flow converges along a corridor of high transmissivity between Pahute Mesa and Oasis Valley.

The location of the lateral PMOV basin boundary is well defined, and this boundary, with a few minor exceptions, represents a no-flow boundary. Some boundary uncertainty exists in the northeastern part of the basin, but potential flow-rate estimates across the northeastern boundary resulting from this uncertainty are small relative to the basin groundwater budget.

Recharge in the PMOV basin is derived from episodic pulses of modern water and the diffuse percolation of old water (greater than 1,000 years). Episodic recharge is a minor recharge component observed as a rise in groundwater levels that occurs 3 months to 1 year following a wet winter. Minor amounts of episodic recharge through an unsaturated zone in excess of 1,000 feet (ft) requires preferential flow through faults and fractures. The dominant recharge component is slow, steady, diffuse percolation of old water through the unsaturated zone. A large component of old water recharging the groundwater system is consistent with observations of isotopically light deuterium and oxygen 18 compositions in water from wells on Pahute Mesa and central Oasis Valley. About half the recharge in the PMOV basin is derived from the eastern Pahute Mesa area. The remaining recharge is derived primarily from other highland areas including Timber Mountain, Belted and Kawich Ranges, and Black Mountain.

The PMOV groundwater system is nearly steady state, where recharge is balanced by the 5,900 acre-feet per year of natural discharge at Oasis Valley. This assumption is reasonable because the basin is dominated by steady-state conditions, where long-term changes in groundwater storage are minimal. Total groundwater withdrawals from 1963 to 2018 have amounted to less than 10 percent of annual groundwater discharge and less than 0.2 percent of the basin's groundwater storage. Therefore, present-day (2020) conditions are considered representative of predevelopment (pre-1950) conditions in nearly all areas of the basin.

The lower PMOV basin boundary is defined at 4,000 ft below the water table to encompass all underground nuclear tests and tritium plumes. This boundary defines the lower boundary of radionuclide migration. However, nearly all flow and tritium transport occur in the upper 1,600 ft of the saturated zone because a transmissivity-with-depth relation indicates that greater than 90 percent of the transmissivity contributing to groundwater flow occurs within 1,600 ft of the water table. Rocks at deeper depths have low transmissivity because argillic and mineralized alterations plug the fractures.

Volcanic rocks form the primary aquifers and confining units in the PMOV basin. Volcanic hydrogeologic units (HGUs) and hydrostratigraphic units (HSUs) have transmissivity distributions that span up to eight orders of magnitude with considerable overlap between distributions. Despite the large overlap between units, mean transmissivities of aquifers are one-to-two orders of magnitude greater than the confining units. However, all volcanic-rock HGUs and HSUs are composite units, meaning that they can function spatially as either an aquifer or confining unit.

Large ranges in transmissivity for HGUs and HSUs can be explained, partly, by these units spanning multiple zones of mineral alteration. Argillic, mineralized, and zeolitic alteration reduce transmissivity and cause rocks to function as confining units. The highest transmissivity intervals occur in rocks with devitrified alteration because fractures are not closed by secondary mineral coatings. The degree and extent of hydraulically connected fractures also cause the large ranges in transmissivity.

Juxtaposition of rocks with similar or different permeabilities across a fault is the most likely mechanism for creating flow-path connections or barriers in the PMOV basin. This concept is supported by large-scale, aquifer test analyses at Pahute Mesa, which show that fault hydraulic properties are similar to nearby HSU hydraulic properties. Hydraulic gradients and transmissivity distributions suggest that only isolated parts of a limited number of faults function as distinct conduits or barriers. Hydraulic evidence on Pahute Mesa does not support faults oriented perpendicular to the regional stress field functioning as barriers or dilated fault zones functioning as conduits.

Tritium and other radionuclides have been detected in wells downgradient of at least four underground nuclear tests on Pahute Mesa; tritium plumes downgradient of other tests are likely but have not been observed. Tritium at the leading edge of the BENHAM plume has moved relatively fast, at a velocity of about 340 to 500 feet per year.

Introduction

Investigation and long-term monitoring of radionuclides at the Nevada National Security Site (NNSS) are the focus of the U.S. Department of Energy (DOE) Underground Test Area activity (U.S. Department of Energy, 2010). One of the objectives of the long-term activity is to assess the extent of contamination on and downgradient of the NNSS. Pahute Mesa, in the northwestern part of the NNSS, is of concern because groundwater is known to be contaminated, transport velocities are fast (up to 600 feet per year [ft/yr]; Russell and others, 2017), and the travel distance for contaminated water to reach publicly accessible lands is relatively short (approximately 12 miles [mi]). Investigations of radionuclide movement away from Pahute Mesa have been occurring since the 1990s (U.S. Department of Energy, 1999, 2009).

Eighty-two nuclear tests were detonated beneath Pahute Mesa and comprised sixty percent of the radionuclide inventory from all underground nuclear tests in the NNSS (Finnegan and others, 2016). The Pahute Mesa nuclear tests were detonated in deep vertical shafts and nearly all these tests occurred at or below the water table (Laczniak and others, 1996; Pawloski and others, 2002). Tests below the water table typically were larger in explosive yield, compared to tests elsewhere on the NNSS, and detonated in deeper shafts to prevent the release of radionuclide-laden gasses to the atmosphere. Sixteen tests, including the three largest (exceeding 1 megaton), were detonated more than 1,000 feet (ft) below the water table (U.S. Department of Energy, 2015). Many of the tests released radionuclides into the groundwater system (Laczniak and others, 1996; Pawloski and others, 2001; Wolfsberg and others, 2002; U.S. Department of Energy, 2019), and these radionuclides are migrating downgradient toward Oasis Valley (Fenelon and others, 2016).

The direction and rate of subsurface transport away from former underground testing areas are controlled, in part, by groundwater flow. Groundwater flow, in turn, is controlled by the hydraulic properties of the rocks transmitting flow and the hydraulic gradient. The primary aquifer property affecting groundwater flow is transmissivity, which quantifies the degree to which groundwater can pass through pore spaces and fractures in a geologic medium. Transmissivity typically is estimated from aquifer tests. Transmissivity of rocks is correlated partly with rock type, secondary mineral alteration, and degree of fracturing. The hydraulic gradient is defined as the difference in hydraulic head between two points divided by the distance between these points and indicates the groundwater-flow potential and direction of flow. Hydraulic head commonly is determined by the water-level altitude in a well. The spatial distribution of hydraulic heads and hydraulic gradients throughout the Pahute Mesa–Oasis Valley (PMOV) groundwater basin has been illustrated by previous authors using potentiometric contours drawn at a regional scale (Waddell and others, 1984; Laczniak and others, 1996; U.S. Department of Energy, 1997; D'Agnese and others, 1998; Harrill and Bedinger, 2010; Fenelon and others, 2010, 2016; Heilweil and Brooks, 2011) or focused on Pahute Mesa (Blankennagel and Weir, 1973; O'Hagan and Laczniak, 1996).

Assessment of radionuclide transport toward Oasis Valley requires an understanding of the flow direction and flow rate through rocks that contain or are susceptible to test-generated contaminants. This report develops refined potentiometric contours, which illustrate hydraulic gradients and groundwater-flow directions in the PMOV basin. Potentiometric contours are developed using a detailed water-level analysis that combines relevant legacy datasets with more recent geologic and hydrologic information. This water-level analysis is integrated with an understanding of lateral and vertical transmissivity distributions, which define the relative ability of aquifers and confining units to transmit and impede flow, respectively. This integrated analysis, combined with information such as the groundwater budget, is used to develop a detailed conceptual model of groundwater flow in the PMOV basin.

Purpose and Scope

The purpose of this report is to provide a detailed conceptual model of groundwater flow in the PMOV basin, with a focus on the region extending from the Pahute Mesa underground nuclear testing area to the downgradient discharge area in Oasis Valley. Geologic, hydrologic, hydraulic-property, and radionuclide data are integrated to develop this groundwater-flow conceptualization. Geologic data were obtained from a three-dimensional hydrostratigraphic framework model (U.S. Department of Energy, 2020a). Geologic units from the hydrostratigraphic framework model are categorized into hydrogeologic units (HGUs) and hydrostratigraphic units (HSUs). HGUs describe the primary lithologic properties, degree of fracturing, and secondary mineral alteration of geologic units, where HGUs of similar character are stratigraphically organized into HSUs (Prothro and others, 2009). Hydrologic data include water levels, natural groundwater-discharge estimates, and groundwater-withdrawal estimates. Hydraulic-property data include transmissivity estimates from aquifer tests and specific capacity. Radionuclide data are restricted to measured tritium concentrations in wells because, unlike other nuclear-test-related radionuclides, tritium is mobile in groundwater and only tritium has been detected above the U.S. Environmental Protection Agency Safe Drinking Water Act standards (Code of Federal Regulations, 2019).

The report summarizes water-level data acquired from nearly 600 wells in and near the study area. All water levels are flagged to indicate their likelihood of representing steady-state conditions or having been affected by nuclear testing or pumping. Basic well-construction information, including a hydrostratigraphic log, are included for about 400 of the wells that had water levels useful for developing potentiometric contours. Well hydrographs and well-construction plots can be displayed using interactive Microsoft® Excel workbooks available in the appendixes of this report.

The direction of groundwater flow in the basin is defined and described in this report, and large-scale changes to the flow system resulting from human activities, such as pumping and nuclear testing, are discussed. Groundwater-flow directions are determined by constructing a potentiometric surface map that is designed to conceptualize and describe predevelopment (steady-state) flow through the volcanic-dominated aquifers and confining units. The map and its component hydraulic heads can be used as calibration targets for groundwater-flow models and can help identify likely groundwater-flow paths.

HGUs and HSUs have been designated previously as aquifers or confining units based on geology and the physical characteristics of the rocks. However, aquifer and confining unit designations have not been validated by comparing to aquifer-test results. Transmissivity estimates from 347 wells, which were compiled from a hydraulic-properties database (Frus and Halford, 2018), were correlated to HGUs, HSUs, and volcanic-rock alteration. Plots of transmissivity distribution by HGU and HSU were used to determine (1) if transmissivity estimates support previously published designations of HGUs and HSUs as aquifers or confining units; (2) the expected range in transmissivities for HGU and HSU groupings; and (3) if HGU and HSU transmissivity distributions are hydraulically unique, meaning that an HGU (or HSU) transmissivity distribution does not greatly overlap with the transmissivity distributions of other units. Plots of transmissivity distribution by volcanic-rock alteration and alteration abundance by HGU were used to help explain the ranges in transmissivity for HGUs and their functionality as aquifers or confining units. Hydraulic-property and alteration analyses are contained within Microsoft® Excel workbooks, which are available in the appendixes of this report.

The lateral and vertical boundaries of the PMOV flow system are examined using groundwater-budget constraints and water-level and hydraulic-property data. Uncertainty in the southeastern segment of the PMOV boundary is analyzed to determine if radionuclides migrating from any of the underground nuclear tests could flow southward across the PMOV basin boundary rather than southwestward to Oasis Valley. The base of the PMOV basin is defined and discussed in terms of active flow and radionuclide transport. The primary basis for determination of the depth of the active flow system is packer-test data from 17 Pahute Mesa deep boreholes, which were used to evaluate hydraulic-property variations with depth. Vertical variations in volcanic-rock alteration were used to help explain hydraulic-conductivity variations with depth.

Horizontal water-level gradients and a mapped transmissivity distribution estimated from a steady-state numerical model of the PMOV basin (Fenelon and others, 2016) are compared to spatially distributed HSUs and HGUs. The lateral distribution of HSUs and HGUs at the potentiometric surface was obtained from a published hydrostratigraphic framework model. The vertical distribution of HSUs and HGUs was evaluated using nine sets of hydrostratigraphic and hydrologic sections that were constructed for this report to portray the hydrostratigraphic framework, underground nuclear tests, and groundwater flow in the basin. Horizontal water-level gradients are analyzed in relation to geologic structures, transmissivity, and HSUs/HGUs to determine potential causes for areas of high or low gradients. Hydraulic properties and water-level gradients also are used to determine whether major geologic structures function as conduits or barriers to flow. The spatial pattern in vertical hydraulic gradients is described and discussed in relation to hydraulic properties and natural recharge and discharge areas.

The groundwater-flow conceptualization in the PMOV basin is discussed in terms of six distinct subareas. The conceptual model for each subarea integrates the following results: groundwater-flow directions, groundwater budgets, horizontal and vertical hydraulic gradients, transmissivity distributions for HGUs and HSUs, inferred relations of faults as conduits or barriers to flow, known tritium plumes migrating downgradient of underground nuclear tests, and the mapped transmissivity distribution of the PMOV basin. The detailed groundwater-flow conceptualization presented in this report provides the basis for future studies of groundwater-flow and radionuclide transport in the PMOV basin.

Description of Study Area

The study area is the PMOV groundwater basin in Nye County, southern Nevada (fig. 1). The basin encompasses about 1,400 square miles (mi^2; 920,000 acres). Of particular focus to this study is the underground nuclear testing area on Pahute Mesa and the downgradient area where groundwater flows to the southwest. Oasis Valley is in the southwestern part of the basin and terminates near Beatty, Nevada. An extensive volcanic plateau (Pahute Mesa, Black Mountain, and Timber Mountain) covers most of the central part of the basin, and several elongated mountain ranges (Kawich and Belted Ranges) and valleys (Gold Flat and Kawich Valley) occur farther north. The eastern boundary of the PMOV basin is the Belted Range, whereas the western boundary is poorly defined, transitioning into Sarcobatus Flat near Black Mountain and Bullfrog Hills. Altitudes range from about 3,500 ft in Oasis Valley to about 8,500 ft in the Belted and Kawich Ranges.

The climate of the study area is arid to semi-arid, characteristic of a high desert region. The climate is characterized by hot summers and mild winters, large fluctuations in daily and annual temperatures, and low precipitation and humidity. Average summertime maximum temperatures in Oasis Valley are nearly 100 °F (National Centers for Environmental Information, 2017), and average wintertime minimum temperatures on Pahute Mesa are about 25 °F (Soulé, 2006). Annual precipitation in the study area ranges from about 6 inches in Oasis Valley to about 8 to 13 inches on the upland areas (Soulé, 2006; National Centers for Environmental Information, 2017). Precipitation occurs primarily in late autumn through early spring and in mid-summer. Precipitation falls primarily as rain and during the winter months at high altitudes as snow. Streams in the study area primarily are ephemeral and flow only for brief periods after infrequent intense rainfall and during and shortly after spring snowmelt. Perennial stream flow in the study area occurs only over short reaches of the Amargosa River downgradient of a few large springs in the Oasis Valley area.

Geology

Geologic units were formed by magmatic activity, volcanism, and depositional processes in the study area. These rocks subsequently have been thrusted and offset. Depositional, magmatic, volcanic, and tectonic processes have juxtaposed geologic units into a complex three-dimensional framework that affects groundwater flow. The geologic history is divided into six periods of deposition and tectonic deformation: (1) Precambrian and Paleozoic marine and non-marine deposition, (2) Late Paleozoic to Early Cenozoic thrust faulting, (3) Mesozoic intrusion, (4) Cenozoic volcanism, (5) Cenozoic normal and strike-slip faulting, and (6) Cenozoic basin-fill deposition.

Precambrian and Paleozoic marine and orogenic processes formed thick sequences of siliciclastic and carbonate rocks (Winograd and Thordarson, 1975; Laczniak and others, 1996). Marine sedimentary rocks, largely siltstones and quartzites, were deposited from Neoproterozoic to Lower Cambrian. The siliciclastic rocks are overlain by thick sequences of Middle Cambrian to Devonian carbonate rocks.

Precambrian and Paleozoic rocks were subjected to compressional tectonic forces from the Late Paleozoic to Early Cenozoic. Siliciclastic and carbonate rocks were offset by regional thrust faulting, which emplaced Neoproterozoic to Lower Cambrian siliciclastic rocks over younger Paleozoic rocks (Faunt and others, 2010). The Belted Range and Bare Mountain have exposed thrust faults. Mesozoic rocks are largely absent due to uplift and erosion of Precambrian and Paleozoic rocks (Faunt and others, 2010). Therefore, Mesozoic rocks are minor and occur as localized granitic intrusions.

Volcanic rocks formed during the Cenozoic and are the dominant rock type in the PMOV basin. From the Oligocene to Miocene, multiple eruptions occurred from at least seven calderas centered on Pahute Mesa, Timber Mountain, and Black Mountain in the southwestern Nevada volcanic field (Blankennagel and Weir, 1973; Sawyer and others, 1994; Grauch and others, 1999; National Security Technologies, LLC, 2007; U.S. Department of Energy, 2020a). Caldera-forming eruptions deposited rhyolitic-to-dacitic lava flows; ash-flow, ash-fall, and reworked tuffs; and tectonic, eruptive, and flow breccias (Winograd and Thordarson, 1975; Laczniak and others, 1996; Faunt and others, 2010). Volcanic rocks are more than 10,000 feet thick (Blankennagel and Weir, 1973; Sawyer and others, 1994; U.S. Department of Energy, 2020a). The estimated volume of rock erupted from these calderas exceeds 3,000 cubic miles (Sawyer and others, 1994).

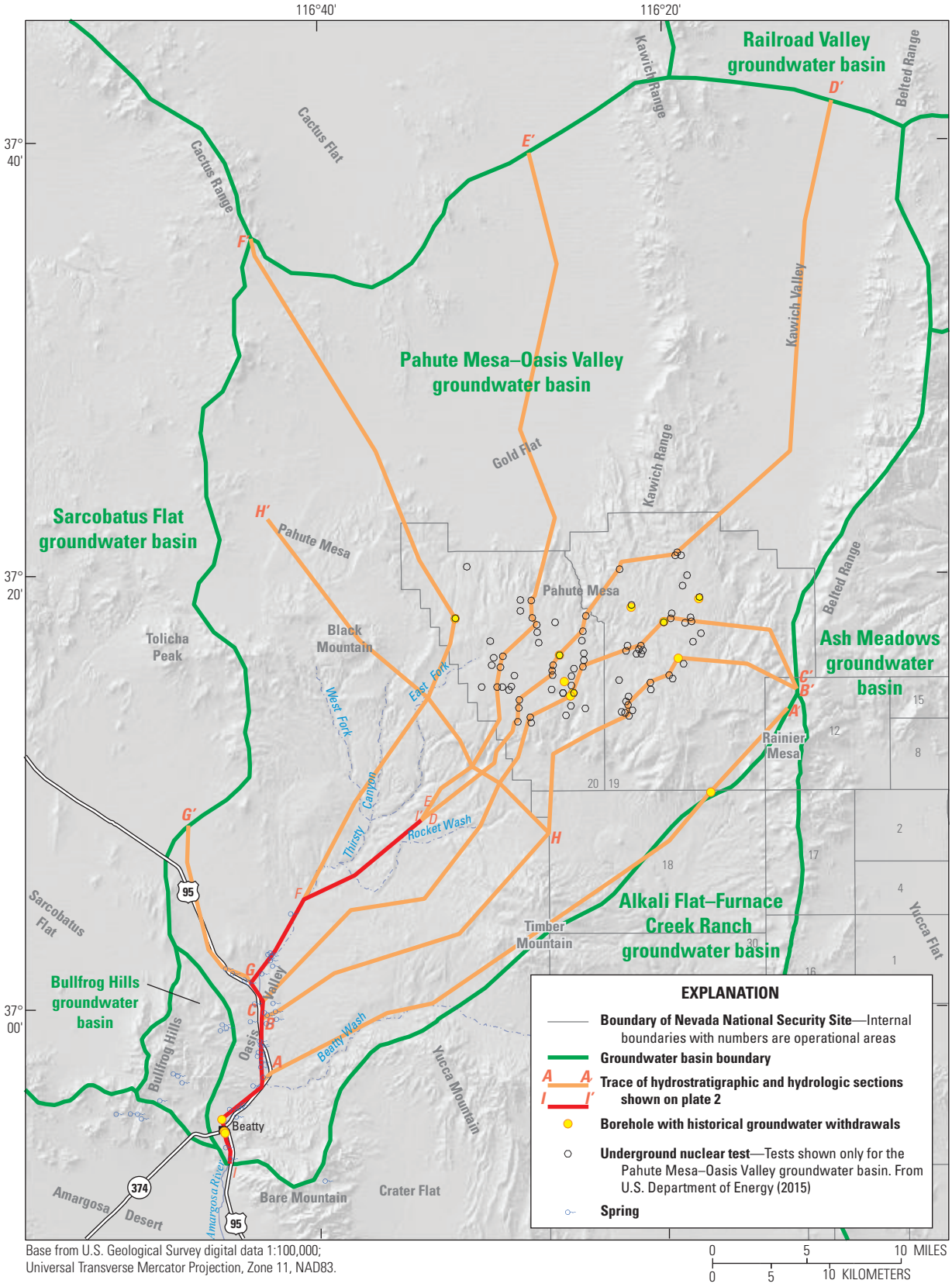

Figure 1. Physiographic and hydrologic features in the Pahute Mesa–Oasis Valley groundwater basin, southern Nevada.

Large-scale normal faulting occurred during and after the period of Cenozoic volcanism (Faunt and others, 2010; U.S. Department of Energy, 2020a). From the Mid-Tertiary to Quaternary, normal faults formed the Basin and Range topography of the Great Basin province. Normal faults are the most common structural feature in the study area and displacement along normal faults continues today (Winograd and Thordarson, 1975). Mid-to-late Cenozoic extensional faulting resulted in northwest- to northeast-striking, high-angle normal faults with up to 1,000 ft of vertical offset on Pahute Mesa (McKee and others, 2001; U.S. Department of Energy, 2020a).

Cenozoic unconsolidated basin fill occurs in Oasis Valley, Kawich Valley, and Gold Flat. Locally thick (greater than 1,000 ft) basin-fill deposits mostly formed from the erosion of nearby volcanic rocks (U.S. Department of Energy, 2020a).

Volcanic Tuff Formation and Alteration

Volcanic tuffs are deposited by a set of complex physical processes. During a volcanic eruption, a turbulent mixture of superheated volcanic gases, molten rock, crystals, and rock fragments is ejected into the atmosphere (Ross and Smith, 1961). The ejected molten rock rapidly cools into glass, forming pumice and fine-grained volcanic ash. Because fine-grained volcanic ash is less dense than other components in the ejected turbulent mixture, wind can transport the ash hundreds to thousands of miles from the eruptive vent (Ross and Smith, 1961). Fine-grained volcanic ash falls out of the atmosphere like rain and is deposited across the landscape, forming an ash-fall tuff. Ash-fall tuffs are called bedded tuffs because they are characterized by bedding structures (Ross and Smith, 1961). Grain sorting in bedded tuff ranges from poorly to well sorted depending on distance traveled from the eruptive vent (Ross and Smith, 1961).

The dense part of the turbulent mixture erupted from the vent initially is ejected thousands of feet into the atmosphere (Ross and Smith, 1961). The weight of the dense mixture causes the volcanic material to fall to land surface. Turbulence and the buoyancy of superheated volcanic gases cause the dense mixture of volcanic material to flow rapidly across the land surface at velocities that can exceed 500 miles per hour (Ross and Smith, 1961). When turbulence and buoyancy effects dissipate, volcanic material is deposited, forming an ash-flow tuff. Ash-flow tuffs range from nonwelded to densely welded, where the degree of welding is based on emplacement temperature, rate of cooling, rate of crystallization, lithostatic load, composition of the tuff, and the composition and amount of volatile gas in the tuff (Ross and Smith, 1961; Winograd, 1971).

As thick ash-flow tuffs cool, their physical and chemical characteristics are altered, forming densely welded tuffs. The top and bottom contacts of a thick ash flow cool rapidly to dense glassy vitrophyre, whereas the interior retains emplacement heat and undergoes a process of devitrification. Devitrification is the crystallization of glass and pumice fragments to minerals, such as tridymite, cristobalite, sanidine, and feldspar (Ross and Smith, 1961; Winograd, 1971). As devitrification propagates outward from the interior of ash-flow tuffs, hot volcanic gas is released from the glass and moves through matrix pores and early formed fractures. The hot volcanic gas is enriched in volatiles from the parent magma and alters the surrounding rock through the process of vapor-phase crystallization. Vapor-phase crystallization is caused by vapor-phase movement of volcanic gas within open spaces and creates minerals such as tridymite, cristobalite, sanidine, zeolites, goethite, hematite, and rutile (Ross and Smith, 1961). Devitrification differs from vapor-phase crystallization in that crystals are formed within the boundary of the glass in devitrification, whereas crystals are formed within open spaces on the exposed surface of glass and pumice fragments in vapor-phase crystallization (Ross and Smith, 1961).

Formation of vitrophyre, devitrification, and vapor-phase crystallization are sequential processes that partly overlap (Stoller-Navarro Joint Venture, 2007b). These processes do not occur in bedded (ash-fall) tuffs or nonwelded (ash-flow) tuffs because emplacement heat, if any, is insufficient to induce crystallization reactions. Partial devitrification does occur in partially welded (ash-flow) tuffs, but the rock is cooled too quickly for the process to complete. The absence or partial completion of crystallization processes causes an initial abundance of thermodynamically unstable volcanic glass in bedded tuffs and nonwelded-to-partially welded tuffs. Therefore, these tuffs are classified as vitric (glassy) tuffs. Densely welded tuffs are classified as devitrified tuff because these tuffs have undergone crystallization processes.

After volcanic tuffs cool, the rocks are altered through the process of diagenesis, defined as the alteration of glass and minerals through rock-water interactions at temperatures below 392 °F and pressures below 300 megapascals (Stoller-Navarro Joint Venture, 2007b). Diagenetic alteration occurs more readily in vitric tuffs, compared to devitrified tuffs, because thermodynamically unstable volcanic glass is prevalent in vitric tuffs. Therefore, altered vitric tuffs, such as bedded or nonwelded tuffs, have better developed diagenetic mineral assemblages compared to devitrified tuffs (Sheppard and Hay, 2001). Two types of diagenetic alteration are zeolitic and argillic alteration. Zeolitic alteration is the alteration of glass or minerals to zeolites. Rhyolitic glass in tuffs is diagenetically altered by hydrolysis to zeolites (clinoptilolite, mordenite). Argillic alteration is the alteration of minerals to clays. For example, potassium feldspar in devitrified tuff is diagenetically altered to smectite. Zeolitic and argillic alteration also can result from hydrothermal alteration.

Volcanic tuffs beneath Pahute Mesa have been subjected to hydrothermal alteration (Benedict and others, 2000). Hydrothermal alteration leaches silica from glass and silica-rich minerals in rhyolitic lavas and tuffs. The leached silica is precipitated along faults and fractures as chalcedony and opal. Hydrothermal fluids rich in potassium, sodium, and calcium commonly replace minerals and glass in volcanic tuffs with potassium feldspar, mica minerals (chlorite, sericite), clays (kaolinite, illite/smectite), and zeolites (analcime, clinoptilolite, mordenite; Utada, 2001). Hydrothermal fluids rich in iron and magnesium cause the alteration of biotite and amphibole to an epidote–chlorite–albite mineral assemblage that commonly occurs with pyrite. Hydrothermal fluids precipitate minerals into fractures and pore spaces, which reduce the porosity and permeability of the volcanic tuffs (Stoller-Navarro Joint Venture, 2007b).

Devitrified rocks are resistant to secondary mineral alteration; however, these rocks can be overprinted by quartzo-feldspathic or textural alteration (Stoller-Navarro Joint Venture, 2007b). Quartzo-feldspathic rocks are rocks that contain an abundance of quartz and feldspar. If devitrification resulted in a rock composed mostly of microcrystalline quartz and feldspar, then the originally formed devitrified rock is also a quartzo-feldspathic rock (Stoller-Navarro Joint Venture, 2007b). Devitrified rocks also can be overprinted by quartzo-feldspathic alteration from hydrothermal processes. Textural alterations commonly associated with devitrified rock are granophyric and spherulitic. Granophyric texture has angular intergrowths of quartz and feldspar, whereas spherulitic texture has spherical phenocrysts within a silica- or feldspar-rich groundmass (Wood, 2007). Fractures within devitrified or quartzo-feldspathic rocks can become closed if filled with hydrothermally precipitated minerals, which reduces the porosity and permeability of the rock.

Hydrostratigraphic Framework

A three-dimensional hydrostratigraphic framework model (HFM) was developed of the PMOV basin and vicinity and is referred to as the Pahute Mesa–Oasis Valley hydrostratigraphic framework model (PMOV HFM; U.S. Department of Energy, 2020a). Geologic units in the HFM were categorized using a geology-based approach and two-level classification scheme (Prothro and others, 2009). Geologic units were classified into HGUs, and then these HGU designations were organized into HSUs (table 1).

HGUs describe the primary lithologic properties, degree of fracturing, and secondary mineral alteration of geologic units, all of which relate to the porosity and permeability of the rocks (Prothro and others, 2009). The HGU classification scheme is consistent with historical classifications of aquifers or confining units based on lithology and on fracture and matrix properties (Blankennagel and Weir, 1973; Winograd and Thordarson, 1975; Laczniak and others, 1996; U.S. Department of Energy, 2020a). Aquifers consist of rocks with high fracture permeability or high matrix porosity and permeability. Rocks with minimal fracturing or low matrix porosity and permeability are classified as confining units.

HGUs of similar character were stratigraphically organized into HSUs, which comprise the primary aquifers, confining units, and composite units in the study area (Prothro and others, 2009). A composite unit is defined as a grouping of rocks composed of aquifers and confining units. Stratigraphic information was integrated into HSU designations so that individual HSUs could be mapped and correlated across the NNSS (Prothro and others, 2009). HSUs are the fundamental mapping units in the PMOV HFM, where each HSU is composed of one or more HGUs (table 1).

The PMOV HFM supersedes a previous HFM that extended from the northern boundary of the NNSS to Beatty, Nevada (Bechtel Nevada, 2002a). The PMOV HFM incorporates HSUs and geologic interpretations from the previous HFM (Bechtel Nevada, 2002a) as well as data from wells drilled after the previous HFM was constructed. The newer PMOV HFM (U.S. Department of Energy, 2020a) is the basis for much of the hydrostratigraphic framework discussion in this report.

Hydrogeologic Units

Geologic units in the PMOV basin have been grouped into nine HGUs: clastic confining unit (CCU), granite confining unit (GCU), intra-caldera intrusive confining unit (IICU), carbonate aquifer (CA), alluvial aquifer (AA), and four types of volcanic rocks (U.S. Department of Energy, 2020a). The volcanic rocks are divided into lava-flow aquifer (LFA), tuff confining unit (TCU), welded-tuff aquifer (WTA), and vitric-tuff aquifer (VTA).

Volcanic HGUs form the principal aquifers and confining units in the PMOV basin because of their widespread distribution (fig. 2; Blankennagel and Weir, 1973; Fenelon and others, 2010). The principal aquifers are the LFAs and WTAs, which consist of rhyolitic-to-dacitic lavas and welded tuffs, respectively. LFAs can have high permeabilities where fractured, but the lavas are restricted areally and in thickness (Prothro and Drellack, 1997). WTAs can have well-connected fracture networks and are widespread, which can provide lateral continuity for water to move through the flow system (Winograd, 1971). The TCU consists of nonwelded and bedded tuffs, which have limited fracture networks and, as a result, have been classified as confining units, especially where they are zeolitized (Blankennagel and Weir, 1973). The VTA is composed of vitric tuffs, which have been classified as aquifers because they are expected to have high matrix porosity and moderate permeability; however, the VTA can function as a confining unit where the unit is zeolitized (U.S Department of Energy, 2020a).

Table 1. Hydrostratigraphic units in the Pahute Mesa–Oasis Valley hydrostratigraphic framework model.

[**Hydrogeologic unit**: AA, alluvial aquifer; CA, carbonate aquifer; GCU, granite confining unit; IICU, intra-caldera intrusive confining unit; LFA, lava-flow aquifer; TCU, tuff confining unit; CCU, clastic confining unit; VTA, vitric-tuff aquifer; WTA, welded-tuff aquifer. Hydrostratigraphic and hydrogeologic unit information from U.S. Department of Energy (2020a, table 4-5)]

Hydrostratigraphic unit (HSU) name	HSU code	Primary hydrogeologic unit(s)
Cenozoic era—Quaternary period		
Alluvial aquifer	AA	AA
Cenozoic era—Tertiary period		
Alluvial aquifer	AA	AA
Younger volcanic composite unit	YVCM	LFA, WTA, VTA
Thirsty Canyon volcanic aquifer	TCVA	WTA, LFA, lesser VTA
Detached volcanics composite unit	DVCM	WTA, LFA, TCU
Detached volcanics aquifer	DVA	WTA, LFA
Shoshone Mountain lava-flow aquifer	SMLFA	LFA
Fortymile Canyon composite unit	FCCM	TCU
Fortymile Canyon upper mafic lava-flow aquifer	FCUMLFA	LFA
Fortymile Canyon upper lava-flow aquifer #1	FCULFA1	LFA, lesser VTA
Fortymile Canyon upper lava-flow aquifer #2	FCULFA2	LFA
Fortymile Canyon upper lava-flow aquifer #3	FCULFA3	LFA
Fortymile Canyon upper lava-flow aquifer #4	FCULFA4	LFA, lesser TCU
Fortymile Canyon upper lava-flow aquifer #5	FCULFA5	LFA
Fortymile Canyon upper lava-flow aquifer #6	FCULFA6	LFA, lesser TCU
Fortymile Canyon upper lava-flow aquifer #7	FCULFA7	LFA, lesser TCU
Fortymile Canyon welded-tuff aquifer #1	FCWTA1	WTA
Fortymile Canyon welded-tuff aquifer	FCWTA	WTA, lesser VTA and TCU
Fortymile Canyon lower lava-flow aquifer	FCLLFA	LFA, lesser TCU
Fortymle Canyon lower mafic lava-flow aquifer	FCLMLFA	LFA
Ammonia Tanks mafic lava-flow aquifer	ATMLFA	LFA
Buttonhook Wash welded-tuff aquifer	BWWTA	WTA
Buttonhook Wash confining unit	BWCU	TCU
Ammonia Tanks welded-tuff aquifer	ATWTA	WTA
Ammonia Tanks caldera confining unit	ATCCU	TCU
Timber Mountain upper welded-tuff aquifer	TMUWTA	WTA, lesser LFA and TCU
Tannenbaum Hill lava-flow aquifer	THLFA	LFA, minor VTA and TCU
Tannenbaum Hill composite unit	THCM	Mostly TCU, lesser WTA
Tannenbaum Hill confining unit	THCU	TCU
Timber Mountain welded-tuff aquifer	TMWTA	WTA, minor VTA
Timber Mountain lower vitric-tuff aquifer	TMLVTA	VTA
Rainier Mesa welded-tuff aquifer	RMWTA	WTA
Fluorspar Canyon confining unit	FCCU	TCU
Windy Wash aquifer	WWA	LFA
Paintbrush composite unit	PCM	WTA, LFA, TCU
Comb Peak aquifer	CPA	LFA
Post-Benham Paintbrush confining unit	PBPCU	TCU
Benham aquifer	BA	LFA
Upper Paintbrush confining unit	UPCU	TCU
Scrugham Peak aquifer	SPA	LFA

Table 1. Hydrostratigraphic units in the Pahute Mesa–Oasis Valley hydrostratigraphic framework model.—Continued

[**Hydrogeologic unit**: AA, alluvial aquifer; CA, carbonate aquifer; GCU, granite confining unit; IICU, intra-caldera intrusive confining unit; LFA, lava-flow aquifer; TCU, tuff confining unit; CCU, clastic confining unit; VTA, vitric-tuff aquifer; WTA, welded-tuff aquifer. Hydrostratigraphic and hydrogeologic unit information from U.S. Department of Energy (2020a, table 4-5)]

Hydrostratigraphic unit (HSU) name	HSU code	Primary hydrogeologic unit(s)
Middle Paintbrush confining unit	MPCU	TCU
Tiva Canyon aquifer	TCA	WTA
Paintbrush vitric-tuff aquifer	PVTA	VTA
Lower Paintbrush confining unit	LPCU	TCU
Paintbrush lava-flow aquifer	PLFA	LFA
Topopah Spring aquifer	TSA	WTA
Yucca Mountain–Crater Flat composite unit	YMCFCM	LFA, WTA, TCU
Calico Hills vitric-tuff aquifer	CHVTA	VTA
Calico Hills zeolitic composite unit	CHZCM	TCU
Calico Hills lava-flow aquifer #1	CHLFA1	LFA
Calico Hills lava-flow aquifer #2	CHLFA2	LFA, very minor TCU
Calico Hills lava-flow aquifer #3	CHLFA3	LFA, minor TCU
Calico Hills lava-flow aquifer #4	CHLFA4	LFA
Calico Hills lava-flow aquifer #5	CHLFA5	LFA
Inlet aquifer	IA	LFA
Crater Flat composite unit	CFCM	Mostly LFA, intercalated with TCU
Crater Flat confining unit	CFCU	TCU
Kearsarge aquifer	KA	LFA
Stockade Wash aquifer	SWA	WTA
Lower vitric-tuff aquifer 2	LVTA2	VTA
Bullfrog confining unit	BFCU	TCU
Belted Range aquifer	BRA	LFA and WTA, lesser TCU
Pre-Belted Range composite unit	PBRCM	TCU, WTA, LFA
Subcaldera volcanic confining unit	SCVCU	TCU
Black Mountain intrusive confining unit	BMICU	IICU
Ammonia Tanks intrusive confining unit	ATICU	IICU
Rainier Mesa intrusive confining unit	RMICU	IICU
Claim Canyon intrusive confining unit	CCICU	IICU
Calico Hills intrusive confining unit	CHICU	IICU
Silent Canyon intrusive confining unit	SCICU	IICU
Redrock Valley intrusive confining unit	RVICU	IICU
Pahute Mesa northern intrusive caldera unit	PMNICU	IICU
Mesozoic era—Cretaceous period		
Mesozoic granite confining unit	MGCU	GCU
Paleozoic era		
Lower carbonate aquifer–thrust plate	LCA3	CA
Lower clastic confining unit-thrust plate	LCCU1	CCU
Upper clastic confining unit	UCCU	CCU
Lower carbonate aquifer	LCA	CA
Lower clastic confining unit	LCCU	CCU
Neoproterozoic era		
Lower clastic confining unit	LCCU	CCU

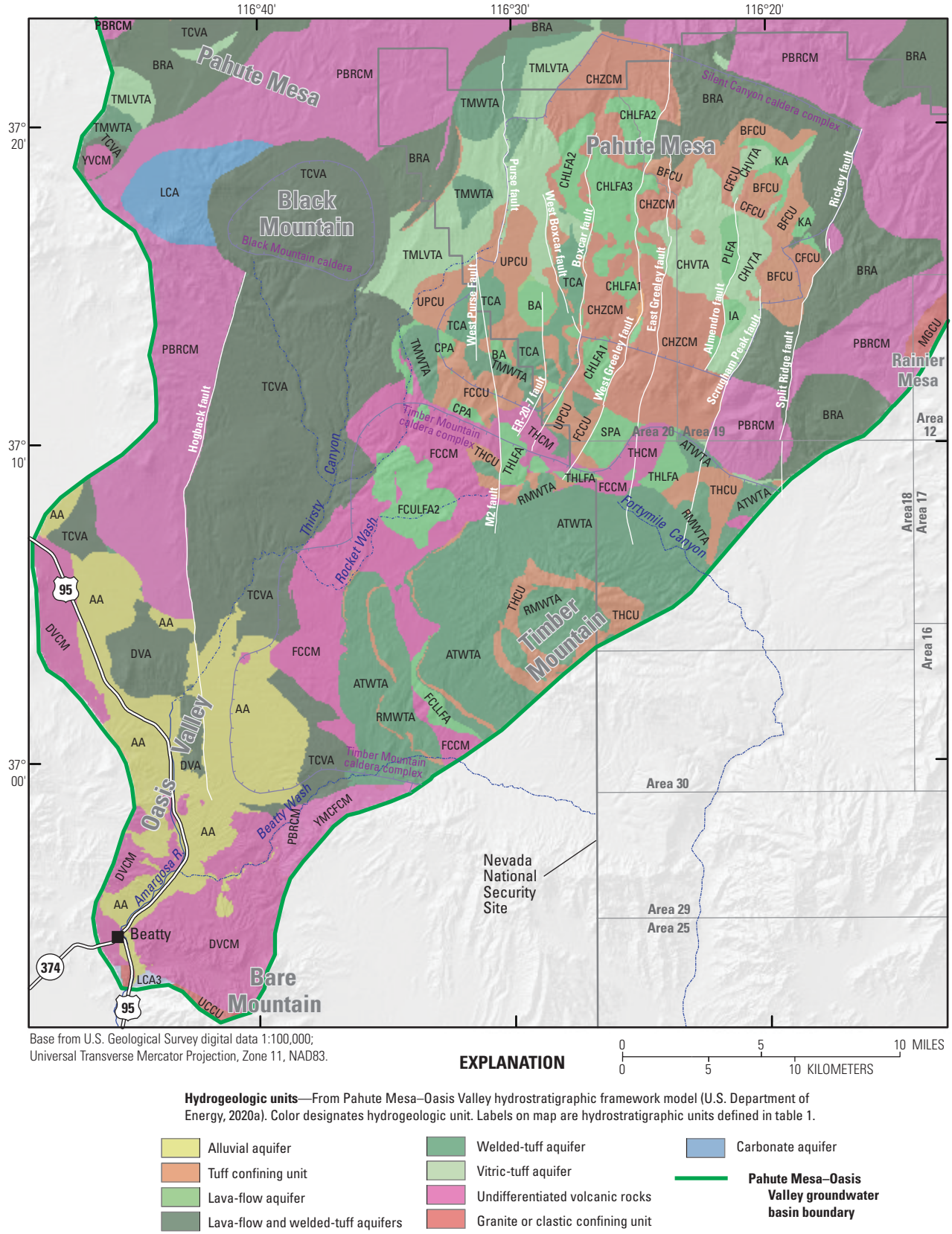

Figure 2. Distribution of hydrogeologic and hydrostratigraphic units at the potentiometric surface in the southern part of the Pahute Mesa–Oasis Valley groundwater basin, southern Nevada.

Nonvolcanic HGUs that function as confining units include the CCU, GCU, and IICU. These HGUs form confining units because rocks within these units have low matrix porosity and permeability and disconnected fractures. The CCU consists of Precambrian to Paleozoic quartzite, argillite, sandstone, siltstone, and shale, and their metamorphic equivalents. The CCU forms the basement of the hydrologic system and composes the Belted and Kawich Ranges and parts of Bare Mountain. The GCU consists of Mesozoic granitic rocks, which occur locally in Black Mountain, Kawich Range, and north of Rainier Mesa. The IICU consists of Cenozoic granite, gabbro, and diorite plutons associated with extension and caldera-related volcanism, such as within calderas beneath Timber Mountain.

Nonvolcanic HGUs that can function as aquifers include the CA and AA. The CA, which consists of Paleozoic limestone and dolomite, occurs locally in the Belted Range, Oasis Valley, Bare Mountain, and near Black Mountain. CAs with high fracture permeability can provide local pathways for groundwater flow. The AA consists of Cenozoic gravels, sands, silts, and clays, which are saturated beneath Oasis Valley (fig. 2), Kawich Valley, and Gold Flat. The AA has high matrix porosity and is expected to have high estimated transmissivities where dominated by sands and gravels (U.S. Department of Energy, 2020a).

Hydrostratigraphic Units

In the HSU classification scheme, stratigraphic information was integrated with aquifer and confining unit designations from the HGU(s) (Prothro and others, 2009). Each HSU is composed of one or more HGUs, and the dominant HGU(s) within the HSU was used to determine whether the HSU was designated an aquifer or confining unit. For example, the Belted Range aquifer (BRA) HSU is composed of three HGUs: LFA, TCU, and WTA (table 1; U.S. Department of Energy, 2020a). The BRA was classified as an aquifer because this HSU contains a larger amount of lava flows (LFA) and welded tuffs (WTA) that are conceptualized to function as aquifers, compared to nonwelded and bedded tuffs (TCU) that are conceptualized to function as confining units. In contrast, the pre-Belted Range composite unit (PBRCM) is composed of three HGUs (LFA, TCU, and WTA) and is conceptualized to function as a composite unit because this unit has relatively equal proportions of aquifers and confining units (table 1).

The PMOV HFM consists of 77 HSUs (table 1). The majority of the HSUs are composed of extruded volcanic rocks, such as the LFA, TCU, VTA, and (or) WTA (62 HSUs). These extruded volcanic HSUs are dominant at the potentiometric surface in the southern part of the PMOV basin (fig. 2). A total of 8 HSUs consist of intra-caldera intrusive confining units (IICUs; table 1) that occur at depth within calderas in the PMOV basin. The AA is common in Oasis Valley (fig. 2), Kawich Valley, and Gold Flat. The remaining six HSUs are pre-Cenozoic rocks that consist of CA, CCU, or GCU. The only pre-Cenozoic rocks exposed at the potentiometric surface are localized areas of Neoproterozoic to Paleozoic lower clastic confining unit (LCCU) in the Belted and Kawich Ranges and southeast of Cactus Range; Paleozoic lower carbonate aquifer (LCA) in Belted Range and west of Black Mountain; Paleozoic lower carbonate aquifer–thrust plate (LCA3) and upper clastic confining unit (UCCU) near Beatty; and Mesozoic granite confining unit (MGCU) at Rainier Mesa (fig. 2).

Study Methods

The groundwater-flow conceptualization integrates water-level, hydraulic-property, and alteration analyses. The direction of groundwater flow in the PMOV basin is defined and described by estimating steady-state hydraulic heads, developing potentiometric contours, and estimating lateral and vertical hydraulic gradients. Hydraulic-property and alteration analyses include depth analyses (relations of hydraulic conductivity and alteration with depth); transmissivity analyses (relations of transmissivity to HSUs, HGUs, and alteration groups); and alteration abundance by HGU. Hydraulic-property and alteration analyses required compilation of transmissivity estimates for wells within the PMOV basin, and the associated steady-state hydraulic head, well construction, and HSU, HGU, and alteration information.

Hydraulic Heads, Potentiometric Contours, and Hydraulic Gradients

Water-level data were compiled, reviewed, and flagged to indicate their likelihood of representing steady-state conditions or having been affected by nuclear testing or pumping. Steady-state water-level data were used to estimate hydraulic heads for potentiometric contouring. Hydraulic heads in the PMOV basin were contoured to portray horizontal hydraulic gradients and groundwater-flow directions. Vertical hydraulic gradients were calculated between all potential well pairs. Uncertainties in hydraulic-head estimates were analyzed and quantified, where appropriate.

Analysis of Water Levels

Water levels from 577 wells in 227 boreholes were compiled, reviewed, and analyzed (appendix 1). Many of the boreholes occur in areas of past underground testing on Pahute Mesa in the northwestern part of the NNSS and downgradient of Pahute Mesa toward Oasis Valley. As used in this report, a well is defined as a single, temporary or permanent completion in a borehole, where the completion defines a unique open interval. Based on this definition, many boreholes in the study area are considered to have multi-well completions.

Multi-well boreholes may consist of temporary completions, where measurements are made in packer-isolated intervals, or permanent completions, such as multiple monitoring tubes installed within the annulus.

Naming conventions for the wells and boreholes referred to in this report are as follows. A well that is the sole completion interval in a borehole is assigned the name of the borehole. In boreholes with multiple completions, wells are differentiated by names that use a parenthetical expression added after the borehole name—for example: *U-19e (5050 ft)*. A single number in the parenthetical expression refers to the depth of the well; two numbers separated by a dash refer to the depth of the top and bottom of the open interval in the well. In some cases, a well name consists of the borehole name followed by one of several non-parenthetical expressions, such as main, piezometer, shallow, intermediate, deep, borehole, or WW. All borehole and well names in this report are consistent with those used in the U.S. Geological Survey National Water Information System (NWIS) database (U.S. Geological Survey, 2020) and are italicized in the text for clarity. Compiled water-level data in appendix 1 are organized by well name and USGS site identification number, and these NWIS names and identification numbers can be cross-referenced in appendix 2 to determine well-construction information.

Nearly 17,000 water levels in 577 wells were measured in the PMOV basin and vicinity from 1941 to 2016 (appendix 1). Each water-level measurement was reviewed for correctness and accuracy, assigned to an open interval, examined to determine the hydrologic condition at the time of measurement, and flagged to indicate if the level reflects steady-state hydrologic conditions or transient conditions imposed by nuclear testing or pumping. The thorough evaluation ensures data integrity and identifies water levels that best represent hydraulic heads for potentiometric contouring. A large part of the water-level analysis was supported by comprehensive evaluations of water levels in Pahute Mesa and the NNSS area (Fenelon, 2000; Elliott and Fenelon, 2010; Jackson and Fenelon, 2018). Water levels and well-construction information are stored in the USGS NWIS database (U.S. Geological Survey, 2020).

As part of the water-level analysis, each water level in appendix 1 was flagged to indicate whether it is representative of each of the following three hydrologic conditions: (1) steady-state conditions, (2) transient conditions resulting from nearby nuclear testing, or (3) transient conditions resulting from pumping. A water level can be representative of more than one condition or none of the conditions. Assignment of a steady-state condition flag assumes that the water level in a well is in a state of dynamic equilibrium and that long-term (50–100 years) changes in storage are negligible. For example, a water level that responds primarily to natural recharge fluctuations is considered representative of steady-state conditions. For some wells, determination of whether water-level measurements represent steady-state conditions was uncertain. Difficulties arose primarily in wells with few water-level measurements or in wells open to low-permeability units, where water levels in the well equilibrate slowly to formation conditions. In these situations, determining whether a water level is equilibrated and representative of long-term aquifer conditions or is affected by borehole conditions or nearby nuclear testing can be problematic.

Several factors were used to determine whether a water level in a low-permeability unit was representative of steady-state conditions. Water levels measured in a well open to a low-permeability unit typically equilibrate slowly from stresses to the system, such as a nearby nuclear test or drilling and developing the well. Water levels in low-permeability units that are representative of steady-state conditions typically change slowly from year to year in response to changes in recharge. If sufficient measurements are available over a long period (greater than 1 year), large changes (greater than 5 ft) in water levels typically suggest non-equilibrated conditions and stable water levels suggest equilibrated conditions. In wells with sparse water-level data of short measurement duration, other factors were considered. These include the elapsed time between the measurement and well completion, the consistency of the measured water-level altitude relative to nearby water-level altitudes, the length of open interval at the well, and any knowledge about the hydraulic conductivity of geologic unit(s) open to the well.

Each water level is assigned one of five uncertainty flags, as follows, for each of the three hydrologic conditions (steady state, nuclear testing, and pumping):

- "Yes"—Water level represents hydrologic condition.
- "Yes?"—Water level probably represents hydrologic condition, but assignment is uncertain.
- "?"—Water level may or may not represent hydrologic condition.
- "No?"—Water level probably does not represent hydrologic condition, but assignment is uncertain.
- "No"—Water level does not represent hydrologic condition

The assignment of these five uncertainty flags allowed for qualitative weighting of the water levels in later analyses. For example, during the potentiometric-surface contouring process, more weight was given to a steady-state water level assigned an uncertainty flag of "Yes" than to a water level assigned a flag of "Yes?" or "?."

Well hydrographs, well locations, water levels, and flag assignments can be displayed interactively from a Microsoft® Excel workbook (appendix 1). The workbook is designed to be an easy-to-use tool to view water levels and other information associated with wells in the study area. Information for an individual well can be selected by using the AutoFilter option available in Excel. An example of the information available in the workbook is provided on figure 3.

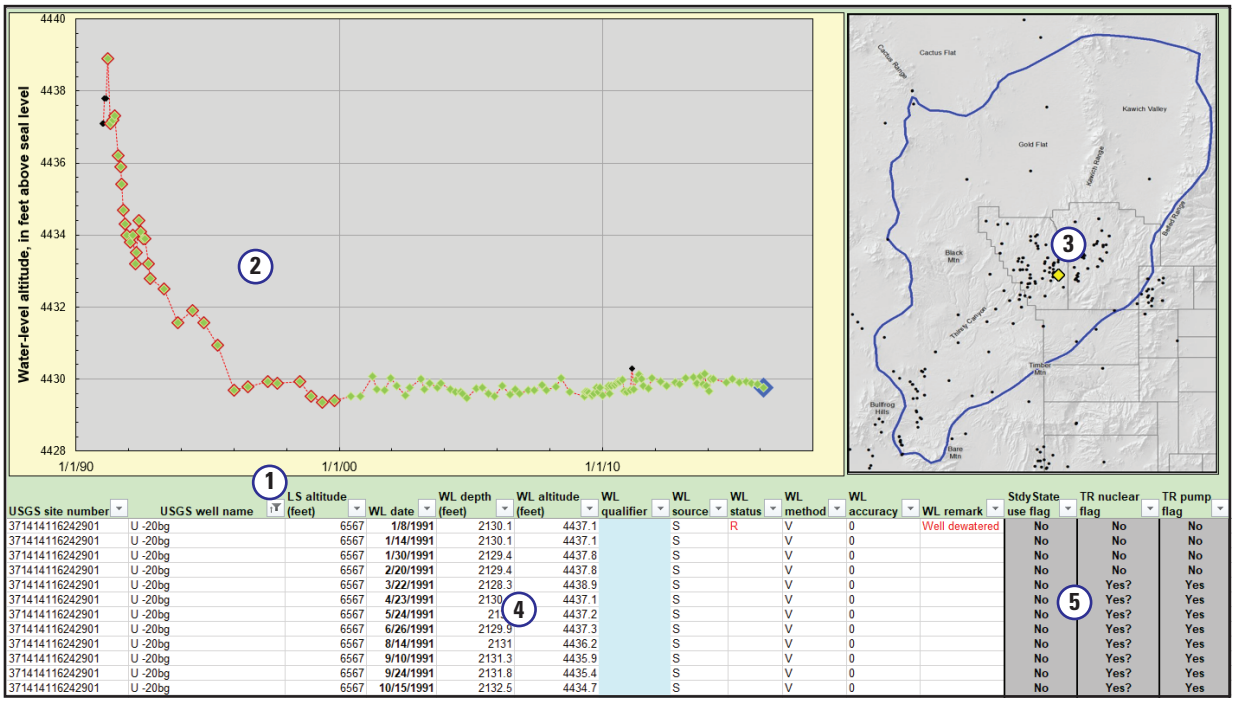

1

USGS site number	USGS well name	LS altitude (feet)	WL date	WL depth (feet)	WL altitude (feet)	WL qualifier	WL source	WL status	WL method	WL accuracy	WL remark	Stdy use flag	State flag	TR nuclear flag	TR pump flag
371414116242901	U -20bg	6567	1/8/1991	2130.1	4437.1		S	R	V	0	Well dewatered	No		No	No
371414116242901	U -20bg	6567	1/14/1991	2130.1	4437.1		S		V	0		No		No	No
371414116242901	U -20bg	6567	1/30/1991	2129.4	4437.8		S		V	0		No		No	No
371414116242901	U -20bg	6567	2/20/1991	2129.4	4437.8		S		V	0		No		No	No
371414116242901	U -20bg	6567	3/22/1991	2128.3	4438.9		S		V	0		No		Yes?	Yes
371414116242901	U -20bg	6567	4/23/1991	2130	4437.1		S		V	0		No		Yes?	Yes
371414116242901	U -20bg	6567	5/24/1991	21	4437.2		S		V	0		No		Yes?	Yes
371414116242901	U -20bg	6567	6/26/1991	2129.9	4437.3		S		V	0		No		Yes?	Yes
371414116242901	U -20bg	6567	8/14/1991	2131	4436.2		S		V	0		No		Yes?	Yes
371414116242901	U -20bg	6567	9/10/1991	2131.3	4435.9		S		V	0		No		Yes?	Yes
371414116242901	U -20bg	6567	9/24/1991	2131.8	4435.4		S		V	0		No		Yes?	Yes
371414116242901	U -20bg	6567	10/15/1991	2132.5	4434.7		S		V	0		No		Yes?	Yes

4

5

Plots highlight the type of information in the spreadsheet: (1) pull-down menu to select well of interest; (2) hydrograph of all water-level measurements for the selected well—steady-state measurements used in contouring are shown as blue diamonds, nonstatic measurements from wellbore equilibration are shown in black, measurements affected by nuclear testing are shown with red outline, and measurements affected by pumping are shown in green; (3) map showing the selected well location as a yellow symbol; (4) water-level data for the well, and (5) water-level flags indicating the likelihood that each water level represents steady-state (natural) conditions, transient conditions resulting from nearby nuclear testing, or transient conditions from nearby pumping.

Figure 3. Image from appendix 1 Microsoft® Excel workbook showing water levels analyzed in well U-20bg.

Estimation of Hydraulic Heads for Potentiometric Contouring

Individual depth-to-water measurements flagged as representative of steady-state conditions (“Yes,” “Yes?,” or “?” in appendix 1) were used to compute steady-state water-level altitudes. Steady-state water-level altitudes were computed for all steady-state depth-to-water measurements by subtracting depth to water from land-surface altitude at the well. All steady-state water-level altitudes were averaged by well to derive a mean water-level altitude for each well. The mean, steady-state, water-level altitude at a well is the hydraulic-head estimate used for potentiometric contouring.

A synoptic set of water-level measurements for all wells in the study area is preferred to using mean water levels, but such a set could not be developed because many of the wells previously measured have been destroyed. Of the 577 wells analyzed for this study, 387 of the wells (appendix 2) had at least one water level identified as representative or potentially representative of steady-state conditions.

An additional 75 land-surface altitudes of springs in Oasis Valley were used in the analysis. Spring land-surface altitudes were estimated from 1:24,000-scale topographic maps (U.S. Geological Survey, 2019a) and a digital elevation model that resampled bare-earth elevation source data every 30 m and reported to the nearest whole meter (Gesch and others, 2009). Each land-surface altitude at a spring and mean, steady-state water-level altitude in a well were assumed equal to the hydraulic-head estimate at the spring orifice or well opening.

The steady-state estimate of the hydraulic head was determined from a single water-level measurement in 144 of the 387 wells. In nearly one-half of these 144 wells, the single measurement could be used only as an upper or lower bound for the steady-state head. For example, on a rising water-level hydrograph that is equilibrating toward steady-state conditions, the last water level can be used as a lower bound for the expected steady-state head in the well. In this example, if the altitude of the last water-level measurement was 4,700 ft, the steady-state head is expected to be greater than 4,700 ft. For measurements made in a dry well, the altitude of the bottom of the well is assigned a “less than” qualifier and is used as an upper bound for contouring. Only hydraulic heads calculated from mean water levels representing steady-state conditions, or those that were assigned a qualifier to constrain the steady-state head, were used to guide the contouring process. One of four qualifiers are used to describe a bounding hydraulic head: “less than” (<), “less than or equal” (≤), “greater than” (>), or “greater than or equal” (≥). The use of “≤“ or “≥” indicates that the hydraulic head is believed to be within a few feet of approximating a steady-state head. A “<” or “>” qualifier provides no information about how close a hydraulic head is to approximating a steady-state head.

Seventy-five spring altitudes and about one-half of the 387 wells with steady-state heads were used for potentiometric contouring. Hydraulic heads were excluded from the contouring dataset primarily because they provided duplicative information. For example, where hydraulic heads were obtained from multiple wells in a single borehole in an area with minimal vertical hydraulic gradient, only one head was chosen as representative of the borehole location. Data quality and representativeness of the geologic units open to the well were considered when determining which heads to exclude. A few wells with "<" or ">" hydraulic-head qualifiers were excluded because they provided only limited information that did not inform the contouring process. Nearly 50 hydraulic heads not used for contouring are shown on plate 1. Many of these heads are anomalously high or low relative to the potentiometric surface and indicate areas of mounded water or large vertical gradients. Appendix 2 shows which well and spring head data were plotted on plate 1 and whether these data were used for contouring the potentiometric surface.

Hydraulic-Head Uncertainty

Hydraulic-head uncertainty characterizes the range of hydraulic-head estimates within which the true value of hydraulic head occurs. Uncertainty includes systematic (measurement) errors and random errors, which result from random fluctuations in the groundwater system. Uncertainty in hydraulic-head estimates can result from limited datasets; incorrect assumptions about the representativeness of a water-level measurement to the well formation; measurement errors; hourly to decadal water-level variability around the long-term average; water-column density differences between wells; and wells with long open intervals, where a hydraulic head is assigned to the center of the interval and assumes no vertical hydraulic gradient.

Uncertainty in a hydraulic-head estimate can occur from incorrectly assuming the water level measured in a well is representative of the formation open to the well. Determination of whether the measured water level is representative of the formation can be subjective if water-level data are sparse. In an undeveloped well or in a well open to a formation of low hydraulic conductivity, the water level in the well can take months to years to equilibrate with the formation (Jackson and Fenelon, 2018; Frus and Halford, 2018). In these cases, a single water-level measurement or a set of measurements that span hours to days may be insufficient to determine if the measurement(s) are representative of the formation. Supplementary information that should be considered to determine the representativeness of the water level include (1) the hole condition at the time of measurement, such as immediately following well construction or bailing the well; (2) any short-term water-level trend that was measured, indicating the water level is equilibrating from activities in the well; (3) the permeability of the formation; and (4) whether the measured water level is anomalous relative to levels in nearby wells. Based on limited water levels and supplementary information, hydrologic judgement is used to determine the representativeness of the water level. An incorrect judgement can lead to a large unquantifiable error in the hydraulic-head estimate. For example, well *PM-2* is open to more than 6,000 ft of mostly volcanic rock (appendix 3). Water-level measurements over a 50-yr period indicate that the hydraulic head in the well is 4,733 ft (appendix 1). However, if only the first measurement from 1966 was available and the measurement was determined incorrectly to be representative of steady-state conditions in the volcanic rocks open to the well, the hydraulic-head estimate would have been 109 ft too low. A determination that the first measurement was representative might have seemed reasonable, considering this measurement was made 4 months after the well was bailed—a seemingly sufficient amount of time for the water level to equilibrate in the well. In hindsight, the water level took more than 2 years to equilibrate.

Most hydraulic-head estimates derived from mean water-level altitudes in the PMOV basin are considered accurate to within 5 to 10 ft based on quantifiable errors discussed below. Uncertainty in hydraulic-head estimates results from multiple factors including the accuracy of the depth-to-water measurement, conversion of depth to water to water-level altitude, and representativeness of the mean water-level measurement to long-term, steady-state conditions. An additional uncertainty of generally less than 10 ft results from assuming that vertical gradients are negligible in a two-dimensional portrayal of the potentiometric surface of the PMOV basin.

The accuracy of individual depth-to-water measurements is affected by the water-level measurement device and by borehole deviation in the measured well. For example, a steel tape is a more accurate device than a geophysical log and a calibrated tape is more accurate than an uncalibrated tape. Measurement-device accuracies of depth-to-water measurements made in the PMOV basin typically range from 0.01 to 1 ft, depending on the device and depth to water. Thirty-three percent of water-level measurements from wells in this study have potential measurement errors exceeding one foot (appendix 1). Errors in measured depth to water in wells also result from borehole deviation, which can cause a measured water level to be deeper than the true vertical depth. Measurement errors resulting from borehole deviation in the PMOV basin are less than 1 ft. In holes where deviations are known to cause errors of greater than 1 ft, the measured water levels were corrected for borehole deviation (Elliott and Fenelon, 2010).

Conversion of a depth-to-water measurement to a water-level altitude creates additional uncertainty because of uncertainty in land-surface altitude. Water-level altitudes for 61, mostly non-surveyed, wells may be in error by 2 to 20 ft due to inaccuracies in estimates of land-surface altitude. Many of these wells are near Oasis Valley; only two are on Pahute Mesa. Land-surface altitudes of all other wells are considered accurate to within 1 ft because the wells were surveyed. Land-surface altitudes for springs were derived from a digital elevation model and topographic-map estimates and are accurate to ± 20 ft. The reported accuracy of the land-surface altitude for each well and spring in the study area is provided in appendix 2.

Steady-state hydraulic head in a well is assumed equal to the mean water-level altitude from all steady-state water levels measured in the well. Uncertainty occurs when the mean water-level altitude does not represent long-term, steady-state conditions. This can occur where limited water-level data for a well do not reflect the total range of natural variation. Daily to seasonal water-level variability of less than one foot occurs in response to changes in earth tides and barometric pressure (Harrison, 1971; Fenelon, 2000). Variability also occurs from responses to long-term (decadal) changes in recharge patterns. In the PMOV basin, long-term water-level variability from recharge generally is less than 5 ft although changes can be larger. For example, water levels in well *U-19bh* rose about 20 ft from 1992 to 2013 in response to recharge (appendix 1; Jackson and Fenelon, 2018). Wells with long-term water-level measurements are more likely to capture natural variability from recharge, resulting in a mean water-level altitude that is representative of steady-state conditions. In contrast, many of the wells in the PMOV basin were measured only for a short period and are biased high or low relative to long-term conditions.

Conversion of water-level altitude to hydraulic head assumes the density of the water is the same between all wells. However, density in the study area can vary because of differences in water temperature, and to a lesser degree, pressure and dissolved solids. The “true” water-level altitude could be several feet lower than the measured, temperature-equivalent water-level altitude in study area wells with long (several thousand feet) water columns and warm water-column temperatures because of abnormally high geothermal gradients. For several wells that were drilled into nuclear-test cavities, the water temperature of the well could be elevated because of heat generated from the test. Carle (2016) calculated hydraulic-head “corrections” for 38 boreholes on Pahute Mesa by accounting for water pressure, gravity, and water temperature relative to an average geothermal gradient on Pahute Mesa. Carle (2016) concluded that nearly all “corrections” were less than 6.6 ft (2 m) and were better applied as uncertainty in the head estimate rather than as a correction. Temperature adjustments were not applied to hydraulic heads because of the large uncertainty in applying an appropriate adjustment to each well and because the magnitude of the temperature adjustment is considered minimal relative to horizontal hydraulic gradients in the study area. Uncertainties in temperature corrections result from poorly constrained estimates of the parameters used to calculate the temperature adjustment, including average water-column temperature at the time of a water-level measurement, zones of inflow into the well, and the average geothermal gradient that should be used to determine if a water-column temperature is anomalous (Fenelon and others, 2010; Carle, 2016).

A final component of hydraulic-head uncertainty occurs from a water level measured in a well with a long (several thousand feet) open interval. In this case, the water level represents an integrated head over the long vertical interval. In a flow system with large vertical hydraulic gradients, a range of depth-dependent heads occur at a single (x,y) location. In most areas of Pahute Mesa, the vertical head difference is relatively small (less than 10 ft). However, larger head differences have been measured, such as a 25-ft difference in borehole *UE-19i* and a 99-ft difference between nested wells *ER-OV-03a2* and *ER-OV-03a3*.

Development of Potentiometric Contours

Hydraulic heads in the PMOV basin were contoured to determine horizontal hydraulic gradients and flow directions. A single set of contours was used to represent the potentiometric surface of the regional flow system. The map approximates present-day (2020) steady-state conditions. In the minor areas where water levels currently are affected by transient pumping effects (Jackson and Fenelon, 2018), the posted water levels represent pre-pumping levels. However, even in areas of pumping, water-level drawdowns are negligible relative to the contour interval. The potentiometric map also approximates predevelopment (pre-1950) conditions, except for a small area near well *U-20 WW* in eastern Area 20 of the NNSS. In this area, heads were as much as 20 ft higher prior to nuclear testing but have been permanently lowered.

Most vertical gradients were considered insignificant when constructing the potentiometric surface because they are small relative to horizontal gradients (see “Calculation of Vertical Hydraulic Gradients” section). Where a large head difference was measured between a well and the contoured surface, indicating a notable vertical gradient, the head was posted on the map and noted as anomalous (plate 1). In areas dominated by confining units where vertical gradients are high relative to horizontal gradients, such as the Bare Mountain or Rainier Mesa areas, the potentiometric surface shown is the water table[1].

[1]The potentiometric surface is the level (height) to which water rises in a well. The potentiometric surface is equivalent to the water table in an unconfined aquifer, whereas the potentiometric surface is above the top of the aquifer if the aquifer is confined because groundwater in these aquifers is under pressure from overlying low-permeability units.

Hydraulic heads were contoured manually and are posted at the well locations. In areas where heads were contradictory, such that all heads could not be contoured, preference was given to (1) heads from wells open to transmissive intervals or to long open intervals, (2) heads with low uncertainty, and (3) heads consistent with surrounding wells. Previous water-level contour maps and conceptualizations were used to guide the contouring and include Blankennagel and Weir (1973), Laczniak and others (1996), O'Hagan and Laczniak (1996), D'Agnese and others (1998), Fenelon and others (2010), and Fenelon and others (2016). As part of the manual contouring process, potentiometric contours were configured in accordance with known or inferred hydraulic gradients, recharge areas, discharge areas, lateral and vertical continuity of aquifers, transmissivity distribution, and known or inferred geology. Specific examples of this manual process include the following:

- In areas where a structure is inferred to impede flow, contours are configured in a tighter pattern to portray an increase in the local head gradient upgradient of the inferred flow barrier (see 4,500 through 4,600-ft contours on northwestern side of Silent Canyon caldera complex, plate 1).
- In areas of recharge on low-permeability rocks, contours are configured to show mounding and high horizontal hydraulic gradients (for example, Rainier Mesa area on plate 1). Conversely, where rocks are permeable, gradients are low (for example, area between 4,400 and 4,500-ft contours in eastern Area 20 on plate 1).
- Contours are drawn to show flow directions consistent with known tritium plumes (for example, downgradient of the BENHAM test [*U-20c*] in southwestern Area 20 on plate 1).
- Contours are drawn so that flow radiates away from recharge areas and converges on discharge areas (for example, Bare Mountain [recharge] and Oasis Valley [discharge] in southwestern part of plate 1).
- Contours are drawn perpendicular to the PMOV basin boundary because the boundary is assumed to be a no-flow boundary.

Calculation of Vertical Hydraulic Gradients

Vertical hydraulic gradient is the difference in hydraulic head between two vertical points in an aquifer system divided by the vertical distance between those points. Ideally, the vertical gradient is calculated using synchronous, static, water-level measurements from two closely paired, short-screened piezometers that are vertically separated. In this study, water-level differences at all potential well pairs were evaluated. The hydraulic gradient at each well pair was calculated as the difference in static water levels between wells divided by the distance between mid-points of the open intervals. Uncertainties in the magnitudes and directions of the computed hydraulic heads resulted from uncertainties in static water-level comparisons and the mid-points being evaluated. Vertical hydraulic gradients were computed with the assumption that water-column temperatures were similar between well pairs, such that measured water levels were equivalent to hydraulic head, because of uncertainty in applying an appropriate temperature adjustment (see "Hydraulic Head Uncertainty" section for details).

Vertical hydraulic gradients were calculated for 58 well pairs in the PMOV basin and vicinity (table 2). Fifty of the well pairs were from multi-completion boreholes. Examples of multi-completion boreholes are two well strings in a single borehole or the deepening of a shallow well. The remaining eight well pairs where vertical hydraulic gradients were calculated consisted of two wells drilled near each other. Wells were within 30 ft of each other for five of the eight well pairs and within 60 to 100 ft of each other for the other three pairs.

Vertical hydraulic-head estimates are affected by water-level uncertainties that result from water-level measurement accuracies, proper attribution of a water level as static, and temporal differences in measurements between paired wells. Measurement accuracies vary by individual measurement and well and depend on a variety of factors. These factors include errors associated with the measurement device, altitude of measuring point, and vertical deviations in well strings. Static water levels for hydraulic-head estimates were selected from water-level measurements flagged as "Yes" or "Yes?" in the column labeled "StdyState Use flag" in appendix 1 (fig. 3). In some cases, the static water level was a qualified estimate, such as "less than" or "greater than," based on water levels in a well that were still equilibrating from aquifer testing at the end of the measurement record. Minimizing temporal variability in water-level measurements provides for more accurate water-level differences. The preference was to calculate water-level differences from measurements made on the same day. For about one-half the well pairs, measurements on the same day were not available.

Table 2. Computed vertical hydraulic gradients for well pairs in the Pahute Mesa–Oasis Valley groundwater basin and vicinity, southern Nevada.

[**Well pair names**: Wells selected for paired well analysis. Shallow well listed on top. U.S. Geological Survey site identification numbers are in appendix 1. **Open interval depths**: Depths, in feet below land surface, to top of uppermost and bottom of lowermost openings in wells. **Water-level altitudes**: Altitude of measured water level, in feet above the National Geodetic Vertical Datum of 1929. **Water-level difference**: Absolute value of water-level altitude in the deep well minus water-level altitude in the shallow well, in feet. **Vertical distance**: Distance between midpoints of open interval depths, in feet. **Vertical gradient**: Calculated absolute value of vertical hydraulic gradient (water-level difference divided by vertical distance), in foot per foot, between well pair. Vertical gradient rounded to one significant digit. **Gradient direction**: Indeterminate (up), calculated gradient is upward, but true direction is indeterminate; Indeterminate (down), calculated gradient is downward but true direction is indeterminate. **Notes**: See footnote(s) pertaining to numbers. **Abbreviations**: mm/dd/yyyy, month/day/year; >, greater than; <, less than; ~, approximately; e, estimated; —, not applicable].

Well site name	Well pair names	Open interval depths	Water-level measurement dates (mm/dd/yyyy)	Water-level altitudes	Water-level difference	Vertical distance	Vertical gradient	Gradient direction	Notes
ER-12-1	ER-12-1 (1641-1846 ft) ER-12-1 (3309-3414 ft)	1,641–1,846 3,309–3,442	10/01/1992 09/25/1992	4,367.12 3,055.12	1,312	1,632	0.8	Down	1
ER-12-3	ER-12-3 piezometer ER-12-3 main	1,244–2,210 2,447–4,908	06/29/2015 06/29/2015	6,147.26 4,283.42	1,864	1,951	1	Down	2
ER-12-4	ER-12-4 piezometer ER-12-4 main	948–1,988 2,563–3,715	03/30/2015 03/30/2015	5,935.83 4,320.38	1,615	1,671	1	Down	2
ER-19-1	ER-19-1-3 (shallow) ER-19-1-1 (deep)	1,301–1,422 3,210–3,560	06/30/2015 06/30/2015	5,136.39 4,362.85	774	2,024	0.4	Down	1
ER-20-4	ER-20-4 shallow ER-20-4 deep	1,520–2,336 2,415–3,053	03/04/2019 03/04/2019	4,214.6 4,214.7	0.1	806	0.0001	Indeterminate (up)	3
ER-20-5	ER-20-5-1 (3-in string) ER-20-5-3	2,249–2,655 3,348–3,954	04/06/2015 04/06/2015	4,189.71 4,190.24	0.5	1,199	0.0004	Indeterminate (up)	3
ER-20-7	ER-20-7 (120-2208 ft) ER-20-7	2,020–2,208 2,292–2,936	06/19/2009 07/09/2009	4,188.9 4,186.7	2.2	500	0.004	Indeterminate (down)	3, 4, 5
ER-20-8	ER-20-8 shallow ER-20-8 intermediate	1,667–2,150 2,440–2,940	05/09/2011 05/10/2011	4,181.41 4,182.28	0.9	782	0.001	Up	—
ER-20-8	ER-20-8 intermediate ER-20-8 deep	2,440–2,940 3,070–3,442	05/10/2011 05/09/2011	4,182.28 4,181.97	0.3	566	0.0005	Down	—
ER-20-12	ER-20-12 p4 ER-20-12 p-3	1,612–2,287 2,510–2,947	01/17/2018 01/17/2018	4,638.3 4,378.0	260	779	0.3	Down	1
ER-20-12	ER-20-12 p-2 ER-20-12 p-1	3,053–3,157 3,343–3,725	05/13/2019 05/13/2019	4,378.2 4,395.3	17	429	0.04	Up	—
ER-20-12	ER-20-12 p-1 ER-20-12 m-1	3,343–3,725 3,916–4,543	05/13/2019 05/13/2019	4,395.3 4,404.3	9	696	0.01	Up	—
ER-30-1	ER-30-1-2 shallow ER-30-1-1 deep	450–628 677–790	06/21/1994 06/21/1994	4,197.09 4,197.2	0.1	195	0.0006	Indeterminate (up)	3, 11
ER-EC-2A	ER-EC-2A (1635-2236 ft) ER-EC-2A (1635-4973 ft)	1,635–2,236 1,635–4,973	12/12/2000 06/28/2000	4,147.49 4,154.25	6.8	1,369	0.005	Up	5, 9
ER-EC-4	ER-EC-4 (952-2295 ft) ER-EC-4 (952-3487 ft)	952–2,295 952–3,487	10/05/2000 08/24/2000	4,010.74 4,010.46	0.3	596	0.0005	Indeterminate (down)	3, 5

Table 2. Computed vertical hydraulic gradients for well pairs in the Pahute Mesa–Oasis Valley groundwater basin and vicinity, southern Nevada.—Continued

[**Well pair names**: Wells selected for paired well analysis. Shallow well listed on top. U.S. Geological Survey site identification numbers are in appendix 1. **Open interval depths**: Depths, in feet below land surface, to top of uppermost and bottom of lowermost openings in wells. **Water-level altitudes**: Altitude of measured water level, in feet above the National Geodetic Vertical Datum of 1929. **Water-level difference**: Absolute value of water-level altitude in the deep well minus water-level altitude in the shallow well, in feet. **Vertical distance**: Distance between midpoints of open interval depths, in feet. **Vertical gradient**: Calculated absolute value of vertical hydraulic gradient (water-level difference divided by vertical distance), in foot per foot, between well pair. Vertical gradient rounded to one significant digit. **Gradient direction**: Indeterminate (up), calculated gradient is upward, but true direction is indeterminate; Indeterminate (down), calculated gradient is downward but true direction is indeterminate. **Notes**: See footnote(s) pertaining to numbers. **Abbreviations**: mm/dd/yyyy, month/day/year; >, greater than; <, less than; ~, approximately; e, estimated; —, not applicable].

Well site name	Well pair names	Open interval depths	Water-level measurement dates (mm/dd/yyyy)	Water-level altitudes	Water-level difference	Vertical distance	Vertical gradient	Gradient direction	Notes
ER-EC-6	ER-EC-6 shallow ER-EC-6 deep	1,507–1,948 3,392–3,820	06/20/2009 06/20/2009	4,179.19 4,178.21	1.0	1,879	0.0005	Down	—
ER-EC-11	ER-EC-11 shallow ER-EC-11 deep	1,663–3,043 3,590–4,148	10/28/2009 10/28/2009	4,179.21 4,180.11	0.9	1,516	0.0006	Up	—
ER-EC-12	ER-EC-12 shallow ER-EC-12 deep	1,854–2,744 3,820–4,069	09/29/2011 09/29/2011	4,170.12 4,173.69	3.6	1,646	0.002	Up	—
ER-EC-13	ER-EC-13 shallow ER-EC-13 deep	1,013–1,541 2,240–2,680	06/16/2015 06/16/2015	4,164.49 4,164.66	0.2	1,183	0.0001	Indeterminate (up)	3
ER-EC-14	ER-EC-14 shallow ER-EC-14 deep	1,295–1,704 1,889–2,378	08/28/2014 08/28/2014	4,162.89 4,162.85	0.04	634	0.0001	Indeterminate (down)	3
ER-EC-15	ER-EC-15 shallow ER-EC-15 deep	1,191–1,768 2,752–3,254	08/28/2014 08/28/2014	4,174.3 4,178.08	3.8	1,524	0.002	Up	—
ER-OV-03a	ER-OV-03a3 ER-OV-03a2	88–160 560–655	07/07/2015 07/07/2015	3,779.53 3,680.7	99	484	0.2	Down	—
ER-OV-03c	ER-OV-03c2 ER-OV-03c	270–321 496–542	06/16/2015 06/16/2015	3,974.37 3,974.28	0.1	224	0.0004	Indeterminate (down)	3
ER-OV-06a	ER-OV-06a2 ER-OV-06a	44–65 488–536	07/07/2015 07/07/2015	3,988.74 3,992.82	4.1	458	0.009	Up	—
Gold Flat	Gold Flat 2a Gold Flat 3	250–360 234–390	05/17/2000 05/17/2000	4,996.55 4,996.42	0.1	7	0.02	Indeterminate (down)	3, 9
Hagestad 1	Hagestad 1 (1600-1904 ft) Hagestad 1 (1874-1904 ft)	1,600–1,904 1,874–1,904	12/10/1958 09/07/1958	6,046.76 <5,918.96	>128	137	>0.9	Down	1
PM-3	PM-3-2 (1442-1667 ft) PM-3-1 (1919-2144 ft)	1,455–1,687 1,872–2,192	06/02/2015 06/02/2015	4,368.22 4,366.24	2	461	0.004	Down	—
Springdale ET	Springdale ET Shallow Well Springdale ET Deep Well	2–5 3–9	06/26/2001 06/26/2001	3,711.95 3,714.52	2.6	3	1	Up	—
TW-1	TW-1 (0-560 ft) TW-1 (3700-4206 ft)	411–560 3,700–4,206	09/30/1960 11/05/1963	5,745.3 4,190.5	1,555	3,468	0.4	Down	1
U-12e.03-1	U-12e.03-1 (430 ft) U-12e.03-1 (834 ft)	1,404–1,825 2,105–2,229	07/12/1959 09/30/1959	>6,167.3 <5,440	>727	553	>1	Down	2

Table 2. Computed vertical hydraulic gradients for well pairs in the Pahute Mesa–Oasis Valley groundwater basin and vicinity, southern Nevada.—Continued

[**Well pair names**: Wells selected for paired well analysis. Shallow well listed on top. U.S. Geological Survey site identification numbers are in appendix 1. **Open interval depths**: Depths, in feet below land surface, to top of uppermost and bottom of lowermost openings in wells. **Water-level altitudes**: Altitude of measured water level, in feet above the National Geodetic Vertical Datum of 1929. **Water-level difference**: Absolute value of water-level altitude in the deep well minus water-level altitude in the shallow well, in feet. **Vertical distance**: Distance between midpoints of open interval depths, in feet. **Vertical gradient**: Calculated absolute value of vertical hydraulic gradient (water-level difference divided by vertical distance), in foot per foot, between well pair. Vertical gradient rounded to one significant digit. **Gradient direction**: Indeterminate (up), calculated gradient is upward, but true direction is indeterminate; Indeterminate (down), calculated gradient is downward but true direction is indeterminate. **Notes**: See footnote(s) pertaining to numbers. **Abbreviations**: mm/dd/yyyy, month/day/year; >, greater than; <, less than; ~, approximately; e, estimated; —, not applicable].

Well site name	Well pair names	Open interval depths	Water-level measurement dates (mm/dd/yyyy)	Water-level altitudes	Water-level difference	Vertical distance	Vertical gradient	Gradient direction	Notes
U-12e.M1 UG	U-12e.M1 UG (631 ft) U-12e.M1 UG (1501 ft)	1,389–2,011 2,865–2,881	10/27/1959 02/25/1960	>6,185.3 <4,674.1	>1,511	1,173	>1	Down	2
U-12s	U-12s (1480 ft) U-12s (1596 ft)	938–1,480 966–1,596	08/17/1966 02/09/1966	5,855.8 >5,828.2	<28	72	<0.4	Indeterminate (down)	3, 7
U-19ab	U-19ab U-19ab 2	2,023–2,250 2,015–2,400	07/17/1980 12/12/1984	4,905.4 4,914.8	9.4	71	0.1	Indeterminate (up)	3, 4, 5, 10
U-19au	U-19au 1 U-19au	2,076–2,167 2,077–2,200	03/02/1988 03/02/1988	4,455.4 4,457.2	1.8	17	0.1	Indeterminate (up)	3, 10
U-19d 2	U-19d 2 (2362-2560 ft) U-19d 2 (2500-2698 ft)	2,362–2,560 2,500–2,698	03/24/1964 03/24/1964	~4,695 4,683.3	~12	138	~0.08	Indeterminate (down)	3, 7
U-19g	U-19g (liner) U-19g (3132-3250 ft)	2,059–e3,210 3,132–3,250	10/29/1975 09/29/1965	4,674.7 <4,680.3	<5.6	e557	<0.01	Indeterminate (up)	3, 5, 7
U-20a 2 WW	U-20a 2 WW (860-2404 ft) U-20a 2 WW (4355-4500 ft)	2,067–2,404 4,355–4,500	02/22/1964 02/22/1964	4,404.7 4,436.3	32	2,192	0.01	Up	—
U-20bb	U-20bb (1900 ft) U-20bb (2220 ft)	1,739–1,900 2,014–2,220	12/18/1989 03/09/1990	>4,487.2 <4,212.6	>275	298	>0.9	Down	1
U-20bd	U-20bd (2100 ft) U-20bd (2261 ft)	1,836–2,100 2,038–2,261	03/14/1989 04/28/1989	>4,648.9 4,447.0	>202	182	>1	Down	1
U-20i	U-20i U-20i (4520-4668 ft)	3,700–4,705 4,520–4,668	08/30/1967 09/02/1967	4,466.2 4,468.5	2.3	392	0.006	Indeterminate (up)	3
U-20y	U-20y (1925 ft) U-20y (2602 ft)	1,858–1,925 2,068–2,602	10/30/1974 12/17/1974	4,398.7 4,188.7	210	444	0.5	Down	1
UE-12t 6	UE-12t 6 (1378 ft) UE-12t 6 (1461 ft)	867–1,378 830–1,461	08/31/1988 06/24/2014	<6,039.8 6,076.76	>37	23	>2	Indeterminate (up)	3, 5, 8
UE-18r	UE-18r (1648-1848 ft) UE-18r (4051-4251 ft)	1,648–1,848 4,051–4,251	02/05/1968 02/03/1968	4,165.6 4,165.1	0.5	2,403	0.0002	Indeterminate (down)	3, 5
UE-19b 1	UE-19b 1 (2190-2374 ft) UE-19b 1 WW	2,190–2,374 2,190–4,500	06/23/1964 06/19/1964	4,677 4,684.9	7.9	1,063	0.007	Indeterminate (up)	3, 4
UE-19c	UE-19c (3078-3284 ft) UE-19c (4266-4520 ft)	3,078–3,284 4,266–4,520	05/09/1964 05/10/1964	4,685.4 4,672.8	12.6	1,212	0.01	Down	—

Table 2. Computed vertical hydraulic gradients for well pairs in the Pahute Mesa–Oasis Valley groundwater basin and vicinity, southern Nevada.—Continued

[**Well pair names**: Wells selected for paired well analysis. Shallow well listed on top. U.S. Geological Survey site identification numbers are in appendix 1. **Open interval depths**: Depths, in feet below land surface, to top of uppermost and bottom of lowermost openings in wells. **Water-level altitudes**: Altitude of measured water level, in feet above the National Geodetic Vertical Datum of 1929. **Water-level difference**: Absolute value of water-level altitude in the deep well minus water-level altitude in the shallow well, in feet. **Vertical distance**: Distance between midpoints of open interval depths, in feet. **Vertical gradient**: Calculated absolute value of vertical hydraulic gradient (water-level difference divided by vertical distance), in foot per foot, between well pair. Vertical gradient rounded to one significant digit. **Gradient direction**: Indeterminate (up), calculated gradient is upward, but true direction is indeterminate; Indeterminate (down), calculated gradient is downward but true direction is indeterminate. **Notes**: See footnote(s) pertaining to numbers. **Abbreviations**: mm/dd/yyyy, month/day/year; >, greater than; <, less than; ~, approximately; e, estimated; —, not applicable].

Well site name	Well pair names	Open interval depths	Water-level measurement dates (mm/dd/yyyy)	Water-level altitudes	Water-level difference	Vertical distance	Vertical gradient	Gradient direction	Notes
UE-19e	UE-19e (2619-2779 ft) UE-19e (4802-5000 ft)	2,619–2,779 4,802–5,000	09/02/1964 09/03/1964	4,686.6 4,665.6	21	2,202	0.01	Down	—
UE-19fS	UE-19fS (2750-2908 ft) UE-19fS (4464-4779 ft)	2,750–2,908 4,464–4,779	08/21/1965 08/23/1965	4,433.7 4,426.3	7.4	1,793	0.004	Down	—
UE-19gS	UE-19gS (2802-2970 ft) UE-19gS (6920-7118 ft)	2,802–2,970 6,920–7,118	03/31/1965 05/08/1965	4,676.5 4,673.6	2.9	4,133	0.0007	Indeterminate (down)	3, 5
UE-19h	UE-19h (2321-2396 ft) UE-19h (2408-2604 ft)	2,321–2,396 2,408–2,604	08/08/1965 08/09/1965	4,671.3 4,668.4	2.9	148	0.02	Indeterminate (down)	3
UE-19i	UE-19i (2910-3068 ft) UE-19i (3460-3618 ft)	2,910–3,068 3,460–3,618	08/04/1965 08/04/1965	>4,614.8 4,589.4	>25	550	>0.05	Down	—
UE-19z	UE-19z (2225 ft) UE-19z (2800 ft)	2,102–2,225 2,197–2,800	07/06/1977 07/12/1977	>4,785.7 4,690.7	>95	335	>0.3	Down	1
UE-20d	UE-20d (2578-2776 ft) UE-20d (4118-4316 ft)	2,578–2,776 4,118–4,316	08/18/1964 08/19/1964	4,174.7 <4,250.5	<76	1,540	<0.05	Up	—
UE-20e 1	UE-20e 1 (1500-2766 ft) UE-20e 1 (4540-6395 ft)	1,832–2,766 4,540–6,395	06/09/1964 06/13/1964	4,465.3 4,474.9	9.6	3,169	0.003	Up	—
UE-20f	UE-20f (4350-4543 ft) UE-20f (4456-13686 ft)	4,350–4,543 4,456–13,686	04/10/1964 01/13/1965	4,259 4,339.7	81	4,625	0.02	Indeterminate (up)	3, 6, 8
UE-20h	UE-20h (2741-2909 ft) UE-20h (3522-7207 ft)	2,741–2,909 3,522–7,207	08/24/1964 08/24/1964	4,441.4 4,446.5	5.1	2,540	0.002	Indeterminate (up)	3, 4, 6, 7
UE-20j	UE-20j (2051-2249 ft) UE-20j (3634-3832 ft)	2,051–2,249 3,634–3,832	10/25/1964 10/26/1964	4,663.2 4,637.3	26	1,583	0.02	Down	—
UE-29a	UE-29a 1 HTH UE-29a 2 HTH	90–215 285–1,383	05/04/2015 05/04/2015	3,894.12 3,890.3	3.8	682	0.006	Down	—
WW-8	WW-8 (30-1198 ft) WW-8 (3428-3524 ft)	1,070–1,198 3,428–3,524	09/21/1962 11/16/1962	4,625 4,618.4	6.6	2,342	0.003	Down	—

[1]Semi-perched shallow aquifer.
[2]Shallow water level is or likely is perched.
[3]Water-level difference is within measurement error.
[4]Low-accuracy method(s) used to measure water levels.
[5]Water-level measurements from different dates.
[6]Water-level measurements have different water temperatures.
[7]Water-level measurement in at least one well represents a nonstatic level.
[8]Static water levels are uncertain because of low-permeability rocks at open intervals.
[9]Vertical gradient is not meaningful because open intervals substantially overlap.
[10]Wells are not located within the same borehole.
[11]Wells may be artificially hydraulically connected.

In these less-than-ideal cases, the potential magnitude of temporal water-level variations between the two measurements was considered when determining if the water-level difference was meaningful.

Long open intervals in wells or overlapping intervals between well pairs can create uncertainty in the magnitude of the vertical hydraulic gradient. For example, 12 of the well pairs had at least one well with an open interval longer than 1,000 ft. The hydraulic-gradient calculation assumes the hydraulic head influencing the water level in the well can be attributed to the open-interval mid-point. Where the zone contributing water to a long open interval is short (for example, along a producing fracture), the mid-point of the open interval may be a poor approximation of the location of the contributing zone. This can lead to errors in the vertical distance between the two hydraulic heads being compared and uncertainties in the magnitude of the hydraulic gradient. Partial overlap between open intervals of a well pair is problematic because vertical separation in the units contributing water to the well is necessary to compute the vertical gradient. The overlapping part of the interval is assumed not to be integral to the overall gradient. Sixteen well pairs had overlapping intervals. Eleven of the pairs had an indeterminate gradient direction, partly based on the uncertainty due to the overlap. Most of the remaining seven well pairs had strong upward or downward gradients (table 2).

Determination of Hydrostratigraphic Units at Well Openings

Top and bottom altitudes of HSUs at each well location were determined from lithologic well logs and from HSU surfaces in the PMOV HFM (U.S. Department of Energy, 2020a). HSUs from land surface to the bottom of each borehole were obtained from the PMOV HFM borehole database (U.S. Department of Energy, 2020a, appendix A) or interpreted from lithologic logs (Wood, 2007). HSUs below the bottom of each borehole were derived from the PMOV HFM and are model interpretations. In areas where data exist, altitudes of HSU surfaces in the PMOV HFM are based on, and in good agreement with, the original lithologic logs (Wood, 2007).

HSUs for the 387 wells with steady-state water levels (appendix 2) and for all boreholes used for underground nuclear testing can be displayed interactively from a Microsoft® Excel workbook (appendix 3). The workbook is designed to view (1) the hydrostratigraphic column, which is interpreted from lithologic wells logs and the PMOV HFM; (2) the mean water level used as the steady-state head, or an estimate of the steady-state head; (3) basic well-construction information for wells in the study area; and (4) the working point (vertical location) of the nuclear detonation, where applicable. The hydrostratigraphic columns provided in appendix 3 extend to almost 10,000 ft below NGVD29. Information for an individual well can be viewed in appendix 3 by selecting the well or borehole from the column-header dropdown list. Two examples from the workbook page, one showing an emplacement borehole for a nuclear detonation and the other showing a monitoring well, are presented on figure 4.

Compilation of Transmissivity Estimates

Transmissivity estimates from 347 wells in 71 boreholes within the PMOV basin were compiled from a hydraulic-properties database (fig. 5; Frus and Halford, 2018). Published transmissivity estimates have assigned qualifiers of “equal to,” “greater than,” or “less than” based on measurement limitations and confounding factors that affected aquifer-test data. Transmissivities were estimated from single-well aquifer tests or specific capacity. Single-well aquifer tests are controlled field experiments that measure water-level changes in a well before, during, and after a known volume of water is either injected or removed from the formation(s) open to the well (Stallman, 1971). Single-well aquifer tests that were analyzed by Frus and Halford (2018) include constant-rate pumping tests (21 wells), variable-rate pumping tests (1 well), pump-and-recovery tests (20 wells), and slug tests (300 wells). Specific capacity is the pumping rate divided by drawdown at an unspecified time and was used to estimate transmissivity in 5 wells.

Most of the slug tests were completed in 236 temporary, packer-isolated intervals in 17 boreholes on Pahute Mesa (fig. 5). These packer-isolated intervals are referred to as wells in this report. Straddle packers were used to isolate and slug test as many as 28 depth intervals (wells) in each of the 17 boreholes (Blankennagel, 1967). Depth intervals typically were 200 ft and the suite of packer-isolated intervals spanned from the water table to the bottom of each borehole. These boreholes have total depths ranging from 3,705 to 13,686 ft below land surface, and depths to water that range from about 1,070 to 2,350 ft and average 2,000 ft below land surface (Frus and Halford, 2018). A pumping aquifer test also was done in each borehole. Summed transmissivity from slug-test results of all temporary wells in each borehole theoretically should equal the transmissivity estimated from the pumping aquifer test of the open borehole. Differences in transmissivity between the sum of slug-test results and the pumping aquifer test occur because slug tests cannot adequately quantify the transmissivity of high-permeability intervals (Frus and Halford, 2018). An integrated borehole analysis was done by Frus and Halford (2018) to reconcile differences in transmissivity by subtracting the sum of slug-test transmissivities from the aquifer-test transmissivity and assigning the excess transmissivity to all high-permeability slug-test intervals. Transmissivities derived solely from each slug test were not used in the hydraulic-property analyses of this study. Instead, revised transmissivity estimates from the integrated borehole analysis of the 236 wells, as reported in Frus and Halford (2018), were used.

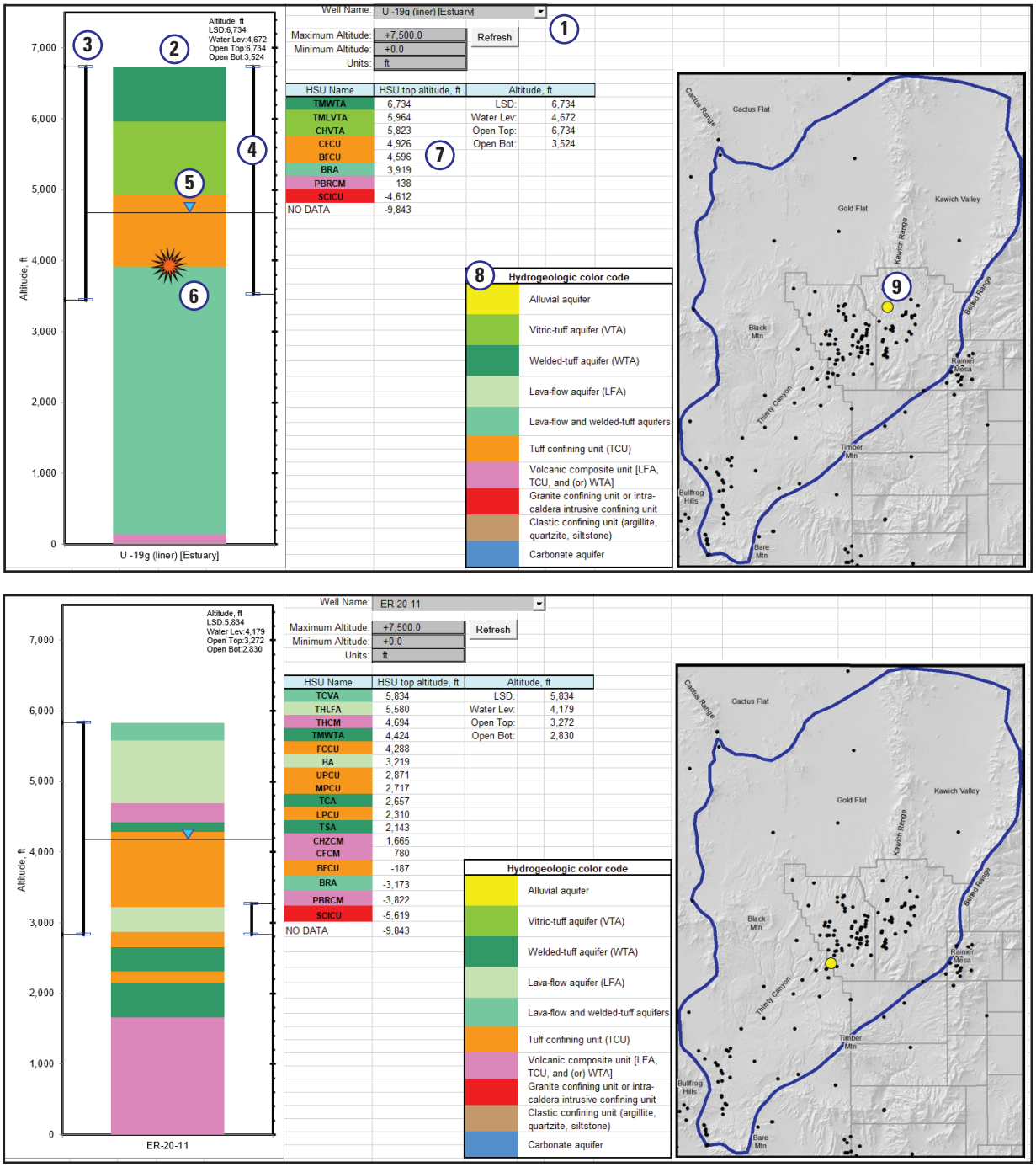

Shown are 2 of the 409 sites (including all underground nuclear detonations) in a workbook for the Pahute Mesa–Oasis Valley groundwater basin. The workbook shows the hydrostratigraphic units (HSUs) penetrated by each borehole and the relation of HSUs to water level and open intervals. Top plot highlights the type of information in the spreadsheet: (1) pull-down menu to select well or borehole of interest; (2) hydrostratigraphic column for selected well; (3) vertical extent of drilled borehole; (4) uppermost and lowermost extent of open interval which, if saturated, could contribute water to well; (5) measured or estimated water level; (6) nuclear detonation working-point depth; (7) tabular information specific to selected well or borehole; (8) explanation for color scheme of hydrostratigraphic column; and (9) map of the Pahute Mesa–Oasis Valley study area showing selected well location as a yellow symbol.

Figure 4. Images from appendix 3 Microsoft® Excel workbook showing well U-19g (liner), which was used for emplacement of the ESTUARY nuclear detonation, and well ER-20-11, which was completed for hydrogeologic investigations.

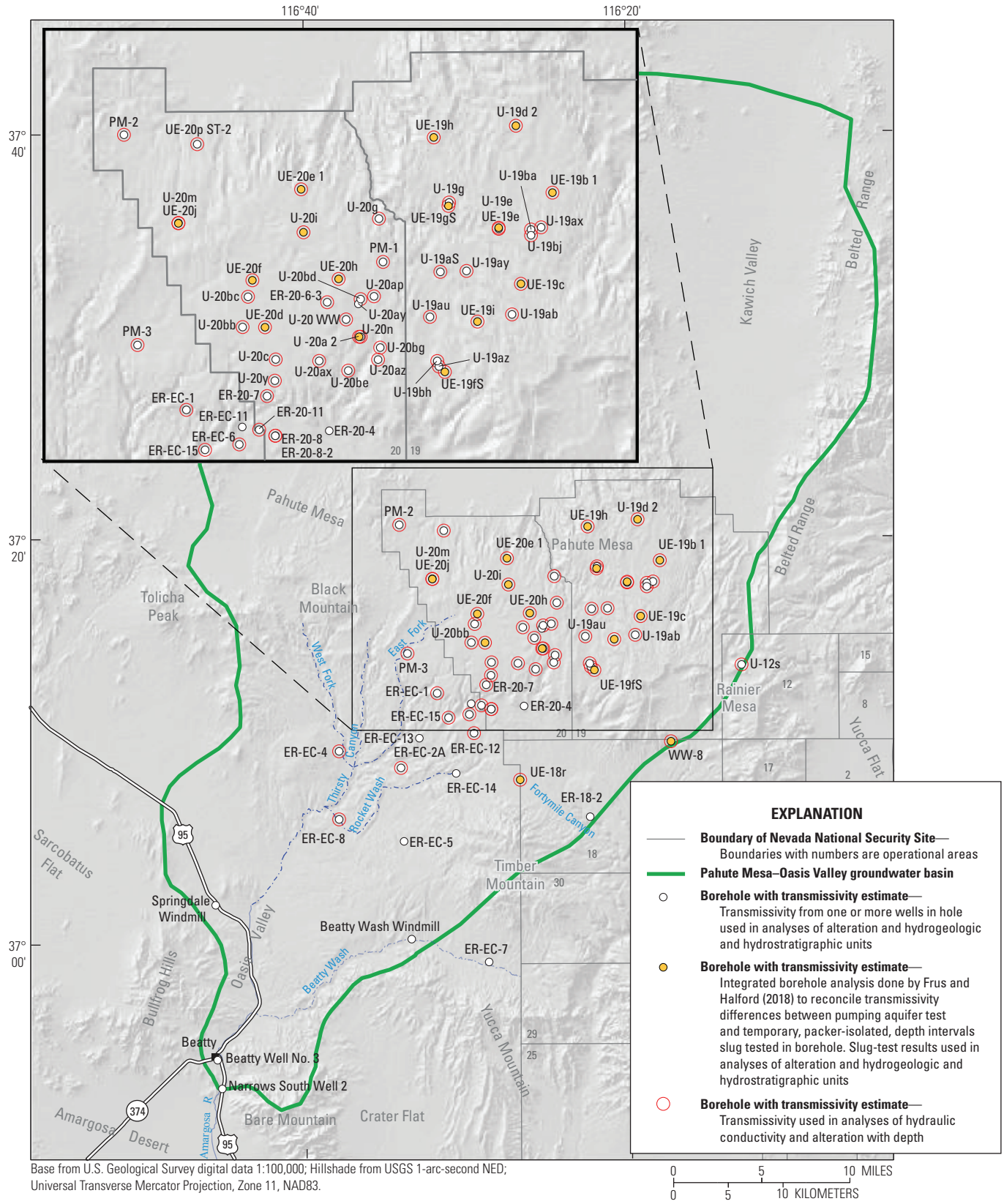

Figure 5. Boreholes with transmissivity estimates from aquifer tests and specific capacity, Pahute Mesa–Oasis Valley groundwater basin and vicinity, southern Nevada.

The remaining 64 of the 300 wells that were slug tested included 23 wells where the entire borehole was slug tested and 41 temporary packer-isolated intervals in 12 boreholes. The 41 tests of discrete depth intervals were not reconciled with integrated borehole analyses and, therefore, slug-test estimates may be biased low (Frus and Halford, 2018).

Depth Analyses

The depth analyses were used to evaluate vertical variations in hydraulic conductivity and volcanic-rock alteration below the water table. In these analyses, the water table is equivalent to the potentiometric surface because the water table is within 30 ft of the steady-state hydraulic-head estimates used to define the potentiometric surface (appendix 2). The analyses of hydraulic conductivity and alteration with depth required compilation of transmissivity estimates from aquifer tests (Frus and Halford, 2018); steady-state hydraulic-head estimates (appendix 2); well-construction information (appendix 3; U.S. Geological Survey, 2020); water-production or flow-log information (appendix 4); and alteration codes from the PMOV HFM borehole database (appendix 5; U.S. Department of Energy, 2020a, appendix A).

Hydraulic Conductivity with Depth

The relation of hydraulic conductivity with depth was analyzed using the hydraulic-properties database from Frus and Halford (2018; fig. 5). The database reports a transmissivity for each well because transmissivity is the most prevalent and reliable aquifer-test result. Hydraulic conductivity equals transmissivity divided by the thickness of rock contributing water to the well, which can be the aquifer thickness or open-interval length of the well.

Analysis of hydraulic conductivity with depth requires the translation of transmissivity to hydraulic conductivity using an appropriate saturated thickness. Saturated thickness is related to the volume of rock investigated from an aquifer test, where the volume of rock investigated is proportional to the volume of water withdrawn from the well. Saturated thickness is assumed equal to the open interval of the well in areas where transmissivity is less than 1,000 ft^2/d or small volumes of water are pumped (less than 100,000 gal), whereas the aquifer thickness is used for saturated rocks where transmissivity exceeds 1,000 ft^2/d or more than 100,000 gal of water are pumped (Halford and others, 2006).

Analysis of hydraulic conductivity with depth is provided in appendix 4. For slug tests, saturated thickness was the difference between the top and bottom of the saturated open interval. For constant-rate, variable-rate, and pump-and-recovery tests, saturated thickness typically equaled the aquifer thickness. When the aquifer thickness is the appropriate saturated thickness, additional data are required to determine intervals contributing flow to the well. Additional data include the following:

1. well-completion diagram to determine position of open interval(s) and confining units;
2. water-production log or flow log to determine interval(s) contributing flow to the well; or
3. multiple-well aquifer test analysis to determine permeable interval(s) that contribute flow to the well.

Volcanic-Rock Alteration with Depth

Volcanic-rock alteration with depth was analyzed using alteration codes assigned to borehole intervals in the PMOV HFM borehole database (U.S. Department of Energy, 2020a, appendix A). Twenty-two alteration codes have been defined to describe volcanic-rock alteration in boreholes within the PMOV HFM (U.S. Department of Energy, 2020a). For each borehole in the PMOV HFM borehole database, geologic units are subdivided into HSUs with unique combinations of secondary mineral alteration codes. A unique combination can consist of as many as four different alteration codes. For example, volcanic rock with the assigned alteration codes of "DV, AR, PY" means that the rock is devitrified (DV), argillic (AR), and pyritic (PY), where the codes are listed from left-to-right in order of dominance.

Fifty-seven boreholes were used in the volcanic-rock alteration with depth analysis. A total of 114 unique combinations of alteration codes were assigned by U.S. Department of Energy (2020a) to volcanic-rock intervals within the 57 boreholes. These boreholes are the same boreholes used in the analysis of hydraulic conductivity with depth (fig. 5). This ensured that the results of hydraulic conductivity with depth can be compared directly to alteration-group abundance with depth.

The analysis of alteration-group abundance with depth categorized the 114 unique alteration combinations into five alteration groups: (1) argillic, (2) mineralized, (3) zeolitic, (4) devitrified, and (5) vitric. The categorization of alteration combinations into alteration groups was done using the "top-down" classification scheme described below.

The argillic-alteration group consists of any alteration combination that includes the argillic or kaolinitic alteration codes (appendix 5). The argillic-alteration group does not consider if the argillic and kaolinitic codes are the dominant type of alteration because the presence of argillic or kaolinitic alteration is considered to have a substantial effect on groundwater flow by plugging fractures and reducing rock permeability (U.S. Department of Energy, 2020a).

The mineralized-alteration group consists of any alteration combination that includes the following fracture-coating mineral codes: albitic; calcite; chloritic; potassic; pyritic; opalline; or silicic–chalcedony. The mineralized-alteration group does not consider if the alteration codes listed above are the dominant type of alteration because the presence of fracture-coating minerals causes fractures to close, which reduces rock permeability (Drellack and others, 1997). None of the alteration combinations in the mineralized-alteration group include the argillic or kaolinitic codes, but 12 alteration combinations in the argillic-alteration group include fracture-coating mineral (mineralized) codes (appendix 5).

The zeolitic-alteration group consists of any alteration combination that contains either the zeolitic, zeolitic–clinoptilolite, or zeolitic–analcime alteration codes, but does not contain the codes listed above from the argillic- or mineralized-alteration groups. For example, argillic- and mineralized-alteration groups have 9 and 16 alteration combinations with a zeolitic code, respectively, but none of the 24 alteration combinations in the zeolitic-alteration group have argillic or mineralized alteration codes (appendix 5).

The devitrified-alteration group consists of any alteration combination that lists first one of the following codes: devitrified; devitrified–vapor phase; pilotaxitic–holocrystalline; quartzo-feldspathic; seriate–holocrystalline; or silicic. Alteration combinations in the devitrified-alteration group do not include codes from the argillic-, mineralized-, or zeolitic-alteration groups (appendix 5). The silicic code is included in the devitrified-alteration group because a silicic designation commonly is used to characterize rock texture, such as granophyric quartz (Stoller-Navarro Joint Venture, 2007b, table D.2-1).

In the vitric-alteration group, glass is listed first in the sequence of alteration combinations, indicating that the volcanic rock is dominated by volcanic glass. Secondary codes listed after glass in the alteration-code sequence include devitrified, quartzo-feldspathic, and silicic (appendix 5).

Analysis of alteration-group abundance with depth required the compilation of alteration codes and their respective top and bottom depths below land surface within the boreholes used in this analysis. Top and bottom contacts for alteration codes in each alteration group were converted from depth below land surface to depth below the water table. The hydraulic-head estimates in appendix 2 were used to approximate the water table. For each alteration group, volcanic-rock thicknesses were binned into 400-foot intervals below the water table. For example, if a borehole is open to devitrified rock from 0 to 483 ft below the water table, then 400 ft is assigned to the 0–400-ft binned interval and 83 ft is assigned to the 401–800-ft interval. If another borehole is open to devitrified rock from 250 to 750 ft below the water table, then 150 ft is assigned to the 0–400-ft binned interval and 350 ft is assigned to the 401–800-ft interval. Within each 400-foot depth interval, thicknesses of each alteration group were summed for all 57 boreholes. In the example above for the two boreholes open to devitrified rock, the cumulative thickness of the 0–400 ft binned interval is 550 ft and the cumulative thickness of the 401–800 ft binned interval is 433 ft. Cumulative thicknesses for each alteration group were plotted in 400-foot depth intervals beginning at the water table. Analysis of alteration-group abundance with depth is provided in appendix 5.

Transmissivity Analyses

Transmissivity analyses were used to evaluate lateral variations in transmissivity by HSU, HGU, and alteration group. Transmissivity analyses in this study retain the transmissivity estimates from aquifer tests to avoid introducing uncertainties related to unknown aquifer thickness at a field site. Transmissivity distributions were developed by distributing transmissivity estimates from wells to HSUs, HGUs, and alteration groups. Quantitative (statistical) and qualitative analyses were done to determine (1) the expected range in transmissivities for HGUs, HSUs, and alteration groups; (2) if transmissivity distributions support previously published designations of HGUs and HSUs as aquifers or confining units; and (3) if transmissivity distributions between HGUs, HSU, or alteration groupings greatly overlap, indicating the transmissivity distributions are hydraulically non-unique.

Distributing Transmissivity to Hydrostratigraphic and Hydrogeologic Units

Relations between transmissivity and HGUs and HSUs were analyzed using the hydraulic-properties database from Frus and Halford (2018). The analyses required the correlation of transmissivity estimates from wells to HGUs and HSUs open to the wells. Boreholes with wells used in the analysis are shown in figure 5. Analyses used to assign transmissivity estimates to HGUs and HSUs are provided in appendix 6.

Transmissivity in each well was distributed to HGUs and HSUs based on lithologic and hydraulic information. Previous designations of HGUs and HSUs as aquifers or confining units were not considered when apportioning the transmissivity because (1) the previous designations are based on geology and the physical characteristics of the rocks, and (2) the purpose of the analysis is to validate these conceptual designations using hydraulic data. The total transmissivity for a well was assigned to one HGU or HSU if one of five criteria were true:

1. open interval had only one HGU or HSU;
2. water-production log or flow log indicated one HGU or HSU contributed nearly all the flow within the open interval;

3. notes based on extensive geophysical logging (temperature, salinometer, and radioactive tracer logs) and slug testing (Blankennagel, 1967; Blankennagel and Weir, 1973) indicated that one HGU or HSU contained the high-permeability interval(s);

4. multiple-well aquifer test analysis indicated one HGU or HSU was orders of magnitude more permeable based on hydraulic-property estimates and, therefore, contributed most of the flow within the open interval; or

5. if a well was open to only alluvial deposits and the lithologic log suggested one HGU or HSU was more permeable, such as gravel versus clay, then transmissivity was assigned to the permeable HGU or HSU.

The total transmissivity for a well was distributed to two or more HGUs or HSUs if information was available from a water-production log or flow log to apportion the percent of total transmissivity by the percent of flow contributed from different HGUs or HSUs. For example, a water-production log for well *ER-EC-8* (Bechtel Nevada, 2004b) indicates that the Fortymile Canyon composite unit (FCCM) contributes about two-thirds of the flow within the open interval, whereas the Buttonhook Wash welded-tuff aquifer (BWWTA) contributes the other one-third of the flow. Using these contributing flow fractions, the FCCM and BWWTA were apportioned 6,900 and 3,500 ft^2/d, respectively, of the total transmissivity (10,400 ft^2/d; appendix 6).

The total transmissivity for a well was assigned equally to two or more HGUs or HSUs if the open interval intersects two or more HGUs or HSUs and the published transmissivity qualifier from the Frus and Halford (2018) database is "less than." This criterion only applied to wells with low transmissivity (less than 10 ft^2/d). For example, well *UE-19i (2896-2910 ft)* has an estimated transmissivity of less than 0.2 ft^2/d and is open to two HSUs: Crater Flat confining unit (CFCU) and Bullfrog confining unit (BFCU; appendix 6). CFCU and BFCU have a low combined transmissivity (less than 0.2 ft^2/d) and no data were available to determine the "most transmissive" HSU. CFCU and BFCU each were assigned the total transmissivity (0.2 ft^2/d) and the published transmissivity qualifier of "less than" was retained.

Transmissivity was apportioned by saturated thickness if the published transmissivity qualifier from the Frus and Halford (2018) database is "equal to," and one of the criteria listed above cannot be used to assign transmissivity to one or more HGUs or HSUs. This criterion only applied to slug tests. For example, well *UE-20j (1858-2056 ft)* has an estimated transmissivity of 14 ft^2/d (Frus and Halford, 2018). The well is open to the BRA and BFCU, which comprise 88 and 12 percent of the open interval, respectively. No information was available to determine the most transmissive HSU; therefore, transmissivity was apportioned by saturated thickness, which resulted in estimated transmissivities of about 12 and 2 ft^2/d for BRA and BFCU, respectively (appendix 6).

For the 278 wells in 29 boreholes that were isolated with straddle packers and slug tested, transmissivity estimates from individual slug tests are summed for each consecutive HGU and HSU in the borehole. For example, 14 wells were slug tested in borehole *UE-19e WW* and each well was open only to one HSU. The upper four wells were open to BFCU, whereas the lower ten wells were open to BRA. Transmissivity estimates from wells open to the BFCU and wells open to the BRA were summed separately, resulting in a single transmissivity estimate for the BFCU and a single estimate for the BRA. Qualifiers were assigned to summed transmissivity estimates of HGUs and HSUs based on published qualifiers from the Frus and Halford (2018) database. A "less than" qualifier was assigned to a summed transmissivity estimate if all or most of the high-transmissivity intervals that were summed in a borehole had qualifiers of "less than." Similar logic was used to assign "equal to" or "greater than" qualifiers to summed transmissivity estimates. Summing transmissivity estimates for each HSU and HGU in a borehole prevented depth dependence from affecting the analysis results.

Distributing Transmissivity to Volcanic-Rock Alteration Groups

Relations between transmissivity and volcanic-rock alteration groups were analyzed using the hydraulic-properties database from Frus and Halford (2018) and alteration codes published in the PMOV HFM borehole database (U.S. Department of Energy, 2020a, appendix A). This analysis was done to determine the expected range in transmissivity for the five previously defined alteration groups: argillic; mineralized; zeolitic; devitrified; and vitric.

The analyses required the correlation of transmissivity estimates from wells to the alteration group(s) within the open intervals of the wells. Boreholes used in the analysis are shown in figure 5. Analyses used to assign transmissivity estimates to volcanic-rock alteration groups are provided in appendix 7. The criteria for distributing transmissivity and assigning qualifiers are the same criteria described in the section "Distributing Transmissivity to Hydrostratigraphic and Hydrogeologic Units."

Statistical and Qualitative Analyses of Transmissivity by Hydrostratigraphic Units, Hydrogeologic Units, and Alteration

Quantitative (statistical) methods were used to analyze transmissivity distributions of HGU, HSU, and alteration groupings that have a minimum number of transmissivity estimates. A minimum sample size was computed to determine the minimum number of transmissivity estimates that were required in a transmissivity distribution to compute statistically significant outcomes. Confounding factors affecting transmissivity analyses were described.

Statistical quantities and analyses were used for analyzing transmissivity distributions that exceeded the minimum number of transmissivity estimates. Qualitative analyses were used for HGU, HSU, and alteration groupings that have limited datasets.

Minimum Sample Size for Statistical Analyses

The purpose of mapping the three-dimensional extents of individual HGUs or HSUs for groundwater-flow or transport models is to extrapolate a unique set of hydraulic or transport properties across each unit's extent (Mirus and others, 2016). Unique hydraulic variability within an HGU (or HSU) is defined as a unit having a transmissivity distribution that is statistically different from the transmissivity distributions of other units. Determining hydraulic variability within alteration groups also is important because each HGU and HSU is composed of multiple alteration groups. Hydraulic variability in the transmissivity distributions of alteration groups can help explain hydraulic variability within HGUs and HSUs.

Statistical analyses can be done to determine whether HGUs, HSUs, or alteration groups have unique hydraulic variability. For example, a two-sample, Student t test statistic (Helsel and Hirsch, 2002, p. 126) can be used to evaluate the mean values of normally distributed (log-transformed) transmissivity distributions. The null hypothesis evaluates whether the estimated means of two transmissivity distributions are equal, or within a specified margin of error that indicates the HGUs, HSUs, or alteration groups are non-unique (non-differentiable) based on hydraulic properties. However, statistically analyzing transmissivity by HGU, HSU, or alteration group requires a sufficient sample size (number of transmissivity estimates). If the sample size is too small, then statistical results will have poor precision and (or) large bias (Helsel and Hirsch, 2002). Computing the minimum sample size (n_{min}) for statistical analyses of transmissivity requires knowledge of three variables given in equation 1 (Helsel and Hirsch, 2002):

$$n_{min} = \left[\frac{t^* \sigma}{E}\right]^2 \quad (1)$$

where

t^* is the critical value;
σ is the standard deviation of the transmissivity distribution; and
E is the desired margin of error.

The critical value (t^*) is determined from the standard normal distribution. A value of t^* equal to 1.96 corresponds to the 95 percent confidence interval.

The variable E is the desired margin of error, which is defined as the maximum difference between the means of two transmissivity distributions and is used to reject the null hypothesis. Note that estimated transmissivities have a variability (error range) that spans a factor of 10 when comparing different analyses of the same aquifer-test data for a well (Halford and others, 2006; Halford, 2016). Therefore, the means of two log-transformed transmissivity distributions are considered the same if their means are within a factor of 10. The margin of error: $E = Log_{10}\ 10 = 1$.

A typical standard deviation of the transmissivity distribution (σ) was estimated by computing the standard deviations of transmissivity distributions for HGUs, HSUs, and alteration groups with five or more transmissivity estimates (appendix 6 and appendix 7). Standard deviations from log-transformed transmissivity distributions ranged from 3.0 to 3.9 for three HGUs, from 0.2 to 4.3 for nine HSUs, and from 1.2 to 4.0 for five alteration groups. These computed standard deviations correspond to transmissivity distributions that span three-to-seven orders of magnitude. Using the average standard deviation of 2.5, the minimum sample size for statistical analyses of transmissivity is 24.

Confounding Factors

Statistical analyses and computations of transmissivity probability distributions were not done for two of five alteration groups, one-half of HGUs, or any HSUs because of limited data and censored estimates. A minimum of 24 transmissivity estimates are required to compute unbiased statistical results. However, only three of five alteration groups (fig. 6) and three of six HGUs (fig. 7) have at least 24 transmissivity estimates, including censored and uncensored data. Censored transmissivity estimates have qualifiers of "greater than" or "less than." Devitrified, mineralized, and zeolitic alteration groups have from 25 to 79 transmissivity estimates, and 27 to 45 percent of these transmissivity estimates are censored (fig. 6). Likewise, between 45 and 70 transmissivity estimates are available in wells open to TCU, WTA, and LFA HGUs, and about 30 to 50 percent of transmissivity estimates are censored (fig. 7). All HSUs have less than 24 transmissivity estimates, where about half of these HSUs have censored estimates (fig. 8). Interpreting transmissivity estimates with censored qualifiers as actual values biases statistical results (Helsel and Cohn, 1988). Likewise, removing censored data from a statistical analysis also biases results.

Computation of Statistical Quantities

Statistical quantities include moment statistics (mean and standard deviation) and percentiles (median and interquartile range). For the three alteration groups and three HGUs with a minimum of 24 transmissivity estimates, statistical quantities were computed using maximum likelihood estimation (MLE; Cohen, 1976) and robust regression on order statistics (ROS; Helsel and Cohn, 1988) approaches. These approaches are recommended to compute statistical quantities from datasets that have censored values at multiple reporting limits (Helsel and Cohn, 1988; Helsel and Hirsch, 2002, p. 364). Percentiles were estimated with the MLE approach, whereas mean and standard deviation were estimated with the ROS approach.

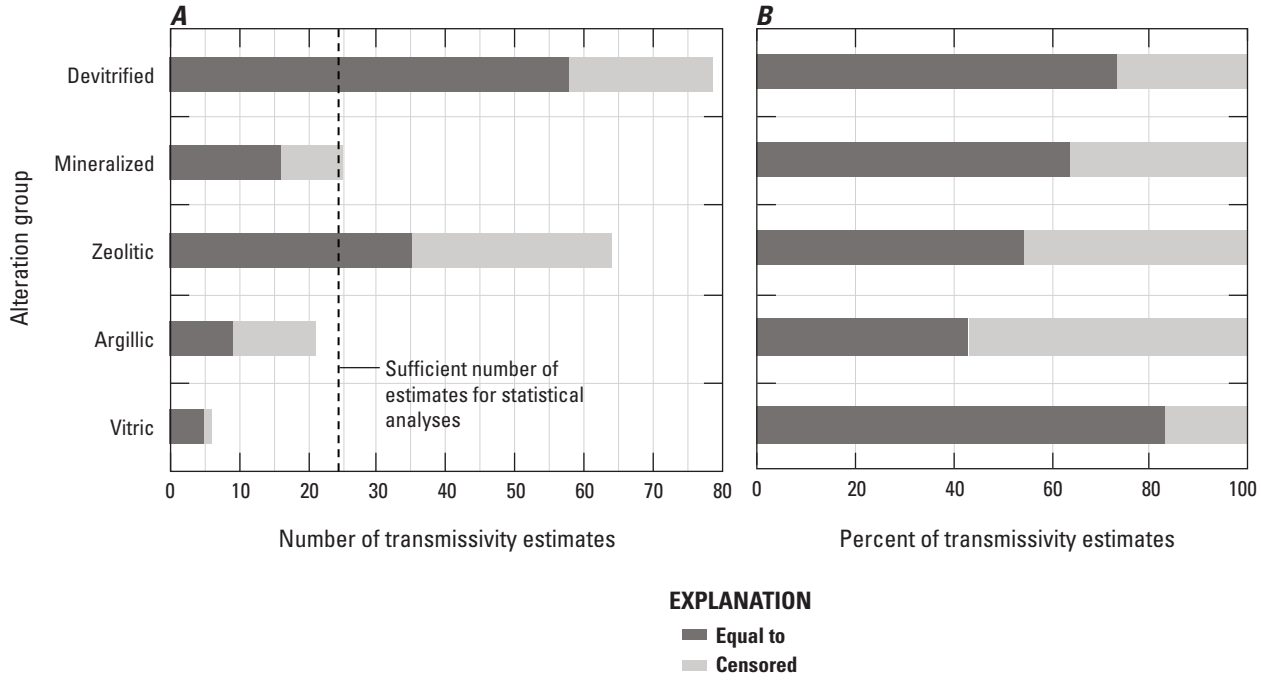

Figure 6. Number and percent of transmissivity estimates that are censored and uncensored, by alteration group. Censored transmissivity estimates have qualifiers of "less than" or "greater than," whereas uncensored estimates have a qualifier of "equal to." Transmissivities estimated from aquifer tests in wells within the Pahute Mesa–Oasis Valley groundwater basin, southern Nevada.

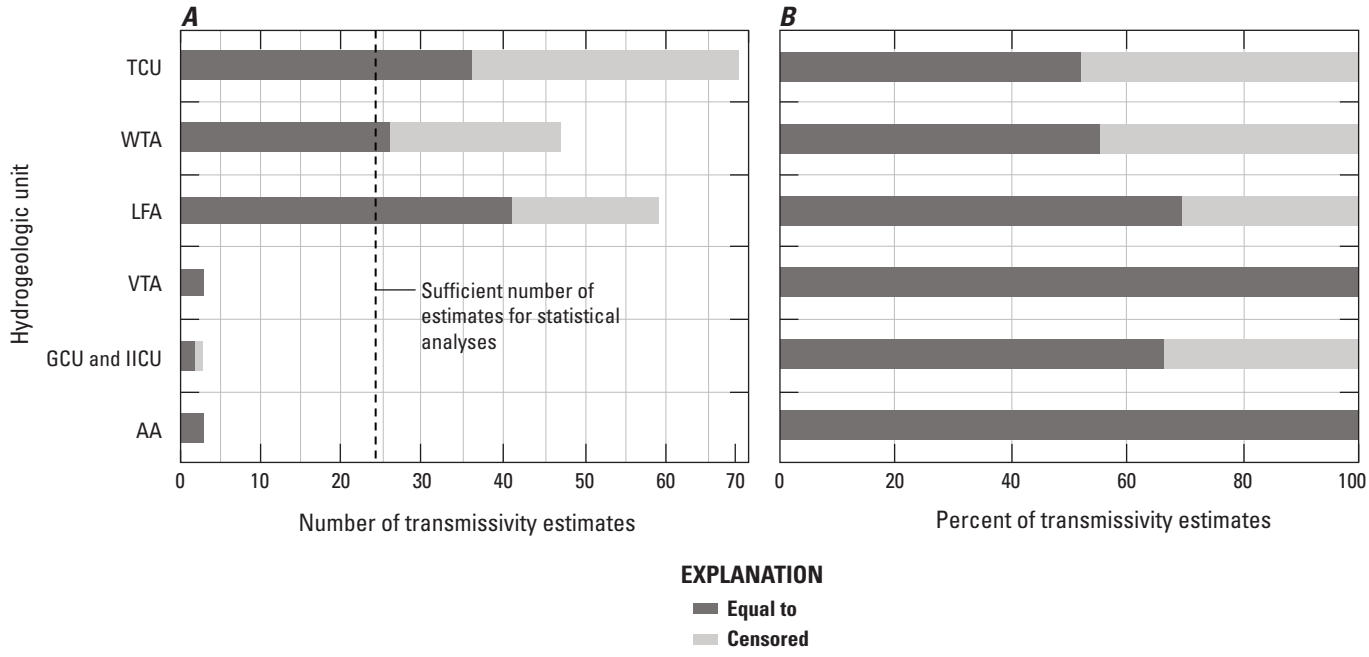

Figure 7. Number and percent of transmissivity estimates that are censored and uncensored, by hydrogeologic unit (HGU). Censored transmissivity estimates have qualifiers of "less than" or "greater than," whereas uncensored estimates have a qualifier of "equal to." Transmissivities estimated from aquifer tests in wells within the Pahute Mesa–Oasis Valley groundwater basin, southern Nevada. Labeled HGUs are defined in table 1.

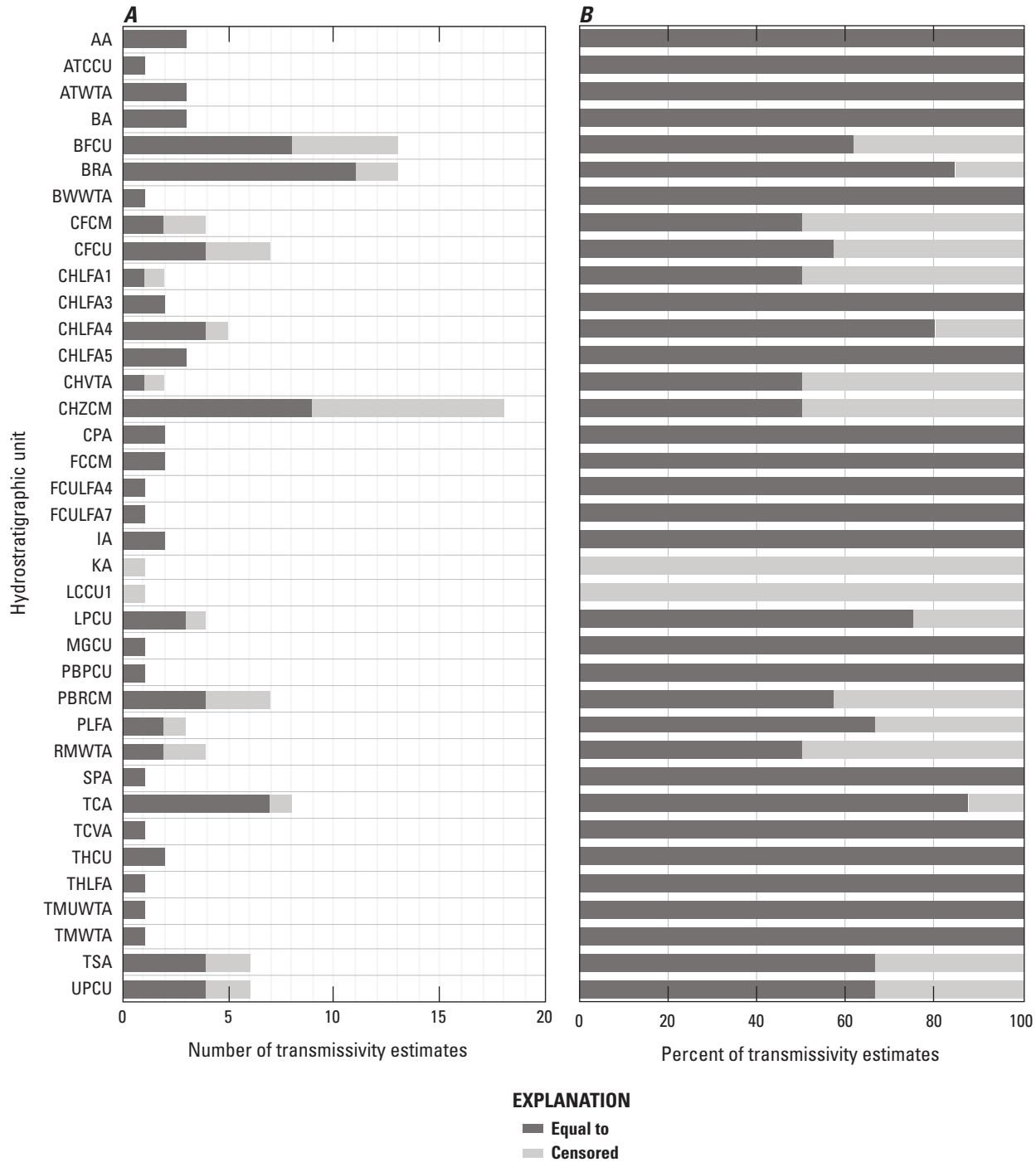

Figure 8. Number and percent of transmissivity estimates that are censored and uncensored, by hydrostratigraphic unit (HSU). Censored transmissivity estimates have qualifiers of "less than" or "greater than," whereas uncensored estimates have a qualifier of "equal to." Transmissivities estimated from aquifer tests in wells within the Pahute Mesa–Oasis Valley groundwater basin, southern Nevada. Labeled HSUs defined in table 1.

The MLE and ROS approaches have been shown to provide unbiased, precise estimates of statistical quantities for (large) datasets with at least 25 samples (Helsel and Gilliom, 1986).

For the alteration groups, HGUs, and HSUs with less than 24 transmissivity estimates, the geometric mean was computed using three different approaches to account for uncertainties from limited data and censored estimates. The minimum geometric mean was computed assuming values of 0 and the detection limit for transmissivities censored as "less than" and "greater than," respectively. The maximum geometric mean was computed assuming values of the detection limit and 100,000 ft^2/d for transmissivities censored as "less than" and "greater than," respectively. An "ROS geometric mean" also was computed using the ROS approach.

Analyses for Limited Datasets

Histograms were used to determine whether individual HGUs and HSUs can be classified as aquifers or confining units. Transmissivities of HGUs and HSUs were binned into three broad categories that represent low (0–10 ft^2/d), moderate (10–1,000 ft^2/d), and high (1,000–100,000 ft^2/d) transmissivity. Broad categories were used to avoid over-interpretation of censored transmissivity estimates. An upper threshold of 10 ft^2/d for low-transmissivity rock and a lower threshold of 1,000 ft^2/d for high-transmissivity rock are consistent with definitions of low and high transmissivity from previous studies (Halford and others, 2006; Halford, 2016; Halford and Jackson, 2020). HGUs and HSUs dominated by high-transmissivity estimates typically function as aquifers, whereas units dominated by low-transmissivity estimates typically function as confining units. HGUs and HSUs with transmissivity estimates that span from low to high are composite units, meaning that the units can function spatially as aquifers or confining units.

Transmissivity distributions were used to determine the expected range and variability in transmissivity for individual HGUs, HSUs, and alteration groups. Geometric means of transmissivity distributions were used to classify aquifers and confining units. Conceptually, HGUs or HSUs classified as aquifers are expected to have higher geometric mean transmissivities compared to confining units. Transmissivity distributions of the five alteration groups were used to explain lateral variations in transmissivity by HGU, and the functionality of HGUs as aquifers or confining units.

Analyses for Sufficiently Large Datasets

Similarity between transmissivity distributions of three HGUs (LFA, TCU, and WTA) and three alteration groups (devitrified, mineralized, and zeolitic) was evaluated qualitatively and quantitatively. MLE was used to fit a normal probability density function to log-transformed transmissivity estimates for each of the three HGUs and three alteration groups. Normal probability density functions were visually compared for overlap as a qualitative assessment of agreement between HGUs and alteration groups. Kendall's tau for categorical data was used to determine whether the three HGUs (LFA, TCU, and WTA) and three alteration groups (devitrified, mineralized, and zeolitic) are non-unique (non-differentiable) based on their transmissivity distributions.

Kendall's tau for categorical data is a contingency table method that can compare two or more datasets and test for differences in the distribution of data among categories (Helsel and Hirsch, 2002, p. 385). This method accounts for large amounts of censoring (greater than 30 percent) at multiple detection limits (Helsel and Hirsch, 2002, p. 375). Transmissivities of the three HGUs and three alteration groups were binned into three broad categories that represent low (0–10 ft^2/d), moderate (10–1,000 ft^2/d), and high (1,000–100,000 ft^2/d) transmissivity. The method computes a modified Kendall's tau and tests its significance using the p-value of the normal distribution, which is obtained from a computed test statistic (z-score) of the normal distribution. The test statistic is compared to the level of significance ($\alpha/2$) of the normal distribution to obtain the two-sided p-value. Comparison of the p-value to the level of significance ($\alpha/2$) evaluates the null hypothesis, which is whether the HGU or alteration group transmissivity distributions are hydraulically similar. For a two-tailed test with a 95-percent confidence interval, the null hypothesis is rejected when the p-value is less than the level of significance ($\alpha/2$), indicating that the compared HGU and alteration group transmissivity distributions are hydraulically distinct.

Volcanic-Rock Alteration Abundance by Hydrogeologic Unit

Analysis of volcanic-rock alteration abundance by HGU required the compilation of HGUs and their respective alteration codes with depth. The analysis only used HGU and alteration information from the saturated portions of boreholes open to volcanic rocks that were used in the analysis of transmissivity by HGU (fig. 5). Limiting analysis to the 71 boreholes allowed results of transmissivity by HGU to be compared directly to alteration-group abundance by HGU. Results of this analysis were used to better understand the ranges in transmissivity for HGUs and their functionality as aquifers or confining units.

The analysis sums the total saturated thickness of each alteration group within each HGU. The five alteration groups are argillic; mineralized; zeolitic; devitrified; and vitric, which are described in the section "Volcanic-Rock Alteration with Depth." Only saturated thicknesses were included because this analysis is used to explain transmissivity distributions from aquifer-test results. Analysis of the thickness of alteration groups by HGU is provided in appendix 5.

Hydraulic-Property and Rock-Alteration Analyses

Hydraulic-property analyses were done to determine lateral and vertical variations in hydraulic conductivity and transmissivity within the study area. Volcanic-rock alteration analyses supplemented hydraulic-property analyses by providing geologic explanations for lateral and vertical variations in hydraulic properties. Transmissivity was analyzed by volcanic-rock alteration group, HGU, and HSU. Hydraulic-property variations with depth were analyzed to define the active part of the flow system and to determine the frequency of permeable zones in complexly bedded volcanic rocks.

Relation of Hydraulic Properties to Volcanic-Rock Alteration, Hydrogeologic Units, and Hydrostratigraphic Units

Hydraulic-property distributions for various HGUs and HSUs in the PMOV basin were examined to determine the expected range and variability of hydraulic properties for individual HGUs and HSUs. This study also determined whether transmissivity distributions support previously published designations of HGUs and HSUs as aquifers or confining units. Relations between transmissivity and volcanic-rock alteration were done to determine the expected range in transmissivity by alteration group. Relations between transmissivity and alteration and the relative abundance of alteration groups for each HGU were used to help explain the ranges in transmissivity for HGUs and their functionality as aquifers or confining units.

Transmissivity Distribution by Volcanic-Rock Alteration

Transmissivity distributions were estimated for devitrified, mineralized, zeolitic, argillic, and vitric alteration groups. A total of 195 transmissivity estimates were used to generate the transmissivity distributions (appendix 7).

The geometric mean transmissivities for the devitrified, mineralized, and zeolitic alteration groups (fig. 9) were computed using all censored and uncensored data. Geometric means computed using the ROS method are best estimates for these alteration groups because sufficient transmissivity estimates are available to compute unbiased means (see section “Minimum Sample Size for Statistical Analyses” for details). The argillic-alteration group likely has a minimally biased ROS geometric mean because this alteration group has 21 transmissivity estimates, which is close to the minimum sample size of 24 for computing unbiased statistical quantities (fig. 6). Minimum and maximum geometric means are used to bracket the ROS geometric means and are especially relevant for the vitric alteration group, which has limited data (fig. 6).

Volcanic rocks are highly heterogeneous with respect to transmissivity, regardless of alteration type (fig. 9). Estimated transmissivities of each of the five alteration groups vary at least four-to-seven orders of magnitude. Because of censored estimates, the actual range in transmissivities likely spans one or more orders of magnitude below the minimum estimate of less than 0.009 ft^2/d and may be greater than the maximum estimate of 50,000 ft^2/d.

Rocks with devitrified alteration generally are more permeable than rocks with mineralized, zeolitic, argillic, or vitric alteration (fig. 9). The ROS geometric mean transmissivity of devitrified rock is 31 ft^2/d, which is one-to-two orders of magnitude greater than the ROS geometric mean transmissivities of the other four alteration groups (fig. 9). High-transmissivity estimates occur mostly in devitrified rocks (fig. 9), likely because fractures are not closed by mineralized, zeolitic, or argillic fracture coatings. As a result, rocks with devitrified alteration probably are the dominant aquifers in the study area. Between 65 and 90 percent of the transmissivity estimates are low (less than 10 ft^2/d) in rocks with mineralized, zeolitic, argillic, or vitric alteration, indicating that these alteration groups typically reduce transmissivity by filling fractures, which causes the rocks to more commonly function as confining units.

Rocks with devitrified alteration are hydraulically distinct from rocks with argillic, mineralized, and zeolitic alteration, based on comparison of normal probability density functions and statistical analyses (fig. 10). Normal probability density functions of transmissivity indicate that the devitrified-alteration group is differentiable from the argillic-, mineralized-, and zeolitic-alteration groups (fig. 10). In figure 10, the argillic-alteration, normal probability density function is shown as a dashed line to indicate that this density function has sample-size bias. Results of the Kendall’s tau for categorical data test provided similar results to the probability density function plots. The test statistic indicates that the transmissivity distribution of the devitrified-alteration group is hydraulically differentiable from the argillic-, mineralized-, and zeolitic-alteration groups, with p-values of less than 0.0001 for all tests.

Transmissivity Distribution by Hydrogeologic Unit

Transmissivity distributions were estimated for TCU, WTA, LFA, VTA, AA, GCU, and IICU. Transmissivity estimates for GCU and IICU were combined because these HGUs have similar rock types (intrusive rock) and limited data. A total of 184 transmissivity estimates from 71 boreholes were used to generate the transmissivity distributions (appendix 6).

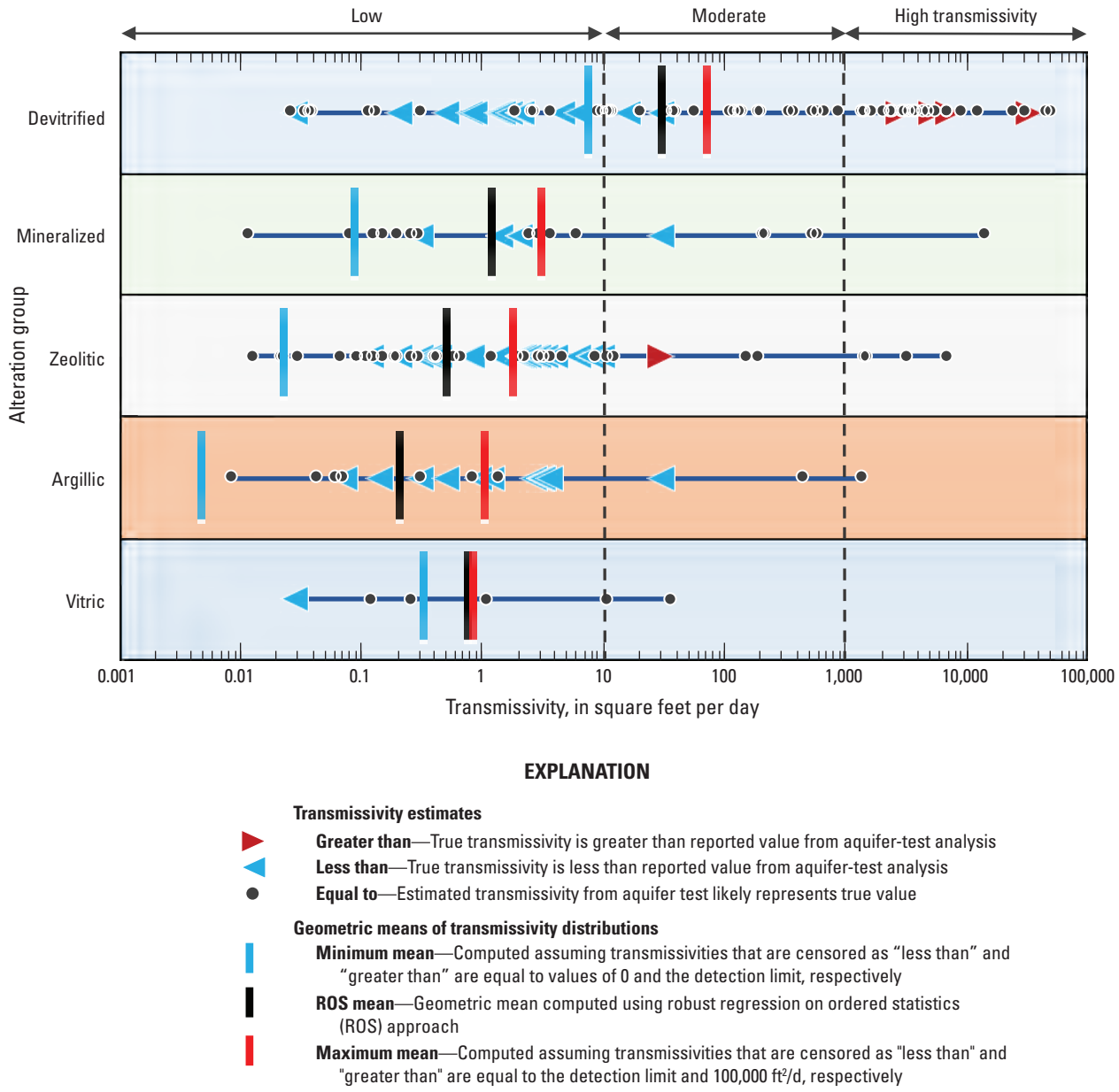

Figure 9. Distributions of transmissivity estimates for five volcanic-rock alteration groups. Transmissivities estimated from aquifer tests in wells within the Pahute Mesa–Oasis Valley groundwater basin, southern Nevada.

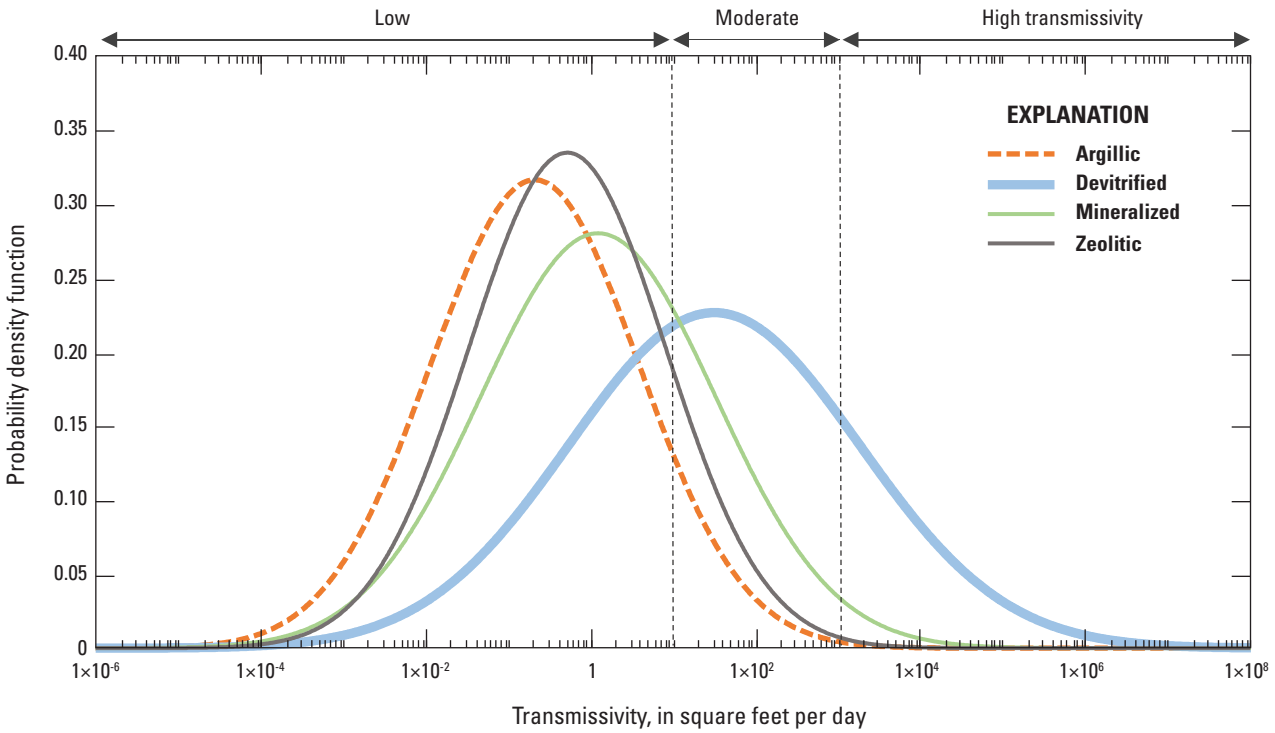

Figure 10. Normal probability density functions of transmissivity for four alteration groups. Normal probability density functions estimated using the maximum likelihood estimation approach and transmissivities from aquifer tests in wells within the Pahute Mesa–Oasis Valley groundwater basin, southern Nevada. The argillic-alteration, normal probability density function has a dashed line to indicate sample-size bias because the argillic-alteration group sample size is less than the minimal sample size for computing an unbiased probability density function.

TCU, WTA, and LFA HGUs are highly heterogeneous with respect to transmissivity (fig. 11). Estimated transmissivities of each of these three HGUs vary six to eight orders of magnitude. Because of censored estimates, the actual range in transmissivities likely spans one or more orders of magnitude below the minimum estimate of less than 0.0014 ft^2/d and may be greater than the maximum estimate of 50,000 ft^2/d. The range of transmissivities estimated for TCU, WTA, and LFA indicate that these HGUs can function spatially as either aquifers or confining units.

Geometric means computed using the ROS method are best estimates for the TCU, WTA, and LFA HGUs (fig. 11). This is because a sufficient number of transmissivity estimates are available to compute an unbiased geometric mean using the ROS method. All transmissivity estimates for the VTA and AA HGUs are uncensored; therefore, minimum, maximum, and ROS geometric means are the same value.

The TCU typically functions as a confining unit but, less commonly, can function as a leaky confining unit or aquifer. The ROS geometric mean transmissivity is 0.5 ft^2/d (fig. 11). Greater than 80 percent of the transmissivity estimates for the TCU are low (fig. 12) because nearly all the rock has undergone argillic, mineralized, or zeolitic alteration (fig. 13). These alterations reduce transmissivity and cause the TCU to function as a confining unit (fig. 9). However, the TCU can contain highly transmissive intervals, as indicated by estimated transmissivities between 1,500 and 7,000 ft^2/d in three boreholes (fig. 11). Highly transmissive intervals in these boreholes occur within zeolitically altered TCU intervals (appendix 7).

The WTA and LFA are more permeable than the TCU. ROS geometric mean transmissivities of the WTA and LFA are 5 and 12 ft^2/d, respectively, which are between 10 and 25 times greater than the ROS geometric mean transmissivity of the TCU (fig. 11). Highly transmissive intervals are more common in the WTA and LFA than in the TCU (fig. 12) because WTA and LFA are dominated by fractured rock with devitrified alteration (fig. 13). Rocks with devitrified alteration contain the most transmissive intervals hydraulically tested in Pahute Mesa (fig. 9) because most fractures are not closed by secondary mineral coatings (Drellack and others, 1997).

Alteration groups comprising the TCU, WTA, and LFA partly explain why these HGUs are highly heterogeneous with respect to transmissivity. TCU, WTA, and LFA consist of rock with devitrified, argillic, mineralized, vitric, and (or) zeolitic alteration, and each of these alteration groups have a large range in transmissivity (fig. 9). The degree and extent of hydraulically connected fractures also causes the large ranges in transmissivity. The large range in transmissivity of TCU, WTA, and LFA indicate that these HGUs can function spatially as aquifers or confining units and are best described as composite units.

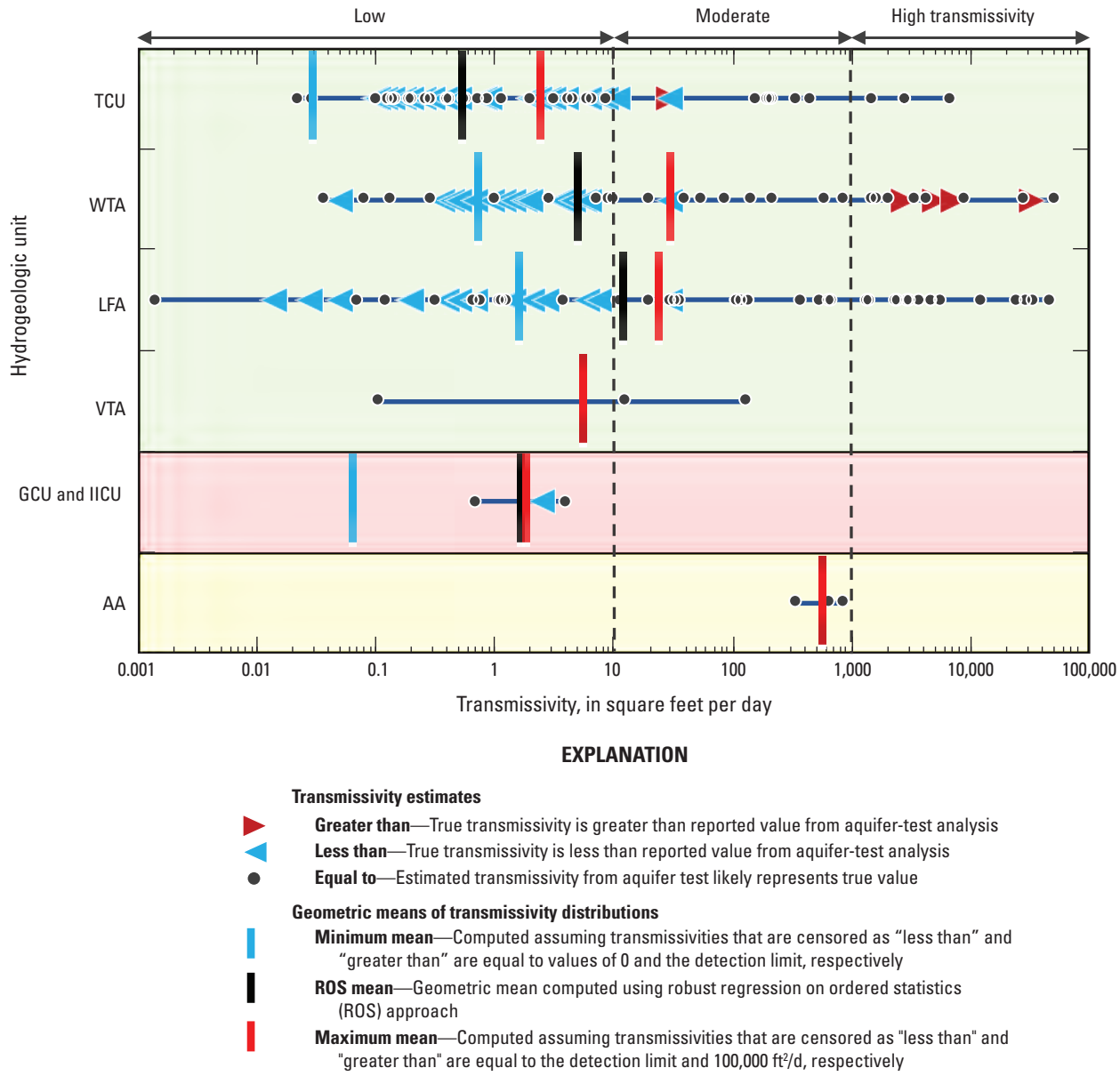

Figure 11. Distribution of transmissivity estimates in seven hydrogeologic units (HGUs). Labeled HGUs are defined in table 1. Transmissivities estimated from aquifer tests in wells within the Pahute Mesa–Oasis Valley groundwater basin, southern Nevada.

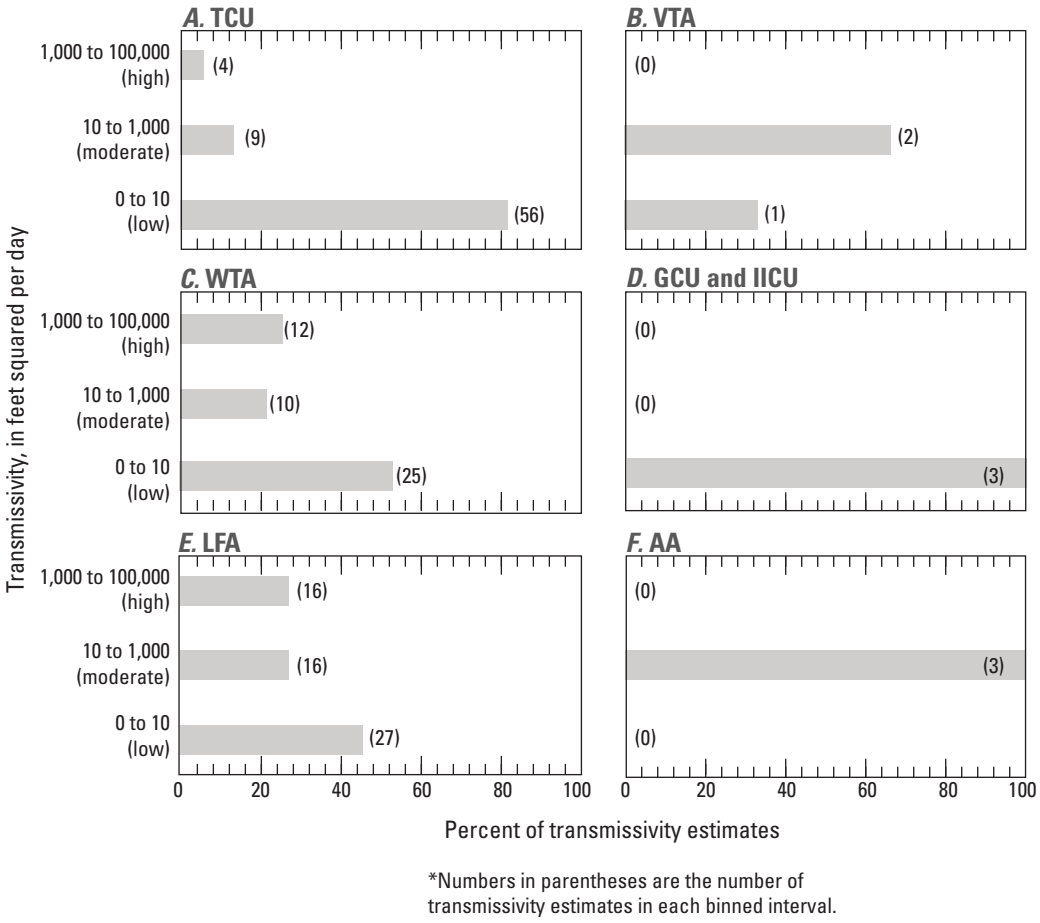

Figure 12. Number and percent of transmissivity estimates in seven hydrogeologic units (HGUs) that have low, moderate, or high transmissivity. Labeled HGUs are defined in table 1. Transmissivities estimated from aquifer tests in wells within the Pahute Mesa–Oasis Valley groundwater basin, southern Nevada.

The WTA and LFA are hydraulically similar, but distinct from the TCU, based on comparison of normal probability density functions and statistical analyses. Normal probability density functions of transmissivity indicate that the WTA and LFA are similar to each other but differentiable from the TCU (fig. 14). Results of the Kendall's tau for categorical data test provided similar results to the probability density function plots (fig. 14). The test statistic indicates that the transmissivity distributions of the WTA and LFA are similar, with a p-value equal to 0.73. The TCU is hydraulically differentiable from the WTA and LFA, with p-values of less than 0.001 for both tests.

Limited hydraulic-testing data are available to determine hydraulic variability in the VTA, combined GCU and IICU, and AA HGUs (fig. 11). Three Pahute Mesa boreholes were open to the VTA, and aquifer-test results suggest this HGU has low to moderate transmissivity. VTA is less permeable than WTA and LFA because the VTA is composed primarily of vitric and zeolitically altered rocks (fig. 13). These alteration groups typically have low to moderate transmissivity (fig. 9) because fracture networks are limited. The intrusive rock (combined GCU and IICU) HGU was hydraulically tested in three boreholes, and estimated transmissivities were low. The IICU HGU is composed of intrusive rocks with devitrified or mineralized alteration (fig. 13). Lack of hydraulically connected fractures and the closing of fractures by fracture coating minerals likely cause intrusive rocks to have low transmissivity. Moderate transmissivities were estimated from specific capacity in three Oasis Valley wells open to AA, where estimated transmissivities range from 300 to 900 ft^2/d.

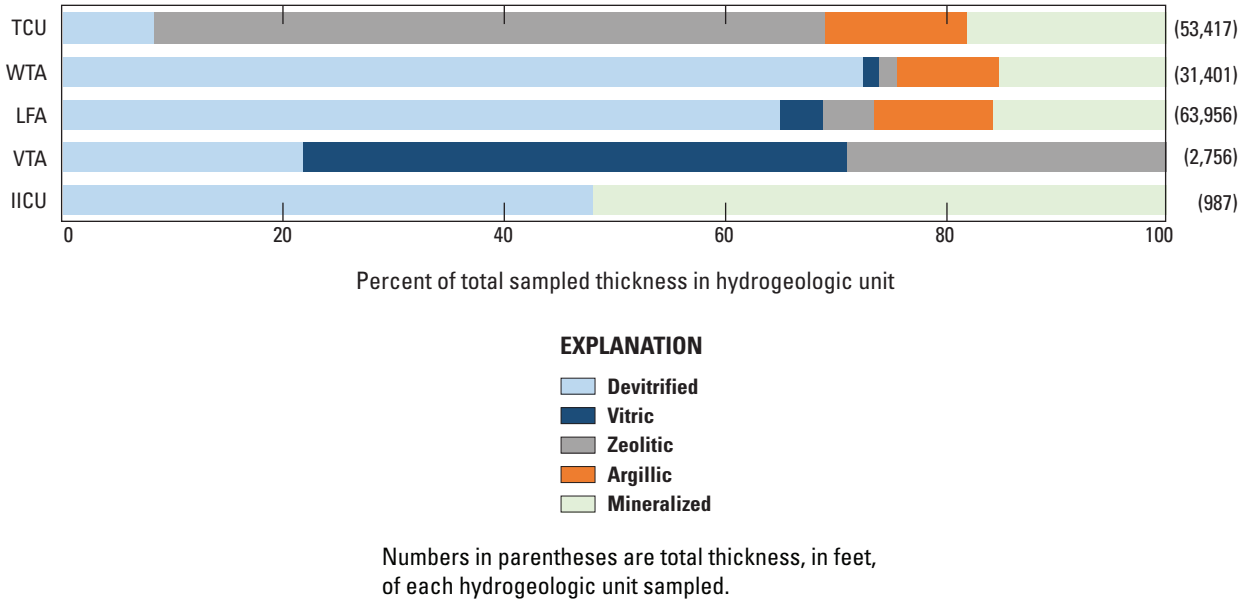

Figure 13. Abundance of five different alteration groups in five volcanic-rock hydrogeologic units (HGUs) in the Pahute Mesa–Oasis Valley groundwater basin, southern Nevada. Labeled HGUs are defined in table 1.

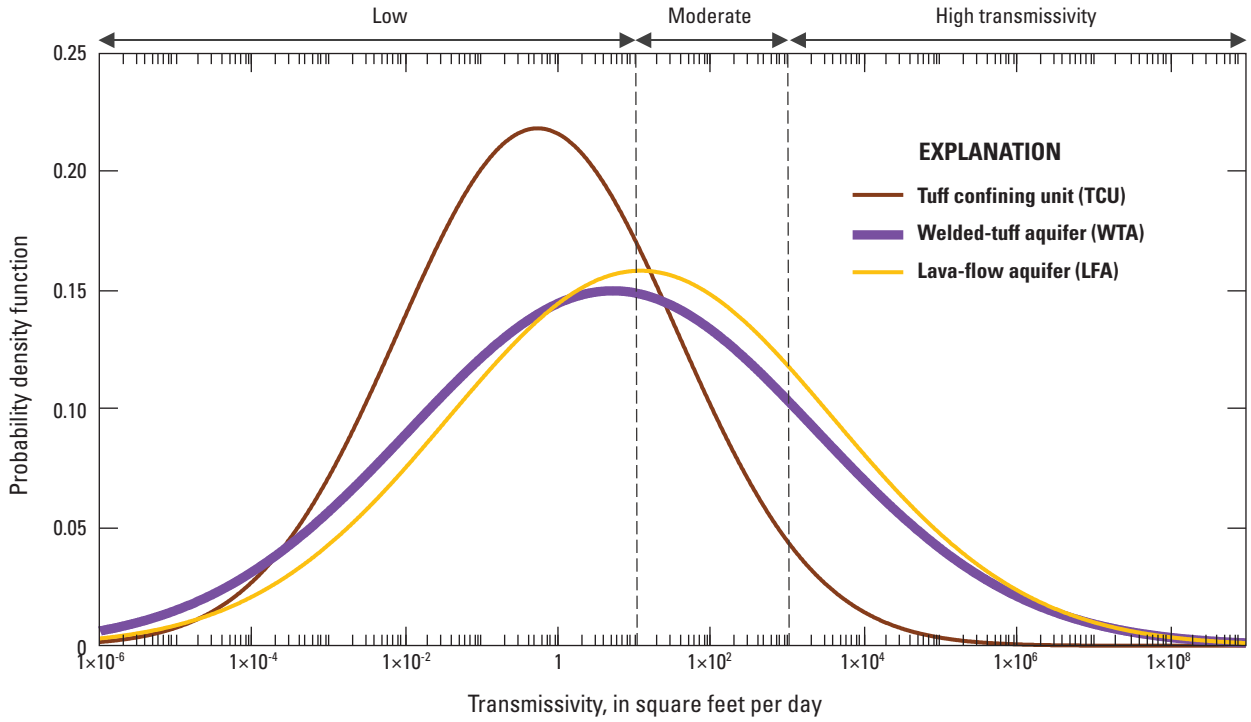

Figure 14. Normal probability density functions of transmissivity in tuff confining unit, welded-tuff aquifer, and lava-flow aquifer hydrogeologic units. Normal probability density functions estimated using the maximum likelihood estimation approach and transmissivities from aquifer tests in wells within the Pahute Mesa–Oasis Valley groundwater basin, southern Nevada.

Hydraulic-Property Distribution by Hydrostratigraphic Unit

Previous studies translated transmissivity estimates from aquifer tests into hydraulic-conductivity estimates using the open interval length of the test well as the saturated thickness. HSU analyses presented in this study retain the transmissivity estimates from aquifer tests to avoid introducing uncertainties related to unknown aquifer thickness at a field site.

The transmissivity by HSU analysis in this study is more comprehensive than analyses from previous studies because this study uses results from a recently published hydraulic-property database (Frus and Halford, 2018). The database compiled and evaluated 1,454 aquifer-test analyses from 347 wells within the PMOV basin to determine the best transmissivity estimate for each well by considering measurement limitations and confounding factors. The database also incorporates results from an integrated borehole analysis that reconciled differences in transmissivity in each borehole that had (1) a borehole transmissivity estimate from a pumping aquifer test, and (2) multiple transmissivity estimates from slug testing discrete depth intervals consecutively from the water table to the bottom of the borehole (Frus and Halford, 2018).

Previous Studies

Two previous studies (Belcher and others, 2002; Stoller Navarro Joint Venture, 2004) determined that volcanic HSUs have overlapping hydraulic-conductivity distributions, based on aquifer-test data. Stoller Navarro Joint Venture (2004) assigned hydraulic-conductivity estimates from aquifer tests to HSUs to determine the expected range of hydraulic conductivities for a given unit. Except for the Thirsty Canyon volcanic aquifer (TCVA), the geometric means of hydraulic conductivities for all HSUs were within two orders of magnitude (fig. 15; Stoller Navarro Joint Venture, 2004). This range is relatively small compared to the estimated hydraulic-conductivity variation within an HSU, which was four to nine orders of magnitude. Hydraulic conductivity also was compared among HSUs grouped by aquifer, composite unit, and confining unit (fig. 15). In general, the mean hydraulic conductivities of the aquifer HSUs are greater than the confining unit HSUs; however, the differences are small relative to the variation within individual HSUs. A similar conclusion was observed from a study of hydraulic-conductivity estimates in the Death Valley regional flow system, which includes the PMOV groundwater basin (Belcher and others, 2002). The geometric-mean hydraulic conductivity varied by no more than two orders of magnitude between 10 investigated volcanic units, whereas the variation within a unit, based on a 95-percent confidence interval, ranged from 3 to nearly 10 orders of magnitude.

Hydraulic-conductivity distributions previously were estimated for volcanic HSUs beneath Pahute Mesa from analysis of multiple-well aquifer tests (MWATs). Sixteen MWATs were completed from 2009 to 2014 in Pahute Mesa near southwestern NNSS Area 20 (Garcia and others, 2017). A cumulative volume of 63 million gallons was pumped during the MWATs and a numerical model simulating the MWATs estimated an integrated area and volume investigated of 60 mi^2 and 30 cubic miles, respectively (Garcia and others, 2017). Simultaneously interpreting between 8 and 16 MWATs resulted in hydraulic-conductivity distributions for 16 volcanic HSUs that spanned between two and six orders of magnitude (Mirus and others, 2016; Garcia and others, 2017). Volcanic HSUs were not hydraulically distinct because hydraulic-conductivity estimates varied more within HSUs than between HSUs and hydraulic-conductivity distributions greatly overlapped (Mirus and others, 2016; Garcia and others, 2017). A similar conclusion was reached regarding volcanic HSUs using a single MWAT at borehole ER-20-11, where the author concludes: "*The hydraulic conductivities of the aquifers, confining units, and composite units show considerable overlap in their estimated values with no discernible trend among the different rock types*" (Navarro, 2016b, p. 5–35).

Current Study

Transmissivities were estimated for 37 HSUs. Transmissivity distributions by HSU were generated from 137 transmissivity estimates from 71 boreholes (appendix 6).

HSUs have been designated previously as aquifers, confining units, or composite units (Drellack and others, 2002; Prothro and others, 2009). HSUs designated as aquifers, such as the BWWTA, were conceptualized to have transmissivity distributions with mostly moderate-to-high transmissivity (10–100,000 ft^2/d), whereas HSUs designated as confining units, such as the BFCU, were conceptualized to have transmissivity distributions with mostly low transmissivity (0–10 ft^2/d). Composite units, such as the pre-Belted Range composite unit (PBRCM), were conceptualized to have a broad range of transmissivities spanning from low to high. Exceptions occur for the Fortymile Canyon composite unit (FCCM) and Calico Hills zeolitic composite unit (CHZCM). Lava flows, conceptualized as aquifers, were delineated and extracted from the originally mapped extents of the FCCM and CHZCM (Bechtel Nevada, 2002a) during revisions for the PMOV HFM (U.S. Department of Energy, 2020a). Seven lava flows were differentiated from the FCCM and designated as Fortymile Canyon upper lava-flow aquifers 1–7 (FCULFA1–FCULFA7). Likewise, five lava flows were differentiated from the CHZCM and designated as Calico Hills lava-flow aquifers 1–5 (CHLFA1–CHLFA5). Because the lava flows conceptualized as aquifers were removed from the original composite units, the revised CHZCM and FCCM are expected to be dominated by TCU and are conceptualized in this report as confining units.

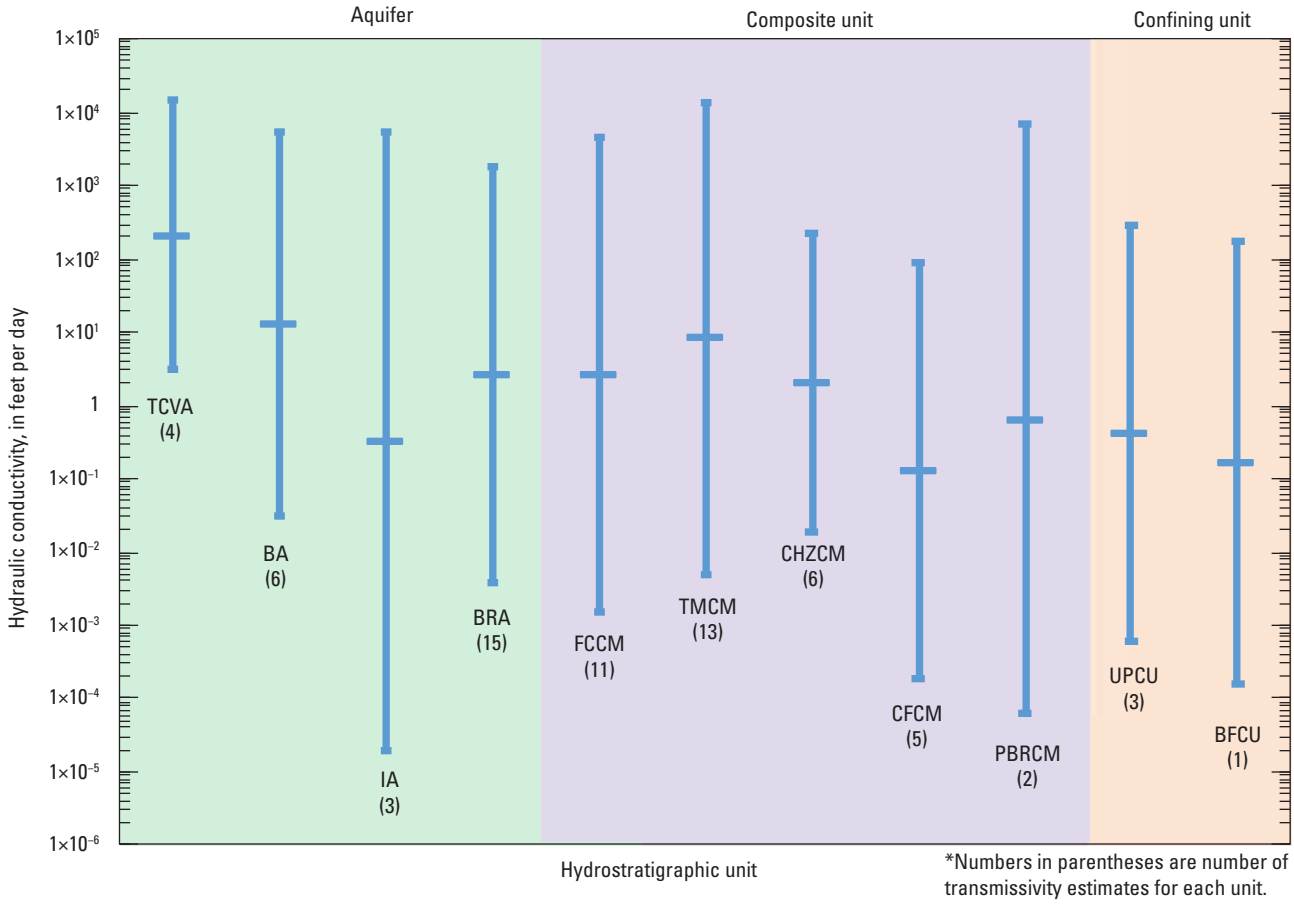

Figure 15. Previously published relation of hydraulic-conductivity distributions among hydrostratigraphic units (HSUs) in the Pahute Mesa–Oasis Valley groundwater basin, southern Nevada. Labeled HSUs are defined in table 1. The hydraulic-conductivity distribution for each HSU is shown as plus or minus two standard deviations (vertical line) from the geometric mean (horizontal hash mark). Distributions from table 5-4 of Stoller Navarro Joint Venture (2004).

Transmissivity data are insufficient to support differentiating the Fortymile Canyon lava flows, FCULFA1–FCULFA7, from the FCCM. No aquifer-test data are available to determine the range in transmissivity of FCULFA1, FCULFA2, FCULFA3, and FCULFA5. Only the FCULFA4 was hydraulically tested in borehole *ER-EC-13*, where the transmissivity is 4,700 ft²/d (fig. 16). Similarly, FCULFA6 and FCULFA7 were hydraulically tested only in well *ER-EC-7*. Total transmissivity from the test was high (12,400 ft²/d), but FCULFA7 likely contributes most of the transmissivity within the open interval based on a water-production log (Bechtel Nevada, 2004a). The transmissivity of FCULFA6 was not estimated but is assumed to be low at this well site.

High transmissivities estimated for FCULFA4 and FCULFA7 suggest these HSUs can function as aquifers, but data are insufficient to determine the range in transmissivity (fig. 16). Greater than 200 ft of FCCM was hydraulically tested in three wells, and water-production logs indicate that FCCM contributes most of the flow within the open interval of two wells: *ER-EC-2A (1635-4973 ft)* and *ER-EC-8* (Bechtel Nevada, 2002b, 2004b). The FCCM transmissivity in the third well, not shown in figure 16, could not be quantified but the transmissivity likely is low based on limited inflows from a flow log (Oberlander and others, 2002). Results indicate that the overall transmissivity of the FCCM probably is variable, with areas of high transmissivity present.

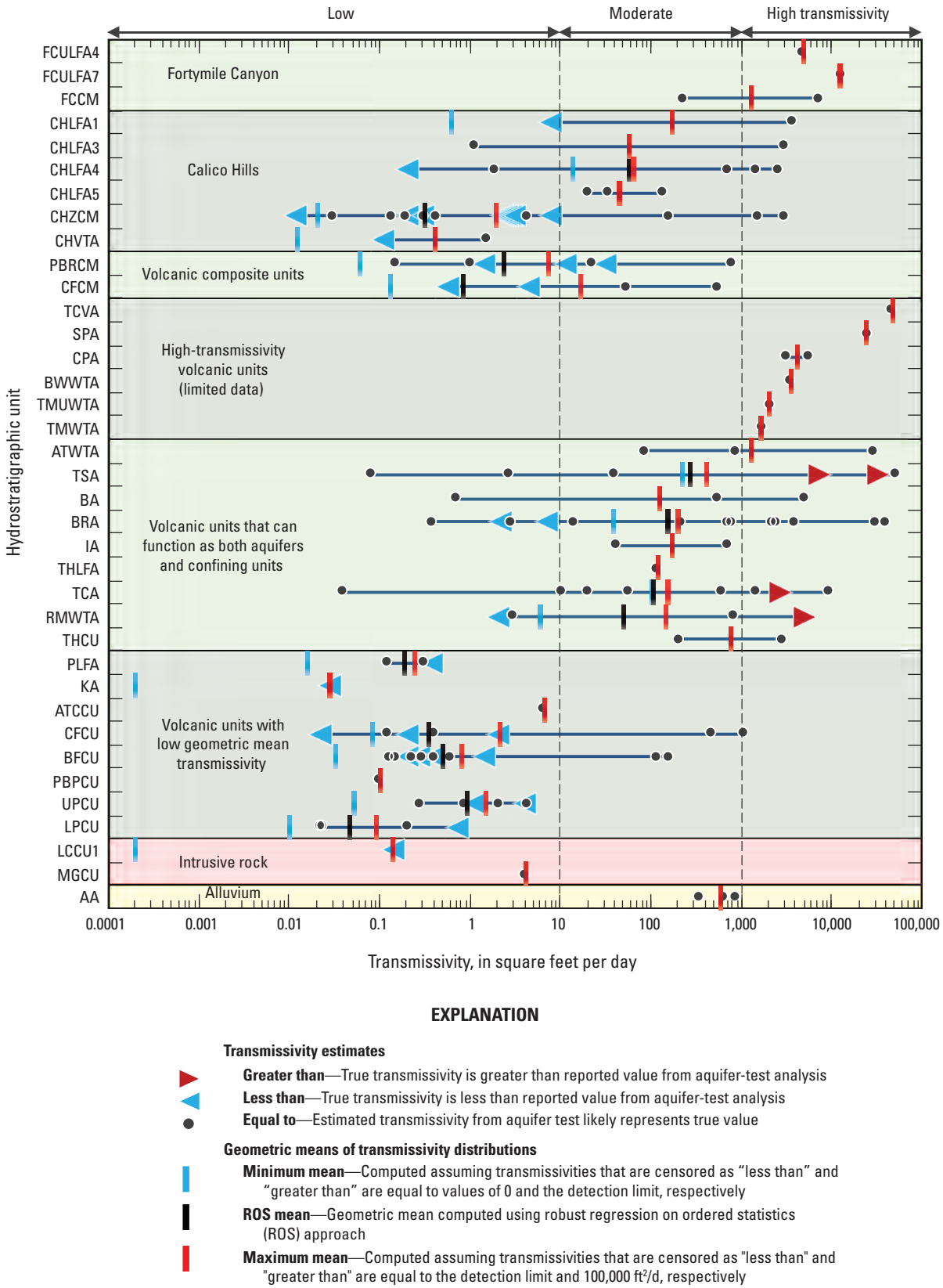

Figure 16. Distribution of transmissivity in hydrostratigraphic units (HSUs). Labeled HSUs are defined in table 1. Transmissivities estimated from aquifer tests in wells within the Pahute Mesa–Oasis Valley groundwater basin, southern Nevada.

Hydraulic data suggest the Calico Hills lava flow HSUs are hydraulically undifferentiable from each other but have higher transmissivities than the CHZCM or Calico Hills vitric tuff aquifer (CHVTA). Lava-flow aquifers CHLFA1, CHLFA3, CHLFA4, and CHLFA5 have similar ROS geometric mean transmissivities that range between 40 and 170 ft^2/d (fig. 16). The Calico Hills lava flow HSUs have overlapping transmissivity distributions that span two to four orders of magnitude, with transmissivity estimates that range from less than one to several thousand feet squared per day (fig. 16). This large range in transmissivity indicates that Calico Hills lava flow HSUs can function spatially as aquifers or confining units. This result is consistent with borehole data and hydraulic-property estimates from previous work (Erikson, 1991; Brikowski, 1992; IT Corporation, 1998; Pawloski and others, 2001; Garcia and others, 2017). The transmissivity distribution of the CHZCM is dominated by low-transmissivity estimates, but two high-transmissivity estimates in the CHZCM indicate that high-permeability intervals can occur in this TCU-dominated unit (fig. 16).

Two HSUs designated as composite units have transmissivity distributions with estimates that span from low to moderate. These HSUs, PBRCM and Crater Flat composite unit (CFCM), conceptually are expected to be heterogeneous and to have a wide range of transmissivities. The PBRCM and CFCM transmissivity distributions shown in figure 16 are heterogeneous, although no high transmissivity intervals were estimated in these HSUs. The transmissivity distributions of these composite units are similar, visually, to many of the distributions from other HSUs that were previously designated as aquifers or confining units.

Limited hydraulic data suggest that some of the HSUs previously designated as aquifers are, in part, highly transmissive. However, one or two high-transmissivity estimates for the Thirsty Canyon volcanic aquifer (TCVA), Scrugham Peak aquifer (SPA), Comb Peak aquifer (CPA), Buttonhook Wash welded tuff aquifer (BWWTA), Timber Mountain upper welded tuff aquifer (TMUWTA), and Timber Mountain welded tuff aquifer (TMWTA) do not demonstrate that these HSUs consistently function as aquifers (fig. 16). The transmissivity distributions of these HSUs likely are similar to distributions of other HSUs previously designated as aquifers.

Transmissivity distributions with estimates that span from low to high occur in HSUs previously designated as aquifers. The Ammonia Tanks welded tuff aquifer (ATWTA), Topopah Spring aquifer (TSA), Benham aquifer (BA), BRA, Inlet aquifer (IA), Tannenbaum Hill lava flow aquifer (THLFA), Tiva Canyon aquifer (TCA), and Rainier Mesa welded tuff aquifer (RMWTA) have transmissivity estimates that span up to six orders of magnitude within an HSU (fig. 16). Transmissivity distributions for HSUs with four or more transmissivity estimates indicate that HSUs previously designated as aquifers function as both aquifers and confining units and have geometric mean transmissivities that mostly are moderate. Even though only two moderate-to-high transmissivity estimates are available for the Tannenbaum Hills confining unit (THCU), these estimates may indicate that the THCU is a composite of aquifers and confining units. In summary, transmissivity distributions of ATWTA, TSA, BA, BRA, IA, THLFA, TCA, RMWTA, and THCU indicate that these HSUs function as composite units. These HSUs are highly heterogeneous with respect to transmissivity (fig. 16) because of spatially variable fracture distributions, ranging from limited fractures to extensive, hydraulically connected fracture networks.

Low-transmissivity volcanic units are dominated by HSUs previously designated as confining units, with several exceptions (fig. 16). The Paintbrush lava flow aquifer (PLFA) and Kearsarge aquifer (KA) were previously designated as aquifers, but limited data suggest these HSUs have low transmissivity. The PLFA and KA lava-flow HSUs likely are hydraulically similar to other lava-flow HSUs, and the limited transmissivity estimates may be from the low end of the true transmissivity distribution. One to 13 transmissivity estimates are available for six HSUs previously designated as confining units: Ammonia Tanks caldera confining unit (ATCCU), Crater Flat confining unit (CFCU), Bullfrog confining unit (BFCU), post-Benham Paintbrush confining unit (PBPCU), upper Paintbrush confining unit (UPCU), and lower Paintbrush confining unit (LPCU). Nearly all the transmissivity estimates, and all the geometric means, are low in these six HSUs. Despite limited hydraulic data, the range in variability is relatively small and the highest transmissivity estimate for all these HSUs is about 1,000 ft^2/d. Therefore, the ATCCU, CFCU, BFCU, PBPCU, UPCU, and LPCU are believed to function primarily as confining units.

The Mesozoic granite confining unit (MGCU), lower clastic confining unit–thrusted (LCCU1), and alluvial aquifer (AA) are the only HSUs tested in the PMOV basin that are not composed of volcanic rock. The MGCU and LCCU1 transmissivity estimates, as expected, are classified as low on figure 16. The AA transmissivity estimates are moderate and have a calculated geometric mean of about 600 ft^2/d.

Relation of Hydraulic Properties to Depth

Hydraulic conductivity and transmissivity with depth were analyzed to evaluate vertical variations in permeability below the water table and land surface. Vertical variations in volcanic-rock alteration abundance were used to help explain hydraulic-property variations with depth.

Transmissivity and Hydraulic Conductivity with Depth

To estimate transmissivity and hydraulic conductivity with depth, transmissivities from single-well aquifer tests and specific capacity in 76 boreholes (fig. 5; Frus and Halford, 2018) were binned into 400-ft depth intervals below the water table (appendix 4). For wells with open intervals greater than 400 ft, total transmissivity was apportioned into 400-ft binned intervals. For example, consider a well open to 800 ft of volcanic rock with a transmissivity of 1,000 ft^2/d. The 800-ft saturated open interval would be binned into two 400-ft saturated intervals, where each interval would have a transmissivity of 500 ft^2/d and a hydraulic conductivity of 1.25 ft/d. Interval-averaged hydraulic conductivity (and transmissivity) was the (arithmetic) average hydraulic conductivity (and transmissivity) from all tests in each 400-ft interval.

Depth-dependent transmissivity variations in volcanic rocks are well defined because slug tests at discrete depth intervals were done consecutively from the water table to the bottom of 17 deep Pahute Mesa boreholes (Blankennagel, 1967; Blankennagel and Weir, 1973; Frus and Halford, 2018). Interval-averaged transmissivities from the 17 Pahute Mesa boreholes indicate that 91 percent of the transmissivity in volcanic rocks occurs within 1,600 ft of the water table (fig. 17). This result was refined by combining interval-averaged transmissivities from the 17 Pahute Mesa boreholes with transmissivities from 59 additional boreholes open to volcanic rocks in the PMOV basin (fig. 5; Frus and Halford, 2018). Using all 76 boreholes, interval-averaged transmissivities indicate that greater than 98 percent of the transmissivity in volcanic rocks in the PMOV basin occurs within 1,600 ft of the water table (fig. 18).

Volcanic-Rock Alteration Abundance and Transmissivity with Depth

An increase in the abundance of argillic and mineralized alteration at depth likely explains the abrupt decrease in transmissivity at depths greater than 1,600 ft below the water table in the PMOV basin. Argillic and mineralized alteration of volcanic rocks are uncommon in the upper 1,600 ft of the saturated zone, where transmissivity is moderate to high (fig. 19). Argillic alteration is persistent at depths greater than 1,600 ft below the water table, and accounts for 11 to 32 percent of the volcanic-rock thickness in each 400-foot depth interval from 1,601 to 6,000 ft below the water table (fig. 19). Likewise, mineralized alteration also is persistent at depths greater than 1,600 ft below the water table, and accounts for 15 to 56 percent of the volcanic-rock thickness in each 400-foot depth interval from 1,601 to 6,000 ft below the water table (fig. 19). The prevalence of argillic and mineralized alteration at deeper depths (greater than 1,600 ft below the water table) is expected based on studies of mineralogical zonation beneath Pahute Mesa (Moncure and others, 1981).

Argillic and mineralized alterations reduce the transmissivity of volcanic rock (Blankennagel and Weir, 1973; Drellack and others, 1997). Volcanic rocks with argillic alteration have the lowest mean transmissivity of any alteration group, with an estimated ROS mean of 0.2 ft^2/d (fig. 9). Volcanic rocks with mineralized alteration also have a low ROS mean transmissivity of 1.2 ft^2/d. Rocks with argillic or mineralized alteration have low transmissivity because most fractures are closed by fracture mineral coatings (Drellack and others, 1997).

The vitric-alteration group does not have a substantial effect on transmissivity with depth. Vitric alteration mostly occurs at shallow depths (within 1,600 ft of the water table), which is expected based on studies of mineralogical zonation beneath Pahute Mesa (fig. 19; Moncure and others, 1981). Similar to argillic and mineralized alteration, estimated transmissivities of vitric rock are predominantly low, spanning from less than 0.03 to 37 ft^2/d (fig. 9). High-transmissivity intervals within the shallow saturated zone are minimally affected by vitric, argillic, and mineralized alterations because the occurrence of these alteration groups is limited near the water table (fig. 19).

Volcanic rocks with devitrified alteration primarily are responsible for the observed trend of most of the transmissivity occurring within 1,600 ft of the water table (fig. 19). High-transmissivity intervals occur more frequently in rocks with devitrified alteration compared to the other alteration groups (fig. 9). Volcanic rocks with devitrified alteration have an estimated ROS mean transmissivity of 31 ft^2/d, which is the highest geometric mean transmissivity for the five alteration groups (fig. 9). Devitrified alteration is abundant at shallow depths, accounting for 33 to 55 percent of the volcanic-rock thickness in each 400-foot depth interval within 1,600 ft of the water table (fig. 19). Devitrified-alteration abundance gradually decreases with depth, where the decreasing abundance of transmissive devitrified rock with depth is correlated with an increasing abundance of low-transmissivity, mineralized- and argillic-altered rock with depth (fig. 19).

No clear trend is observed in the abundance of zeolitic alteration with depth below the water table (fig. 19). Zeolitic alteration occurs in every 400-foot depth interval and comprises from 3 to 55 percent of each depth interval (fig. 19). However, zeolitic alteration is more common, on average, in the upper 1,600 ft of the saturated zone than at deeper depths. Estimated transmissivities for volcanic rocks with zeolitic alteration typically are low (fig. 9). Zeolitic alteration does not explain the decrease in transmissivity with depth, although zeolitic alteration contributes to lowering the overall transmissivity of the volcanic rocks by sealing fractures.

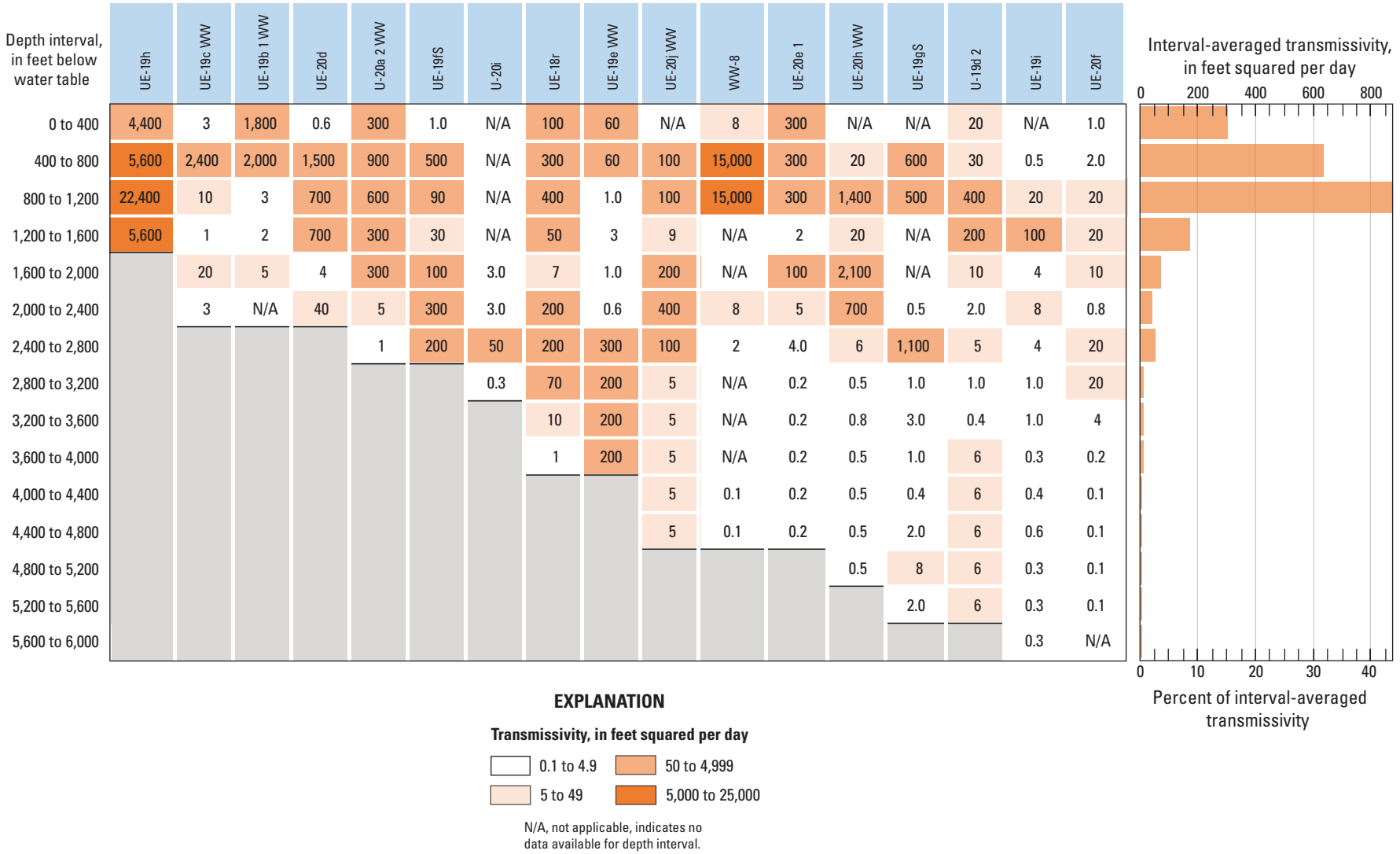

Figure 17. Distribution of transmissivity with depth in 17 boreholes open to volcanic rock at Pahute Mesa, southern Nevada. Transmissivities estimated from slug testing discrete depth intervals consecutively from the water table to the bottom of the 17 boreholes (Frus and Halford, 2018).

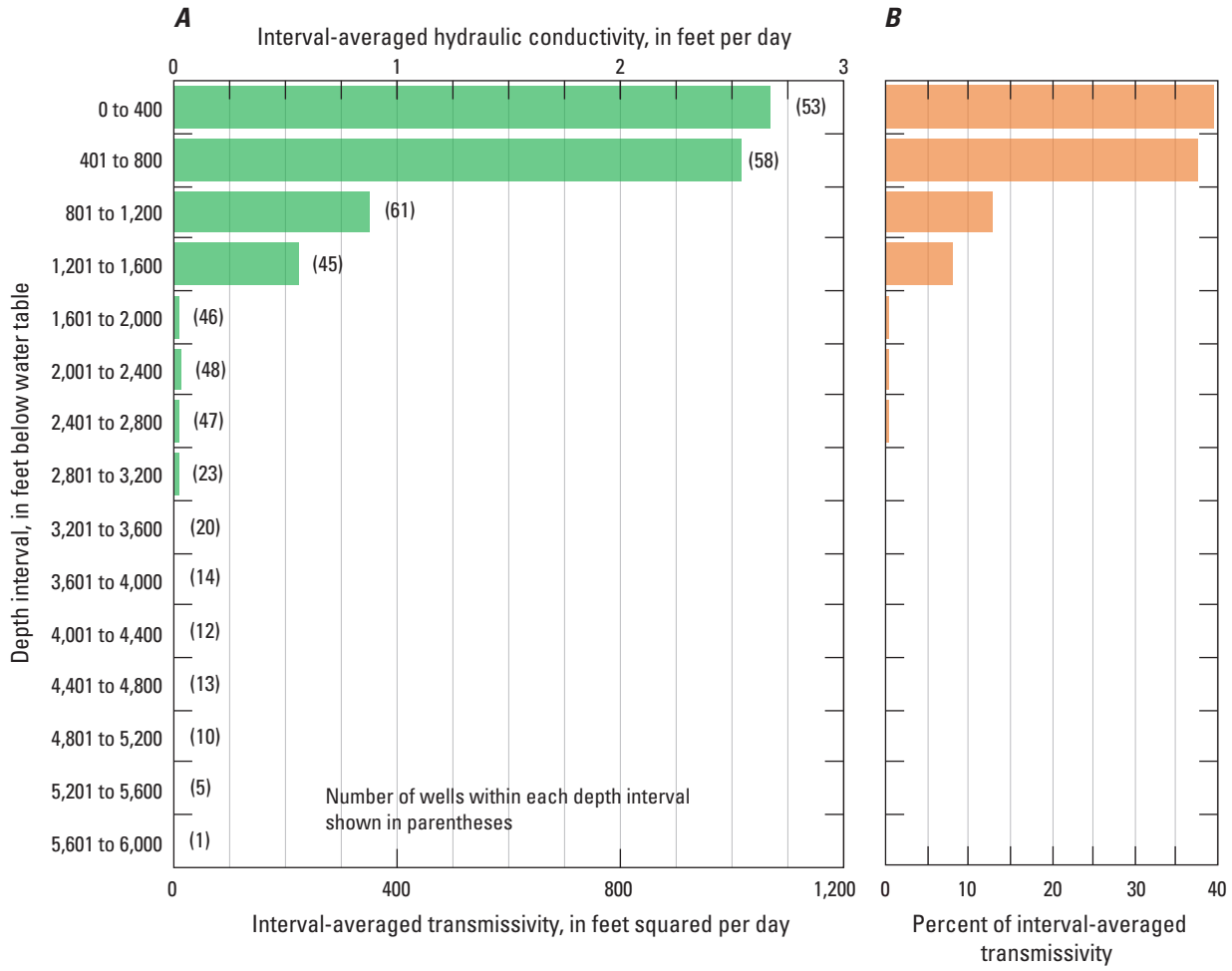

Figure 18. Distribution of hydraulic conductivity and transmissivity with depth in volcanic rocks within the Pahute Mesa–Oasis Valley (PMOV) groundwater basin, southern Nevada. Hydraulic conductivity and transmissivity estimated using aquifer-test results from the 17 boreholes in figure 17 plus an additional 59 boreholes in the PMOV basin (Frus and Halford, 2018).

Hydraulic Conductivity as a Function of Depth Decay

Hydraulic conductivity in the volcanic rocks underlying the PMOV basin does not decrease smoothly as a function of depth below land surface, as conceptualized in depth-decay models. These models assume that permeability decreases with depth as geostatic and hydrostatic load increases, which decreases widths of pore spaces and fracture apertures (Bernabé and others, 2003; Cardenas and Jiang, 2010). Hydraulic conductivity previously has been correlated weakly with depth below land surface (Stoller-Navarro Joint Venture, 2004; Belcher and Sweetkind, 2010).

Relations between hydraulic conductivity and depth below land surface have been analyzed for volcanic rocks at Pahute Mesa. Hydraulic-conductivity estimates by HGU were compiled by Belcher and others (2002) and a regression analysis concluded that, for the volcanic HGUs, "*relations between depth and log hydraulic conductivity had a correlation coefficient that ranged from virtually zero to 0.52*" (Belcher and Sweetkind, 2010, p. 118). This weak correlation also has been observed in depth-dependence analyses of hydraulic conductivity by HSU. An analysis of hydraulic conductivities from slug-test results of 10 HSUs at Pahute Mesa concluded that "*there is no clear depth dependence in hydraulic conductivity for any of the HSUs. In some cases, what appear to be changes in K [hydraulic conductivity] with depth may actually be spatial variability*" (Stoller-Navarro Joint Venture, 2004, p. 5–17). The main conclusion from analysis of volcanic HGUs and HSUs is that "*the hydraulic conductivity of the volcanics, as a group, appear to decrease with depth, but there is a great deal of scatter in the values*" (see fig. 5-9 of Stoller-Navarro Joint Venture, 2004, p. 5–15). Weak correlations between hydraulic conductivity and depth have no predictive value because individual hydraulic-conductivity estimates range between 1×10^{-6} ft/d and 1 ft/d at similar depths within 4,000 ft below land surface (Stoller-Navarro Joint Venture, 2004, p. 5–15).

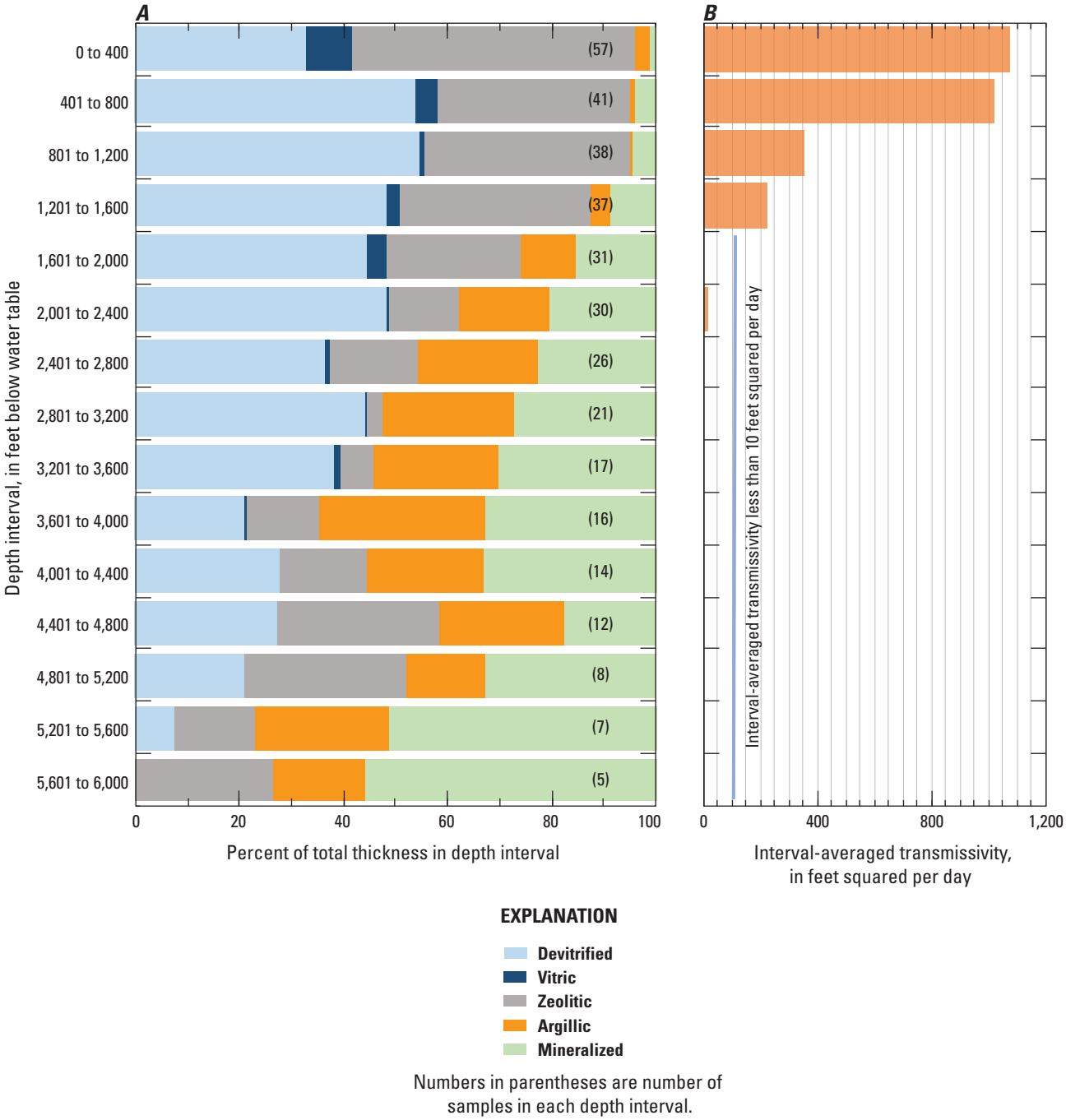

Figure 19. Distribution of alteration abundance and transmissivity with depth in boreholes open to volcanic rocks within the Pahute Mesa–Oasis Valley groundwater basin, southern Nevada.

Hydraulic conductivity with depth below land surface was analyzed in this study using compiled hydraulic-property data (Frus and Halford, 2018). Results for this study are similar to previous studies because hydraulic conductivity generally decreases with depth, but scatter within the data yields correlation coefficients that range from 0.02 to 0.35 for volcanic HGUs. Hydraulic variations with depth are consistent with complex bedded and fractured rocks that have been observed in outcrops in the study area (Sweetkind and others, 2010, p. 71). These observable hydraulic and structural heterogeneities cannot be represented adequately with a depth-decay model.

Volcanic rocks can be divided into shallow permeable rocks and deep low-permeability rocks as an alternative to a depth-decay model. The division between shallow and deep rocks at 1,600 ft below the water table is supported by depth-dependent hydraulic-conductivity data (fig. 18). Depth-dependent variations in volcanic rocks beneath Pahute Mesa are well defined in 17 boreholes, where 16 of the 17 boreholes were completed in volcanic rocks at depths greater than 1,600 ft below the water table (fig. 17). The decreasing abundance of high-transmissivity devitrified rock at depth, which is correlated to an increasing abundance of low-transmissivity rock with argillic and mineralized alteration at depth, likely explains the abrupt decrease in transmissivity at depths greater than 1,600 ft below the water table in the PMOV basin. Permeable shallow rocks transmit most of the groundwater between recharge and discharge areas, whereas deep rocks have low permeability and transmit a minor component of the flow. The shallow-deep concept has been used previously within the study area and on the NNSS (Fenelon and others, 2008, 2010, 2012; Halford and Jackson, 2020).

Frequency of Permeable Intervals in Volcanic Rock

Most of the transmissivity in the volcanic rocks underlying Pahute Mesa is restricted to thin, infrequent permeable zones. A permeable zone is defined as having a moderate or high transmissivity that exceeds 10 ft^2/d. Permeable zones occur within 77 of 219 depth-discrete intervals slug tested in 17 Pahute Mesa boreholes. A total of 45,000 ft of saturated volcanic rock was slug tested, where the 77 slug tests with permeable zones cumulatively tested about 18,500 ft of the 45,000 ft of volcanic rocks. Only part of the 18,500 ft of volcanic rock is permeable because zones of moderate or high transmissivity caused by flowing fractures are much thinner than the tested interval lengths. Results from slug tests and geophysical logs, including temperature, salinometer, radioactive tracer, and borehole flow, indicate that zones of flowing fractures range from 10- to 70-ft thick, and average 40 ft (Blankennagel, 1967; Blankennagel and Weir, 1973). Therefore, permeable flowing fractures account for, on average, about 40 ft of each 200-ft interval tested, which equates to 20 percent of the tested interval. Assuming only 20 percent of the 18,500 ft of permeable test intervals is permeable, then about 3,700 ft of the 45,000 ft of volcanic rock tested contains permeable flowing fractures (fig. 20), which implies that eight percent of the volcanic-rock volume contains 99.6 percent of the transmissivity (fig. 20).

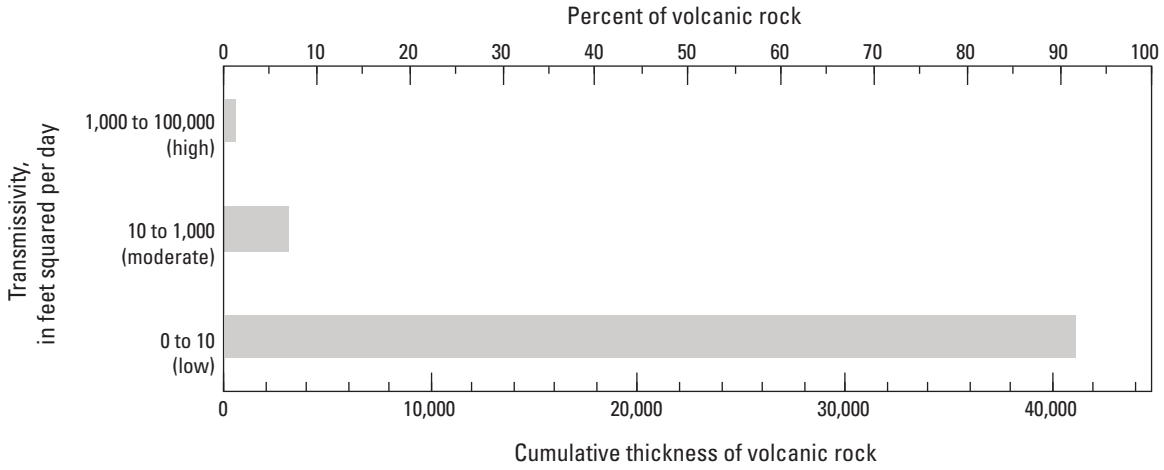

Figure 20. Cumulative thickness and percent of volcanic rock that has low, moderate, or high transmissivity. Transmissivities estimated from 219 discrete depth intervals in 17 Pahute Mesa boreholes within the Pahute Mesa–Oasis Valley groundwater basin, southern Nevada.

Groundwater Flow Conceptualization of the Pahute Mesa–Oasis Valley Groundwater Basin

Conceptualization of groundwater flow in the PMOV basin requires an integrated understanding of the geology, hydraulic properties, basin boundaries, groundwater budget, water levels, and radionuclide distribution within the basin. Lateral and vertical boundaries of the PMOV basin define the three-dimensional volume of the flow system. The groundwater budget provides a constraint on the amount and distribution of groundwater flow between recharge and discharge areas. Water levels are analyzed to develop a potentiometric surface that portrays horizontal hydraulic gradients and regional groundwater-flow directions. Radionuclide data are used to ascertain consistency of radionuclide-transport directions to groundwater-flow paths derived from the potentiometric surface map. Relations of hydraulic properties to geologic materials and major geologic structures are used to determine where groundwater is likely to flow and whether specific structures can be characterized as barriers or conduits to flow. The groundwater-flow conceptualization in the PMOV basin is discussed in terms of six distinct subareas, where geologic, hydrologic, and radionuclide data are integrated.

Plate 1 shows the potentiometric contours, horizontal flow arrows, data locations, hydraulic-head estimates, areas of recharge and discharge, and geologic structures. Additionally, nine sets of hydrostratigraphic and hydrologic sections were constructed to portray the hydrostratigraphic framework, underground nuclear tests, and groundwater flow in the basin. Eight of the sections (sections *A–A′* to *G–G′* and *I–I′* on plate 2) are oriented approximately parallel to regional flow and one section (*H–H′* on plate 2) is oriented perpendicular to flow.

Lateral Basin Boundary

The lateral boundary of the PMOV basin (fig. 21) defines where recharge occurs, moves downgradient, and discharges to Oasis Valley. The boundary was developed based on regional water-level contours, geologic controls, and knowledge of water-budget constraints in adjacent flow systems (Fenelon and others, 2016). Internal consistency of the boundary was tested by matching measured water levels, groundwater discharges, and transmissivities with simulated results from groundwater-flow models (Fenelon and others, 2016; Halford and Jackson, 2020).

The boundary of the PMOV basin, which extends eastward to the Belted Range and incorporates all underground nuclear tests on Pahute Mesa, is consistent with updated estimates of discharges in the PMOV and AFFCR groundwater basins. A previous interpretation of the groundwater-basin boundary that defined the contributing area to Oasis Valley was first published by Waddell (1982) and later republished and discussed by Waddell and others (1984) and Laczniak and others (1996). The previous basin delineation, referred to as the Oasis Valley groundwater basin (fig. 21), is about one-third the size of the PMOV basin and excludes most of the underground testing area on Pahute Mesa. In the Waddell (1982) interpretation, groundwater underlying most of the Pahute Mesa testing area flows south toward Fortymile Canyon and discharges in the Amargosa Desert or at Death Valley, about 50 miles to the south or southwest, respectively. The small area defined by Waddell (1982) for the Oasis Valley groundwater basin was a reasonable conceptualization at the time because the area was consistent with the small historical estimate of groundwater discharge in Oasis Valley. The reconnaissance estimate of 2,000 acre-ft/yr (Malmberg and Eakin, 1962) used by Waddell (1982) is three times less than the current, refined estimate of 5,900 acre-ft/yr (Reiner and others, 2002). Most of the Pahute Mesa testing area that was excluded from the Oasis Valley groundwater basin by Waddell (1982) was instead included in the AFFCR groundwater basin to account for a large, historical groundwater-discharge estimate in the AFFCR basin. The historical estimate of 16,000 acre-ft/yr (Walker and Eakin, 1963; Hunt and others, 1966; Waddell, 1982) is twice the current estimate of 8,000 acre-ft/yr (Fenelon and others, 2016).

Southerly flow paths through Fortymile Canyon from any of the underground tests on Pahute Mesa are unlikely, based on revised basin budgets (Fenelon and others, 2016) and by potentiometric data (plate 1) that indicate southwesterly flow. The southeastern segment of the PMOV basin boundary is a no-flow boundary that parallels these southwesterly flow paths. The erroneous postulation of southerly flow paths through Fortymile Canyon by many investigators (for example, Laczniak and others, 1996; Thomas and others, 2002; Kwicklis and others, 2005; Rose and others, 2006; Stoller-Navarro Joint Venture, 2009; Hershey and others, 2016) is based largely on ambiguous geochemical interpretations and the outdated conceptualization (Waddell, 1982) of the delineated groundwater basin. The Oasis Valley groundwater basin was delineated based on historical discharge estimates and limited water-level data (Waddell, 1982, plate 1). Wells were not drilled between Oasis Valley and the western boundary of NNSS Area 20 (plate 1) until after 1995.

Interbasin Flow

The lateral basin boundary of the PMOV basin represents a no-flow boundary, although minor amounts of water may cross into or out of the basin in several places. These locations of potential interbasin flow are along the southern and southeastern boundaries (Fenelon and others, 2016). Depending on the area, interbasin flow can occur as groundwater or surface-water flow.

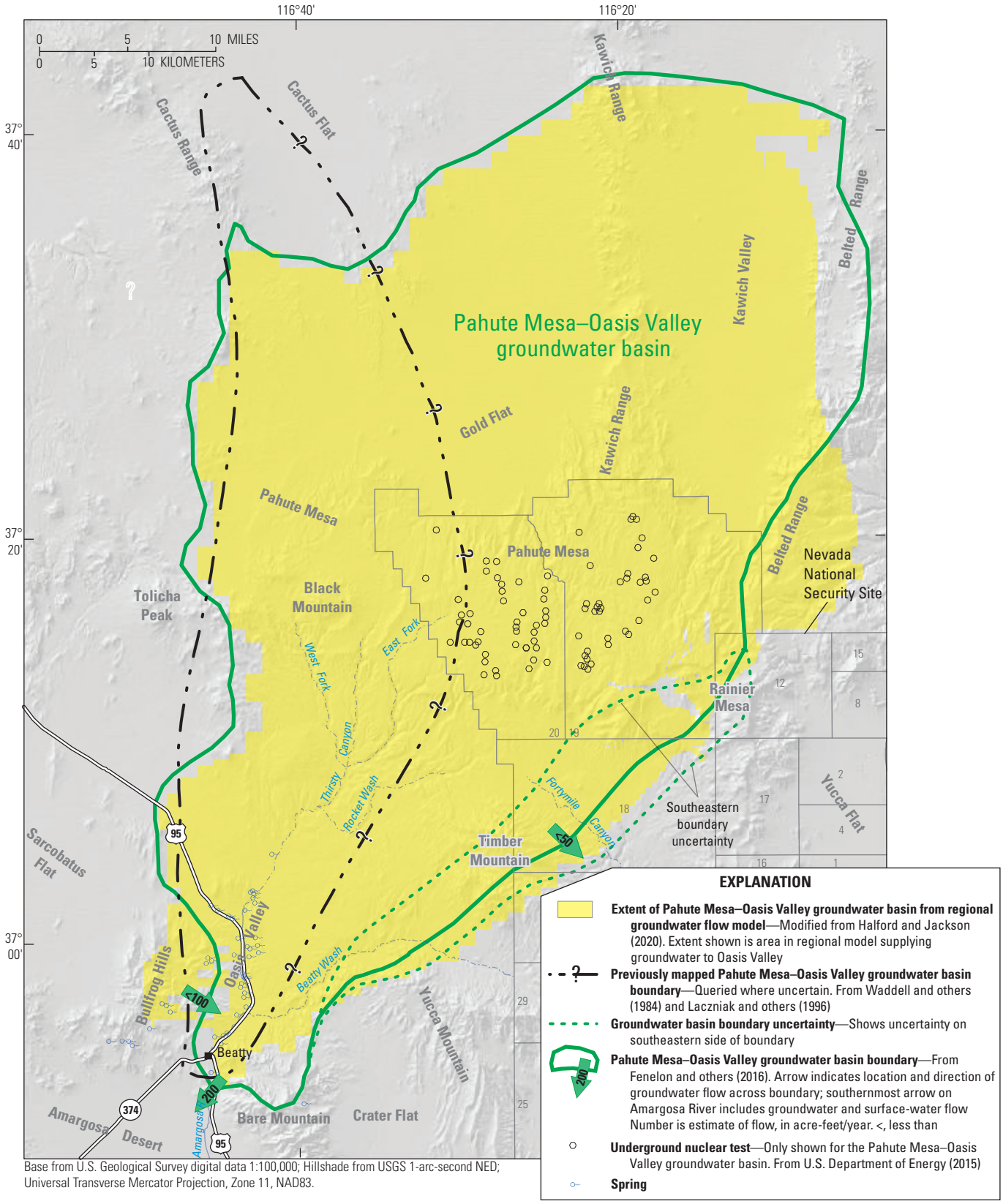

Figure 21. Pahute Mesa–Oasis Valley groundwater basin boundary showing area of boundary uncertainty and comparison to previously published extents.

About 200 acre-ft/yr of groundwater entering the northern part of the AFFCR groundwater basin is interbasin flow derived from the southern terminus of the PMOV basin (fig. 21). An estimated 100 acre-ft/yr of groundwater underflows the PMOV basin boundary through alluvium underlying the Amargosa River (Reiner and others, 2002). Additionally, water in the Amargosa River that originates in the PMOV basin as runoff from spring flow and flood events flows southward past USGS gaging station 10251217 (Amargosa River at Beatty, Nev.) and into the Amargosa Desert. About 100 acre-ft/yr of this surface water is estimated to infiltrate the river channel as groundwater recharge in the AFFCR groundwater basin (U.S. Geological Survey, 2015; Stonestrom and others, 2007).

Some groundwater seeps eastward across the PMOV basin boundary from Bullfrog Hills (fig. 21), but the flux is considered negligible (Fenelon and others, 2016). These hills consist of low-permeability rocks and contain small springs that are sourced by localized flow paths from recharge in the nearby highlands (White, 1979; Reiner and others, 2002). Most of the groundwater from the highlands is captured by the springs with only a minor component crossing into the PMOV basin. A regional, steady-state, groundwater-flow model simulated 60 acre-ft/yr of flow from Bullfrog Hills into Oasis Valley (Halford and Jackson, 2020).

A final small source of interbasin flow is surface water in Fortymile Canyon that provides recharge to the AFFCR groundwater basin (fig. 21). The downgradient part of this ephemeral drainage flows infrequently during wet periods (less than once a year, on average). Savard (1998) estimated a long-term recharge rate of about 90 acre-ft/yr from streamflow infiltration through the channel of Fortymile Canyon and Fortymile Wash. No more than 50 acre-ft/yr of this infiltration is attributed to precipitation falling in the catchment area of the PMOV basin.

Boundary Uncertainty

Areas of uncertainty in the no-flow boundary of the PMOV groundwater basin were identified by Fenelon and others (2016). Two areas were identified where the potential for significant unaccounted flow could occur and a third area was identified that could affect the fate of radionuclide transport from some of the southeasternmost underground nuclear tests. The first two areas are the northwestern PMOV boundary, bounded by Cactus and Kawich Ranges, and the northeastern PMOV boundary, bounded by Kawich and Belted Ranges. The third area of uncertainty is the southeastern PMOV boundary between Bare Mountain and Rainier Mesa. Other less important areas of boundary uncertainty are discussed in Fenelon and others (2016).

Uncertainty in the northwestern PMOV boundary was analyzed thoroughly in Fenelon and others (2016, p. 24–28) and is summarized in this report. Location of the northwestern boundary is uncertain because water-level data in Cactus Flat are insufficient to determine if groundwater flows into or away from the PMOV basin. An alternative boundary was investigated that incorporated 520 mi^2 of Cactus Flat and assumed that water flows from Cactus Flat into the PMOV basin.

The alternative boundary incorporating Cactus Flat was not a plausible alternative based on multiple lines of evidence (Fenelon and others, 2016). First, a regional water-budget analysis suggested that too much recharge was generated in the alternative PMOV basin compared to the discharge from the basin. Second, a numerical groundwater-flow model of the alternative basin required physically unrealistic transmissivities in Gold Flat to simulate large amounts of groundwater flowing southward from Cactus Flat into Gold Flat. The large amounts of water were generated by recharge in the ranges bounding Cactus Flat. Third, a chloride mass-balance analysis demonstrated a poorer fit to chloride concentrations in discharge waters at Oasis Valley using the larger alternative PMOV basin.

The northeastern boundary of the PMOV basin at the northern end of Kawich Valley (fig. 22) likely is a no-flow boundary (Fenelon and others, 2016). Water-level measurements in this area are sparse and the water-level gradient is relatively flat, resulting in boundary uncertainty between the PMOV and Railroad Valley South groundwater basins. Despite this uncertainty, the actual boundary cannot extend significantly northward of the currently mapped extent because of groundwater-budget constraints.

Groundwater-budget constraints support the location of the northeastern boundary of the PMOV basin, as defined by Fenelon and others (2016). Groundwater in southern Reveille and Railroad Valleys generally flows from recharge areas that include Quinn Canyon, Reveille, and central Kawich Ranges to discharge areas primarily north of Railroad Valley South groundwater basin (fig. 22). Recharge generated from Belted and southern Kawich Ranges flows southward from Kawich Valley to the discharge area in Oasis Valley (Fenelon and others, 2016, plate 1). Greater amounts of precipitation and recharge occur in highland areas surrounding the Railroad Valley South groundwater basin, compared to the PMOV basin, because highland areas within the PMOV basin have altitudes up to 8,500 ft, whereas highland areas surrounding Railroad Valley South groundwater basin have altitudes up to 11,300 ft (Fenelon and others, 2016, plate 1). Groundwater in southern Reveille and Railroad Valleys likely flows 40 mi north to a major (80,000 acre-ft/yr; Van Denburgh and Rush, 1974) discharge area rather than 50 mi south to a relatively small (5,900 acre-ft/yr; Reiner and others, 2002) discharge area in Oasis Valley (Fenelon and others, 2016, plate 1). Extending the northeastern PMOV boundary farther northward to intercept additional recharge water is not necessary because regional water-balance analyses indicate that recharge generated within the PMOV basin is sufficient to support discharge in Oasis Valley (Fenelon and others, 2016; Halford and Jackson, 2020).

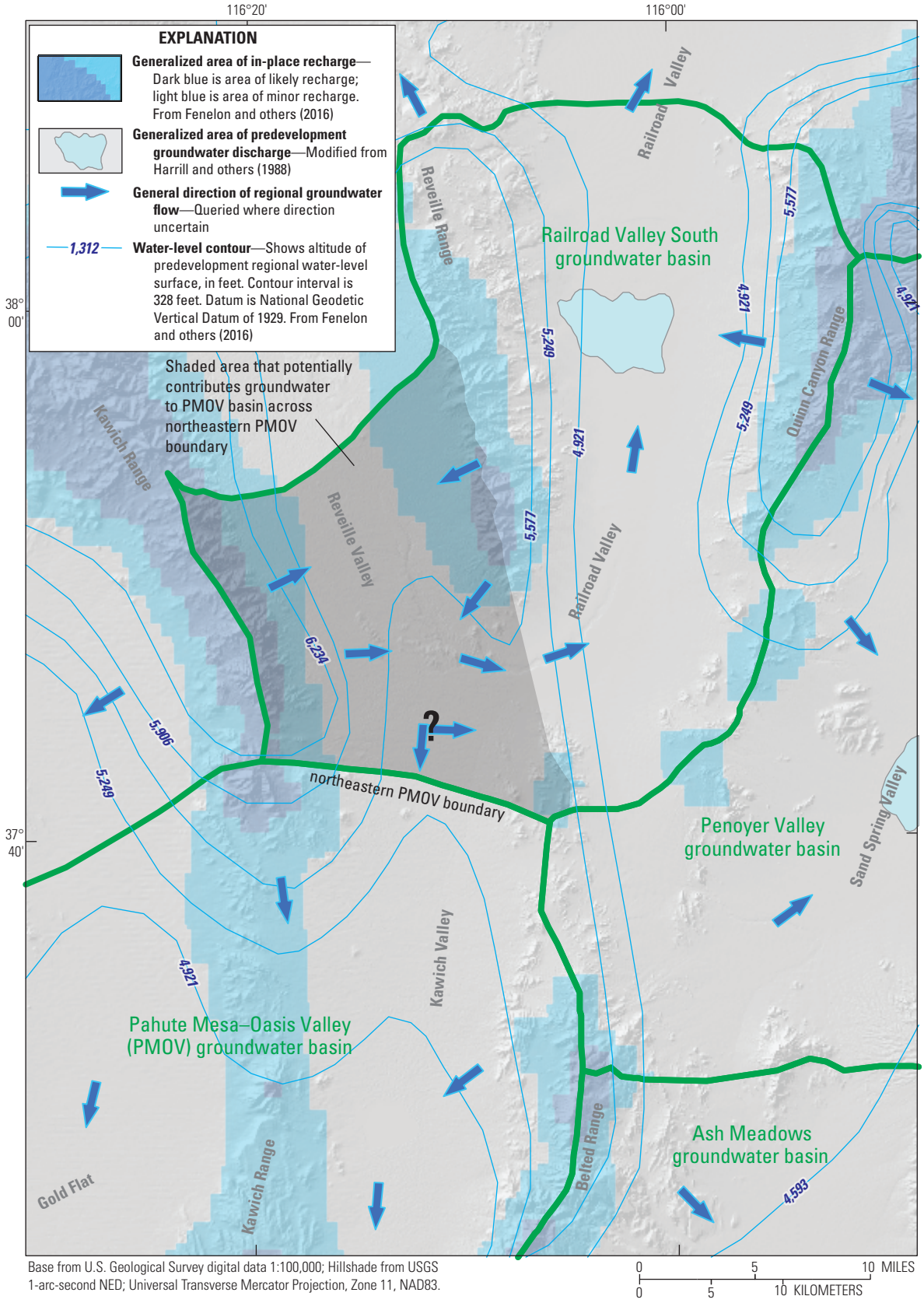

Figure 22. Recharge areas and groundwater-flow paths in Railroad Valley South and northeastern Pahute Mesa–Oasis Valley groundwater basins, southern Nevada.

If the northeastern PMOV boundary actually extends to the northern end of its uncertainty range (fig. 22), less than 450 acre-ft/yr of groundwater is expected to be generated from additional recharge based on a local Maxey-Eakin relation. The Maxey-Eakin method (Maxey and Eakin, 1951; Avon and Durbin, 1994; Fenelon and others, 2016) is a simple analysis that balances measured discharge with estimated recharge within a groundwater basin. Recharge is estimated by scaling a precipitation distribution to the measured discharge. The area of Reveille Valley that possibly contributes a component of flow to the PMOV basin is 120,000 acres (see dark shaded area in fig. 22). The annual precipitation volume for this area from a modeled precipitation distribution (PRISM Climate Group, 2012) totals 97,000 acre-ft for areas where precipitation rates exceed 0.4 ft/yr. Using a local modified Maxey-Eakin relation, 900 acre-ft/yr of recharge is estimated for the northeastern area of uncertainty. This estimate assumes that 0.9 percent of the annual precipitation volume in excess of 0.4 ft/yr is converted to recharge (Fenelon and others, 2016). The 900 acre-ft of recharge either moves as groundwater flow from Reveille Valley to Railroad Valley or bifurcates, with part of the flow moving southward into the PMOV basin through Kawich Valley (see queried flow arrows on fig. 22). Less than 50 percent, or less than about 450 acre-ft/yr, of the local recharge can potentially flow southward to Oasis Valley because local hydraulic gradients require a significant component of the flow in Reveille Valley to move eastward into Railroad Valley. An estimated flow of 0 to 450 acre-ft/yr from this area of uncertainty is similar to estimates of 1,000 acre-ft/yr or less from previous studies (Blankennagel and Weir, 1973; Van Denburgh and Rush, 1974; Harrill and others, 1988; Fenelon and others, 2016).

The most critical aspect of the current PMOV basin boundary, with respect to radionuclide transport from nuclear tests on Pahute Mesa, is uncertainty associated with the location of the southeastern boundary. Uncertainty along this boundary segment allows for the actual boundary to be as much as 2–4 mi northwest or 1–2 mi southeast of the mapped boundary (fig. 21). Uncertainty ranges were developed by extending the boundary as far north or south as possible while still honoring water-level measurements and hydraulic gradients. Rainier Mesa, Timber Mountain, and Bare Mountain were used as anchor points, based on the assumption that these highlands contain low-permeability rocks or sufficient recharge to create groundwater mounds beneath them (see "Timber Mountain" section for details). The envelope of uncertainty shown on figure 21 does not incorporate any of the Pahute Mesa nuclear tests, demonstrating that transport from these tests will be directed toward Oasis Valley.

If a component of groundwater moves across the southeastern boundary into Crater Flat in the vicinity of wells *ER-0V-03c* and *Beatty Wash Windmill*, then the amount of flow likely is limited based on geologic evidence (Fridrich and others, 1999). Groundwater flow into Crater Flat west of well *ER-0V-03c* is prohibited because basin fill and volcanic rocks in Oasis Valley terminate against siliciclastic and carbonate rocks in Bare Mountain along the Bullfrog Hills–Fluorspar Canyon detachment (plate 1). The carbonate rocks, if permeable, are localized, discontinuous, northward-dipping blocks enclosed within siliciclastic rocks composed of low-permeability argillite and fine-grained quartzite (Fridrich and others, 1999; Hildenbrand and others, 1999). Therefore, rocks in Bare Mountain are a barrier to groundwater flow (Schenkel and others, 1999). A groundwater-flow path has been postulated into Crater Flat between wells *ER-0V-03c* and *Beatty Wash Windmill* (plate 1) based on isotopic analysis (see fig. 18 of Kwicklis and others, 2005). If southerly flow into Crater Flat occurs, the amount of flow is limited to a 5-mi-wide, east-west corridor of saturated volcanic rocks (U.S. Department of Energy, 2020a). Estimated flow through the postulated flow corridor would be about 15 acre-ft/yr. This estimate was computed using a horizontal hydraulic gradient of 125 ft/mi between wells *ER-0V-03c* and *Crater Flat 1*, and an estimated transmissivity of 1,100 ft^2/d, which was based on the geometric mean of transmissivity estimates from wells *Crater Flat 1* and *Beatty Wash Windmill* (Frus and Halford, 2018).

Uncertainty in the location of the southeastern segment of the PMOV basin boundary was tested with a regional groundwater-flow model that simulated predevelopment (steady-state) and groundwater-development conditions in the PMOV, AFFCR, and Ash Meadows groundwater basins (Halford and Jackson, 2020). This numerical model can reasonably quantify flow across the southeastern PMOV boundary because greater than 97 percent of predevelopment discharge was specified, and recharge was estimated based on basin water balances. The shaded area in figure 21 is the extent of the PMOV basin, as defined by simulation results of predevelopment flow. Results indicate that the current location of the southeastern boundary is a good approximation of the groundwater divide (fig. 21). The shaded area in figure 21 that is outside the southeastern boundary defined by Fenelon and others (2016) accounts for less than 4 percent (230 acre-ft/yr) of the total discharge in Oasis Valley (Halford and Jackson, 2020).

The southeastern boundary, defined by predevelopment water levels and discharges, is susceptible to pumping because water-level declines near the boundary can cause the boundary to move. Regional analysis of historical (1913–2010) and potential future (2011–2100)[2] groundwater development indicates that the PMOV groundwater basin largely is isolated from the effects of pumping in neighboring AFFCR and Ash Meadows groundwater basins (Halford and Jackson, 2020). Water-level declines from historical and potential future pumping within the PMOV basin are small (less than 5 ft) and do not extend to the PMOV basin boundary.

[2]Halford and Jackson (2020) used a regional numerical model to simulate a potential future groundwater-development scenario in which pumping at current (2010) rates is assumed to continue through 2100.

Uncertainty in the location of the eastern segment of the PMOV basin boundary along the Belted Range (fig. 21) also was tested with a regional groundwater-flow model (Halford and Jackson, 2020). The shaded area in figure 21 east of the Belted Range, which is outside of the PMOV basin boundary defined by Fenelon and others (2016), is associated with a net inflow of 20 acre-ft/yr into the PMOV basin (Halford and Jackson, 2020). A simulated net inflow of 20 acre-ft/yr is negligible compared to the total discharge from the PMOV basin. Other shaded areas outside of the PMOV basin boundary defined by Fenelon and others (2016) also are associated with negligible amounts of groundwater, indicating that the PMOV basin extent defined by Fenelon and others (2016) is a good approximation of the area contributing groundwater to Oasis Valley.

Lower Flow System and Lower Basin Boundaries

The *lower boundary of the groundwater-flow system* defines the active part of the flow system where nearly all flow occurs. The lower flow system boundary was determined from detailed analyses of hydraulic conductivity (and transmissivity) with depth. Depth-analysis results indicate that greater than 90 percent of the total transmissivity contributing to groundwater flow and radionuclide transport occurs within 1,600 ft of the water table (fig. 18). As a result, most of the flow in the PMOV basin occurs in shallow saturated rocks that are within 1,600 ft of the water table. Therefore, the lower flow system boundary is defined at 1,600 ft below the water table.

Hydrologic sections on plate 2 show the active (high transmissivity) and less active (low transmissivity) parts of the flow system. The dashed line on the hydrologic sections in plate 2, which separates the active and less active parts of the flow system at a depth of 1,600 ft below the water table, is the lower flow system boundary. Groundwater in the deep (less active) part of the system has limited interaction with the shallow part because flow is restricted by rocks with low hydraulic conductivities.

The *lower boundary of the PMOV basin* defines the lower boundary of radionuclide migration and was determined from consideration of likely radionuclide transport depths. The lower PMOV basin boundary extends below the lower flow system boundary and encompasses some of the deep low-permeability rocks, because radionuclides from some of the large underground nuclear tests were emplaced in these deep rocks. Depths of detonation and radionuclide distributions around the nuclear tests were considered when defining the lower PMOV basin boundary. Radionuclides shortly after a nuclear test are assumed to be distributed within an exchange volume of no more than three cavity radii (U.S. Congress, 1989; U.S. Department of Energy, 2018). Cavity radius, and three cavity radii, are calculated based on the reported maximum yield from U.S. Department of Energy (2015) and equation 1 of Pawloski (1999). Of the 82 Pahute Mesa underground nuclear tests, 14 tests have exchange volumes, assuming three cavity radii, that extend below the active flow system boundary at 1,600 ft below the water table (Stoller-Navarro Joint Venture, 2009, table 4-3). These 14 nuclear tests include 13 of the 16 largest tests, based on maximum yield, on the NNSS (U.S. Department of Energy, 2015).

The lower boundary of the PMOV basin is defined at a depth of 4,000 ft below the water table. Hydrologic sections on plate 2 are truncated at the lower boundary of the basin. A depth of 4,000 ft below the water table is sufficiently deep to encompass all nuclear tests and tritium plumes. The deepest nuclear test beneath the water table is HANDLEY, which was detonated at about 2,700 ft below the water table (section *F–F'* on plate 2). The exchange volume for HANDLEY, assuming three cavity radii, extends to about 3,700 ft below the water table (Stoller-Navarro Joint Venture, 2009, table 4-3). Extending the lower PMOV basin boundary to a depth greater than 4,000 ft below the water table is not necessary because test-induced alteration of the rocks surrounding a nuclear test and thermal buoyancy effects cause upward migration of tritium and other mobile radionuclides from a nuclear test, as explained below.

Detonation of a nuclear device underground locally alters the surrounding rock. When a nuclear device is detonated, an immense amount of thermal and mechanical energy is released (U.S. Congress, 1989). The explosion produces high temperatures and pressures in the rocks surrounding the detonation location. Vaporization and compression of rocks surrounding the detonation point create and expand an open, approximately spherical cavity volume filled with steam and vaporized rock (Carroll and Lacomb, 1993). Formation of the open cavity is generally followed by a collapse of overburden material and the generation of a rubblized vertical chimney hours to days after the test. This collapse evolves from the reduction of cavity temperatures and pressures and the condensation of most cavity gases into melted rock and water (Carroll and Lacomb, 1993). The composition of the cavity zone after collapse includes a mixture of melted rock and infallen rubble. The chimney might extend as far upward as the ground surface in the form of a surface crater or up to some intermediate elevation. Beyond the cavity, the explosion generates a compressive shock wave that moves radially away through more distant, intact rock and produces permanently altered zones of crushed, compressed, and fractured rock around the cavity (Carroll and Lacomb, 1993).

Following the detonation, residual test-related radionuclides will be present in the cavity, melted rock accrued at the bottom of the cavity and, to some extent, in the rocks surrounding the cavity. The subsequent movement of radionuclides within the cavity-chimney system will be influenced by the residual heat, degree of water saturation, and permeability of the altered rocks (Carle and others, 2003). The residual heat and generally higher permeability of the cavity-chimney system, compared to the native rock, can drive water and (or) gas phase movements upward through the chimney in a convectively (buoyancy) driven recirculation process (Pawloski and others, 2001), which, in turn, can transport radionuclides resident in water and (or) gas phases outward and upward, away from the cavity (Carle and others, 2003). In this sense, the chimney becomes a potential pathway for radionuclides to move into permeable zones above the cavity. For tests conducted below the water table, much of the movement will occur under saturated flow conditions. Outside of preexisting background hydraulic gradients, there are few test-related forces that tend to drive fluid flow and radionuclide transport to deeper locations from the cavity-chimney system. Downward movement of radionuclides from the cavity-chimney system also is inhibited by relatively impermeable melted rock at the bottom of the cavity.

Potential radionuclide migration from underground nuclear tests beneath Pahute Mesa will occur primarily in shallow permeable rocks within 1,600 ft of the water table and, to a lesser extent, in deep, low-permeability rocks from 1,600 to 4,000 ft below the water table. Vertically upward movement of radionuclides into shallow, permeable rocks is evidenced by higher measured tritium in shallow wells compared to deeper wells downgradient of nuclear tests (Navarro-Intera, LLC, 2015; U.S. Department of Energy, 2019). For example, tritium from the BENHAM nuclear test has been detected in shallow well *ER-20-5-1*, open to TSA, and deeper well *ER-20-5-3*, open to CHLFA5 (section *D–D´* on plate 2). The open intervals of these shallow and deep wells are about 1,900 and 600 ft above the BENHAM test burial depth, respectively (appendix 3). Measured tritium in shallow well *ER-20-5-1* is 300 times greater than the measured tritium in deeper well *ER-20-5-3* because the permeability of the TSA likely is higher than the permeability of the deeper CHLFA5.

Groundwater Budget

The groundwater budget consists of recharge entering the PMOV basin by infiltration of precipitation and discharge leaving the basin through springs and pumped wells. The groundwater system is assumed to be in steady state, where recharge and discharge are approximately in balance. Changes in groundwater storage resulting from temporal variability in recharge and small amounts of groundwater pumping negligibly affect the long-term (century-scale) steady-state budget.

Discharge

More than 98 percent of natural groundwater flow in the PMOV basin discharges from springs and seeps at Oasis Valley (Reiner and others, 2002; Fenelon and others, 2016). Discharge from Oasis Valley is thought to be controlled by the general thinning of volcanic rocks toward Oasis Valley and their termination against low-permeability siliciclastic rocks, which crop out near Oasis Valley (section *I–I´* on plate 2; Fridrich and others, 1999; Reiner and others, 2002). The siliciclastic rocks impede southward flow and force groundwater upward through faults in the Oasis Valley area (Laczniak and others, 1996). An estimated 5,900 acre-ft/yr of groundwater discharges to Oasis Valley from springs or by diffuse upward flow into shallow alluvium, where the water is evaporated or transpired by phreatophytes. Spring locations and areas of evapotranspiration are shown on plate 1. Subsurface outflow from Oasis Valley to the Amargosa Desert through alluvium in southern Oasis Valley accounts for the remaining natural discharge in the PMOV basin and is estimated to be about 80 acre-ft/yr (Reiner and others, 2002).

The natural groundwater-discharge estimate for Oasis Valley is reasonably certain because this estimate is based on a detailed, site-specific, field study (Reiner and others, 2002). Discharge to springs and seeps is estimated to be accurate to ± 15 percent, or to range from 5,000 to 6,800 acre-ft/yr (Fenelon and others, 2016) with a best estimate of 5,900 acre-ft/yr. Subsurface outflow into the Amargosa Desert is estimated to range from 30 to 130 acre-ft/yr with a best estimate of 80 acre-ft/yr (Reiner and others, 2002).

Groundwater has been withdrawn in the PMOV basin from wells on the NNSS and near Beatty since 1963 (fig. 1). Through 2018, a total of 12,700 acre-ft was withdrawn from 14 wells in 10 boreholes on the NNSS (U.S. Geological Survey, 2019b). Three of these wells—*U-20 WW*, *UE-19c WW*, and *WW-8 (30-2031 ft)*—accounted for 90 percent of the withdrawals. Groundwater withdrawals for the town of Beatty are the only other significant source of pumping in the PMOV basin. Three public-supply wells located in Beatty account for most of the withdrawals. From 1963 to 2010, a total of about 13,000 acre-feet were withdrawn from these wells (Elliott and Moreo, 2018). During this period, an additional estimated 330 acre-ft was withdrawn from 22 domestic wells near Beatty (Elliott and Moreo, 2018). Average withdrawals in the PMOV basin of 500 acre-ft/yr from the NNSS and Beatty account for less than 10 percent of the 5,900 acre-ft/yr of natural, groundwater discharge from the basin.

Less than 0.2 percent of groundwater has been withdrawn from storage in the PMOV basin from 1963 to 2018. Groundwater withdrawals from storage were calculated as the ratio of total groundwater withdrawals to total groundwater storage in the PMOV basin. Total groundwater withdrawals through 2018 in the PMOV basin are about 26,000 acre-ft. Total groundwater storage in the 920,000-acre PMOV basin is estimated to be 15,000,000 acre-feet, assuming a fractured-rock effective porosity of 0.01 and a saturated thickness of 1,600 ft for the active part of the flow system.

Groundwater development in adjacent groundwater basins has not captured natural groundwater discharge or groundwater from storage in the PMOV basin. Results from a regional groundwater-flow model, which simulated predevelopment conditions and groundwater development from 1913 to present-day (2020), indicate that simulated water-level declines from regional pumping in nearby AFFCR and Ash Meadows groundwater basins do not extend into the PMOV basin (Halford and Jackson, 2020). This simulated result is consistent with measured water-level data in wells within and near the PMOV basin boundary. Water levels in these wells are unaffected by pumping and show multi-decadal, rising water-level trends in response to multiple winters with greater-than-average precipitation (Jackson and Fenelon, 2018).

Recharge

Recharge in the PMOV basin occurs on volcanic highlands, such as Pahute Mesa and Timber Mountain, and as infiltration of runoff from highlands into alluvial fans. Recharge primarily replenishes volcanic and alluvial aquifers in the basin. Most recharge occurs when winter precipitation collects in surface fractures and openings of permeable volcanic rocks and infiltrates downward by way of interconnected fractures or through the rock matrix to depths beyond the influence of evaporation and transpiration.

Lesser amounts of recharge occur in highland areas composed of siliciclastic and other low-permeability rocks, such as Kawich and Belted Ranges. On these highlands, most of the precipitation from snowmelt or high-intensity rainfall events is conceptualized to run off as surface or shallow subsurface flow. Recharge from surface runoff occurs where streamflow moves downgradient on top of low-permeability rocks in highland areas and infiltrates adjacent, permeable, alluvial-fan deposits or basin fill in ephemeral channels at lower elevations (Hevesi and others, 2003; Flint and others, 2004). Recharge from shallow subsurface flow occurs where infiltrating water encounters low-permeability rocks above the regional potentiometric surface and forms perched or semi-perched zones. These zones are unconfined, saturated volumes of groundwater that form localized recharge mounds and are separated from the underlying regional groundwater system by discontinuous low-permeability rocks. The shallow saturated zone is considered perched if the top of the underlying low-permeability rocks is unsaturated, whereas a semi-perched zone has no intervening unsaturated zone. Perched zones are known to occur east of the study area in Rainier Mesa (Winograd and Thordarson, 1975) but have not been observed in the PMOV basin. Semi-perched conditions have been observed in multi-well completions on Pahute Mesa. Low-permeability rocks forming perched and semi-perched zones impede infiltration because vertical hydraulic conductivities of these rocks are less than local infiltration rates. As a result, water is impounded, and excess infiltrating water is diverted laterally. This excess water moves laterally downslope until sufficiently permeable, saturated rocks of the regional system are encountered that can accept the shallow flow (Feth, 1964; Winograd, 1971).

A conceptual distribution of recharge areas in the PMOV basin is shown on plate 1. The delineation of areas of potential recharge was guided by (1) modeled net infiltration derived from a distributed parameter, local water-balance model (Hevesi and others, 2003; Hevesi, 2006); (2) highland areas exceeding altitudes of about 6,000 ft; and (3) drainage channels with large ephemeral discharges and wide valley bottoms. The east side of Pahute Mesa, centered on NNSS Area 20, likely provides a large proportion of the recharge in the PMOV basin (Hevesi, 2006; Fenelon and others, 2016). Most recharge occurring in eastern Pahute Mesa is consistent with groundwater chloride concentrations, which are low in Area 20 of eastern Pahute Mesa and to the south near Timber Mountain (Rose and others, 2006). These areas of relatively high recharge rates result in less evapo-concentration of initial chloride concentrations in precipitation (Cooper and others, 2013).

Recharge Components

The dominant component of recharge is slow, steady, diffuse percolation through the unsaturated zone. Diffuse recharge is difficult to observe in water-level records because this steady source of recharge to the water table is offset by a steady drainage of water out of the flow system, resulting in no net change in groundwater storage. Fenelon and others (2016) estimated that 150,000,000 acre-ft of pore water are stored in the unsaturated zone of the PMOV basin and that residence times of this pore water may be 15,000 years or more. These calculations suggest that some modern-day infiltration below the root zone will not reach the water table for many thousands of years and that diffuse recharge entering the water table today is old (greater than 10,000 years). To restate, the dominant component of recharge is old water within pore spaces in the unsaturated zone that slowly percolates through the unsaturated zone and recharges the groundwater system. This conceptual idea of old water recharging the groundwater system is consistent with observations of isotopically light deuterium and oxygen 18 compositions in water from wells on Pahute Mesa and central Oasis Valley (Thomas and others, 2002; Kwicklis and others, 2005).

A second, minor component of recharge in the PMOV basin occurs as pulses of episodic recharge following wet winters. Episodic recharge is observed in the PMOV basin as a rise in groundwater levels following a wet winter, where water levels begin to rise within three months to one year after a winter that is 125 to 200 percent wetter than average (Jackson and Fenelon, 2018). Rising water levels after wet winters are observed in many wells in the PMOV basin, suggesting that episodic recharge is pervasive. A minor amount of rapid recharge through an unsaturated zone in excess of 1,000 ft requires preferential flow through faults and fractures.

Reconciling Old Groundwater with Modern Recharge Inputs

The isotopically light deuterium and oxygen 18 compositions of groundwater on Pahute Mesa and central Oasis Valley are inconsistent with modern recharge, which is isotopically heavy (Thomas and others, 2002; Kwicklis and others, 2005). Isotopically light groundwater suggests that recharge to the water table at Pahute Mesa is from precipitation during a colder climatic period such as the late Pleistocene. Kwicklis and others (2005) concluded that isotopically light groundwater beneath Pahute Mesa can be explained by a significant component of old (greater than 10,000 years) soil water entering the water table, which has taken a long time to move through the thick unsaturated zone.

Reconciling the apparently contradictory observations of 10,000-year old recharge water and rapid water-level responses to winter recharge might be explained as follows. The observed rapid water-level responses result from minor amounts of recharge that occur primarily as focused, preferential flow in ephemeral channels, faults, or permeable outcrop areas. In contrast, the steady input of old, diffuse recharge is unobserved but dominates across large areas underlain by the thick unsaturated zone. The rapid recharge events at focused locations will cause hydraulic responses that propagate outward from the points of recharge and may be observed as pressure changes in distant wells where old recharge predominates. Hydraulic responses can propagate through volcanic rocks on Pahute Mesa because hydraulic connections are common, even across geologic structures and mapped confining units. For example, pumping-induced drawdown was observed in many instances in observation wells located as much as 3 mi away from pumped wells and across major geologic structures (Garcia and others, 2017; Russell and others, 2017).

Steady-State Assumption and Future Hydroclimate

Recharge water generated within the PMOV basin nearly equals the 5,900 acre-ft/yr of discharged water in Oasis Valley. Recharge nearly equals discharge because the basin boundary, with a few minor exceptions of interbasin flows (fig. 21), is a no-flow boundary. Additionally, long-term (century-scale) changes in groundwater storage are minimal because flow in the basin is dominated by steady-state conditions (Jackson and Fenelon, 2018). Therefore, although year-to-year recharge rates may fluctuate because of variability in episodic, winter recharge events, the long-term, average, annual recharge rate remains approximately constant.

Annual recharge rates are expected to decrease with future hydroclimate in the Death Valley regional flow system, which includes the PMOV basin (Meixner and others, 2016). Hydroclimate models predict that future (2050–2100) temperatures will be warmer than today (2020) in the southwestern United States (Garfin and others, 2013). Projected warmer temperatures are expected to decrease winter precipitation and snowpack and to increase evapotranspiration, which will decrease future rates of infiltration below the root zone (Garfin and others, 2013). However, the magnitude of decreased future infiltration is highly uncertain because of uncertainties in future winter precipitation (Meixner and others, 2016).

A decrease in annual recharge with time will result in a decrease in water discharged to Oasis Valley. Groundwater flow volumes and flow rates are a function of recharge rates, where flow volumes and rates will decrease as recharge decreases. The PMOV groundwater system is expected to equilibrate slowly to a gradual decrease in annual recharge, possibly on the order of one-hundred years or more. A long timescale for equilibration is expected because, as a rule, small groundwater basins have short equilibration (steady-state) timescales, whereas large groundwater basins, such as the PMOV groundwater basin, have long steady-state timescales (Jackson and Fenelon, 2018). Additionally, in areas where the unsaturated zone is thick, slow percolation rates cause a long lag time between infiltration of water below the root zone and recharge at the water table.

A future hydroclimate with less recharge is expected to decrease radionuclide transport rates. Radionuclide transport rates are a function of recharge and groundwater-flow rates. A decrease in recharge results in a decrease in groundwater-flow rates and advective flow velocities, which decreases radionuclide transport rates. Therefore, a decrease in the recharge rate would be approximately proportional to the decrease in the transport rate.

A steady-state future hydroclimate assumption is adequate, especially for forecasting the extent of tritium migration from Pahute Mesa. Tritium is the contaminant of concern in Pahute Mesa (U.S. Department of Energy, 2020b) because (1) tritium is the only radionuclide that has been (and likely will be) detected in groundwater samples above the Safe Drinking Water Act standards (U.S. Department of Energy, 2019), and (2) tritium currently is nearly 90 percent of the Pahute Mesa radionuclide inventory (Finnegan and others, 2016). The timing for tritium in nuclear-test cavities to radioactively decay to below the SDWA standards is about 150 years. Therefore, a century-scale, steady-state climate assumption is adequate for forecasting tritium transport.

Regional Potentiometric Contours and Flow Paths

The potentiometric contours and flow arrows from plate 1 are reproduced on figure 23 for easier viewing. The potentiometric map is a two-dimensional portrayal of the "regional" groundwater surface, representative of 2020 conditions. The potentiometric map is not a water-table map, although in many areas the water table and mapped potentiometric surface are coincident. The map is intended to represent the potentiometric head in the most transmissive rocks at any given horizontal location. As such, the map ignores vertical gradients or areas where two aquifers with different potentiometric surfaces are present. In most areas of the PMOV basin, a single potentiometric surface is adequate to represent hydraulic heads through the flow system. In areas with spatially limited water-level data, or where all water levels are from shallow wells, it could not be determined if these limited data best represent hydraulic head with depth. In these areas, data were contoured with the assumption that they represent the regional groundwater surface. In areas where water levels in shallow wells are elevated relative to the contoured potentiometric surface, the shallow water levels are denoted as elevated on plate 1 but not contoured. Likewise, anomalously low water levels in wells relative to the regional surface are denoted but not contoured.

Groundwater in the PMOV basin generally flows from north to south-southwest, discharging at Oasis Valley (fig. 23). Flow is southwesterly from the NNSS to Oasis Valley and is well-constrained by water-level data. The northern part of the basin (north of the NNSS) and the far western part of the basin are data limited. Potentiometric contours in these areas are uncertain, especially in high-altitude areas where groundwater mounding in low-permeability rocks may be much greater than shown.

The effect of regional-scale (basin-scale) horizontal anisotropy on groundwater flow is unknown but likely is minor within the PMOV basin. Hydraulic gradients and flow-path directions inferred from the potentiometric map (fig. 23; plate 1) assume an isotropic flow field. At a local scale (tens of feet), horizontal anisotropy can cause flow to take tortuous paths that may differ from the regional flow direction. At an intermediate scale, faults may function as transverse conduits or barriers through juxtaposition, where an aquifer is juxtaposed with another aquifer or with a confining unit, respectively. Because most faults on Pahute Mesa are oriented north-northeast, horizontal anisotropy may occur at an intermediate scale where aquifers and confining units are juxtaposed at faults. At a regional scale, anisotropy occurs because of low-permeability, north-south trending mountain ranges, such as the Belted and Kawich Ranges, that impede east-west flow. This type of horizontal anisotropy is accounted for in the potentiometric contours that were developed assuming that the mountains are composed of low-permeability rocks. Regional-scale anisotropy also could occur on Pahute Mesa because of a regional stress field that conceptually allows preferentially oriented faults to function as conduits and non-preferentially oriented faults to function as barriers (Parashar and others, 2018). Hydraulic evidence does not support the concept that dilated fault zones on Pahute Mesa function as regional conduits. Preferentially oriented faults with respect to the regional stress field (conceptual conduits) on Pahute Mesa are oriented from about N15°E to N30°E (Reeves and others, 2017). These fault-strike directions are slightly different from average regional flow directions of about N45°E, as determined from hydraulic-head measurements (plate 1). Even if there was an anisotropic flow field as a result of preferentially oriented faults, flow directions in most areas would deviate only slightly southward from flow directions on plate 1.

Relation of Transmissivity to Groundwater Flow

A simulated transmissivity distribution in the PMOV basin and regional potentiometric contours from plate 1 are shown in figure 24. The transmissivity distribution is derived from a one-layer, steady-state, groundwater-flow model, where simulated results were matched to measured water levels, groundwater discharges, and transmissivities (Fenelon and others, 2016). The transmissivity distribution is more certain where data constrain the model results, primarily in the western half of Area 19, Area 20, and downgradient of the southwestern part of Area 20. North and west of the NNSS, data are sparse, and the transmissivity distribution is poorly constrained. The transmissivity distribution in figure 24 indicates a high degree of heterogeneity for the volcanic rocks in the Pahute Mesa underground testing area (NNSS Areas 19 and 20; fig. 2), which is consistent with hydraulic-property analyses in this report (figs. 11, 16).

Saturated-rock transmissivities are a major control on groundwater flow between recharge and discharge areas. Groundwater-flow paths tend to converge in areas of high transmissivity and diverge in areas of low transmissivity. Groundwater flow is proportional to transmissivity; therefore, areas of high transmissivity allow more groundwater to move through a geologic medium compared to areas with low transmissivity. Rocks with moderate-to-high transmissivity are relatively continuous from Pahute Mesa to Oasis Valley (fig. 24). The highest transmissivities occur along a corridor on the eastern side of Area 20 that continues to the southwest off the NNSS (fig. 24). Groundwater flow converges in the eastern Area 20 corridor and moves downgradient toward Thirsty Canyon and Oasis Valley. Much of the northern and eastern parts of the PMOV basin are dominated by low-transmissivity rocks that limit groundwater flow.

Groundwater flow and transmissivity are inversely proportional to horizontal hydraulic gradients. Areas of low hydraulic gradients, portrayed by the large spacing between potentiometric contours in figure 24, coincide with areas of high-transmissivity rocks. These high-transmissivity rocks typically consist of LFA, WTA and AA (figs. 2, 11).

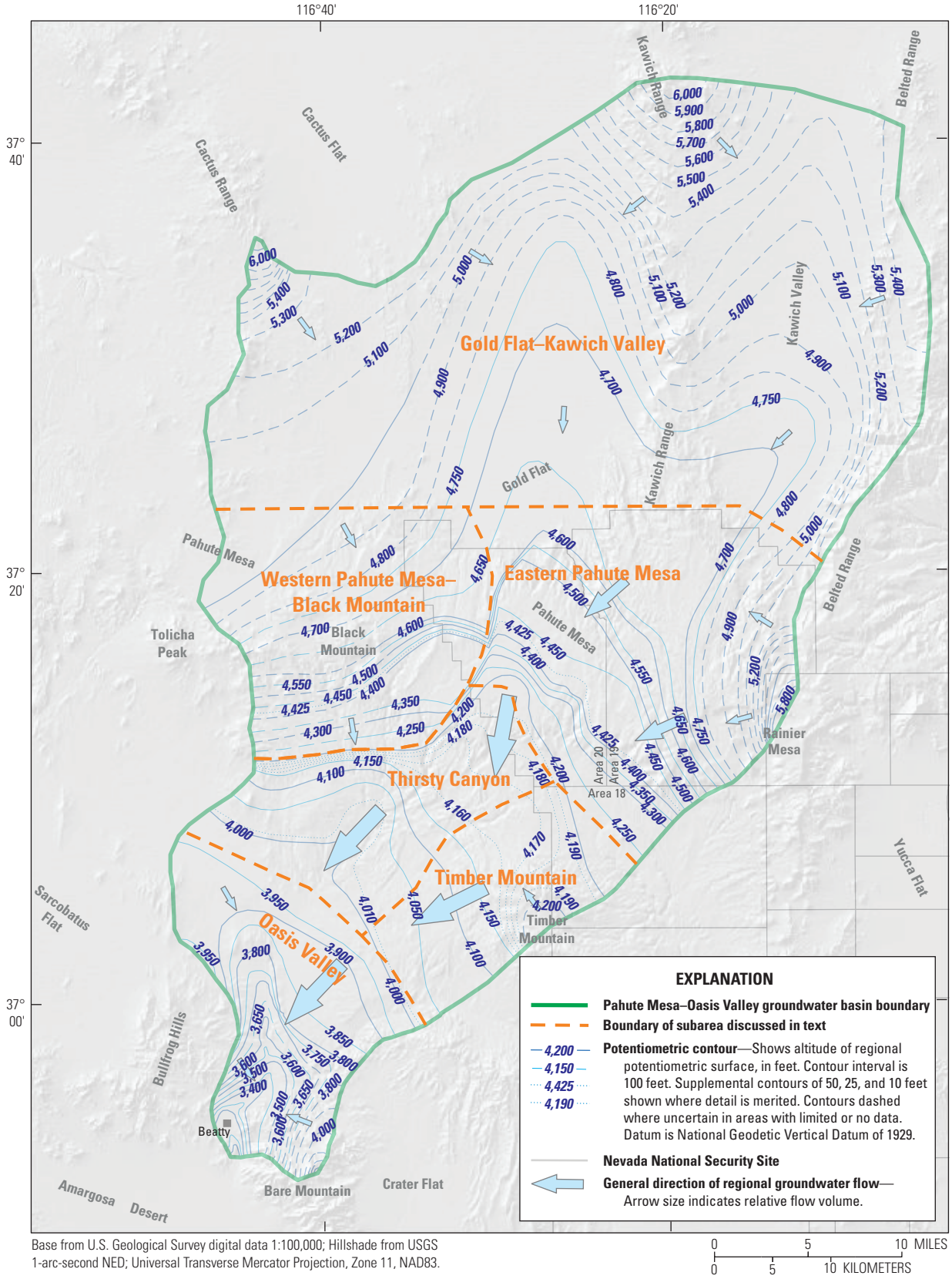

Figure 23. Potentiometric contours and regional groundwater-flow paths in the Pahute Mesa–Oasis Valley groundwater basin, southern Nevada.

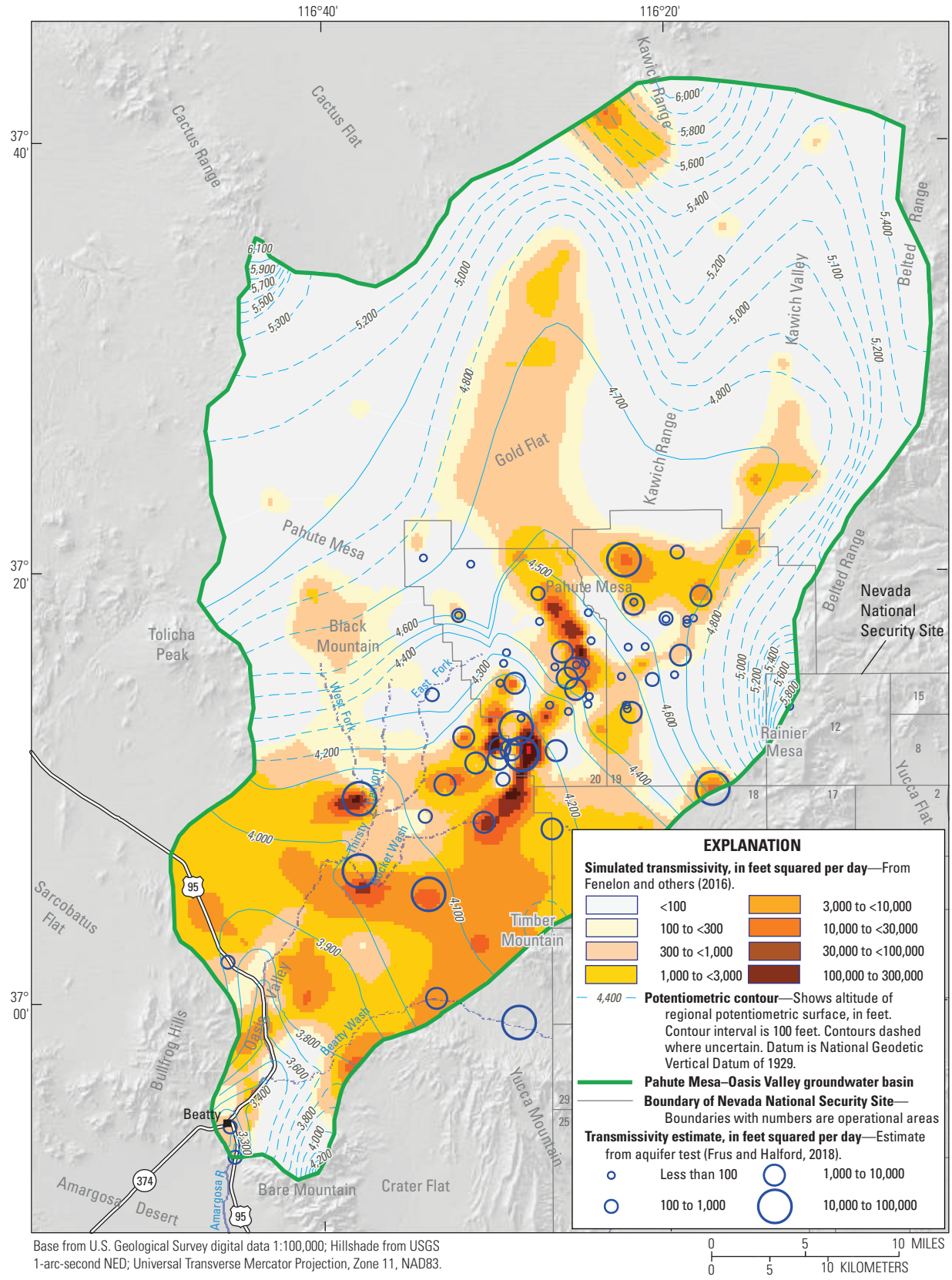

Figure 24. Regional potentiometric contours, estimated transmissivities at wells, and spatial distribution of modeled transmissivity in the Pahute Mesa–Oasis Valley groundwater basin, southern Nevada.

Conversely, areas of high hydraulic gradients, portrayed by the close spacing between potentiometric contours in figure 24, coincide with areas of low-transmissivity rocks that impede groundwater flow. These areas of high gradients generally coincide with areas of low-transmissivity siliciclastic (CCU), intrusive (GCU and IICU), or volcanic rocks in the study area (figs. 2, 11). High gradients also partially result from mounding of water in areas of recharge and constriction of groundwater flow into a small area, such as at Oasis Valley.

Water-Level Trends and Hydraulic Gradients

Water levels, measured from 1941 to 2016, are available for 577 wells in 227 boreholes in the PMOV basin and vicinity (appendix 1). Depth to water exceeds 1,500 ft in most wells in the Pahute Mesa underground testing area, whereas depth to water near Oasis Valley commonly is less than 50 ft. About 70 of the 577 wells had sufficiently long records to analyze for water-level trends (Jackson and Fenelon, 2018).

Of the 577 wells analyzed for this study, 387 had at least one water level identified as representative or potentially representative of steady-state conditions (appendix 2). These steady-state water levels, as well as 75 land-surface altitudes of springs in Oasis Valley, were used to determine hydraulic-head distributions and hydraulic gradients in the PMOV basin.

The hydraulic-head distribution, in part, controls the direction and rate of groundwater flow in the PMOV basin. The difference in hydraulic head along a given length of flow path defines the hydraulic gradient and describes the groundwater-flow potential. Hydraulic head commonly is equated to water-level altitude, and at a well, is estimated by subtracting a depth-to-water measurement from the land-surface altitude. This simple computation assumes that the water-level measurement is representative of steady-state groundwater conditions in the formation open to the well.

Water-Level Trends

An analysis of water-level trends through 2016 in the PMOV basin is presented in Jackson and Fenelon (2018). A summary of this analysis is provided below. Water-level trends were grouped into the following three categories based on the dominant hydrologic stress or stresses, in parentheses, affecting the trend in each well: nonstatic (wellbore equilibration); transient (pumping, nuclear testing); or steady state (recharge, evapotranspiration).

Nonstatic water-level trends are observed in a few wells open to low-permeability formations, where equilibration from the addition or removal of water in the borehole can take months to years. Interpreting these trends correctly is important for estimating accurate static water levels and in order not to attribute the trend to a transient stress, such as distant pumping. Nonstatic water levels are useful as ad hoc slug or injection tests to estimate hydraulic conductivities of low-permeability formations (Halford and others, 2005).

Transient trends are observed in wells affected by nuclear testing and (or) pumping. Pumping stresses are restricted to two small areas in the PMOV basin near Beatty, Nevada and on Pahute Mesa. About 1 ft of drawdown was observed in the alluvium in *Beatty Wash Terrace Well*, about 3 mi north of municipal withdrawal wells for Beatty. The drawdown is confined to a small part of the alluvial valley of the Amargosa River near Beatty (Halford and Jackson, 2020). Pumping drawdown on Pahute Mesa is restricted to a 2.2 mi^2 area centered on water-supply well *U-20 WW*. Water levels near well *U-20 WW* also may be permanently lowered by a nuclear test. Other observed nuclear-test effects on Pahute Mesa typically were short-lived (less than 1 yr) or localized to within 1 mi of a test.

Groundwater underlying most of the PMOV basin reflects steady-state conditions, where short-term changes in recharge and evapotranspiration cause water levels to naturally oscillate around long-term (century-scale) average conditions. Most wells in the PMOV basin with steady-state water levels had upward trends from 1995 to 2016. The upward trends resulted from a relatively wet period from 1968 to 2011, where episodic recharge from multiple wet winters caused a system-wide rise in water levels. Although water levels typically have risen throughout the PMOV basin, differences in trend patterns occur geographically. Differences result from the influences of transmissivity, unsaturated zone thickness, and (or) proximity to a recharge area, where each area has a unique, temporally variable, recharge pattern (Jackson and Fenelon, 2018).

Steady-state water-level trends from representative wells in the PMOV basin and vicinity are shown on figure 25. Most wells have overall rising trends from 1985 to 2017, although trends in many of the wells have flattened or begun declining since about 2014. This recent change in trend suggests that no significant episodic recharge events have occurred in the PMOV basin since about 2012.

Maximum measured water-level fluctuations for most wells in the PMOV basin are less than 5 ft, with many wells having overall changes of 1 to 2 ft (Jackson and Fenelon, 2018). These changes are small relative to horizontal hydraulic gradients in the PMOV basin, which range from 10 to 100 ft/mi. Therefore, natural water-level changes have little effect on groundwater velocities, radionuclide transport rates, or basin groundwater fluxes.

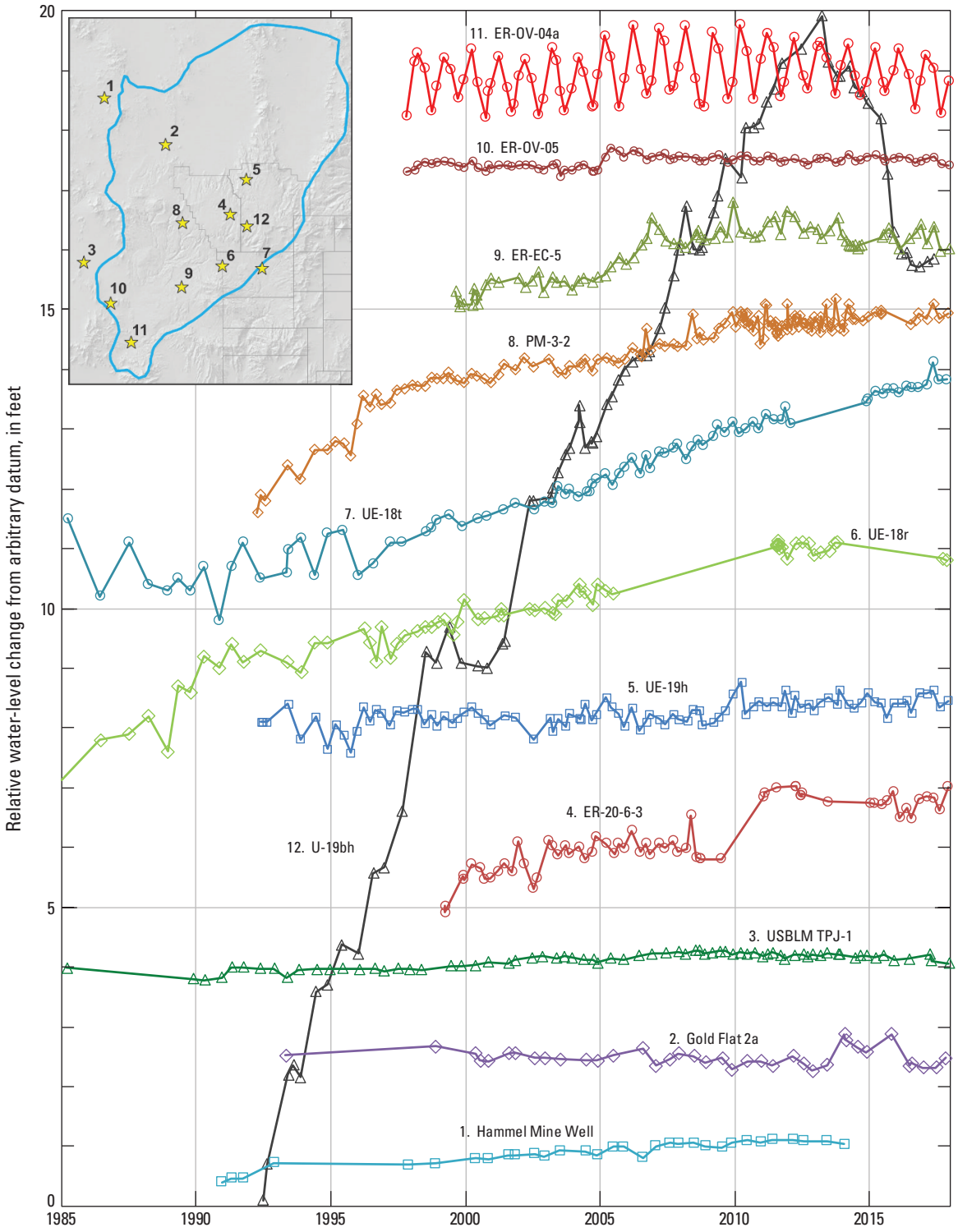

Figure 25. Steady-state water-level trends in the Pahute Mesa–Oasis Valley groundwater basin and vicinity, southern Nevada, 1985–2017.

Locally, water-level fluctuations can be large in wells open to low-permeability rocks, such as wells *U-19bh* (fig. 25) or *U-12s (1480 ft)* (appendix 1). Water levels in these wells have changed about 20 and 40 ft, respectively, in 25 years. These large water-level responses result from small amounts of recharge water seeping into rocks with low storativity, which amplifies the response. The amplified response is maintained for long periods because the low permeability of the rocks provides no mechanism for the water to efficiently drain. Therefore, large water-level responses may occur in low-permeability rocks directly connected to infiltration recharge, but smaller responses are typical in hydraulically connected rocks where most of the groundwater flow occurs in the PMOV basin.

Horizontal Hydraulic Gradients

Horizontal hydraulic gradients range from 10 to 100 ft/mi in most areas of the PMOV basin (fig. 26). This gradient range is typical of rocks that are relatively transmissive (greater than 100 ft^2/d; fig. 24). Horizontal gradients are lowest in the most transmissive areas, specifically along the central axis of the basin from southern Kawich Valley to northern Oasis Valley. Gradients along this axis typically range from 10 to 50 ft/mi and are consistently low (15 ft/mi) from southwestern Area 20 of the NNSS to northern Oasis Valley (fig. 26).

Horizontal gradients are highest in recharge areas with low-transmissivity rocks and where flow converges at the discharge area in Oasis Valley (figs. 24, 26). Low-transmissivity rocks occur in the highlands on the periphery of the basin. These rocks include nonwelded tuffs and granite at Rainier Mesa, siliciclastic rocks in the Belted, Kawich, and Cactus Ranges, and siliciclastic and carbonate rocks at Bare Mountain (Fenelon and others, 2016). Horizontal gradients in these highlands range from 100 to 400 ft/mi (fig. 26). Overall, the groundwater flux in these high-gradient areas is relatively low because, even though gradients in highlands are 4 to 10 times higher than gradients in the central part of the basin, transmissivities are 100 to 1,000 times lower in the highlands (fig. 24).

Calculating horizontal gradients between individual wells with small water-level differences requires caution. Considerations of head uncertainty and vertical gradients must be considered whenever horizontal gradients are calculated between well pairs. For example, an apparent northward hydraulic gradient is calculated in western Area 20 if water levels in wells *ER-20-5-3* and *U-20c (12-4800 ft)* are used (plate 1). These wells have estimated hydraulic heads of 4,190 and 4,184 ft, respectively (appendix 2). Between these wells, the hydraulic gradient is definitively southward, as demonstrated by a tritium plume detected at well *ER-20-5-3* from the BENHAM nuclear test, detonated at the site of well *U-20c (12-4800 ft)* (Wolfsberg and others, 2002; U.S. Department of Energy, 2019). The wrong gradient and flow direction result from uncertainties in hydraulic-head estimates at these wells. Measurement uncertainty is caused by a single uncalibrated measurement at well *U-20c (12-4800 ft)*. Temporal uncertainty occurs because the measurement was made more than 40 years before measurements in well *ER-20-5-3*. Vertical hydraulic gradients and water-column temperature effects also may contribute to small (generally less than 2 ft) hydraulic-head uncertainties because of differences in the open intervals of the wells.

Vertical Hydraulic Gradients

The direction of the vertical hydraulic gradient is upward in 12 of 58 well pairs, downward in 24 well pairs, and indeterminate in 22 well pairs (table 2). An indeterminate direction was assigned to well pairs where the water-level difference was judged to be less than the uncertainty in the paired measurements. Upward and downward gradients were categorized as large and small based on the water-level difference and the magnitude of the hydraulic gradient (fig. 27).

Blankennagel and Weir (1973, p. B21) concluded from packer tests in 17 Pahute Mesa boreholes that vertical gradients are indeterminate to depths of 2,500 ft below the saturated zone. Below these depths, Blankennagel and Weir stated that gradients are predominantly downward on the eastern part of Pahute Mesa (east of the red dashed line on fig. 27) and upward to the west. This spatial portrayal of vertical gradients implies that a large, hydraulically connected aquifer underlies the eastern part of Pahute Mesa at great depth (greater than 4,500 ft below land surface). Downward-moving groundwater would enter this hypothetical deep aquifer and be conveyed westward. West of the red dashed line on figure 27, groundwater would move upward and discharge to a shallower aquifer.

In contrast to the Blankennagel and Weir (1973) assessment, no clear spatial pattern is evident in the distribution of upward and downward gradients in the PMOV basin (fig. 27). This conclusion is based on evaluation of 58 well pairs for the current study (table 2), including a re-evaluation of the packer tests in the 17 boreholes evaluated by Blankennagel and Weir (1973). Vertical gradients are more likely to be downward to the east and upward to the west, but the pattern is not as consistent as portrayed in Blankennagel and Weir (1973). Nearly all the computed upward and downward gradients occur at depths of less than 2,500 ft below the water table.

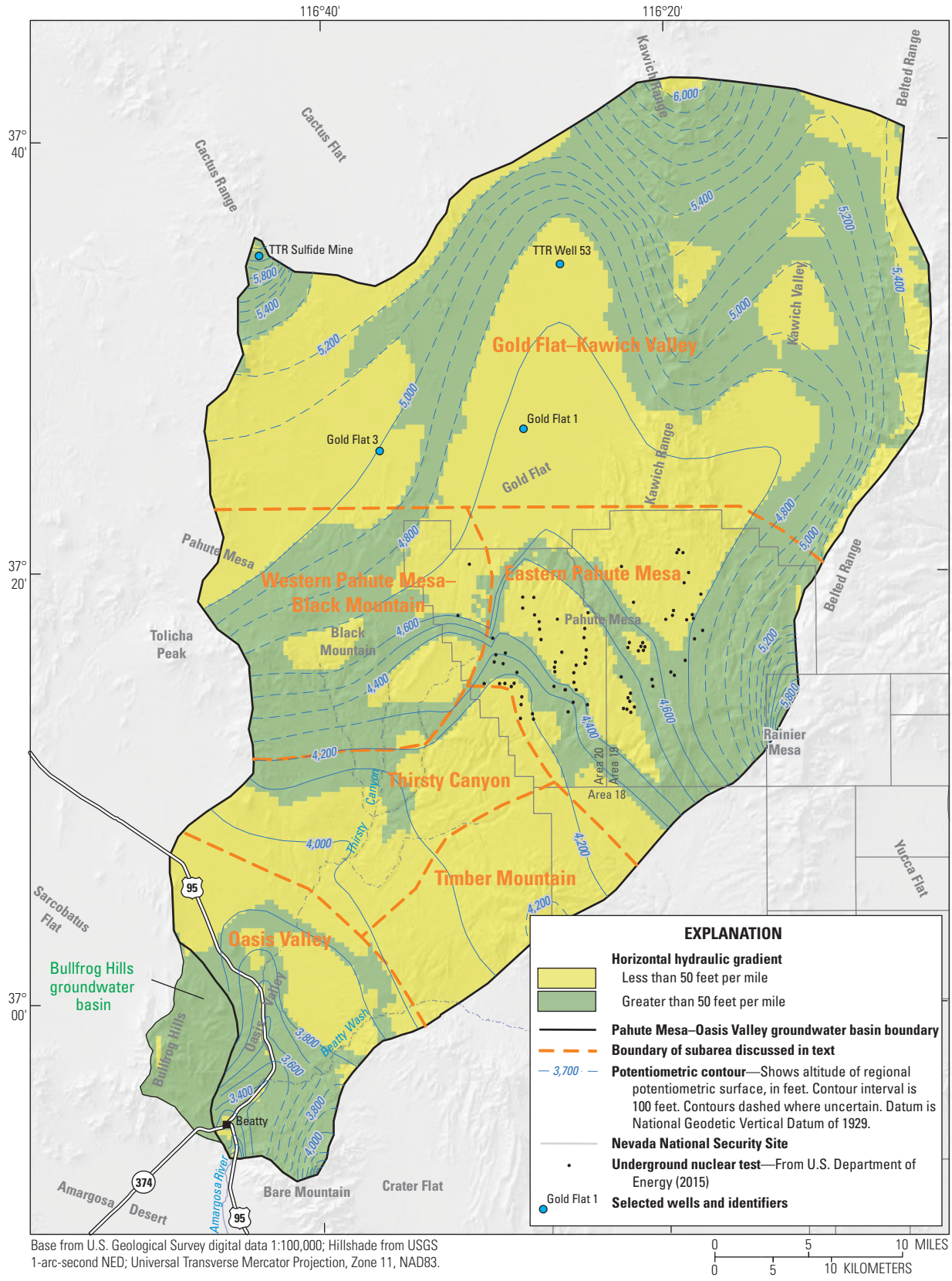

Figure 26. Potentiometric contours and delineated areas of low and high horizontal hydraulic gradients in the Pahute Mesa–Oasis Valley groundwater basin, southern Nevada.

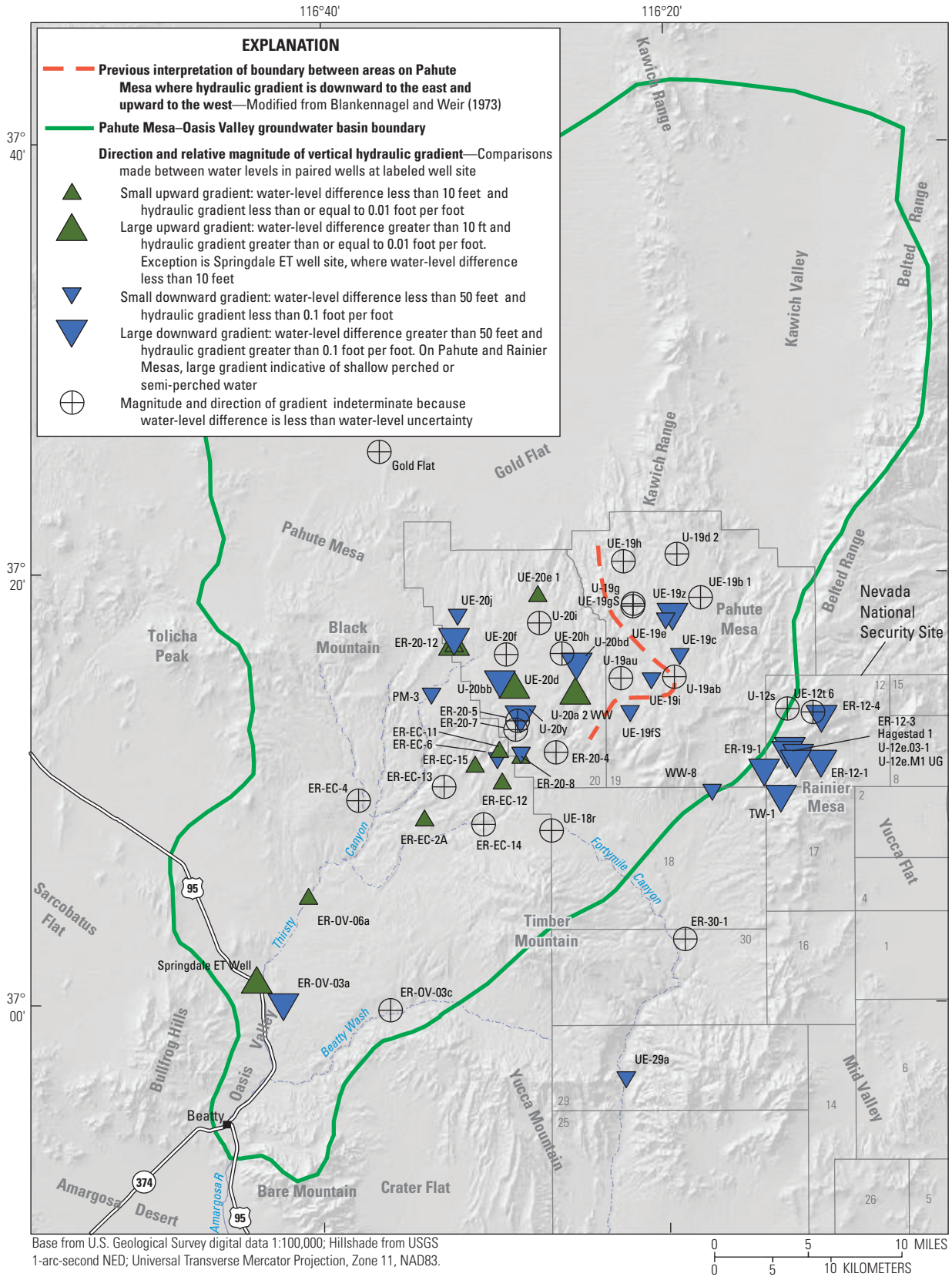

Figure 27. Direction and relative magnitude of vertical hydraulic gradients in the Pahute Mesa–Oasis Valley groundwater basin and vicinity, southern Nevada.

Downward vertical gradients are most common in recharge areas in the PMOV basin. Large downward gradients are conceptualized to occur where downward movement of recharge water is impeded by a shallow confining unit, which forms a mound of perched or semi-perched groundwater above the regional potentiometric surface. On Rainier Mesa, recharge is high and shallow confining units predominate, which results in consistently large, downward vertical gradients. Observations of large downward gradients near the water table on Pahute Mesa are sporadic (fig. 27). Large downward gradients on Pahute Mesa are attributed to localized confining units at or near the water table that elevate water levels by restricting downward movement of recharge. These large gradients usually were observed during drilling near the water table. After a drill hole penetrated through a shallow confining unit with an elevated water level, the water level would drop abruptly to an altitude consistent with regional water levels. An example of a localized semi-perched aquifer overlying the regional system, at borehole *ER-20-12*, is discussed in detail in the "Western Pahute Mesa–Black Mountain" section. Areas of large downward gradients near the water table on Pahute Mesa probably are more prevalent than shown on fig. 27.

Upward vertical gradients occur throughout the PMOV basin (fig. 27). On Pahute Mesa, upward gradients are conceptualized to occur where low-permeability units obstruct flow and cause groundwater to move vertically upward from one permeable unit into another. Upward gradients are expected in Oasis Valley. The general thinning of volcanic rocks toward Oasis Valley and their termination against low-permeability siliciclastic rocks forces groundwater upward through faults to discharge at springs and seeps in Oasis Valley (Fridrich and others, 1999; Reiner and others, 2002). The large downward gradient in Oasis Valley at borehole *ER-OV-03a* is anomalous and likely is the result of a fault that hydraulically isolates shallow and deep saturated rocks (Robledo and others, 1998).

Relation of Faults to Groundwater Flow

Faults commonly are characterized at Pahute Mesa as barriers or conduits to groundwater flow (Fridrich and others, 1999; Mission Support and Test Services, LLC, 2018). Juxtaposition of rocks with similar or different permeabilities across a fault is commonly accepted as a mechanism for creating flow-path connections or barriers, respectively (Laczniak and others, 1996; Faunt, 1997; Schenkel and others, 1999; Kwicklis and others, 2006; Pawloski and others, 2010; U.S. Department of Energy, 2020a). An alternative concept suggests that fault permeability is controlled, in part, by the present-day regional stress field, where faults parallel to the maximum stress likely are conduits for groundwater flow, and faults oriented between 45 and 90 degrees to the maximum stress tend to impede or deflect groundwater flow (Snow, 1965; Faunt, 1997; Kwicklis and others, 2006; Reeves and others, 2017; Parashar and others, 2018). In addition to the regional stress field, the degree of influence of the fault damage zone and fault-gouge zone also needs to be considered when categorizing faults as conduits or barriers to regional groundwater flow (Faunt, 1997; Schenkel and others, 1999; Mission Support and Test Services, LLC, 2018). Several studies, discussed below, have addressed the relation of faults to groundwater flow based on regional stress fields and hydraulic-property data.

Regional Stress and Fault Permeability

The effect of regional tectonic stress on the permeability of major faults and the function of fault zones as barriers or conduits to groundwater flow was investigated at Pahute Mesa (Reeves and others, 2017). Conceptually, fault transmissivity is proportional to the cube of fault aperture (Snow, 1965). Aperture increases by either decreasing the normal stress acting on the fault wall (dilation) or increasing the ratio of shear stress to normal stress, which results in fault displacement, or slip (Morris and others, 1996; Ferrill and others, 1999). Reeves and others (2017) computed the dilation tendency and slip tendency of 394 faults and caldera margins mapped by Slate and others (1999) and the Phase II Pahute Mesa HFM (Day and Kincaid, 2013; Day and others, 2013; Kincaid and others, 2013), which is an intermediate version of the HFM between Bechtel Nevada (2002a) and U.S. Department of Energy (2020a). Results indicate that faults and caldera margins oriented northeast-to-southwest have the highest dilation and slip tendencies, whereas faults and caldera margins oriented northwest-to-southeast have the lowest dilation and slip tendencies. Reeves and others (2017, p. 46) state: "*A direct relationship between either dilation tendency [T_d] or slip tendency [T_s] and fault permeability does not exist, and therefore faults are arbitrarily considered enhanced for fluid flow in this study when either dilated: $T_d \geq 0.80$ or critically stressed: $T_s \geq 0.60$.*" Using this arbitrary relation, 157 of the 394 faults tested, or 40 percent, were identified as potential conduits to groundwater flow. This method did not consider hydraulic information to determine whether these major structural features are conduits to flow.

Flowing Intervals and Fracture Permeability in Boreholes

At the borehole scale, fracture orientation and spacing are not correlated with the occurrence of permeable flowing fractures in volcanic rocks at Pahute Mesa. Borehole geophysical logging was done to assess the number and orientation of fractures in seven Pahute Mesa boreholes (Reeves and others, 2017). A total of 294 fractures were logged in these boreholes, where estimated lineal fracture densities ranged from 0.006 to 0.04 fractures per foot, which equates to average vertical fracture spacings that range from 25 to 167 ft (Reeves and others, 2017). Comparisons of fracture locations to intervals of inflow from borehole flowmeter data (Oberlander and others, 2002) indicate that 25 of the 294 fractures, or about 9 percent of the fractures, contribute flow to the wells (Reeves and others, 2017). Borehole fracture orientations were compared to nearby major faults to compute dilation and slip tendencies and results indicate that only 1 of the 25 flowing fractures is considered a conduit to groundwater flow when using the arbitrary regional-scale stress relations of dilation tendency greater than 0.8 and slip tendency greater than 0.6 (Reeves and others, 2017). Reeves and others (2017, p. iv) concluded that "*the [regional] stress field does not play a significant role in influencing fluid flow through smaller, background fractures at the borehole scale. This may be explained by the dominance of cooling fractures within lava and welded tuff units, which create complex connectivity patterns for fluid flow that are unrelated to and minimally influenced by tectonic stress*."

Dickerson and others (2006) compared changes in flow to fracture locations within seven Pahute Mesa boreholes and results indicate there is no obvious correlation between flow and fracture locations. Few to no fractures accounted for the significant increases in flow within the boreholes. Even though the azimuths of fractures in these boreholes typically are oriented parallel to the strike of major faults, most of the fractures do not control groundwater flow.

Hydraulic Properties and Faults

Regression analyses and correlations were done to relate volcanic-rock hydraulic conductivities in wells on Pahute Mesa to distance to the nearest fault (Navarro, 2020). Hydraulic conductivities were derived from pumping aquifer test results in Frus and Halford (2018) and fault distances were extracted from the PMOV HFM (U.S. Department of Energy, 2020a). No correlations were found between hydraulic conductivity and fault distance when all pumping-test data were evaluated (Navarro, 2020). A strong negative correlation was reported between log-transformed hydraulic conductivities in wells and distance to the nearest fault when only faults within 1,000 ft of a well were considered. This negative correlation, which only considered 10 wells, indicates that a zone of enhanced permeability occurs near the faults. However, multiple-well aquifer test results in 8 of these 10 wells show that nearby faults are neither conduits nor barriers to groundwater flow (Garcia and others, 2011, 2017; Mirus and others, 2016). For example, borehole *ER-20-8* intersects the ER-20-8 fault and is about 1,200 ft east of the ER-20-7 fault (plate 1). Pumping in borehole *ER-20-8* propagated across the ER-20-7 fault and induced drawdowns in borehole *ER-EC-6*, which is about 1.3 mi southwest of borehole *ER-20-8* (plate 1; Garcia and others, 2017). This result indicates that the ER-20-7 fault is not a flow barrier and that the ER-20-7 and ER-20-8 faults also are not important conduits. If these faults were high-transmissivity conduits, they would attenuate the pumping signal and drawdown would not be observed greater than one mile from the faults in borehole *ER-EC-6* (Garcia and others, 2011).

Analysis of large-scale, multiple-well aquifer test results at Pahute Mesa was used to infer whether major faults and caldera margins are conduits or barriers to groundwater flow. Eight multiple-well aquifer tests were simulated in regional-scale groundwater models to characterize the hydraulic properties of volcanic rocks in Pahute Mesa (Mirus and others, 2016). Hydraulic properties were distributed spatially across HSUs using the Phase II Pahute Mesa HFM, and faults were implemented implicitly by offset of juxtaposed HSUs. Determination of whether a fault is a barrier to flow was based on the propagation of pumping signals across structural blocks between a pumping well and observation wells. Mirus and others (2016) developed a second HFM that added more complexity to the Phase II Pahute Mesa HFM. The second HFM explicitly mapped fault zones so that hydraulic properties could be estimated independently for HSUs and fault zones. Adding faults explicitly as unique hydrologic features did not improve model calibration; instead, independently estimating fault hydraulic properties degraded the hydraulic uniqueness of modeled HSUs. Fault hydraulic properties also were similar to the hydraulic properties of nearby HSUs, indicating that faults are not hydraulically distinct features and that fault offset between HSUs likely is more important for simulation of groundwater flow than explicit simulation of fault zones.

Sixteen multiple-well aquifer tests at Pahute Mesa were simulated by Garcia and others (2017) using the Phase II Pahute Mesa HFM. Heterogeneous hydraulic-property distributions were estimated for HSUs. Large-scale anisotropy of faults was accounted for with large contrasts in hydraulic properties within HSUs because heterogeneity and anisotropy are correlated. Garcia and others (2017, p. 1) concluded the following: "*Drawdown was detected at distances greater than 3 miles from pumping wells and propagated across hydrostratigraphic units and major structures, indicating that neither faults nor structural blocks noticeably impede or divert groundwater flow in the study area.*" Specific faults investigated for the aquifer-test analysis included the M2 fault, ER-20-7 fault, southern part of the Boxcar fault, northern structural margin of the Ammonia Tanks and Rainier Mesa calderas, and the Northern Timber Mountain moat structural zone (NTMMSZ; plate 1).

The NTMMSZ has been posited as a potentially important hydraulic barrier that could have a strong influence on radionuclide transport (Parashar and others, 2018); however, the migration of a tritium plume across the NTMMSZ indicates that this structure is not a hydraulic barrier. Tritium from the BENHAM nuclear test has been detected upgradient of the NTMMSZ in wells *ER-20-5-1*, *ER-20-5-3*, and *ER-20-7* (plate 1; section *D–D′* on plate 2; U.S. Department of Energy, 2019). Tritium from the BENHAM nuclear test also has been detected downgradient of the NTMMSZ in boreholes *ER-20-8*, *ER-20-8-2*, *ER-20-11*, and *ER-EC-11* (plate 1; section *C–C′* on plate 2; U.S. Department of Energy, 2019). The NTMMSZ is neither a barrier nor conduit to tritium transport; instead, tritium migrates from older volcanic rocks into younger volcanic rocks across the NTMMSZ because younger volcanic rocks are offset (down-dropped) more than 1,000 ft south of the NTMMSZ (sections *C–C′, E–E′*, and *F–F′* on plate 2; Pawloski and others, 2010). The tritium plume predominantly occurs in the TSA north of the NTMMSZ and juxtaposition causes the migration of the tritium plume from the older TSA into, predominantly, the younger BA.

Most faults cannot be differentiated hydraulically from adjacent host rocks and have no direct hydraulic significance. The West Greeley fault in Pahute Mesa has been conceptualized as a conduit for groundwater flow and radionuclide transport (Kwicklis and others, 2006; Stoller-Navarro Joint Venture, 2009). This interpretation was tested during analysis of a multiple-well aquifer test in well *U-20 WW* (plate 1), where drawdown propagated across the fault (Garcia and others, 2011). Results showed that the estimated hydraulic conductivity of the 400-ft wide fault zone was similar to the hydraulic conductivity of the surrounding volcanic rocks, indicating that West Greeley fault is neither a significant conduit nor barrier to flow.

Hydraulically Significant Faults

A limited number of faults and caldera margins are considered flow barriers or conduits based on hydraulic information. These faults typically function as conduits or barriers to flow over segments of the fault rather than along the entire length. For example, the Boxcar fault has been identified as a transverse barrier to groundwater flow based on hydraulic-head differences on each side of the fault (U.S. Department of Energy, 2009). Examination of the potentiometric surface on the east side of the Boxcar fault suggests that the fault may impede westward flow in the area between boreholes *UE-20h WW* and *U-20be* (plate 1). In this area, flow is directed southward, nearly paralleling the Boxcar fault. However, water-level data suggest that the northern part of the fault does not significantly affect groundwater flow.

Borehole *ER-20-8* intersects the ER-20-8 fault and this fault was postulated to provide a vertical hydraulic connection between three aquifers separated by confining units in the borehole (Navarro-Intera, LLC, 2012). The vertical hydraulic connection along the ER-20-8 fault was postulated based on minimum attenuation of drawdowns in wells *ER-20-8 shallow* (open to SPA), *ER-20-8 intermediate* (open to TCA), and *ER-20-8 deep* (open to TSA) during pumping from either the main upper completion (open to TCA) or main lower completion (open to TSA) of the borehole. Alternatively, these unattenuated drawdowns that were measured may be attributed to the MPCU and LPCU functioning as leaky confining units between these aquifers.

Rocks near the northern margin of the Ammonia Tanks caldera between wells *ER-EC-12* and *ER-EC-14* (plate 1) have transmissivities exceeding 100,000 ft^2/d (Garcia and others, 2017). These high transmissivities may occur where large volcanic blocks were deposited along a steep, unstable caldera margin. The small hydraulic gradient between wells *ER-EC-12* and *ER-EC-14* (plate 1) may be the result of the permeable rubble zone that formed inside the caldera rim.

The Thirsty Canyon lineament (plate 1) likely is a barrier to groundwater flow on its northern end and a conduit farther south. This lineament is a buried north-northeast trending feature that parallels the western structural margins of the Silent Canyon and Timber Mountain caldera complexes (Mankinen and others, 1999). The steep west-to-east hydraulic gradient coincident with the lineament (plate 1) may be attributed to structural features related to the lineament, including the Silent Canyon caldera complex and the Purse and West Purse faults (Blankennagel and Weir, 1973; Laczniak and others, 1996; Kwicklis and others, 2006). The steep gradient, indicating a hydraulic barrier, likely formed because structural features associated with the Thirsty Canyon lineament caused considerable vertical offset of HSUs that juxtaposed permeable rock on the east against impermeable rock on the west (Blankennagel and Weir, 1973; Schenkel and others, 1999; Kwicklis and others, 2006; section *H–H′* on plate 2). Farther south along Thirsty Canyon, near boreholes *ER-EC-4* and *ER-EC-8*, potentiometric contours indicate converging flow paths in the vicinity of the Thirsty Canyon lineament (plate 1). Converging flow paths suggest an area of high transmissivity nearly coincident with the lineament, indicating a preferred flow path or conduit for flow.

Some of the major faults in Oasis Valley are thought to control spring locations by functioning as conduits or barriers to groundwater flow. Faults identified as likely to influence groundwater flow and spring locations are the Hogback, Bare Mountain, Beatty, Colson Pond, Fleur-de-Lis, and Hot Spring faults, and the Bullfrog Hills–Fluorspar Canyon detachment (plate 1; Fridrich and others, 1999; Reiner and others, 2002). Springs in Oasis Valley likely occur near faults because of

1. juxtaposition of permeable rocks against low-permeability rocks, which has formed springs near Colson Pond fault;

2. abrupt thinning of the volcanic aquifer, which has formed springs west of the Hogback fault between the Colson Pond and Hot Spring faults; or

3. termination of aquifer continuity against low-permeability siliciclastic rocks, such as along the Beatty fault (Fridrich and others, 1999; Schenkel and others, 1999; Reiner and others, 2002).

Groundwater-Flow Characterization by Subarea

The groundwater-flow conceptualization in the PMOV basin is discussed in terms of six distinct subareas: Gold Flat–Kawich Valley; eastern Pahute Mesa; western Pahute Mesa–Black Mountain; Thirsty Canyon; Timber Mountain; and Oasis Valley. Water budgets, potentiometric contours, water-level trends, groundwater-flow paths, hydraulic gradients, hydraulic properties, radionuclide data, and hydraulically significant faults are used to characterize groundwater flow within each of the six subareas.

Gold Flat–Kawich Valley

The area of Gold Flat and Kawich Valley, north of the NNSS, encompasses about half of the PMOV basin. Most groundwater flow is focused from the highland areas into the alluvial valleys of Gold Flat and Kawich Valley. Water levels in the highland areas are elevated because of minor amounts of recharge infiltrating low-permeability rocks. Water levels are conceptualized to have high east-west gradients away from the mountains and lower southward gradients through adjacent valleys (fig. 26). For example, the horizontal hydraulic gradient between southern Cactus Range and Gold Flat is 90 ft/mi, based on water levels in wells *TTR Sulfide Mine* and *Gold Flat 3*. In contrast, the gradient through Gold Flat is much lower (8 ft/mi), as determined from wells *TTR Well 53* and *Gold Flat 1*. The low gradients in the valleys generally coincide with alluvial deposits (AA), which can have moderate-to-high transmissivities (fig. 11). Total flow into the southern half of the PMOV basin from the Gold Flat–Kawich Valley area is estimated to be relatively small at about 13 percent of the PMOV basin budget (fig. 28).

Eastern Pahute Mesa

Groundwater from recharge areas in northwestern Rainier Mesa and southern Belted Range radiates northwest, west, and southwest into the eastern Pahute Mesa area (plate 1). Flow paths ultimately align in a southwesterly direction before entering the Thirsty Canyon and Timber Mountain areas (fig. 23). About one-half of the recharge for the PMOV basin is generated in the uplands within the eastern Pahute Mesa area and 65 percent of the groundwater discharging at Oasis Valley flows through the southwestern boundary of this area (fig. 28).

The volcanic rocks at the water table in NNSS Areas 19 and 20 are progressively younger to the west. This occurs because a series of north-south trending normal faults cause the geologic units to stair-step downwards in a westward direction (sections *B–B′* and *C–C′* on plate 2). For example, the BRA HSU occurs at the water table in the east-central part of Area 19 (fig. 2). About 15 mi west, near the Purse and West Purse faults in Area 20, the BRA is down-dropped to depths of about 6,000 ft below the water table. On the western side of the Purse and West Purse faults, the BRA is uplifted by these faults and occurs again at the water table (section *F–F′* on plate 2).

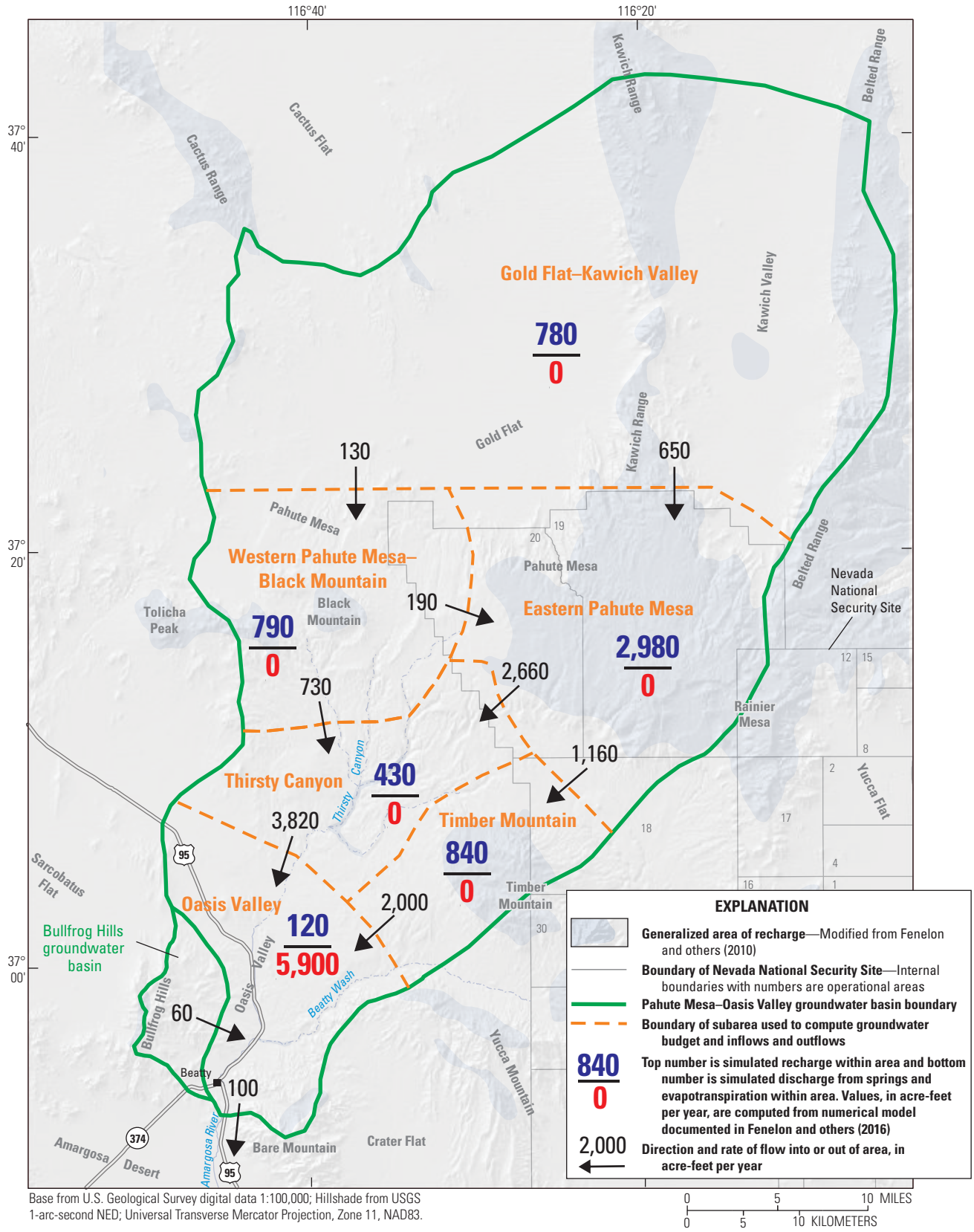

Figure 28. Groundwater budgets and inflows and outflows between areas in the Pahute Mesa–Oasis Valley groundwater basin, southern Nevada.

The large juxtaposition of rock units from east to west in the eastern Pahute Mesa area results in lateral discontinuities. Because groundwater follows "the path of least resistance," groundwater within a permeable HSU upgradient of a discontinuity will flow into the closest permeable HSU downgradient of the discontinuity. Consequently, groundwater will flow through many HSUs as it moves downgradient. Furthermore, the transmissivities of rocks deeper than about 1,600 ft below the water table are low (fig. 18), ensuring that most groundwater will stay shallow as it moves through permeable HSUs across lateral discontinuities.

Pool–Dam Conceptualization

Groundwater encounters an alternating sequence of low- and high-transmissivity rock as it moves from east to west across eastern Pahute Mesa (fig. 24). Low- and high-transmissivity rock coincide with high- and low-gradient areas, referred to as dams and pools, respectively (fig. 26). Groundwater dams occur where permeable deposits, such as lava flows, pinch out against less permeable units or where permeable units are juxtaposed with low-permeability units along faults (fig. 29). Within a permeable pool, groundwater flow primarily is horizontal (low vertical hydraulic gradient) and the horizontal hydraulic gradient is low. Where a permeable pool ends, the horizontal gradient increases, and flow paths diverge in the low-permeability unit to compensate for the lower hydraulic conductivity of the unit. Vertical hydraulic gradients are likely to be highest near the edges of permeable units, where water flows from deeper to shallower units, or vice versa.

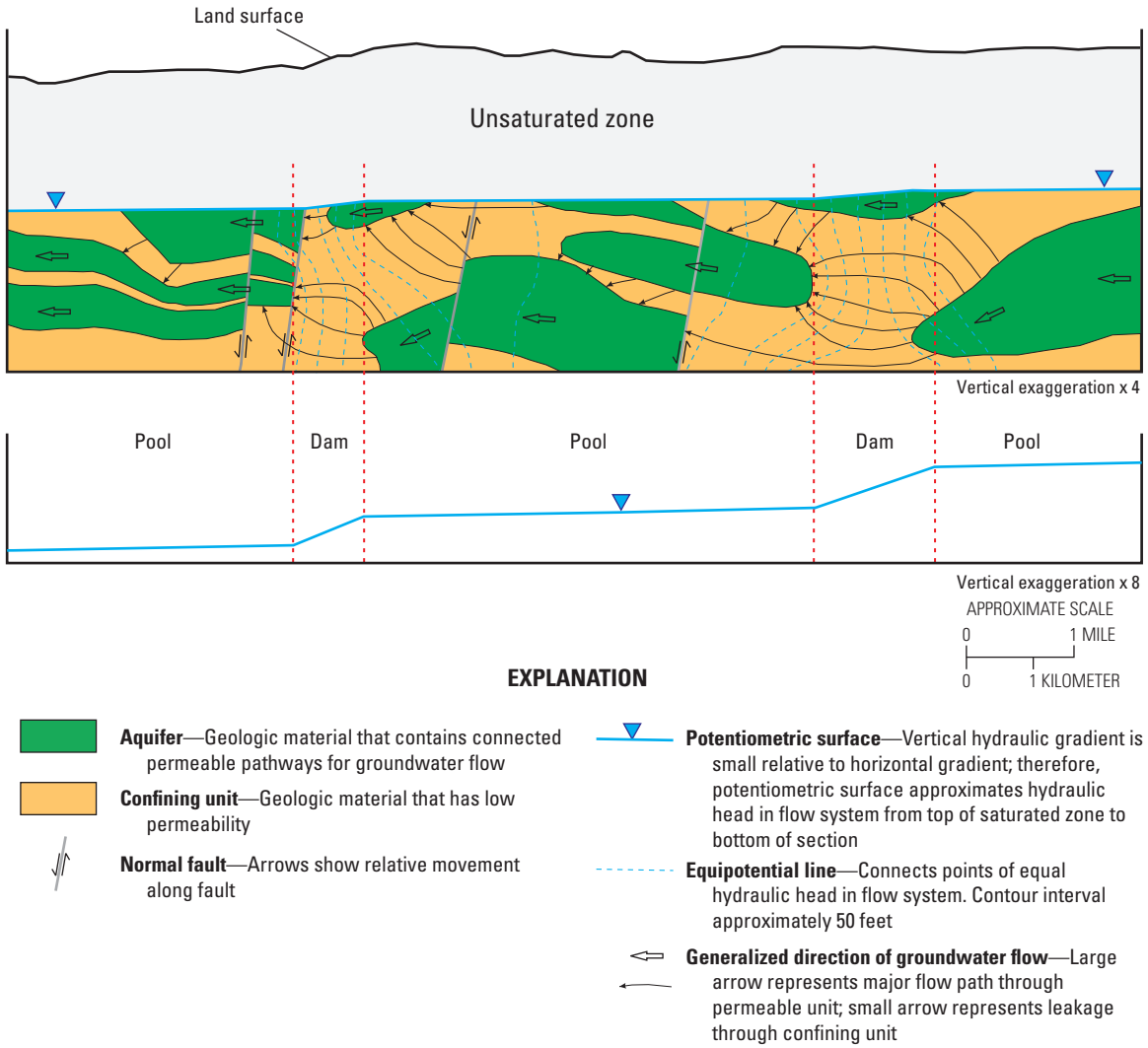

Figure 29. Conceptual hydrogeologic section through areas of low and high horizontal gradients (pools and dams) at eastern Pahute Mesa, southern Nevada.

Confining units are hydraulic barriers to groundwater flow and function as groundwater dams. These confining units hydraulically separate permeable units and impede the propagation of pumping signals. For example, groundwater withdrawals from an aquifer test at well *U-20 WW* caused water-level declines 1.2 mi to the southeast in observation well *UE-20bh 1*, where both wells are open to Calico Hills lava flows in a groundwater pool between the 4,500- and 4,400-foot contours (plate 1; appendix 3; Garcia and others, 2011). Lack of detected water-level declines in observation well *U-20bf* indicate that drawdown from pumping at well *U-20 WW* did not propagate 0.8 mi southwest to this observation well. Well *U-20bf* is in a groundwater dam, as indicated by the steepening of water-level contours (plate 1; Garcia and others, 2011). Well *U-20bf* is open to CHZCM (appendix 3) and aquifer-test results indicate this HSU functions as a confining unit between the 4,400- and 4,300- or 4,200-foot contours in the eastern Pahute Mesa area (fig. 26).

Groundwater pools and dams in the eastern Pahute Mesa area coincide with specific HSUs or HGUs in the upper 1,600 ft of the saturated zone. Some of the pool–dam boundaries also coincide with fault boundaries; the coincidence results from juxtaposition of permeable units with low-permeability units at the fault boundaries. Within the eastern Pahute Mesa area, there are two distinct pools and three dams. The easternmost dam is expressed as an area of high hydraulic gradient associated with low-permeability volcanic tuffs and granite (TCU and GCU) at Rainier Mesa. As portrayed on figure 26, this high-gradient area extends westward to about the 4,700-foot contour line. Much of the high-gradient area between the 5,000- and 4,700-foot contours has no water-level data (plate 1) to constrain the contours so that the high-gradient area could be less extensive to the east by several miles. A low-gradient pool occurs between the 4,700- and 4,600-foot contours in northern NNSS Area 20 (fig. 26). This area is dominated at shallow depths by the BRA, an HSU with moderate transmissivity (fig. 16). Downgradient of the pool is a groundwater dam between the 4,600- and 4,500-foot contours extending from eastern Area 19 to southcentral Area 20 (fig. 26). The dam is caused by low-transmissivity HSUs—CFCU, BFCU, and CHZCM—that dominate in the shallow part of the flow system. Another pool occurs between the 4,500- and 4,400-foot contours (fig. 26), where moderate transmissivity Calico Hills lava flows (fig. 16) are pervasive at shallow depths. At the downgradient end of the eastern Pahute Mesa area, another dam occurs between the 4,400- and 4,300- or 4,200-foot contours (fig. 26). In this area, CHZCM, UPCU, and LPCU are dominant at shallow depths and are composed of low-transmissivity TCU. The pool-dam pattern confirms the transmissivity analysis of HGUs, which showed that LFAs and WTAs can be relatively permeable and TCUs have lower permeability (fig. 11). Hydrologic sections *B–B´* through *E–E´* (plate 2) show the sequence of HSUs or HGUs that occur near the water table and how they relate to the pools and dams, which are delineated on the sections as low- and high-gradient areas, respectively. The relation shown on the sections is not perfect because (1) the sections are a two-dimensional representation of a three-dimensional system, (2) the HSUs or HGUs are heterogeneous and do not always function as an aquifer or a confining unit, and (3) the potentiometric contours and geologic unit extents are uncertain where unconstrained by data.

Elevated Water Levels

Elevated water levels, indicative of semi-perched conditions in shallow rocks, are not uncommon in the eastern Pahute Mesa area. Elevated water levels in rocks near the water table have been observed in more than 20 shallow wells (plate 1). Water levels in these wells are elevated tens of feet to several hundred feet above levels in deeper units and result in large downward hydraulic gradients (fig. 27; table 2). Water levels in semi-perched zones are elevated because vertical hydraulic conductivities of underlying low-permeability rocks are less than local infiltration rates, which impounds water and laterally diverts flow. These low-permeability rocks that impede recharge commonly are composed of TCUs, such as the BFCU, CFCU, CHZCM, UPCU, and LPCU. Mapping areas of semi-perched water in eastern Pahute Mesa is difficult because well coverage defining the extent of semi-perched areas is limited and the hydraulic conductivities of the rock units are heterogeneous. An example of a semi-perched area is a cluster of elevated water levels measured in NNSS Area 19 between boreholes *UE-19c* and *U-19aq* (shown as red-circle well symbols on plate 1). Some of the boreholes in this semi-perched area are shown on section *B–B´* (*UE-19c*, *UE-19i*, and *U-19x* on plate 2); however, the semi-perched system is not delineated on plate 2 because water-level data are limited. CFCU, BFCU, and CHZCM occur at or near the water table in the area of these boreholes and is the primary cause of the elevated water levels. The cause of the elevated water level in the shallow part of borehole *UE-19c* is not as obvious. Nearly all of borehole *UE-19c* is open to BRA. The shallowest interval, well *UE-19c (2421-2884 ft)*, has a water level that is at least 20 ft higher than deeper intervals in the BRA. The likely cause of the elevated water level is a heterogeneous BRA that has a low permeability near the top of the unit. The BRA in the shallow part of the hole consists of interbedded lava and nonwelded tuff (Wood, 2007) and has a hydraulic conductivity of less than 0.01 ft/d (Frus and Halford, 2018). This low-permeability section directly overlies lavas and lava breccias with a high hydraulic conductivity (12 ft/d) and a lower water level.

Permanent, Large-Scale Nuclear Testing Effect on Water Levels

Nuclear testing may have permanently lowered water levels within a several-square-mile area of eastern Pahute Mesa that includes wells *U-20 WW*, *UE-20bh 1*, *UE-20n 1*, *U-20n PS 1DD-H*, and *U-20bg* (plate 1). These wells have similar water-level trends (fig. 30) and previous studies have documented the effects of pumping well *U-20 WW* on water levels in these wells (Fenelon, 2000; Garcia and others, 2011). In the absence of any groundwater stress except pumping from well *U-20 WW*, water-level declines in these five wells would be expected to recover to pre-pumping levels after pumping ceases. Full recovery from pumping that ceased in 1999 is expected by 2005 based on a water-level model analysis by Jackson and Fenelon (2018). A declining trend of about 19 ft between pre-pumping and post-pumping water levels in these five wells indicates that the water-level decline cannot be attributed only to pumping from well *U-20 WW* (fig. 30; Jackson and Fenelon, 2018). The declining trend potentially was caused by the breach of a confining unit from a nearby nuclear test, which permanently lowered the hydraulic head in the volcanic rocks open to the wells (Jackson and Fenelon, 2018).

A breach scenario occurs when a nuclear detonation forms a chimney through a confining unit or fractures a confining unit that separates two aquifers with different hydraulic heads. The breach in the confining unit causes a hydraulic connection between the aquifers, allowing groundwater to flow to the aquifer with lower hydraulic head. Groundwater levels equilibrate with time to a new steady-state condition with a new composite hydraulic head.

The vertical breach of a confining unit plausibly explains the permanent dewatering of the groundwater pool near wells *U-20 WW*, *UE-20bh 1*, *UE-20n 1*, *U-20n PS 1DD-H*, and *U-20bg*. These five wells are open to CHLFA4, CHZCM, or both (appendix 3). On February 22, 1964, a 32-ft upward gradient was measured in borehole *U-20a 2 WW* (table 2) between the shallower CHLFA4 and deeper CHZCM. After 1964, chimney formation from a nearby nuclear test, such as the CHESHIRE test (*U-20n*; plate 1) detonated on February 14, 1976 in the CHLFA4, may have breached low-permeability rock, causing a hydraulic connection between the CHLFA4 and CHZCM (section *C–C′* on plate 2). Water-level trends from the five wells (fig. 30**)** indicate that heads equilibrated to a new steady-state condition by 2005. If the CHESHIRE test dewatered the groundwater pool near these wells, then water levels equilibrated within 29 years, from 1976 to 2005.

Radionuclides may have experienced a period of accelerated transport rates if a confining unit was breached from a nuclear test. The delineated area around wells *U-20 WW*, *UE-20bh 1*, *UE-20n 1*, *U-20n PS 1DD-H*, and *U-20bg* (plate 1) is the area likely affected by the breach. Assuming the groundwater system was permanently dewatered 19 ft within the delineated area (6.2×10^7 ft^2), then about 27,000 acre-ft (8.9 billion gallons) of groundwater was released from storage. The maximum downgradient distance radionuclides could have been displaced can be estimated from the average linear velocity, where the distance is equal to the total groundwater released from storage divided by the cross-sectional area multiplied by the porosity. Using a thickness-porosity product of 50 ft (Fenelon and others, 2016) for the approximately 16,000-ft wide delineated area, radionuclides could have been displaced as much as 0.3 miles farther downgradient than under pre-test, steady-state flow conditions.

Western Pahute Mesa–Black Mountain

Groundwater flow in the western Pahute Mesa–Black Mountain area is south-southeasterly (fig. 23). Most of the flow is sourced from recharge occurring on Black Mountain and highlands to the west. About 75 percent of the flow moves southeast into the Thirsty Canyon area, although a small amount (25 percent) moves into eastern Pahute Mesa (fig. 28). Total flow through the western Pahute Mesa–Black Mountain area is relatively minor, comprising less than 15 percent of the PMOV basin budget. Relatively minor flow is consistent with much of the western area having high horizontal hydraulic gradients (fig. 26), indicative of low-permeability rocks and limited flow.

Groundwater Source

The western Pahute Mesa–Black Mountain area and eastern Pahute Mesa area have groundwater sourced from different recharge areas and distinct flow paths (plate 1). The two areas are separated by the Thirsty Canyon lineament in western NNSS Area 20. The lineament is conceptualized to be a groundwater barrier, with a high west-to-east hydraulic gradient across the lineament. No water-level data provide direct evidence for the high gradient co-located with the lineament or associated Purse and West Purse faults, as portrayed on plate 1. However, water levels west of the lineament are about 200 ft higher than levels east of the lineament, indicating a high eastward gradient somewhere in this area. The high gradient likely is indicative of low-permeability rocks and limited eastward flow in the vicinity of the lineament. A separation of groundwater flow west and east of the Thirsty Canyon lineament is indicated by geochemically distinct groundwater. Rose and others (2006) reported high chloride and sulfate concentrations and relatively low deuterium values in the western Pahute Mesa–Black Mountain area compared to eastern Pahute Mesa. Downgradient, water in the Thirsty Canyon area appears to be a mixture of these two water types.

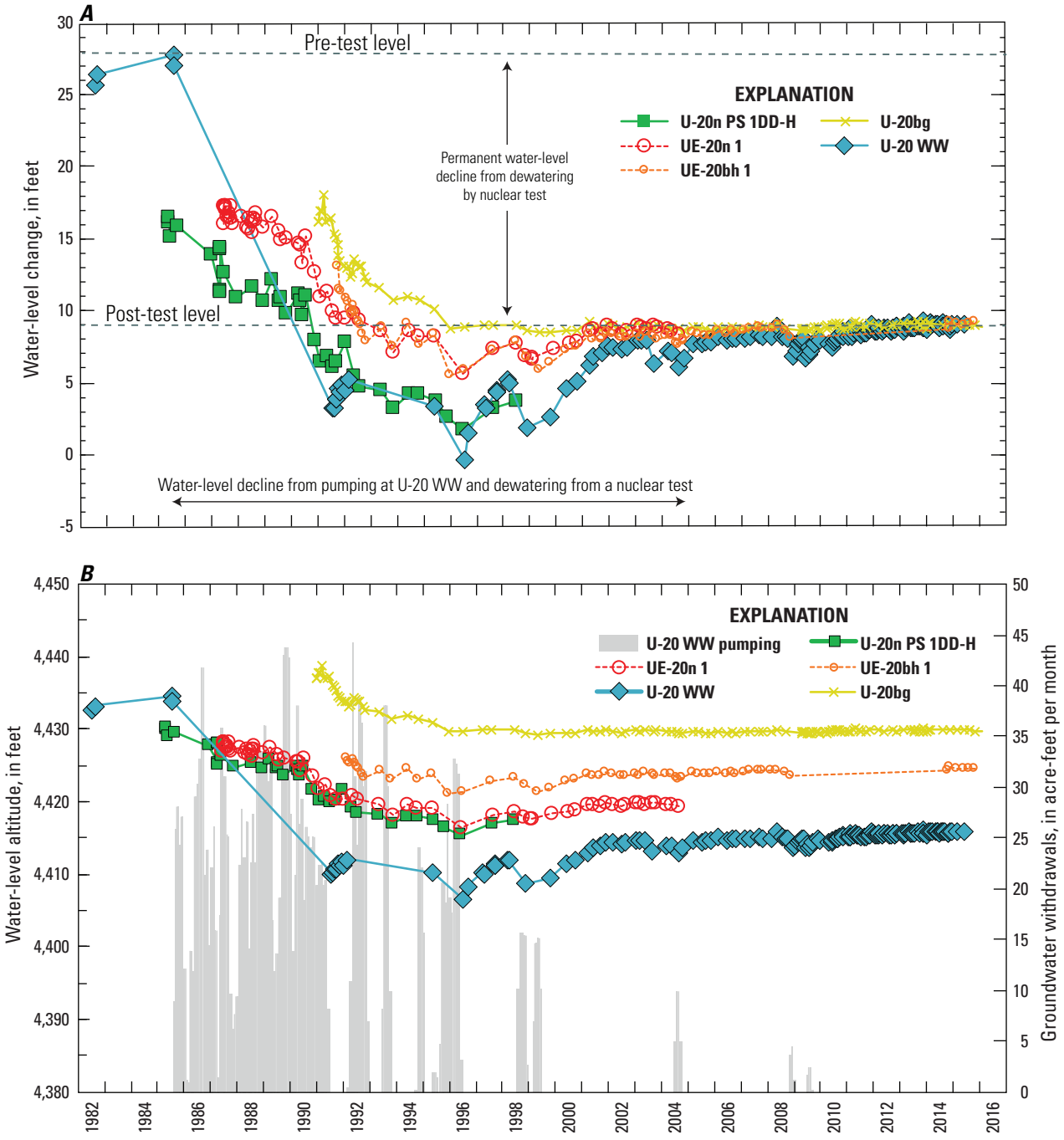

Figure 30. Comparison of (*A*) water-level change and (*B*) groundwater withdrawals in well U-20 WW and water-level altitudes in wells U-20WW, UE-20bh 1, UE-20n 1, U-20n PS 1DD-H, and U-20bg, Pahute Mesa–Oasis Valley groundwater basin, southern Nevada.

Conceptualization of Semi-Perched and Regional Aquifers near HANDLEY Nuclear Test

A semi-perched aquifer above the regional system was encountered during completion of hole *ER-20-12* in 2016 (Navarro, 2016a). The water level in the shallow aquifer is about 260 ft higher than in the regional system. As discussed in the "Elevated Water Levels" section, semi-perched aquifers are not uncommon on Pahute Mesa. Both the shallow and regional aquifers in hole *ER-20-12* are contaminated with radionuclides from the HANDLEY nuclear test, about 1.4 mi to the north-northeast (fig. 31; Russell and others, 2017; Navarro, 2018). Downgradient contamination of the shallow aquifer demonstrates that groundwater in a semi-perched aquifer can flow laterally for several miles before water moves downward into the regional system.

An examination of the hydrostratigraphic sequences between hole *UE-20j*, about 75 ft southwest of the HANDLEY test, and hole *ER-20-12* (fig. 31) indicates that several HSUs hydraulically separate the semi-perched aquifer from the regional system (fig. 32). The water level in the shallow welded-tuff aquifer (TMWTA) at hole *ER-20-12* is elevated. This aquifer is hydraulically separated from a deeper lava-flow aquifer (CHLFA5) by vitric tuff (TMLVTA) and tuff confining unit (UPCU; fig. 32). Limited aquifer-test data suggest that the TMLVTA HSU has low transmissivity (VTA in fig. 11), but probably not low enough to fully isolate the shallow aquifer from the deeper aquifer. North of *ER-20-12*, the UPCU connects with TCUs within the CHZCM and LPCU. Combined, these tuffs likely isolate the shallow TMWTA and TMLVTA from deeper aquifers, such as CHLFA5, BRA, and TCA.

The extent of the shallow, semi-perched system in the area of hole *ER-20-12* is unknown but can be conceptualized from HSU extents, measured water levels, and the regional potentiometric surface shown on plate 1. The UPCU is the primary HSU that isolates the semi-perched aquifer from the underlying regional system (fig. 32). The UPCU intersects the water table southeast of *ER-20-12* (fig. 31) and is conceptualized to form a groundwater barrier to southeastward and downward flowing waters. The semi-perched aquifer is supplied by a small amount of recharge that is sufficient to elevate the head in the TMWTA and TMLVTA. Recharge rates in this area likely are variable, with higher rates of focused recharge occurring in drainage channels or in areas vegetated with trees. In order for the water to pool in the shallow aquifer, the recharge rate must exceed the vertical hydraulic conductivity of the UPCU. Recharge rates likely are less than 1×10^{-4} ft/d, whereas the hydraulic conductivity of the UPCU likely is greater than 1×10^{-5} ft/d. The only alternative source of water that potentially could supply the semi-perched aquifer is shallow groundwater in the BRA northwest of *ER-20-12*. For the BRA to be a source, the water table in the BRA would have to be elevated 100 ft or more above the mapped potentiometric surface shown on figure 31.

The pooled water in the semi-perched aquifer either seeps uniformly through the UPCU into the underlying regional system, flows into underlying units where the UPCU pinches out, or leaks downward through discrete fractures, faults, or small breaches in the UPCU. The extent of the semi-perched aquifer extends at least from the HANDLEY test to *ER-20-12*, because radionuclides from the test were detected in the semi-perched aquifer at *ER-20-12* (U.S. Department of Energy, 2019). The TMWTA at hole *UE-20j*, adjacent to the HANDLEY test, is hydraulically isolated by LPCU, which is the functional equivalent of UPCU in this area. The southern extent of the semi-perched aquifer is unknown but could extend as far south as *PM-3* (fig. 31). Alternatively, the terminus of the semi-perched aquifer could be the Ribbon Cliff structural zone if a fault breach allows water to leak downward into the underlying TCA (fig. 32).

A conceptual set of potentiometric contours for the semi-perched aquifer is illustrated in this report (fig. 31) because the semi-perched aquifer is contaminated with radionuclides from the HANDLEY nuclear test. The potentiometric map is based on a conceptualization in which the recharge rate to the shallow system exceeds the hydraulic conductivity of the underlying UPCU, and the TCVA and BRA are the primary outlets for shallow lateral flow. Flow in the semi-perched aquifer is south-southwest, nearly parallel to regional flow north of hole *ER-20-12* and perpendicular to regional flow farther south. Semi-perched aquifers with similar local-scale flow systems to the one shown on figure 31 may occur elsewhere in the PMOV basin, especially where water levels are denoted as elevated above the regional system (plate 1). Water tables in other local-scale flow systems are not contoured because water-level data are limited, radionuclide data do not indicate contamination, and this report is focused on basin-scale flow.

Thirsty Canyon

The Thirsty Canyon area, between the NNSS and Oasis Valley, is characterized by high transmissivities, relatively low recharge, and low hydraulic gradients. Transmissivities are especially high just southwest of the NNSS, where they locally exceed 100,000 ft^2/d as a result of thick, fractured LFAs and WTAs (fig. 24; Navarro-Intera, LLC, 2011; Garcia and others, 2017). These rocks promote flow to Oasis Valley, with nearly two-thirds of the water discharged in the PMOV basin passing through the Thirsty Canyon area (fig. 28).

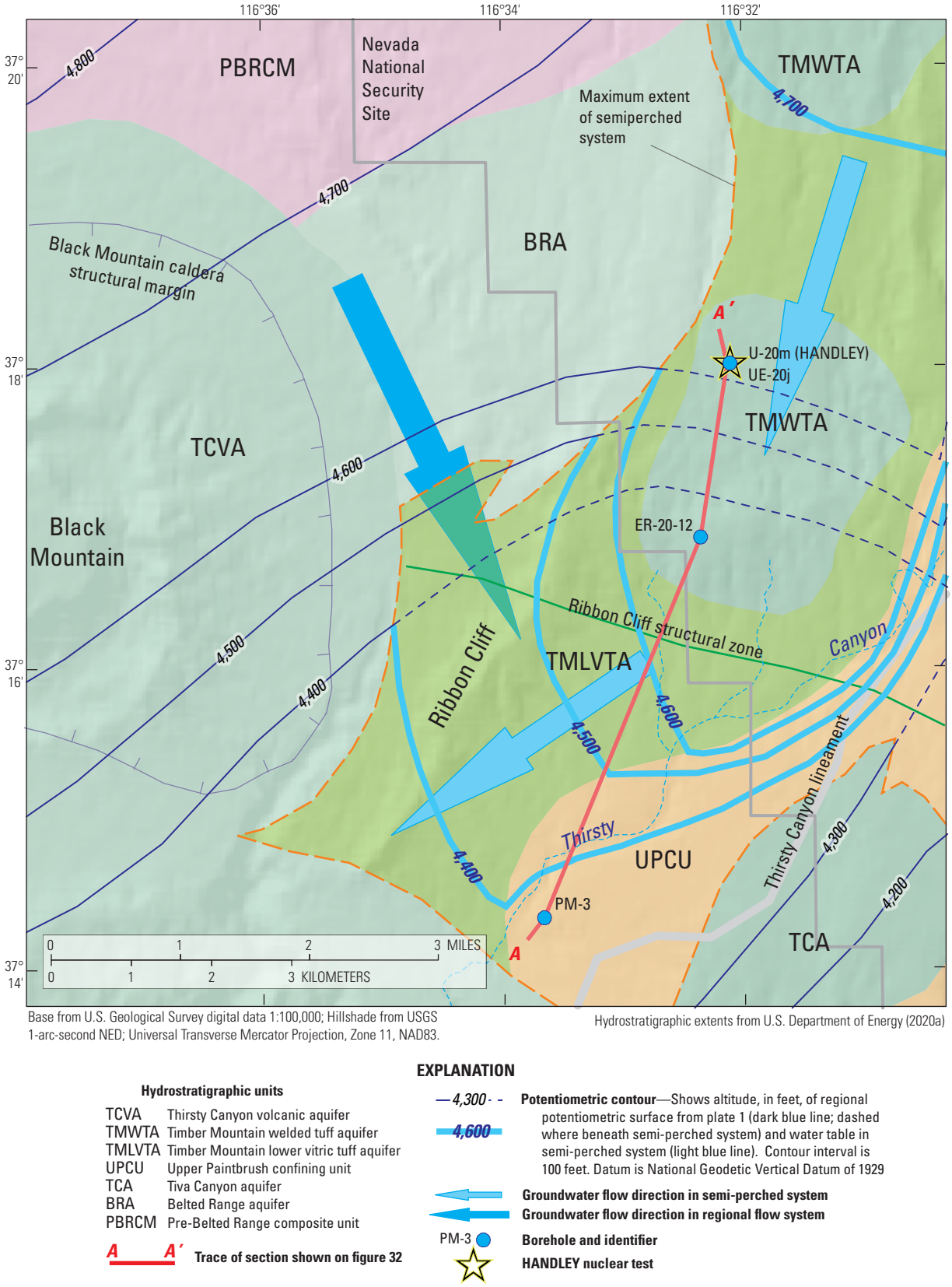

Figure 31. Hydrostratigraphic units at the water table, wells, groundwater-flow paths, and potentiometric contours of the shallow semi-perched system and regional system in western Pahute Mesa, southern Nevada.

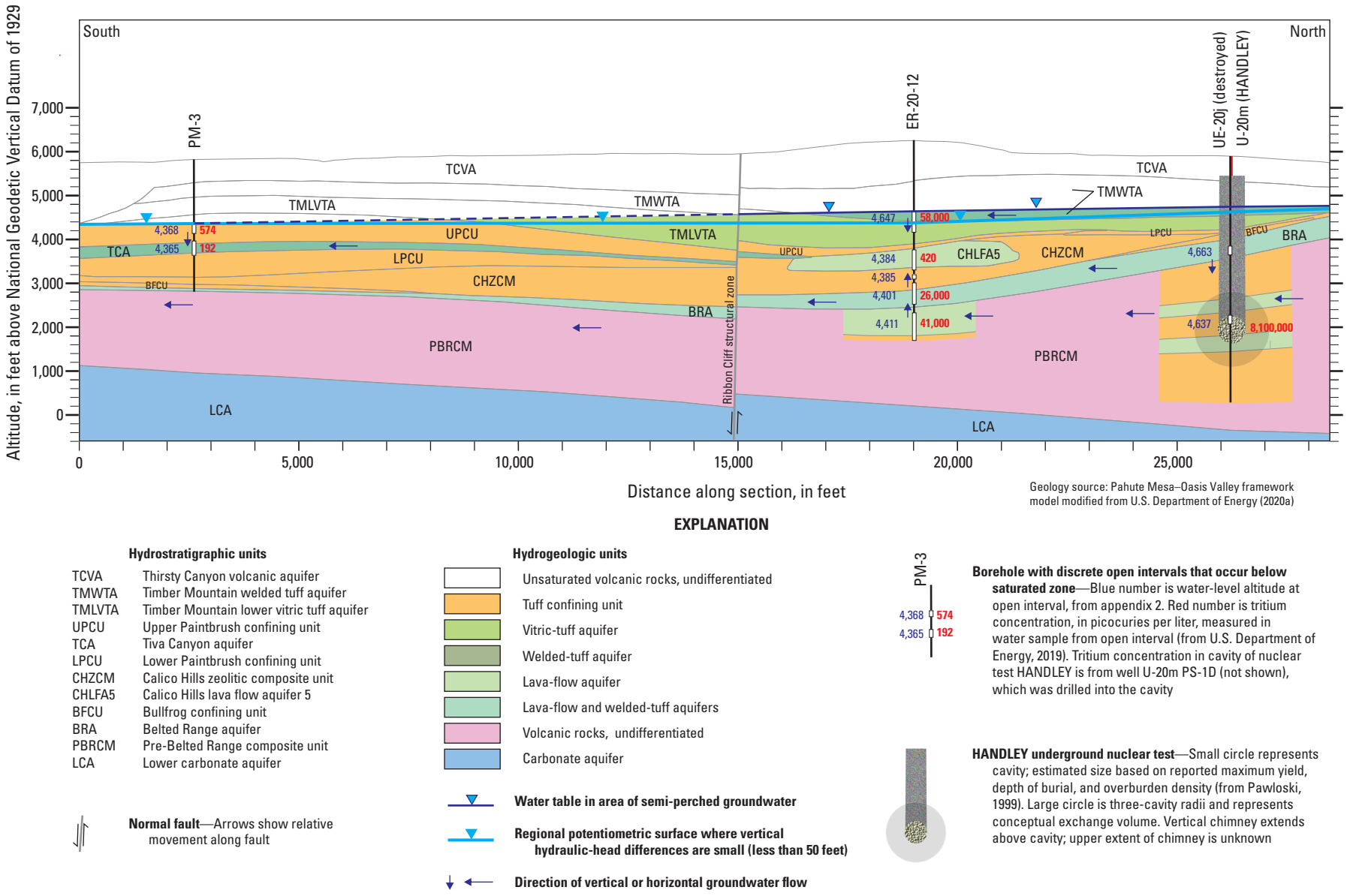

Figure 32. Hydrogeologic and hydrostratigraphic section from HANDLEY nuclear test to borehole PM-3, showing potentiometric surfaces, groundwater-flow directions, and tritium in wells, western Pahute Mesa, southern Nevada.

TCUs function as leaky confining units or aquifers within a groundwater pool between the 4,200- and 4,160-foot contours in the Thirsty Canyon area (fig. 23). The area between the contours has been referred to as the Bench (U.S. Department of Energy, 2020a). Conceptually, a leaky confining unit partially separates an aquifer from an underlying or overlying aquifer. In terms of pumping, a leaky confining unit attenuates, but does not impede, the propagation of a pumping signal through the unit into an adjacent aquifer. For example, two constant-rate tests were done at well *ER-EC-11 main*, where a packer was used to isolate and hydraulically test the TCA separately from the TSA (Navarro-Intera, LLC, 2011). Pumping from either TCA or TSA at well *ER-EC-11 main* caused water-level declines in observation wells *ER-EC-6 shallow*, *ER-EC-6 intermediate*, and *ER-EC-6 deep* (fig. 33), which are open to the BA, TCA, and TSA, respectively (section *D–D´* on plate 2). A water-level decline in the BA at well *ER-EC-6 shallow* indicates that pumping from the TCA at well *ER-EC-11 main* propagated across the UPCU into the BA and pumping from the TSA at *ER-EC-11 main* propagated across the LPCU, TCA, and UPCU. HSUs designated as confining units may leak in the Bench area because of intense fracturing or faulting that breaches and creates hydraulic pathways through the TCUs.

Leaky confining units that were observed during large-scale aquifer testing (Garcia and others, 2017) may not be restricted to the Bench area. The lack of pervasive vertical gradients on Pahute Mesa suggests that TCUs probably leak in other areas. For example, downgradient of the Bench, two aquifer-test results indicate that the FCCM has transmissivities of 200 and 7,000 ft^2/d in the Thirsty Canyon area (fig. 16). The FCCM HSU is composed predominantly of TCU (table 1). Moderate-to-high transmissivities in the FCCM indicate that TCUs can function as aquifers.

Water converges toward a groundwater trough in the upgradient part of the Thirsty Canyon area (plate 1). The low-gradient convergence area begins near borehole *UE-20d*, about 2 mi northeast of the NNSS boundary. From this borehole to borehole *ER-EC-2A*, a distance of 8.6 mi, the hydraulic gradient is extremely low at 3.7 ft/mi. Groundwater from the Black Mountain area, west of the NNSS, converges with water from NNSS Area 20. This converging groundwater initially flows south-southwest and then southwest along the trough, which coincides with Thirsty Canyon and the Thirsty Canyon lineament. The water ultimately reaches the upgradient end of Oasis Valley.

Timber Mountain

A groundwater mound is conceptualized at Timber Mountain, in the absence of water-level data, because high precipitation rates on the mountain suggest the occurrence of a localized recharge mound (plate 1). Winter precipitation rates on Timber Mountain, based on data from 2010 to 2019, were almost as great as on Rainier Mesa (Lyles and others, 2012; National Oceanic and Atmospheric Administration, 2019). Rainier Mesa is an area where the occurrence of recharge and mounded groundwater is well documented (Fenelon and others, 2008; U.S. Department of Energy, 2018). Most recharge in the PMOV basin results from winter precipitation, when evapotranspiration rates are low and excess water can infiltrate below the root zone (Winograd and others, 1998; Smith and others, 2017). Recharge and infiltration models indicate maximum recharge rates beneath Timber Mountain of 0.6 in/yr (Hevesi and others, 2003), 0.8 in/yr (Russell and Minor, 2002), and 2 in/yr (U.S. Department of Energy, 1997). Low groundwater-chloride concentrations in wells surrounding Timber Mountain are consistent with Timber Mountain being a recharge location (Fenelon and others, 2016). A moderate amount of recharge (totaling about 15 percent of the discharge at Oasis Valley) was estimated for the Timber Mountain area (fig. 28).

The degree of mounding beneath Timber Mountain is proportional to the recharge rate and inversely proportional to saturated-rock transmissivities. The recharge rate is expected to be moderate, ranging from 0.6 to 2 in/yr, based on recharge and infiltration models, as discussed above. The transmissivity of the core of Timber Mountain is unknown, but transmissivities are high (greater than 1,000 ft^2/d) in five of six wells that ring the outer flanks of the mountain (fig. 24). These five wells (*Beatty Wash Windmill*, *ER-EC-5*, *ER-EC-7*, *ER-EC-14 deep*, and *UE-18r*) have a geometric mean transmissivity of 6,000 ft^2/d (Frus and Halford, 2018). Transmissive rocks beneath Timber Mountain will cause localized recharge to spread and dissipate so that hydraulic gradients are low and only a slightly elevated mound is formed, as portrayed on plate 1.

The presence of even a slight groundwater mound beneath Timber Mountain creates a hydraulic barrier to groundwater flow in the center of the southeastern boundary of the PMOV basin. The southeastern boundary is defined by groundwater mounds at Rainier Mesa, Timber Mountain, and Bare Mountain, and the boundary parallels groundwater-flow paths between these mounds. Recharge from Timber Mountain forces southwestward flowing water from Pahute Mesa to remain on the northwestern side of the mountain as it flows to Oasis Valley.

Geochemical evidence suggests that groundwater north of Timber Mountain flows toward Oasis Valley. Stable isotopes oxygen-18 and deuterium were analyzed in groundwater throughout the PMOV basin (Kwicklis and others, 2005). The distribution of these isotopic compositions indicates that isotopically light groundwater from Areas 19 and 20 on Pahute Mesa flows around the western side of Timber Mountain toward Oasis Valley rather than southward toward Yucca Mountain. Groundwater south of Timber Mountain in Fortymile Wash, upper Beatty Wash and Yucca Mountain is isotopically heavier, suggesting no significant influx of groundwater from Pahute Mesa.

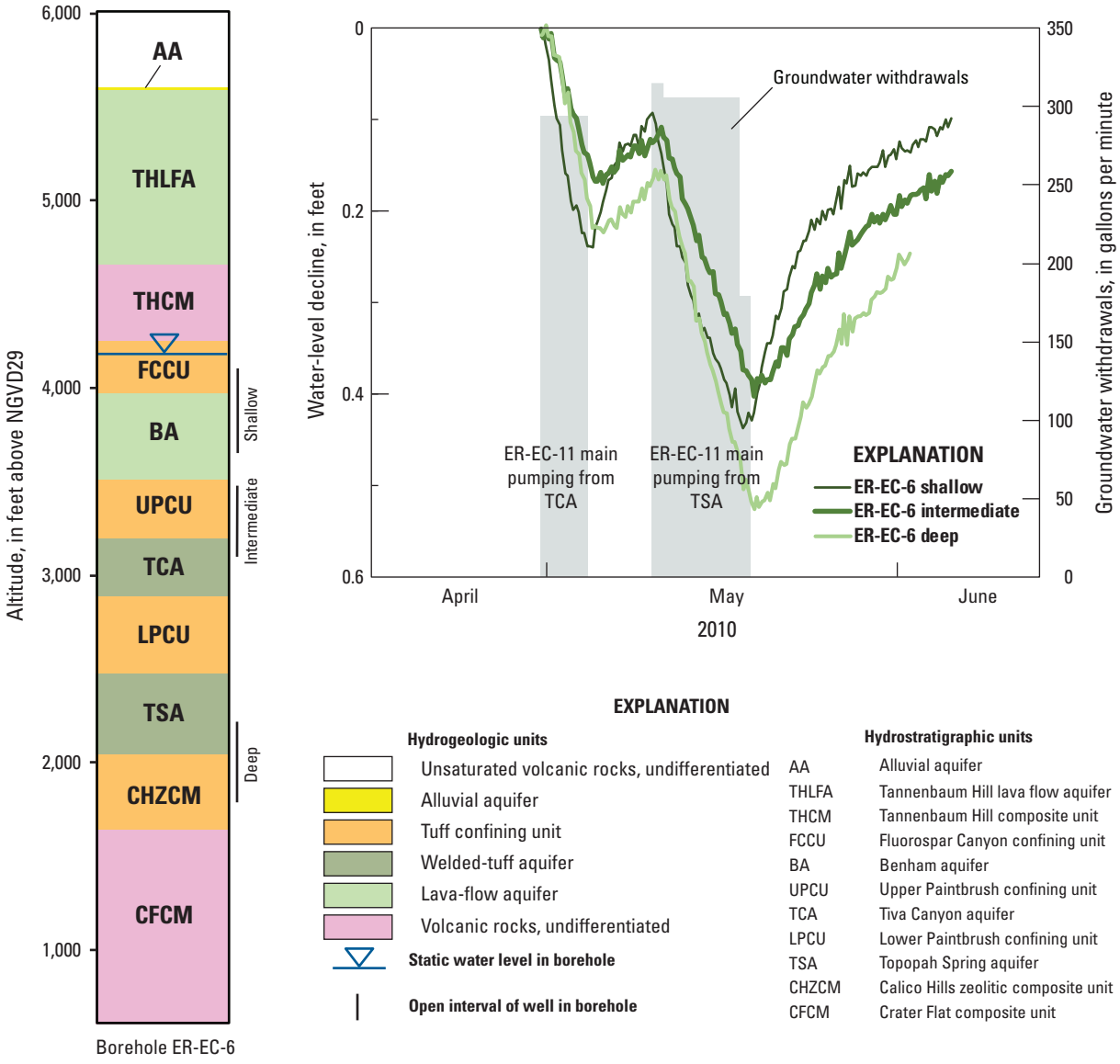

Figure 33. Water-level declines in wells ER-EC-6 shallow, ER-EC-6 intermediate, and ER-EC-6 deep in response to pumping from well ER-EC-11 main during multiple-well aquifer testing in the Thirsty Canyon area, Pahute Mesa–Oasis Valley groundwater basin, southern Nevada.

Kwicklis and others (2005) also concluded, based on isotopic analysis, that groundwater from upper Beatty Wash, between wells *ER-0V-03c* and *Beatty Wash Windmill*, likely flows south into Crater Flat rather than southwest towards Oasis Valley as is portrayed on plate 1. Upper Beatty Wash lies within the area of uncertainty for the southeastern boundary of the PMOV basin (plate 1), which was defined based on uncertainty in the potentiometric surface. If the isotopic interpretation is correct, then the southeastern boundary of the PMOV basin near upper Beatty Wash can be moved as much as several miles north without contradicting hydraulic-head data. Moving the southeastern boundary of the PMOV basin northward also would not affect groundwater-flow paths from all Pahute Mesa nuclear tests, which are toward Oasis Valley.

Oasis Valley

All groundwater in the PMOV basin flows into Oasis Valley to discharge at springs and seeps. Ninety-eight percent of this water is discharged by evapotranspiration in areas of shallow groundwater adjacent to the Amargosa River, whereas the remaining two percent flows south through alluvium underlying the Amargosa River and into the AFFCR groundwater basin. More than 60 discrete springs have been identified in Oasis Valley (plate 1), including clusters of springs at Goss Springs, Hot Springs, Ute Springs, Beatty Springs, and Revert Springs.

Discharge from Hot Springs is about 105 °F, indicating upward movement of water adjacent to the Beatty fault from deeper in the flow system (Reiner and others, 2002), with little time to cool before discharging. Water does not need to travel to great depths to reach this warm temperature. A correlation analysis was done between measured groundwater temperatures and depth at 31 wells in the Pahute Mesa and Thirsty Canyon areas, based on data from Blankennagel and Weir (1973) and Reiner (2007). Results of the analysis show that half of the wells have water temperatures greater than 105 °F within the active part of the flow system, at a depth of less than 1,600 ft below the water table.

Horizontal and vertical hydraulic gradients are high where groundwater converges into the discharge area in Oasis Valley. Horizontal gradients are as much as 150 ft/mi where water flows east or west toward the springs (fig. 26; plate 1). Vertical gradients in the discharge area are expected to be upward as groundwater moves to land surface. Vertical gradients were measured at three sites in the Oasis Valley area; two were upward and one was downward (fig. 27).

The large downward gradient in Oasis Valley occurs near the Hogback fault at site *ER-OV-03a* (section *B–B´* on plate 2). Vertical gradients at the site suggest that shallow groundwater in alluvium discharges from nearby springs at altitudes of about 3,838 ft (plate 1), whereas deeper groundwater moves downward, likely aided by the Hogback fault. The water level in the deepest well at site *ER-OV-03a* has an altitude of 3,681 ft, nearly equal to the land-surface altitude at the downgradient Goss Springs (plate 1). These nearly equal altitudes suggest that groundwater moving downward along the fault near site *ER-OV-03a* likely discharges at Goss Springs.

Relation of Radionuclide Transport to Groundwater Flow

Potentiometric contours indicate groundwater-flow paths from all 82 underground nuclear-test locations on Pahute Mesa terminate in the Oasis Valley discharge area (Fenelon and others, 2016; Halford and Jackson, 2020). Nearly all the tests were conducted in the eastern Pahute Mesa area, with two tests in the western Pahute Mesa–Black Mountain area (fig. 26). Potentiometric contours in the nuclear-test areas are well-constrained by water-level data. Therefore, there is a low probability that radionuclides from any nuclear test on Pahute Mesa will move south through Fortymile Canyon or toward Yucca Mountain, as has been simulated in some previous studies (U.S. Department of Energy, 1997; Stoller-Navarro Joint Venture, 2009; Zhu and others, 2009).

Pahute Mesa hosted the 14 largest detonations at the NNSS, based on their maximum announced yields (U.S. Department of Energy, 2015). These detonations have either a specified yield greater than one megaton [Mt] or the maximum of the announced yield range is 1 Mt or greater. Two detonations have specified yields: BENHAM at 1.15 Mt and BOXCAR at 1.3 Mt (fig. 34; U.S. Department of Energy, 2015). Twelve detonations have unspecified yields: (1) HANDLEY at greater than 1 Mt; (2) COLBY at 500 to 1,000 kilotons (kt); (3) JORUM at less than 1 Mt; and (4) nine detonations at 200 to 1,000 kt (ALMENDRO, CAMEMBERT, FONTINA, INLET, KASSERI, MAST, MUENSTER, PIPKIN, and TYBO; fig. 34). Sixty percent of the radionuclides released during nuclear testing at the NNSS were on Pahute Mesa (Finnegan and others, 2016), despite having only 10 percent of the tests (U.S. Department of Energy, 2015).

Although the working points of more than half the tests on Pahute Mesa are above the water table (fig. 34), only three tests are more than three calculated cavity radii above the water table (Pawloski, 1999; U.S. Department of Energy, 2015). Therefore, nearly all tests likely redistributed radionuclides below or immediately above the water table.

Figure 34 shows the distribution of boreholes where one or more wells were sampled for tritium and the relative groundwater concentrations of tritium in the Pahute Mesa area. Tritium data were derived from Stoller-Navarro Joint Venture (2007a) and U.S. Department of Energy (2019). Only wells sampled for tritium after all underground nuclear testing ceased (post-1992) are shown on figure 34. Tritium samples from wells drilled directly into test cavities are not shown.

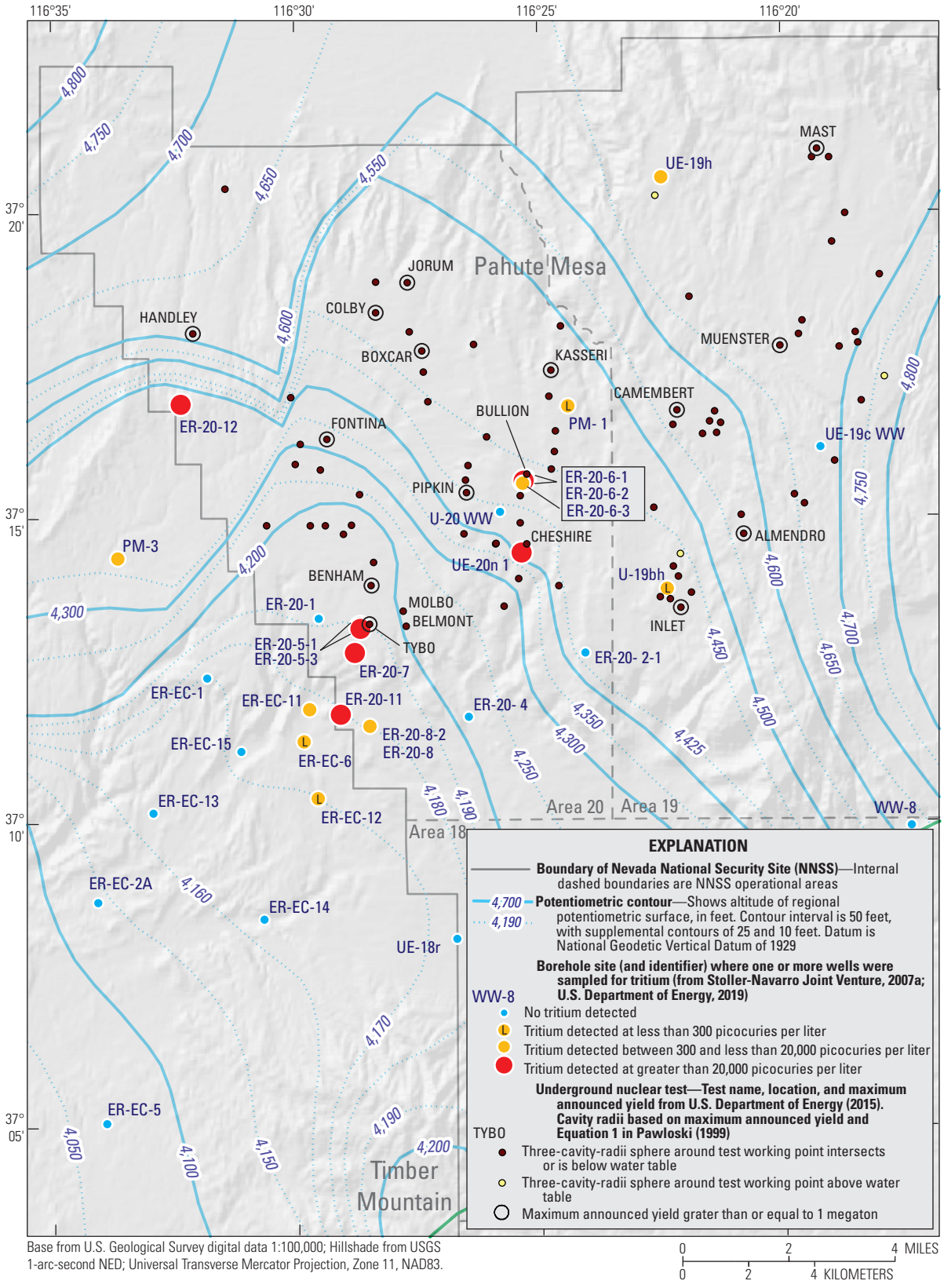

Figure 34. Potentiometric surface, underground nuclear tests, and boreholes where one or more wells were sampled for tritium on Pahute Mesa, Nevada National Security Site, southern Nevada.

Radionuclide plumes in the Pahute Mesa area, discussed in the following paragraphs, have been observed downgradient of at least four underground nuclear tests: BULLION, CHESHIRE, BENHAM, and HANDLEY (IT Corporation, 1998; Sawyer and others, 1999; Wolfsberg and others, 2002; Russell and others, 2017). Localized tritium plumes downgradient of many other nuclear tests on Pahute Mesa are likely but have not been observed because of limited observation wells immediately downgradient of most tests. However, widespread radionuclide contamination across Pahute Mesa has not been observed, based on limited data. Several boreholes downgradient of tests, but not associated with plumes from BULLION, CHESHIRE, BENHAM, and HANDLEY, have no detectable tritium (fig. 34). These boreholes include *UE-19c WW*, *U-20 WW*, *ER-20-1*, *ER-20-2-1*, *ER-20-4*, and *ER-EC-1*. Several other boreholes along the southeastern PMOV boundary had no detectable tritium. These include *WW-8* (fig. 34) and *UE-18t* and *ER-18-2*, about 3 and 6 mi, respectively, to the southwest of *WW-8*. Low concentrations of tritium (less than 300 picocuries per liter [pCi/L]) were detected in boreholes *U-19bh* and *PM-1*, and a moderate concentration of tritium was detected in borehole *UE-19h*. The latter borehole had a tritium concentration of 1,970 pCi/L from a single sample in 1999; however, a confirmation sample was never collected to verify this result. Assuming tritium is present in borehole *UE-19h*, the likely source is the nuclear test, MAST, about 3 mi to the northeast (fig. 34; section *D–D´* on plate 2).

Wells *ER-20-6-1*, *ER-20-6-2*, and *ER-20-6-3* are 500 to 1,000 ft downgradient of the BULLION test (fig. 34). Wells *ER-20-6-1* and *ER-20-6-2* had tritium concentrations greater than 20,000 pCi/L in 1996, shortly after drilling the wells (Stoller-Navarro Joint Venture, 2007a); however, more recent samples collected in 2017 indicated tritium concentrations were near or below the detection limit of about 300 pCi/L (U.S. Department of Energy, 2019). The farthest downgradient well, *ER-20-6-3*, had tritium concentrations as high as 4,000 pCi/L in 1997, but concentrations in 2017 were below detection.

CHESHIRE test, with an announced yield of 200 to 500 kilotons, was detonated in 1976 (U.S. Department of Energy, 2015). Well *UE-20n 1* was completed in CHLFA4, 980 ft downgradient of CHESHIRE (fig. 34; section *C–C´* on plate 2). Radionuclides, including high levels of tritium attributed to CHESHIRE, were detected the year the well was completed in 1987 (Sawyer and others, 1999). This equates to a minimum transport velocity[3] in the CHLFA4 of 70 ft/yr if transport is measured from the edge of the cavity and 20 ft/yr if transport is measured from the edge of a three-cavity-radii sphere, where both calculations are based on a maximum yield of 500 kilotons. This simplified calculation ignores transient effects from test-induced heating and cooling of nearby groundwater and infilling of water into the cavity and chimney after the test (Pawloski and others, 2001; Carle and others, 2003). The southwesterly transport direction from CHESHIRE is consistent with the flow direction indicated from potentiometric contours (plate 1).

Tritium and other radionuclides have been detected in multiple wells downgradient of the BENHAM test. The BENHAM test was detonated in 1968 and, at 1.15 megatons, has one of the largest announced yields on the NNSS. Radionuclides were detected initially in 1996 in shallow well *ER-20-5-1*, open to TSA, and deeper well *ER-20-5-3*, open to CHLFA5 (section *D–D´* on plate 2). Plutonium detected in both wells was attributed to the BENHAM test (Kersting and others, 1999), despite the TYBO[4] test being much closer (900 ft versus 4,300 ft) to the *ER-20-5* well site. Tritium has been detected at moderate-to-high concentrations in five additional boreholes downgradient of the BENHAM test (fig. 34). Two other boreholes, *ER-EC-6* and *ER-EC-12*, have low-level (4–7 pCi/L) tritium concentrations that may be part of the leading edge of the plume. Although much of the tritium detected downgradient can be attributed to the BENHAM test, several tests south of the BENHAM test cannot be ruled out as contributing to the tritium plume.

A transport velocity that ranges from greater than 340 to 500 ft/yr is estimated for the leading edge of tritium transport from the BENHAM test. This velocity range is based on linear transport distances of 14,000 and 22,000 ft from the BENHAM test to holes *ER-20-8* and *ER-EC-12*, respectively. Elapsed times ranged from less than 41 years in hole *ER-20-8* to 44 years in hole *ER-EC-12*—tritium was detected during drilling of hole *ER-20-8* in 2009 and was first detected in hole *ER-EC-12* in 2012 (Navarro-Interra, LLC, 2012; U.S. Department of Energy, 2019). If the downgradient tritium is derived from a different nearby test (TYBO, BELMONT, or MOLBO; fig. 34), then the transport velocity could range from greater than 300 to 700 ft/yr. Transport directions are south-southwest and directions computed from any of the four tests listed in this paragraph are consistent with flow directions derived from the potentiometric map.

Radionuclides have been observed downgradient of the HANDLEY test in the western Pahute Mesa–Black Mountain area (Navarro, 2018). The HANDLEY test was detonated in 1970 and had a reported yield of greater than 1 megaton (U.S. Department of Energy, 2015). Low concentrations of tritium (less than 50 pCi/L) were detected in downgradient hole *PM-3* in 2000, but the detections were flagged as uncertain (Navarro-Intera, LLC, 2015). In 2010, low levels of tritium were detected again, but with a high level of certainty. Hole *ER-20-12*, drilled in 2016, encountered high levels of tritium and confirmed the presence of a plume between the HANDLEY test and hole *PM-3* (fig. 34).

[3]Calculated transport velocities are not average linear velocities. Transport velocities are reported to provide a mechanism for comparing transport distances and times between tritium plumes from different nuclear tests.

[4]TYBO test, with an announced yield of 200 to 1,000 kilotons, was detonated in 1975 (U.S. Department of Energy, 2015).

A transport velocity of 600 to 800 ft/yr, or about 2 ft/d, is estimated for the leading edge of tritium transport from the HANDLEY test to hole *PM-3*. This velocity is based on a linear transport distance of 23,600 ft and an elapsed time of 30 or 40 years. The slower velocity estimate assumes that the initial tritium detections in hole *PM-3* were false positives and that tritium arrived at hole *PM-3* in 2010. The transport direction is south-southwest and consistent with the flow direction indicated from the potentiometric contours.

Several observations on groundwater-flow paths between the HANDLEY test and hole *PM-3* can be made based on water-level and tritium measurements and transmissivity estimates. The HANDLEY test was detonated in a TCU within the PBRCM, with 300- to 400-ft-thick LFAs directly above and below the test (fig. 32). Radionuclides likely circulated within the test cavity and chimney and exited through the most permeable units. Based on hydraulic testing in adjacent hole *UE-20j*, the BRA and a 600-ft section of rock directly above the cavity that includes lava and adjacent tuffs have the highest transmissivities of all tested intervals (200 and 800 ft^2/d, respectively; see HSU analysis in appendix 6). Although not hydraulically tested, the TMWTA at the HANDLEY site has a saturated thickness of about 100 ft near the water table. This moderately welded tuff likely has at least moderate transmissivity (between 10 and 1,000 ft^2/d) based on the high concentration (greater than 20,000 pCi/L) of tritium detected at the water table in hole *ER-20-12* (fig. 34). High concentrations of tritium in hole *ER-20-12* also were detected in the BRA and the lava flow in the upper part of the PBRCM. The PBRCM lava flow was hydraulically tested and found to have a moderate transmissivity of 40 to 90 ft^2/d (Navarro, 2018). The zones where high concentrations of tritium were detected in hole *ER-20-12* are consistent with the zones of high transmissivity observed in hole *UE-20j*. Low concentrations of tritium in hole *ER-20-12* were detected in the CHLFA5, which is isolated from the HANDLEY test by several HSUs consisting of TCU. Farther downgradient, low concentrations of tritium in hole *PM-3* were detected in the TCA and UPCU. The TCA in hole *PM-3* has a moderate transmissivity (600 ft^2/d; see HSU analysis in appendix 6) and likely is the primary migration pathway for tritium to hole *PM-3*. However, the underlying BRA and PBRCM were not sampled. A direct hydraulic connection between the BRA in hole *ER-20-12* and the TCA and UPCU in hole *PM-3* was observed during drilling of *ER-20-12* (Navarro, 2018). This hydraulic connection suggests that the groundwater-flow path and transport route from *ER-20-12* to *PM-3* is not a direct route through a single HSU, but rather that vertical pathways may exist. A final observation regarding radionuclide transport from the HANDLEY test is that radionuclides are not likely to move into the underlying carbonate aquifer (LCA). In hole *ER-20-12*, the hydraulic gradient is upward from the upper part of the PBRCM to the BRA, which suggests that the BRA is the drain for groundwater in this area rather than the deeper LCA.

Summary

This report presents a detailed conceptual model of groundwater flow in the Pahute Mesa–Oasis Valley (PMOV) groundwater basin. The conceptual model integrates geologic, hydrologic, hydraulic-property, and radionuclide data. Geologic data were obtained from a previously published hydrostratigraphic framework model of the PMOV basin, referred to as the PMOV HFM. Geologic units from the PMOV HFM are categorized into hydrogeologic units (HGUs) and hydrostratigraphic units (HSUs). Hydrologic data include water levels, natural groundwater-discharge estimates, and groundwater-withdrawal estimates. Hydraulic-property data include transmissivity estimates from wells in the PMOV basin, which were compiled from a previously published hydraulic-properties database. Radionuclide data are restricted to measured tritium in wells. The groundwater-flow conceptualization provides a framework for the development of groundwater flow and radionuclide transport models in the PMOV basin.

The PMOV basin flow conceptualization includes descriptions of the following:

1. the lateral PMOV basin boundary;
2. the lower boundary of the active part of the flow system;
3. the lower PMOV basin boundary, which is based on radionuclide transport depths;
4. the PMOV basin groundwater budget, including areas of recharge and discharge;
5. a potentiometric surface constructed for the PMOV basin, which portrays horizontal hydraulic gradients and regional groundwater-flow directions;
6. the spatial pattern in transmissivity;
7. the spatial pattern in vertical hydraulic gradients;
8. steady-state water-level trends;
9. the spatial extent of water levels affected by transient (pumping or nuclear testing) stresses, and the effect of these stresses on regional groundwater flow;
10. the function of faults as conduits or barriers to flow;
11. the vertical distribution of HSUs, HGUs, and flow directions, as determined from nine sets of hydrostratigraphic and hydrologic cross sections constructed in this study;
12. the relation of radionuclide transport to groundwater flow; and

13. hydraulic-property and alteration analyses, which include depth analyses (relations of hydraulic conductivity and alteration with depth); transmissivity analyses (relations of transmissivity to HSUs, HGUs, and alteration); and alteration abundance by HGU.

Potentiometric contours indicate that groundwater in the PMOV basin generally flows south-southwest and discharges at Oasis Valley. Flow is southwesterly from the northwestern part of the NNSS to Oasis Valley and is well-constrained by water-level data. Nearly two-thirds of the water discharging to Oasis Valley passes through the Thirsty Canyon area, which is characterized by abundant high-transmissivity rocks that result in large areas of low hydraulic gradients. In Oasis Valley, horizontal and vertical hydraulic gradients are high where groundwater converges into the discharge area. Warm (105 °F) water discharging from some Oasis Valley springs likely becomes heated at relatively shallow depths. Measurements of groundwater temperature in wells in the Pahute Mesa and Thirsty Canyon areas indicate that about half the wells have water temperatures greater than 105 °F within the active part of the flow system, at a depth of less than 1,600 ft below the water table.

The lateral boundary of the PMOV basin defines the area over which recharge occurs, moves downgradient, and discharges to Oasis Valley. The boundary is consistent with updated estimates of discharge in the PMOV and Alkali Flat–Furnace Creek Ranch (AFFCR) groundwater basins. The lateral boundary of the PMOV basin generally represents a no-flow boundary, although minor amounts of interbasin flow occur along the southern and southeastern boundaries. Some boundary uncertainty exists in the northeastern part of the basin, but potential flow-rate estimates across the northeastern boundary resulting from this uncertainty are small relative to the basin groundwater budget.

The southeastern PMOV boundary between Bare Mountain and Rainier Mesa is a no-flow boundary, as indicated by geologic data, water levels, groundwater-budget constraints, and results from a regional numerical model. Rainier Mesa, Timber Mountain, and Bare Mountain were used as anchor points for delineating the southeastern PMOV boundary, based on the assumption that these highlands contain low-permeability rocks or sufficient recharge to create groundwater mounds beneath them. A postulated, but likely, recharge mound beneath Timber Mountain forms a hydraulic flow barrier in the center of the southeastern PMOV basin boundary. Moderate recharge rates and geochemical evidence support a groundwater mound beneath Timber Mountain, which forces groundwater from eastern Pahute Mesa around the western side of Timber Mountain and toward Oasis Valley rather than southward toward Yucca Mountain. Some uncertainty exists in the location of the southeastern part of the PMOV boundary between Bare and Timber Mountains. Even allowing for uncertainty, flow paths from all 82 underground nuclear tests on Pahute Mesa are toward Oasis Valley.

There are two components of recharge in the PMOV basin: episodic and diffuse. Episodic recharge is a minor recharge component observed as a rise in groundwater levels that occurs three months to one year following a wet winter. Episodic recharge through an unsaturated zone in excess of 1,000 ft requires preferential flow through faults and fractures. Water-level data documenting the occurrence of episodic recharge demonstrate that a preferential-flow component of modern recharge is contributing to the PMOV water budget. Diffuse recharge is the dominant recharge component, which occurs as old water (greater than 10,000 years) within pore spaces in the unsaturated zone slowly percolates through the unsaturated zone and recharges the groundwater system. Most water recharging the groundwater system today likely is old based on residence-time calculations that suggest some modern-day infiltration will take many thousands of years to move through the thick unsaturated zone. Old recharge is consistent with observations of isotopically light deuterium and oxygen 18 compositions in groundwater on Pahute Mesa and central Oasis Valley. Isotopic evidence that suggests a large fraction of recharge water is old can be reconciled with observations of episodic modern recharge as follows. Rapid recharge events at focused locations account only for a small amount of the total basin recharge, but the high hydraulic diffusivity of fractured rocks allows rapid transmission of hydraulic responses to distant wells where old recharge predominates.

Most, about 65 percent, of the recharge in the PMOV basin is derived from eastern Pahute Mesa and Timber Mountain. Limited recharge occurs from highlands north and west of Pahute Mesa because these highland areas are composed of low-permeability rocks, which impede infiltration and induce steep gradients.

Western and eastern Pahute Mesa have groundwater sourced from different recharge areas and distinct flow paths. The two areas are separated by the Thirsty Canyon lineament. A separation of groundwater flow east and west of the lineament is supported by geochemically distinct isotopic, chloride, and sulfate groundwater compositions. Water downgradient of these areas converges and appears to be a mixture of the two water types.

The groundwater system in the PMOV basin is nearly steady state, where recharge and natural discharge are assumed to be in balance. This assumption is reasonable because the lateral basin boundary is a no-flow boundary, and the basin is dominated by steady-state conditions, where long-term changes in groundwater storage from recharge and groundwater pumping are minimal. Therefore, present-day (2020) conditions are considered representative of predevelopment (pre-1950) conditions in nearly all areas of the basin. An estimated 5,900 acre-ft/yr of groundwater discharges to Oasis Valley from springs or by diffuse upward flow into shallow alluvium, where the water is evaporated or transpired by phreatophytes. Groundwater has been withdrawn in the PMOV basin from wells on the Nevada National Security Site (NNSS) and near Beatty since 1963. However, total groundwater withdrawals through 2018 account for less than 10 percent of annual groundwater flow and less than 0.2 percent of groundwater storage in the PMOV basin.

Nuclear testing does not affect the steady-state assumption for regional groundwater flow in the PMOV basin. Observed nuclear-test effects on water levels in Pahute Mesa typically were short-lived (less than 1 yr) or localized to within 1 mi of a test. One large-scale, nuclear-testing effect on water levels has been documented near the CHESHIRE nuclear test, but water levels re-equilibrated to steady-state conditions by 2005. The large-scale, nuclear testing effect permanently lowered water levels within a several-square-mile area near the CHESHIRE nuclear test in eastern Pahute Mesa. Similar declining water-level trends in multiple wells potentially were caused by the breach of a confining unit from a nearby nuclear test, which permanently lowered the hydraulic head in the volcanic rocks open to the wells. Water-level trends from the wells indicate that heads equilibrated to a new steady-state condition within 29 years. During the 29-year re-equilibration period, radionuclides may have experienced a period of accelerated transport rates if a confining unit was breached from a nuclear test. An estimated 27,000 acre-ft (8.9 billion gallons) of groundwater was released from storage, which could have displaced radionuclides as much as 0.3 miles farther downgradient than would have occurred under pre-test, steady-state flow conditions.

Elevated water levels, indicative of semi-perched conditions in shallow rocks, are not uncommon in the Pahute Mesa area. Semi-perched zones are unconfined, saturated volumes of groundwater that form localized recharge mounds and are separated from the underlying regional groundwater system by saturated low-permeability rocks. Water levels in semi-perched zones are elevated because vertical hydraulic conductivities of underlying low-permeability rocks are less than local infiltration rates, which impounds water and laterally diverts flow. These low-permeability rocks that impede downward movement of recharge commonly are tuff confining units and cause large, downward, vertical gradients.

A semi-perched aquifer above the regional system was encountered during completion of hole *ER-20-12* in western Pahute Mesa. Both the shallow and regional aquifers in hole *ER-20-12* are contaminated with radionuclides from the HANDLEY nuclear test. Downgradient contamination of the shallow aquifer demonstrates that groundwater in a semi-perched aquifer can flow laterally for several miles before water moves downward into the regional system.

The lower boundary of the PMOV basin is defined at a depth of 4,000 ft below the water table. This boundary defines the lower boundary of radionuclide migration and was determined from consideration of likely radionuclide transport depths. A depth of 4,000 ft below the water table is sufficiently deep to encompass all nuclear tests and tritium plumes. Extending the lower PMOV basin boundary to a depth greater than 4,000 ft below the water table is not necessary because formation of the cavity-chimney system and thermal buoyancy effects cause the upward migration of tritium from a nuclear test.

The lower boundary of the groundwater-flow system occurs above the lower boundary of the PMOV basin and defines the active part of the flow system where nearly all flow occurs. The lower flow system boundary was determined from the relation of transmissivity with depth. The transmissivity-with-depth relation indicates that greater than 90 percent of the total transmissivity contributing to groundwater flow occurs within 1,600 ft of the water table. As a result, most of the flow in the PMOV basin occurs in shallow saturated rocks and the lower flow system boundary is defined at 1,600 ft below the water table.

Volcanic-rock alteration likely explains the low transmissivity at depth. Argillic and mineralized alterations, which reduce the transmissivity of volcanic rock, are common at depths greater than 1,600 ft below the water table. Fractured rocks likely have low transmissivity at depth because most fractures are closed by fracture mineral coatings. Hydraulic conductivity does not decrease smoothly as a function of depth below either land surface or the water table. However, volcanic rocks can be divided into shallow permeable rocks and deep low-permeability rocks at 1,600 ft below the water table as an alternative to depth decay.

Most of the transmissivity in the volcanic rocks underlying Pahute Mesa is restricted to thin, infrequent permeable zones. Analysis of 219 packer-isolated and slug-tested intervals in 17 Pahute Mesa boreholes indicates that 8 percent of the volcanic-rock volume contains 99.6 percent of the total transmissivity.

All volcanic-rock HGUs and HSUs are composite units, meaning that they can function as either an aquifer or confining unit, and their functionality varies spatially within each unit. For example, welded-tuff aquifer (WTA), lava-flow aquifer (LFA), and tuff confining unit (TCU) HGUs have transmissivity distributions that span up to eight orders of magnitude, and each of these HGUs has a higher occurrence of low-transmissivity estimates (less than 10 ft^2/d) compared to moderate (10–1,000 ft^2/d) or high (greater than 1,000 ft^2/d) transmissivity estimates. Greater than 80 percent of the TCU transmissivity estimates are low because nearly all the rock has undergone argillic, mineralized, or zeolitic alteration.

These alterations reduce transmissivity and cause the TCU to function as a confining unit. However, the TCU does contain a few highly transmissive intervals within zeolitically altered zones. Spatial variability in transmissivity causes the TCU to function primarily as a confining unit in Pahute Mesa, but to function as a leaky confining unit or aquifer downgradient in the Thirsty Canyon area. WTA and LFA HGUs have a higher occurrence of high-transmissivity intervals compared to the TCU. The higher transmissivity in WTA and LFA HGUs is associated with devitrified rocks that do not have fractures closed by secondary mineral coatings. Volcanic HSUs have transmissivity distributions that span up to seven orders of magnitude. This result is consistent with previous studies. In general, mean transmissivities of aquifer HGUs and HSUs are greater than confining unit HGUs and HSUs.

Groundwater encounters an alternating sequence of low- and high-transmissivity rock as it moves from east to west across the eastern Pahute Mesa area. Low- and high-transmissivity rock coincide with high and low horizontal-gradient areas, referred to as dams and pools, respectively. Even though groundwater pools and dams coincide with specific HSUs or HGUs, these units are heterogeneous and do not always function as aquifers (pools) or confining units (dams).

Numerous studies have investigated whether major geologic structures at Pahute Mesa function as conduits or barriers to groundwater flow. One theory is that a regional stress field allows preferentially oriented faults to function as conduits and non-preferentially oriented faults to function as barriers. However, hydraulic evidence does not support dilated fault zones on Pahute Mesa functioning as conduits. At the borehole scale, fracture orientation and spacing are not correlated with the occurrence of permeable flowing fractures in volcanic rocks at Pahute Mesa. A strong negative correlation was reported between hydraulic conductivities in 10 Pahute Mesa wells and distance to the nearest fault when only faults within 1,000 ft of a well were considered. However, multiple-well aquifer test results in 8 of these 10 wells show that nearby faults are neither conduits nor barriers to groundwater flow. Analysis of large-scale, multiple-well aquifer test results at Pahute Mesa showed that fault hydraulic properties were similar to nearby HSU hydraulic properties, indicating that faults are not hydraulically distinct features. More likely, juxtaposition of rocks with similar or different permeabilities across a fault creates flow-path connections or barriers.

Hydraulic data suggest that parts of a limited number of faults act as conduits or barriers to groundwater flow in the PMOV basin. Westward flow across part of the Boxcar fault may be impeded because water-level data indicate that flow is directed southward, nearly paralleling the Boxcar fault. Water-level data indicate that the Thirsty Canyon lineament likely is a barrier and conduit to flow in specific areas. A steep west-to-east hydraulic gradient across the Thirsty Canyon lineament suggests that this lineament acts as a barrier between western and eastern Pahute Mesa. Potentiometric contours along Thirsty Canyon indicate converging flow paths nearly coincident with the lineament, suggesting the lineament is a conduit for flow in this area. Some of the major faults in Oasis Valley are thought to control spring locations by functioning as conduits or barriers to flow. Faults identified as likely to influence groundwater flow and spring locations are the Hogback, Bare Mountain, Beatty, Colson Pond, Fleur-de-Lis, and Hot Spring faults, and the Bullfrog Hills–Fluorspar Canyon detachment.

Tritium and other radionuclides have been detected in wells downgradient of at least four underground nuclear tests: BULLION, CHESHIRE, BENHAM, and HANDLEY. Localized tritium plumes downgradient of other nuclear tests on Pahute Mesa are likely but have not been observed because of limited observation wells immediately downgradient of most tests. Radionuclide-transport directions from BULLION, CHESHIRE, BENHAM, and HANDLEY nuclear tests are consistent with flow directions derived from potentiometric contours. Tritium at the leading edge of the BENHAM plume has moved between 3 and 4 mi, resulting in a transport velocity of about 340 to 500 ft/yr.

Acknowledgments

The authors gratefully acknowledge the contractors, GeoHydros, LLC, and Navarro Research and Engineering, Inc., for providing information from their Pahute Mesa–Oasis Valley hydrostratigraphic framework model. Kevin Day (GeoHydros, LLC), Ken Rehfeldt (Navarro), Tim Vogt (Navarro), and Jeff Wurtz (Navarro) worked collaboratively with authors of this report to provide hydrostratigraphic framework model output integral to (1) developing cross sections, (2) constructing the hydrostratigraphic well logs shown in appendix 3, and (3) analyzing transmissivity by alteration and hydrostratigraphic and hydrogeologic units. We thank Andrew Tompson, Lawrence Livermore National Laboratory, for providing technical guidance concerning radionuclide transport depths. We thank Don Sweetkind, U.S. Geological Survey, for providing geologic insights and technical guidance during development of the cross sections. We thank Keith Halford, U.S. Geological Survey (retired), for providing hydrologic expertise and guidance throughout the project. The authors also gratefully acknowledge the reviewers of this report for their helpful comments: Steven F. Carle (Lawrence Livermore National Laboratory), Philip M. Gardner (U.S. Geological Survey), and Shana L. Mashburn (U.S. Geological Survey).

References Cited

Avon, L., and Durbin, T.J., 1994, Evaluation of the Maxey-Eakin method for estimating recharge to ground-water basins in Nevada—American Water Resources Association: Water Resources Bulletin, v. 30, no. 1, p. 99–111, https://onlinelibrary.wiley.com/doi/abs/10.1111/j.1752-1688.1994.tb03277.x.

Bechtel Nevada, 2002a, A hydrostratigraphic model and alternatives for the groundwater flow and contaminant transport model of Corrective Action Units 101 and 102—Central and western Pahute Mesa, Nye County, Nevada: U.S. Department of Energy Report DOE/NV /11718–706, 383 p., https://www.osti.gov/biblio/799777-hydrostratigraphic-model-alternatives-groundwater-flow-containment-transport-model-corrective-action-units-central-western-pahute-mesa-nye-county-nevada.

Bechtel Nevada, 2002b, Completion report for well ER-EC-2A: U.S. Department of Energy DOE/NV/11718--591, 115 p., https://www.osti.gov/biblio/793382-completion-report-well-er-ec

Bechtel Nevada, 2004a, Completion report for well ER-EC-5: U.S. Department of Energy DOE/NV/11718--424, 103 p.

Bechtel Nevada, 2004b, Completion report for well ER-EC-7: U.S. Department of Energy DOE/NV/11718--467, 95 p., https://www.osti.gov/biblio/840518-completion-report-well-er-ec.

Belcher, W.R., and Sweetkind, D.S., eds., 2010, Death Valley regional groundwater flow system, Nevada and California—Hydrogeologic framework and transient groundwater flow model, U.S. Geological Survey Professional Paper 1711, 398 p., https://doi.org/10.3133/pp1711.

Belcher, W.R., Sweetkind, D.S., and Elliott, P.E., 2002, Probability distributions of hydraulic conductivity for the hydrogeologic units of the Death Valley regional ground-water flow system, Nevada and California: U.S. Geological Survey Water-Resources Investigations Report 2002–4212, 24 p., https://doi.org/10.3133/wri024212.

Benedict, F.C., Jr., Rose, T.P., and Zhou, X., 2000, Mineralogical, chemical, and isotopic characterization of fracture-coating minerals in borehole samples from western Pahute Mesa and Oasis Valley, Nevada: Lawrence Livermore National Laboratory Report UCRL-ID-152919, 113 p.

Bernabé, Y., Mok, U., and Evans, B., 2003, Permeability-porosity relationships in rocks subjected to various evolution processes: Pure and Applied Geophysics, v. 160, no. 5, p. 937–960, https://doi.org/10.1007/PL00012574.

Blankennagel, R.K., 1967, Hydraulic testing techniques of deep drill holes at Pahute Mesa, Nevada test site: U.S. Geological Survey Open-File Report 67–18, 51 p., https://doi.org/10.3133/ofr6718.

Blankennagel, R.K., and Weir, J.E., Jr., 1973, Geohydrology of the eastern part of Pahute Mesa, Nevada test site, Nye, County, Nevada: U.S. Geological Survey Professional Paper 712–B, 35 p., https://doi.org/10.3133/pp712B.

Brikowski, T.H., 1992, Estimates of potential radionuclide migration at the Bullion site: Reno, Nevada, Desert Research Institute, Publication no. 45097, 26 p., https://doi.org/10.2172/138468.

Cardenas, B.M., and Jiang, X.W., 2010, Groundwater flow, transport, and residence times through topography-driven basins with exponentially decreasing permeability and porosity: Water Resources Research, v. 46, no. 11, 9 p., https://doi.org/10.1029/2010WR009370.

Carle, S.F., 2016, Spreadsheet for estimation of uncertainty of potentiometric head variation of water temperature and gravity within the water column of Pahute Mesa boreholes: Lawrence Livermore National Laboratory LLNL-MI-693218, 1 spreadsheet.

Carle, S.F., Maxwell, R.M., and Pawloski, G.A., 2003, Impact of test heat on groundwater flow at Pahute Mesa, Nevada Test Site: Lawrence Livermore National Laboratory Report UCRL-ID-152599, 144 p.

Carroll, R.D., and Lacomb, J.W., 1993, Borehole techniques identifying subsurface chimney heights in loose ground–Some experiences above underground nuclear explosions: International Journal of Rock Mechanics and Mining Sciences & Geomechanics Abstracts, v. 30, no. 6, p. 575–590, https://doi.org/10.1016/0148-9062(93)91218-8.

Code of Federal Regulations, 2019, Title 40 Code of Regulations, Part 141–National Primary Drinking Water Regulations: U.S. Government Printing Office, Washington, D.C., https://www.govinfo.gov/content/pkg/CFR-2017-title40-vol25/xml/CFR-2017-title40-vol25-part141.xml.

Cohen, A.C., 1976, Progressively censored sampling in the three parameter log-normal distribution: Technometrics, v. 18, no. 1, p. 99–103, https://doi.org/10.2307/1267922.

Cooper, C.A., Hershey, R.L., Healey, J.M., and Lyles, B.F., 2013, Estimation of groundwater recharge at Pahute Mesa using the chloride mass-balance method: Desert Research Institute Publication No. 45251, 99 p., https://www.osti.gov/biblio/1113247-estimation-groundwater-recharge-pahute-mesa-using-chloride-mass-balance-method.

D'Agnese, F.A., Faunt, C.C., and Turner, A.K., 1998, An estimated potentiometric surface of the Death Valley region, Nevada and California, developed using Geographic Information System and automated interpolation techniques: U.S. Geological Survey Water-Resources Investigations Report 97–4052, 15 p., https://doi.org/10.3133/wri974052.

Day, K.E., and Kincaid, T.R., 2013, Benefits of Automation in Hydrostratigraphic Framework Modeling—A New HFM for Pahute Mesa, Nevada: MODFLOW and More 2013: Translating Science into Practice, conference paper: Golden, Colorado, Colorado School of Mines, http://www.geohydros.com/images/Pubs/geohydros_2013_New_PahuteMesa_HFM_ExtAbs_MODFLOW2013.pdf.

Day, K.E., Kincaid, T.R., Vogt, T., Ruskauff, G., Drellack, S., Prothro, L., and Reed, D., 2013, A new hydrostratigraphic framework model (HFM) of Pahute Mesa, Nevada—2, Lava flow aquifers (LFAs)—MODFLOW and More 2013—Translating Science into Practice, poster presentation: Golden, Colorado, Colorado School of Mines, http://www.geohydros.com/images/Pubs/geohydros_2013_New_PahuteMesa_HFM_Poster2_MODFLOW2013.pdf.

Dickerson, R., Fryer, B., and Hand, J., 2006, Letter report: Fracture database evaluation and analysis: Stoller-Navarro Joint Venture report, 62 p., https://doi.org/10.13140/2.1.1364.5602.

Drellack, S.L., Jr., Prothro, L.B., Roberson, K.E., Schier, B.A., and Price, E.H., 1997, Analysis of fractures in volcanic cores from Pahute Mesa, Nevada Test Site: U.S. Department of Energy Report DOE/NV/11718-160, 203 p., https://digital.library.unt.edu/ark:/67531/metadc691651/m2/1/high_res_d/623041.pdf.

Drellack, S.L., Jr., Prothro, L.B., and Gonzales, J.L., 2002, A hydrostratigraphic model of the Pahute Mesa–Oasis Valley area, Nye County, Nevada: U.S. Department of Energy Report DOE/NV/11718-646, 14 p., https://www.osti.gov/biblio/790074.

Elliott, P.E., and Fenelon, J.M., 2010, Database of groundwater levels and hydrograph descriptions for the Nevada Test Site area, Nye County, Nevada (ver. 10.0, February 2020): U.S. Geological Survey Data Series 533, 16 p., https://doi.org/10.3133/ds533.

Elliott, P.E., and Moreo, M.T., 2018, Update to the groundwater withdrawals database for the Death Valley regional groundwater flow system, Nevada and California, 1913–2010: U.S. Geological Survey data release, https://doi.org/10.5066/F75H7FH3.

Erikson, S.J., 1991, Report of drilling and radionuclide migration investigations at UE20n#1, Pahute Mesa, Nevada Test Site, 1987: U.S. Department of Energy Report DOE/NV/10384--35, Desert Research Institute Publication No. 45081, 127 p., https://inis.iaea.org/search/search.aspx?orig_q=RN:22083862.

Faunt, C.C., 1997, Effect of faulting on ground-water movement in the Death Valley region, Nevada and California: U.S. Geological Survey Water-Resources Investigations Report 95–4132, 42 p., 1 pl., https://doi.org/10.3133/wri954132.

Faunt, C.C., Sweetkind, D.S., and Belcher, W.R., 2010, Three-dimensional hydrogeologic framework model, chap. E *of* Belcher, W.R., and Sweetkind, D.S., eds., Death Valley regional groundwater flow system, Nevada and California—Hydrogeologic framework and transient groundwater flow model: U.S. Geological Survey Professional Paper 1711, p. 161–249, https://doi.org/10.3133/pp1711.

Fenelon, J.M., 2000, Quality assurance and analysis of water levels in wells on Pahute Mesa and vicinity, Nevada Test Site, Nye County, Nevada: U.S. Geological Survey Water-Resources Investigations Report 2000–4014, 68 p., https://doi.org/10.3133/wri004014.

Fenelon, J.M., Laczniak, R.J., and Halford, K.J., 2008, Predevelopment water-level contours for aquifers in the Rainier Mesa and Shoshone Mountain area of the Nevada Test Site, Nye County, Nevada: U.S. Geological Survey Scientific Investigations Report 2008–5044, 38 p., https://doi.org/10.3133/sir20085044.

Fenelon, J.M., Sweetkind, D.S., and Laczniak, R.J., 2010, Groundwater flow systems at the Nevada Test Site, Nevada—A synthesis of potentiometric contours, hydrostratigraphy, and geologic structures: U.S. Geological Survey Professional Paper 1771, https://doi.org/10.3133/pp1771.

Fenelon, J.M., Sweetkind, D.S., Elliott, P.E., and Laczniak, R.J., 2012, Conceptualization of the predevelopment groundwater flow system and transient water-level responses in Yucca Flat, Nevada National Security Site, Nevada: U.S. Geological Survey Scientific Investigations Report 2012–5196, 61 p., https://doi.org/10.3133/sir20125196.

Fenelon, J.M., Halford, K.J., and Moreo, M.T., 2016, Delineation of the Pahute Mesa–Oasis Valley groundwater basin, Nevada (ver. 1.1, May 2016): U.S. Geological Survey Scientific Investigations Report 2015–5175, 40 p., https://doi.org/10.3133/sir20155175.

Ferrill, D.A., Winterle, J., Wittmeyer, G., Sims, D., Colton, S., Armstrong, A., and Morris, A.P., 1999, Stressed rock strains groundwater at Yucca Mountain, Nevada: GSA Today, v. 9, no. 5, p. 1–7, https://www.geosociety.org/gsatoday/archive/9/5/pdf/gt9905.pdf.

Feth, J.H., 1964, Hidden recharge: Ground Water, v. 2, no. 4, p. 14–17, https://doi.org/10.1111/j.1745-6584.1964.tb01780.x.

Finnegan, D.L., Bowen, S.M., Thompson, J.L., Miller, C.M., Baca, P.L., Olivas, L.F., Geoffrion, C.G., Smith, D.K., Goishi, W., Esser, B.K., Meadows, J.W., Namboodiri, N., and Wild, J.F., 2016, Nevada National Security Site underground radionuclide inventory, 1951–1992—Accounting for radionuclide decay through September 30, 2012: Los Alamos National Laboratory Report LA-UR-16-21749, 53 p., https://www.osti.gov/biblio/1242909-nevada-national-security-site-underground-radionuclide-inventory-accounting-radionuclide-decay-through-september.

Flint, A.L., Flint, L.E., Hevesi, J.A., and Blainey, J.M., 2004, Fundamental concepts of recharge in the Desert Southwest—A regional modeling perspective, *in* Hogan, J.F., Phillips, F.M., and Scanlon, B.R., eds., Groundwater recharge in a desert environment—The southwestern United States—Water Science and Applications Series v. 9: Washington, D.C., American Geophysical Union, p. 159–184, https://ca.water.usgs.gov/pubs/FLint_recharge-concepts-modeling_2004.pdf, https://doi.org/10.1029/009WSA10.

Fridrich, C.J., Minor, S.A., and Mankinen, E.A., 1999, Geologic evaluation of the Oasis Valley basin, Nye County, Nevada: U.S. Geological Survey Open-File Report 99–533–A, 55 p., https://pubs.er.usgs.gov/publication/ofr99533A.

Frus, R.J., and Halford, K.J., 2018, Documentation of single-well aquifer tests and integrated borehole analyses, Pahute Mesa and vicinity, Nevada: U.S. Geological Survey Scientific Investigations Report 2018–5096, 22 p., https://doi.org/10.3133/sir20185096.

Garcia, C.A., Fenelon, J.M., Halford, K.J., Reiner, S.R., and Laczniak, R.J., 2011, Assessing hydraulic connections across a complex sequence of volcanic rocks—Analysis of U-20 WW multiple-well aquifer test, Pahute Mesa, Nevada National Security Site, Nevada: U.S. Geological Survey Scientific Investigations Report 2011–5173, 24 p., https://doi.org/10.3133/sir20115173.

Garcia, C.A., Jackson, T.R., Halford, K.J., Sweetkind, D.S., Damar, N.A., Fenelon, J.M., and Reiner, S.R., 2017, Hydraulic characterization of volcanic rocks in Pahute Mesa using an integrated analysis of 16 multiple-well aquifer tests, Nevada National Security Site, 2009–14: U.S. Geological Survey Scientific Investigations Report 2016–5151, 62 p., https://doi.org/10.3133/sir20165151.

Garfin, G., Jardine, A., Merideth, R., Black, M., and LeRoy, S., eds., 2013, Assessment of climate change in the southwest United States—A report prepared for the National Climate Assessment: Washington, DC, Island Press, 506 p., https://climas.arizona.edu/sites/default/files/pdf2013sw-nca-color-finalweb.pdf, https://doi.org/10.5822/978-1-61091-484-0.

Gesch, D., Evans, G., Mauck, J., Hutchinson, J., and Carswell, W.J., Jr., 2009, The National Map—Elevation: U.S. Geological Survey Fact Sheet 2009–3053, 4 p., https://doi.org/10.3133/fs20093053.

Grauch, V.J.S., Sawyer, D.A., Fridrich, C.J., and Hudson, M.R., 1999, Geophysical framework of the southwestern Nevada volcanic field and hydrogeologic implications: U.S. Geological Survey Professional Paper 1608, 39 p., https://doi.org/10.3133/pp1608.

Halford, K.J., 2016, T-COMP—A suite of programs for extracting transmissivity from MODFLOW models: U.S. Geological Survey Techniques and Methods, book 6, chap. A54, 17 p., https://doi.org/10.3133/tm6A54.

Halford, K.J., and Jackson, T.R., 2020, Groundwater characterization and effects of pumping in the Death Valley regional groundwater flow system, Nevada and California, with special reference to Devils Hole: U.S. Geological Survey Professional Paper 1863, 198 p., https://doi.org/10.3133/pp1863.

Halford, K.J., Laczniak, R.J., and Galloway, D.L., 2005, Hydraulic characterization of overpressured tuffs in central Yucca Flat, Nevada Test Site, Nye County, Nevada: U.S. Geological Survey Scientific Investigations Report 2005–5211, 36 p., https://doi.org/10.3133/sir20055211.

Halford, K.J., Weight, W.D., and Schreiber, R.P., 2006, Interpretation of transmissivity estimates from single-well pumping aquifer tests: Ground Water, v. 44, no. 3, p. 467–471, https://doi.org/10.1111/j.1745-6584.2005.00151.x.

Harrill, J.R., and Bedinger, M.S., 2010, Estimated model boundary flows, *in* Belcher, W.R., and Sweetkind, D.S., eds., Appendix 2 of Death Valley regional groundwater flow system, Nevada and California—Hydrogeologic framework and transient groundwater flow model: U.S. Geological Survey Professional Paper 1711, https://doi.org/10.3133/pp1711.

Harrill, J.R., Gates, J.S., and Thomas, J.M., 1988, Major ground-water flow systems in the Great Basin region of Nevada, Utah, and adjacent states: U.S. Geological Survey Hydrologic Investigations Atlas HA-694-C, 2 sheets, https://doi.org/10.3133/ha694C.

Harrison, J.C., 1971, New computer programs for the calculation of earth tides: Boulder, Colorado, Cooperative Institute for Research in Environmental Sciences, National Oceanic and Atmospheric Administration/University of Colorado, 58 p.

Heilweil, V.M., and Brooks, L.E., eds., 2011, Conceptual model of the Great Basin carbonate and alluvial aquifer system, U.S. Geological Survey Scientific Investigations Report 2010–5193, 191 p., https://doi.org/10.3133/sir20105193.

Helsel, D.R., and Cohn, T.A., 1988, Estimation of descriptive statistics for multiply censored water quality data: Water Resources Research, v. 24, no. 12, p. 1997–2004, https://doi.org/10.1029/WR024i012p01997.

Helsel, D.R., and Gilliom, R.J., 1986, Estimation of distributional parameters for censored trace level water quality data—2. Verification and applications: Water Resources Research, v. 22, no. 2, p. 147–155, https://doi.org/10.1029/WR022i002p00147.

Helsel, D.R., and Hirsch, R.M., 2002, Statistical methods in water resources: U.S. Geological Survey Techniques of Water-Resources Investigations of the United States Geological Survey, Book 4, Hydrologic Analysis and Interpretation, Chapter A3, 510 p., https://doi.org/10.3133/twri04A3.

Hershey, R.L., Fereday, W., and Thomas, J.M., 2016, Dissolved organic carbon 14C in southern Nevada groundwater and implications for groundwater travel times: Desert Research Institute Publication No. 45268; U.S. Department of Energy DOE/NV/0000939-34, 59 p., https://www.osti.gov/biblio/1287225-dissolved-organic-carbon-southern-nevada-groundwater-implications-groundwater-travel-times.

Hevesi, J.A., 2006, Net infiltration of the Death Valley regional ground-water system, Nevada and California: U.S. Geological geospatial data, https://water.usgs.gov/GIS/metadata/usgswrd/XML/pp1711_rch_model1.xml.

Hevesi, J.A., Flint, A.L., and Flint, L.E., 2003, Simulation of net infiltration and potential recharge using a distributed-parameter watershed model of the Death Valley region, Nevada and California: U.S. Geological Survey Water-Resources Investigations Report 03–4090, 161 p., https://pubs.usgs.gov/wri/wri034090/.

Hildenbrand, T.G., Langenheim, V.E., Mankinen, E.A., and McKee, E.H., 1999, Inversion of gravity data to define the pre-Tertiary surface and regional structures possibly influencing ground-water flow in the Pahute Mesa–Oasis Valley region, Nye County, Nevada: U.S. Geological Survey Open-File Report 99–49, 26 p., https://doi.org/10.3133/ofr9949.

Hunt, C.B., Robinson, T.W., Bowles, W.A., and Washburn, A.L., 1966, Hydrologic basin, Death Valley, California: U.S. Geological Survey Professional Paper 494–B, 138 p., https://doi.org/10.3133/pp494B.

IT Corporation, 1998, Report and analysis of the Bullion forced-gradient experiment: Las Vegas, Nev., U.S. Department of Energy DOE/NV/13052-042, 190 p., https://www.osti.gov/biblio/305939-report-analysis-bullion-forced-gradient-experiment.

Jackson, T.R., and Fenelon, J.M., 2018, Conceptual framework and trend analysis of water-level responses to hydrologic stresses, Pahute Mesa–Oasis Valley groundwater basin, Nevada, 1966–2016: U.S. Geological Survey Scientific Investigations Report 2018–5064, 89 p., https://doi.org/10.3133/sir20185064.

Kersting, A.B., Efurd, D.W., Finnegan, D.L., Rokop, D.J., Smith, D.K., and Thompson, J.L., 1999, Migration of plutonium in groundwater at the Nevada Test Site: Nature, v. 397, 4 p., https://www.nature.com/articles/16231.

Kincaid, T.R., Day, K.E., Vogt, T., Ruskauff, G., Drellack, S., Prothro, L., and Reed, D., 2013, A new hydrostratigraphic framework model (HFM) of Pahute Mesa, Nevada—1, Hydrostratigraphic units (HSUs), faults, and calderas—MODFLOW and More 2013—Translating Science into Practice—Poster presentation: Golden, Colorado, Colorado School of Mines, http://www.geohydros.com/images/Pubs/geohydros_2013_New_PahuteMesa_HFM_Poster1_MODFLOW2013.pdf.

Kwicklis, E.M., Rose, T.P., and Benedict, F.C., Jr., 2005, Evaluation of groundwater flow in the Pahute Mesa–Oasis Valley flow system using groundwater chemical and isotopic data: Los Alamos National Laboratory Report LA-UR-05-4344, 90 p.

Kwicklis, E., Broxton, D., Vaniman, D., and Wolfsberg, A., 2006, Appendix B—Investigation of the influence of faults on groundwater movement in the Pahute Mesa/Oasis Valley flow model domain, *in* Ruskauff, G., Groundwater flow model of Corrective Action Units 101 and 102—Central and western Pahute Mesa, Nevada Test Site, Nye County, Nevada: Stoller-Navarro Joint Venture Report S-N/99205--076, 1101 p. https://www.osti.gov/biblio/921957-groundwater-flow-model-corrective-action-units-central-western-pahute-mesa-nevada-test-site-nye-county-nevada-revision.

Laczniak, R.J., Cole, J.C., Sawyer, D.A., and Trudeau, D.A., 1996, Summary of hydrogeologic controls on ground-water flow at the Nevada Test Site, Nye County, Nevada: U.S. Geological Survey Water-Resources Investigations Report 96–4109, 59 p., https://doi.org/10.2172/257364.

Laczniak, R.J., LaRue Smith, J., Elliott, P.E., DeMeo, G.A., Chatigny, M.A., and Roemer, G.J., 2001, Ground-water discharge determined from estimates of evapotranspiration, Death Valley Regional Flow System, Nevada and California: U.S. Geological Survey Water-Resources Investigations Report 01–4195, 51 p. https://doi.org/10.2172/790204.

Lyles, B., McCurdy, G., Chapman, J., and Miller, J., 2012, Timber Mountain precipitation monitoring station: Desert Research Institute Publication No. 45239, 17 p., https://www.osti.gov/biblio/1046471-timber-mountain-precipitation-monitoring-station.

Malmberg, G.T., and Eakin, T.E., 1962, Ground-water appraisal of Sarcobatus Flat and Oasis Valley, Nye and Esmeralda Counties, Nevada: Nevada Department of Conservation and Natural Resources, Ground-Water Resources Reconnaissance Series Report 10, 39 p., http://images.water.nv.gov/images/publications/recon%20reports/rpt10-Sarcobatus_flat.pdf.

Mankinen, E.A., Hildenbrand, T.G., Dixon, G.L., McKee, E.H., Fridrich, C.J., and Laczniak, R.J., 1999, Gravity and magnetic study of the Pahute Mesa and Oasis Valley region, Nye County, Nevada: U.S. Geological Survey Open-File Report 99–303, 58 p., https://doi.org/10.3133/ofr99303.

Maxey, G.B., and Eakin, T.E., 1951, Ground water in Railroad, Hot Creek, Reveille, Kawich, and Penoyer Valleys, Nye, Lincoln, and White Pine Counties, Nevada, *in* Eakin, T.E., Maxey, G.B., Robinson, T.W., Fredericks, J.C., and Loeltz, O.J., Contributions to the hydrology of eastern Nevada: Nevada Water Resources Bulletin No. 12, p. 127–171, http://water.nv.gov/bulletins.aspx.

McKee, E.H., Phelps, G.A., and Mankinen, E.A., 2001, The Silent Canyon Caldera—A three-dimensional model as part of a Pahute Mesa–Oasis Valley, Nevada, hydrogeologic model: U.S. Geological Survey Open-File Report 2001–1297, 23 p., https://doi.org/10.3133/ofr01297.

Meixner, T., Manning, A.H., Stonestrom, D.A., Allen, D.M., Ajami, H., Blasch, K.W., Brookfield, A.E., Castro, C.L., Clark, J.F., Gochis, D.J., Flint, A.L., Neff, K.L., Niraula, R., Rodell, M., Scanlon, B.R., Singha, K., and Walvoord, M.A., 2016, Implications of projected climate change for groundwater recharge in the western United States: Journal of Hydrology (Amsterdam), v. 534, p. 124–138, https://doi.org/10.1016/j.jhydrol.2015.12.027.

Mirus, B.B., Halford, K.J., Sweetkind, D.S., and Fenelon, J.M., 2016, Testing the suitability of geologic frameworks for extrapolating hydraulic properties across regional scales: Hydrogeology Journal, v. 24, no. 5, p. 1133–1146, https://doi.org/10.1007/s10040-016-1375-1.

Mission Support and Test Services, LLC, 2018, Nevada National Security Site, Environmental report 2017, Attachment A, Site description: U.S. Department of Energy Report DOE/NV/03624--0270, 88 p., https://www.osti.gov/biblio/1473975-nevada-national-security-site-environmental-report-attachment-site-description.

Moncure, G.K., Surdam, R.C., and McKague, H.L., 1981, Zeolite diagenesis below Pahute Mesa, Nevada test site: The Clay Minerals Society, v. 29, no. 5, p. 385–396, http://www.clays.org/journal/archive/volume%2029/29-5-385.pdf.

Morris, A., Ferrill, D.A., and Henderson, D.B., 1996, Slip tendency analysis and fault reactivation: Geology, v. 24, no. 3, p. 275–278, https://doi.org/10.1130/0091-7613(1996)024<0275:STAAFR>2.3.CO;2.

National Centers for Environmental Information, 2017, 1981–2010 U.S. climate normals: National Oceanic and Atmospheric Administration, National Centers for Environmental Information web page, accessed July 2017, at https://www.ncdc.noaa.gov/data-access/land-based-station-data/land-based-datasets/climate-normals/1981-2010-normals-data.

National Oceanic and Atmospheric Administration, 2019, Air Resources Laboratory / Special Operations and Research Division (SORD): National Oceanic and Atmospheric Administration webpage, accessed June 1, 2019, at https://www.sord.nv.doe.gov/.

National Security Technologies, LLC, 2007, A hydrostratigraphic model and alternatives for the groundwater flow and contaminant transport model of Corrective Action Unit 99—Rainier Mesa–Shoshone Mountain, Nye County, Nevada: U.S. Department of Energy Report DOE/NV/25946—146, 302 p., https://digital.library.unt.edu/ark:/67531/metadc899397/

Navarro, 2016a, Completion report for well ER-20-12, Corrective Action Units 101 and 102, Central and Western Pahute Mesa: U.S. Department of Energy Report DOE/NV-1549, 237 p., https://www.osti.gov/biblio/1295560-completion-report-well-er-corrective-action-units-central-western-pahute-mesa.

Navarro, 2016b, Pahute Mesa well development and testing analyses for well ER-20-11, Nevada National Security Site, Nye County, Nevada: Navarro Report N/0002653-028-REV. 0, 175 p., https://www.osti.gov/biblio/1464519-pahute-mesa-well-development-testing-analyses-well-er-nevada-national-security-site-nye-county-nevada-revision.

Navarro, 2018, Pahute Mesa phase II well ER-20-12 well development, testing, and sampling data and analysis report: Navarro Report N/0002653-046, 269 p., https://www.osti.gov/biblio/1468441-pahute-mesa-phase-ii-well-er-well-development-testing-sampling-data-analysis-report-revision.

Navarro, 2020, Hydrologic data for the groundwater flow and contaminant transport model of corrective action units 101 and 102: Central and Western Pahute Mesa, Nye County, Nevada: Navarro Report S-N/99205-002, 422 p.

Navarro-Intera, LLC, 2011, Pahute Mesa well development and testing analyses for wells ER-20-7, ER-20-8 #2, and ER-EC-11: Navarro-Intera, LLC Report N-I/28091-037, 161 p., https://www.osti.gov/biblio/1031914-pahute-mesa-well-development-testing-analyses-wells-er-er-er-ec-revision.

Navarro-Intera, LLC, 2012, Pahute Mesa well development and testing analyses for wells ER-20-8 and ER-20-4, Nevada National Security Site, Nye County, Nevada: Navarro-Intera Re-port N-I/28091-061, 186 p., https://www.osti.gov/biblio/1052206-pahute-mesa-well-development-testing-analyses-wells-er-er-nevada-national-security-site-nye-county-nevada-revision.

Navarro-Intera, LLC, 2015, Evaluation of PM-3 chemistry data and possible interpretations of 3H observations: Navarro-Intera Report N-I/28091-092, 159 p., https://www.osti.gov/biblio/1172309-evaluation-pm-chemistry-data-possible-interpretations-observations-revision.

O'Hagan, M.D., and Laczniak, R.L., 1996, Ground-water levels beneath eastern Pahute Mesa and vicinity, Nevada Test Site, Nye County, Nevada: U.S. Geological Survey Water-Resources Investigations Report 96–4042, 1 map, https://doi.org/10.3133/wri964042.

Oberlander, P.L., Lyles, B.F., and Russell, C.E., 2002, Summary report, Borehole testing and characterization of western Pahute Mesa–Oasis Valley ER-EC wells: Desert Research Institute Publication 45195, 56 p.

Parashar, R., Pham, H.V., and Reeves, D.M., 2018, Letter report—Investigation of primary flow paths in western Pahute Mesa using models accounting for the influence of regional stress on fault permeability: U.S. Department of Energy Report DOE/NV/0003590-24, 41 p.

Pawloski, G.A., 1999, Development of phenomenological models of underground nuclear tests on Pahute Mesa, Nevada Test Site—BENHAM and TYBO: Lawrence Livermore National Laboratory Report UCRL-ID-136003, 46 p., https://www.osti.gov/biblio/822992-development-phenomenological-models-underground-nuclear-tests-pahute-mesa-nevada-test-site-benham-tybo.

Pawloski, G.A., Tompson, A.F.B., Carle, S.F., Bourcier, W.L., Bruton, C.J., Daniels, J.I., Maxwell, R.M., Shumaker, D.E., Smith, D.K., and Zavarin, M., 2001, Evaluation of the hydrologic source term from the underground nuclear tests on Pahute Mesa at the Nevada Test Site—The CHESHIRE Test: Lawrence Livermore National Laboratory Report UCRL-ID-147023, 507 p., https://www.osti.gov/biblio/15005874.

Pawloski, G.A., Rose, T.P., Meadows, J.W., Deshler, B.J., and Watrus, J., 2002, Categorization of underground nuclear tests on Pahute Mesa, Nevada Test Site, for use in radionuclide transport models: Lawrence Livermore National Laboratory Report UCRL-TR-208347, 235 p.

Pawloski, G.A., Wurtz, J., and Drellack, S.L., 2010, The Underground Test Area Project of the Nevada Test Site—Building confidence in groundwater flow and transport models at Pahute Mesa through focused characterization studies: Waste Management Conference, conference paper, Phoenix, Arizona, United States, 12 p., https://xcdsystem.com/wmsym/archives//2010/pdfs/10337.pdf.

PRISM Climate Group, 2012, PRISM climate data, 30-year normal, Norm81m data set, created July, 2012: Oregon State University PRISM Climate Group web page, accessed May 2014, at http://prism.oregonstate.edu.

Prothro, L.B., and Drellack, S.L., Jr., 1997, Nature and extent of lava-flow aquifers beneath Pahute Mesa, Nevada Test Site: U.S. Department of Energy Report DOE/NV/11718-156, 50 p., https://www.osti.gov/biblio/653925-nature-extent-lava-flow-aquifers-beneath-pahute-mesa-nevada-test-site.

Prothro, L.B., Drellack, S.L., Jr., and Mercadante, J.M., 2009, A hydrostratigraphic system for modeling groundwater flow and radionuclide migration at the corrective action unit scale, Nevada Test Site and surrounding areas, Clark, Lincoln, and Nye Counties, Nevada: U.S. Department of Energy Report DOE/NV/25946--630, 145 p., https://www.osti.gov/biblio/950486-hydrostratigraphic-system-modeling-groundwater-flow-radionuclide-migration-corrective-action-unit-scale-nevada-test-site-surrounding-areas-clark-lincoln-nye-counties-nevada.

Reeves, D.M., Smith, K.D., Parashar, R., Collins, C., and Heintz, K.M., 2017, Investigating the influence of regional stress on fault and fracture permeability at Pahute Mesa, Nevada National Security Site: Desert Research Institute Publication 45275: U.S. Department of Energy DOE/NV/0000939-41, 133 p., https://www.osti.gov/biblio/1358216.

Reiner, S.R., 2007, Ground-water temperature data, Nevada Test Site and vicinity, Nye, Clark, and Lincoln Counties, Nevada, 2000–2006: U.S. Geological Survey Data Series 269, 20 p., https://doi.org/10.3133/ds269.

Reiner, S.R., Laczniak, R.J., DeMeo, G.A., Smith, J.L., Elliott, P.E., Nylund, W.E., and Fridrich, C.J., 2002, Ground-water discharge determined from measurements of evapotranspiration, other available hydrologic components, and shallow water-level changes, Oasis Valley, Nye County, Nevada: U.S. Geological Survey Water-Resources Investigations Report 2001–4239, 65 p., https://doi.org/10.3133/wri014239.

Robledo, A.R., Ryder, P.L., Fenelon, J.M., and Paillet, F.L., 1998, Geohydrology of monitoring wells drilled in Oasis Valley near Beatty, Nye County, Nevada, 1997: U.S. Geological Survey Water-Resources Investigations Report 98–4184, 40 p., https://doi.org/10.3133/wri984184.

Rose, T.P., Benedict, F.C., Thomas, J.M., Sicke, W.S., Hershey, R.L., Paces, J.B., Farnham, I.M., and Peterman, Z.E., 2006, Geochemical data analysis and interpretation of the Pahute Mesa–Oasis Valley groundwater flow system, Nye County, Nevada, August 2002: Lawrence Livermore National Laboratory Report UCRL-TR-224559, 155 p.

Ross, C.S., and Smith, R.L., 1961, Ash-flow tuffs—Their origin, geologic relations and identification: U.S. Geological Survey Professional Paper 366, 80 p., https://doi.org/10.3133/pp366.

Russell, C.E., and Minor, T., 2002, Reconnaissance estimates of recharge based on elevation-dependent chloride mass-balance approach: Desert Research Institute Publication 45164: U.S. Department of Energy DOE/NV/11508-37, 57 p., https://www.osti.gov/biblio/808504-reconnaissance-estimates-recharge-based-elevation-dependent-chloride-mass-balance-approach.

Russell, C.E., DeNovio, N.M., Farnham, I.M., and Wurtz, J.A., 2017, ER-20-12—A case-study of corrective action investigation in a challenging environment: Phoenix, Ariz., Proceedings of the Waste Management 2017 Conference, March 5–10, 2017, #17236, 15 p.

Savard, C.S., 1998, Estimated ground-water recharge from streamflow in Fortymile Wash near Yucca Mountain, Nevada: U.S. Geological Survey Water-Resources Investigations Report 97–4273, 30 p., https://doi.org/10.3133/wri974273.

Sawyer, D.A., Fleck, R.J., Lanphere, M.A., Warren, R.G., Broxton, D.E., and Hudson, M.R., 1994, Episodic caldera volcanism in the Miocene southwestern Nevada volcanic field—Revised stratigraphic framework, 40Ar/39Ar geochronology, and implications for magmatism and extension: Geological Society of America Bulletin, v. 106, no. 10, p. 1304–1318, https://doi.org/10.1130/0016-7606(1994)106<1304:ECVITM>2.3.CO;2.

Sawyer, D.A., Thompson, J.L., and Smith, D.K., 1999, The Cheshire migration experiment, A summary report: Los Alamos National Laboratory, LA-13555-MS, 32 p., https://digital.library.unt.edu/ark:/67531/metadc622886/.

Schenkel, C.J., Hildenbrand, T.G., and Dixon, G.L., 1999, Magnetotelluric study of the Pahute Mesa and Oasis Valley regions, Nevada: U.S. Geological Survey Open-File Report 99–355, 39 p., https://doi.org/10.3133/ofr99355.

Sheppard, R.A., and Hay, R.L., 2001, Formation of zeolites in open systems, *in* Bish, D.L., and Ming, D.W., eds., Natural zeolites—Occurrence, properties, applications: Reviews in Mineralogy and Geochemistry, v. 45, p. 261–276, https://doi.org/10.1515/9781501509117-010.

Slate, J.L., Berry, M.E., Rowley, P.D., Fridrich, C.J., Morgan, K.S., Workman, J.B., Young, O.D., Dixon, G.L., Williams, V.S., McKee, E.H., Ponce, D.A., Hildenbrand, T.G., Swadley, W.C., Lundstrom, S.C., Ekren, E.B., Warren, R.G., Cole, J.C., Fleck, R.J., Lanphere, M.A., Sawyer, D.A., Minor, S.A., Grunwald, D.J., Laczniak, R.J., Menges, C.M., Yount, J.C., and Jayko, A.S., 1999, Digital geologic map of the Nevada Test Site and vicinity, Nye, Lincoln, and Clark Counties, Nevada, and Inyo County, California: U.S. Geologic Survey Open File Report 99–554–A, 53 p., https://pubs.usgs.gov/of/2000/ofr-00-0554/ofr-99-0554-met.html.

Smith, D.W., Moreo, M.T., Garcia, C.A., Halford, K.J., and Fenelon, J.M., 2017, A process to estimate net infiltration using a site-scale water-budget approach, Rainier Mesa, Nevada National Security Site, Nevada, 2002–05: U.S. Geological Survey Scientific Investigations Report 2017–5078, 22 p., https://doi.org/10.3133/sir20175078.

Snow, D.T., 1965, A parallel plate model of fractured permeable media: Berkeley, USA, University of California Ph.D. dissertation, https://www.nrc.gov/docs/ML0319/ML031910452.pdf.

Soulé, D.A., 2006, Climatology of the Nevada Test Site: National Oceanic and Atmospheric Administration, Air Resources Laboratory, Special Operations and Research Division Technical Memorandum SORD 2006-3, 165 p.

Stallman, R.W., 1971, Aquifer-test design, observation, and data analysis: U.S. Geological Survey Techniques of Water-Resources Investigations, book 3, chap. B1, 26 p., https://doi.org/10.3133/twri03B1.

Stoller-Navarro Joint Venture, 2004, Hydrologic data for the groundwater flow and contaminant transport model of Corrective Action Units 101 and 102—Central and western Pahute Mesa, Nye County, Nevada: Stoller-Navarro Joint Venture Report S-N/99205--002, Shaw/13052-204, Revision No. 0, 422 p., https://www.osti.gov/biblio/1119864-hydrologic-data-groundwater-flow-contaminant-transport-model-corrective-action-units-central-western-pahute-mesa-nye-county-nevada-revision.

Stoller-Navarro Joint Venture, 2007a, Geochem07.mdb and a user's guide to the comprehensive water quality database for groundwater in the vicinity of the Nevada Test Site, Stoller-Navarro Joint Venture S-N/99205--059, Revision 2.

Stoller-Navarro Joint Venture, 2007b, Phase I contaminant transport parameters for the groundwater flow and contaminant transport model of Corrective Action Unit 97—Yucca Flat/Climax Mine, Nevada Test Site, Nye County, Nevada: Stoller-Navarro Joint Venture Report S-N/99205--096, 918 p., https://www.osti.gov/servlets/purl/915816.

Stoller-Navarro Joint Venture, 2009, Phase I transport model of Corrective Action Unit 101 and 102—Central and western Pahute Mesa, Nevada Test Site, Nye County, Nevada: Stoller-Navarro Joint Venture Report S-N/99205--111, Revision No. 1, 696 p., https://www.osti.gov/biblio/948559-phase-transport-model-corrective-action-units-central-western-pahute-mesa-nevada-test-site-nye-county-nevada-errata-sheet-revision.

Stonestrom, D.A., Prudic, D.E., Walvoord, M.A., Abraham, J.D., Stewart-Deaker, A.E., Glancy, P.A., Constantz, J, Laczniak, R.J., and Andraski., B.J., 2007, Focused ground-water recharge in the Amargosa Desert basin, chap. E *of* Stonestrom, D.A., Constantz, J., Ferre, T.P.A., and Leake, S.A., eds., Ground-water recharge in the arid and semiarid southwestern United States: U.S. Geological Survey Professional Paper 1703–E, p. 107–136, https://doi.org/10.3133/pp1703E.

Sweetkind, D.S., Belcher, W.R., Faunt, C.C., and Potter, C.J., 2010, Geology and hydrogeology, Chap. B *of* Belcher, W.R., and Sweetkind, D.S., eds., Death Valley regional ground-water flow system, Nevada and California—Hydrogeologic framework and transient ground-water flow model: U.S. Geological Survey Professional Paper 1711, p. 19–94, https://doi.org/10.3133/pp1711.

Thomas, J.M., Benedict, F.C., Jr., Rose, T.P., Hershey, R.L., Paces, J.B., Peterman, Z.E., Farnham, I.M., Johannesson, K.H., Singh, A.K., Stetzenbach, K.J., Hudson, G.B., Kenneally, J.M., Eaton, G.F., and Smith, D.K., 2002, Geochemical and isotopic interpretations of groundwater flow in the Oasis Valley flow system, southern Nevada: Desert Research Institute Publication 45190; U.S. Department of Energy DOE/NV/11508-56, 102 p., https://www.osti.gov/biblio/806667-geochemical-isotopic-interpretations-groundwater-flow-oasis-valley-flow-system-southern-nevada.

U.S. Congress, 1989, The containment of underground nuclear explosions: Office of Technology Assessment, U.S. Government Printing Office, Washington, DC, OTA-ISC-414, 80 p., https://www.nnss.gov/docs/docs_LibraryPublications/OTA-ISC-414.pdf.

U.S. Department of Energy, 1997, Regional groundwater flow and tritium transport modeling and risk assessment of the Underground Test Area, Nevada Test Site, Nevada: U.S. Department of Energy Report DOE/NV-477, 396 p., https://www.osti.gov/biblio/788792-regional-groundwater-flow-tritium-transport-modeling-risk-assessment-underground-test-area-nevada-test-site-nevada.

U.S. Department of Energy, 1999, Corrective action investigation plan for Corrective Action Units 101 and 102—Central and western Pahute Mesa, Nevada Test Site, Nevada: U.S. Department of Energy DOE/NV-516, 350 p.

U.S. Department of Energy, 2009, Phase II corrective action investigation plan for Corrective Action Units 101 and 102—Central and western Pahute Mesa, Nevada Test Site, Nye County, Nevada: U.S. Department of Energy Report DOE/NV-1312, Rev. 2, 255 p., https://www.osti.gov/biblio/1121444-phase-ii-corrective-action-investigation-plan-corrective-action-units-central-western-pahute-mesa-nevada-test-site-nye-county-nevada-revision-rotc.

U.S. Department of Energy, 2010, Environmental restoration: U.S. Department of Energy Fact Sheet DOE/NV-537, Rev 4, 2 p. https://www.nnss.gov/docs/fact_sheets/DOENV_537.pdf.

U.S. Department of Energy, 2015, United States nuclear tests, July 1945 through September 1992: U.S. Department of Energy Report DOE/NV-209-REV 16 129 p., https://www.osti.gov/biblio/1351809-united-states-nuclear-tests-july-through-september-september.

U.S. Department of Energy, 2018, Rainier Mesa/Shoshone Mountain flow and transport model report, Nevada National Security Site, Nevada: U.S. Department of Energy Report DOE/NV-1588, 908 p., https://www.osti.gov/biblio/1465819-rainier-mesa-shoshone-mountain-flow-transport-model-report-nevada-national-security-site-nevada-revision.

U.S. Department of Energy, 2019, Calendar year 2018 Underground Test Area annual sampling report, Nevada National Security Site, Nevada: U.S. Department of Energy Report DOE/NV-0009-REV. 1, 182 p., https://www.osti.gov/biblio/1577125-calendar-year-underground-test-area-annual-sampling-report-nevada-national-security-site-nevada-revision.

U.S. Department of Energy, 2020a, Pahute Mesa–Oasis Valley hydrostratigraphic framework model for Corrective Action Units 101 and 102—Central and western Pahute Mesa, Nye County, Nevada: U.S. Department of Energy Report DOE/EMNV-0014, 708 p.

U.S. Department of Energy, 2020b, Update to the Phase II Corrective Action Investigation Plan for Corrective Action Units 101 and 102, Central and Western Pahute Mesa, Nevada National Security Site, Nye County, Nevada: U.S. Department of Energy Report DOE/EMNV-0018, 52 p.

U.S. Geological Survey, 2015, USGS 10251217 AMARGOSA RV AT BEATTY, NV, in USGS water data for the Nation: U.S. Geological Survey National Water Information System data-base, accessed January 2015, at https://doi.org/10.5066/F7P55KJN. [Site information directly accessible at http://waterdata.usgs.gov/nv/nwis/inventory/?site_no=10251217&agency_cd=USGS&amp.]

U.S. Geological Survey, 2019a, The National Map–Data Delivery web page, accessed June 26, 2019, at https://www.usgs.gov/core-science-systems/ngp/tnm-delivery/topographic-maps.

U.S. Geological Survey, 2019b, U.S. Geological Survey—U.S. Department of Energy Cooperative Studies in Nevada Groundwater Withdrawals web page, accessed April 14, 2019, at https://nevada.usgs.gov/doe_nv/water_withdrawals.html.

U.S. Geological Survey, 2020, USGS water data for the nation: U.S. Geological Survey National Water Information System database, accessed May 2020, at https://doi.org/10.5066/F7P55KJN.

Utada, M., 2001, Zeolites in hydrothermally altered rocks, *in* Bish, D.L., and Ming, D.W., eds., Natural zeolites—Occurrence, properties, applications: Reviews in Mineralogy and Geochemistry, v. 45, p. 305–322. https://doi.org/10.1515/9781501509117-012.

Van Denburgh, A.S., and Rush, F.E., 1974, Water-resources appraisal of Railroad and Penoyer Valleys, east-central Nevada: Nevada Department of Conservation and Natural Resources, Water Resources—Reconnaissance Series Report 60, 61 p., http://water.nv.gov/reconreports.aspx.

Waddell, R.K., 1982, Two-dimensional, steady-state model of ground-water flow, Nevada Test Site and vicinity, Nevada–California: U.S. Geological Survey Water-Resources Investigations Report 82–4085, 77 p., https://doi.org/10.3133/wri824085.

Waddell, R.K., Robison, J.H., and Blankennagel, R.K., 1984, Hydrology of Yucca Mountain and vicinity, Nevada–California—Investigative results through mid-1983: U.S. Geological Survey Water-Resources Investigations Report 84–4267, 72 p., https://doi.org/10.3133/wri844267.

Walker, G.E., and Eakin, T.E., 1963, Geology and ground water of Amargosa Desert, Nevada-California: Nevada Department of Conservation and Natural Resources, Water Resources—Reconnaissance Series Report 14, 45 p., http://images.water.nv.gov/images/publications/recon%20reports/rpt14-Amargosa_valley.pdf.

White, A.F., 1979, Geochemistry of ground water associated with tuffaceous rocks, Oasis Valley, Nevada: U.S. Geological Survey Professional Paper 712–E, 25 p., https://doi.org/10.3133/pp712E.

Winograd, I.J., 1971, Hydrogeology of ash flow tuff—A preliminary statement: Water Resources Research, v. 7, no. 4, p. 994–1006, https://agupubs.onlinelibrary.wiley.com/doi/pdf/10.1029/WR007i004p00994,https://doi.org/10.1029/WR007i004p00994.

Winograd, I.J., and Thordarson, W., 1975, Hydrogeologic and hydrochemical framework, south-central Great Basin, Nevada–California, with special reference to the Nevada Test Site: U.S. Geological Survey Professional Paper 712–C, 126 p., https://doi.org/10.3133/pp712C.

Winograd, I.J., Riggs, A.C., and Coplen, T.B., 1998, The relative contributions of summer and cool-season precipitation to groundwater recharge, Spring Mountains, Nevada, USA: Hydrogeology Journal, v. 6, no. 1, p. 77–93, https://doi.org/10.1007/s100400050135.

Wolfsberg, A., Glascoe, L., Lu, G., Olson, A., Lichtner, P., McGraw, M., Cherry, T., and Roemer, G., 2002, TYBO/BENHAM—Model analysis of groundwater flow and radionuclide migration from underground nuclear tests in southwestern Pahute Mesa, Nevada: Los Alamos National Laboratory Report LA-13977, 490 p., https://www.osti.gov/biblio/821548-tybo-benham-model-analysis-groundwater-flow-radionuclide-migration-from-underground-nuclear-tests-southwestern-pahute-mesa-nevada.

Wood, D.B., 2007, Digitally available interval-specific rock-sample data compiled from historical records, Nevada National Security Site and vicinity, Nye County, Nevada (ver. 2.2, February 2017): U.S. Geological Survey Data Series 297, 23 p., https://doi.org/10.3133/ds297.

Zhu, J., Pohlmann, K.F., Chapman, J.B., Russell, C.E., Carroll, R.W.H., and Shafer, D.S., 2009, Uncertainty and sensitivity of contaminant travel times from the upgradient Nevada Test Site to the Yucca Mountain area: Desert Research Institute Publication No. 45230, 247 p., https://www.osti.gov/biblio/947196-uncertainty-sensitivity-contaminant-travel-times-from-upgradient-nevada-test-site-yucca-mountain-area.

Appendix 1. Water Levels Measured in the Pahute Mesa–Oasis Valley Groundwater Basin and Vicinity, Southern Nevada, 1941–2016

Hydrographs and locations for the 577 wells that have measured water levels in the Pahute Mesa–Oasis Valley groundwater basin and vicinity are tabulated and can be displayed interactively from a Microsoft® Excel workbook. The workbook is designed to be an easy-to-use tool to view water levels and other associated information for wells in the study area. Information for an individual well can be selected by using the AutoFilter option available in Excel. The information presented for a selected well includes

- USGS site identification number,
- Well name,
- Land-surface altitude,
- Water-level date,
- Water-level depth,
- Water-level altitude,
- Water-level qualifier,
- Water-level source,
- Water-level status,
- Water-level method,
- Water-Level accuracy,
- Water-level remark,
- Steady state, transient (nuclear), and transient (pumping) flags,
- Latitude, and
- Longitude.

Appendix 2. Well and Spring Data for Potentiometric Contouring of the Pahute Mesa–Oasis Valley Groundwater Basin, Southern Nevada

Summary tables that include information for the 387 wells and 75 springs used to develop potentiometric contours in the Pahute Mesa–Oasis Valley groundwater basin. Summary tables are available in a Microsoft® Excel workbook. For each well, the hydraulic-head estimate is the mean of all water-level altitudes flagged as representative or potentially representative of predevelopment (steady-state) conditions. Hydraulic-head estimates at springs are the spring land-surface altitudes, which were estimated from 1:24,000-scale topographic maps and a digital elevation model that sampled 1:24,000-scale maps every 30 m and reported to the nearest whole meter. The information presented for each well includes

- USGS site identification number,
- USGS well name,
- USGS borehole name,
- Latitude*,
- Longitude*,
- Land-surface altitude*,
- Land-surface altitude accuracy*,
- Borehole depth,
- Well depth,
- Top opening altitude,
- Bottom opening altitude,
- Number of steady-state water levels,
- Water-level date range,
- Hydraulic-head estimate*,
- Water-level measurement accuracy,
- Does hydraulic head represent steady-state conditions? *,
- Show hydraulic head on map? *, and
- Map use of hydraulic head for potentiometric contouring*.

The information presented for each spring include the spring name and the listed information above with an asterisk (*).

Appendix 3. Hydrostratigraphic Units for Wells and Underground Nuclear Test Holes in the Pahute Mesa–Oasis Valley Groundwater Basin, as Determined from Well Logs and Projected from Hydrostratigraphic Framework Models

The hydrostratigraphic units (HSUs) and corresponding hydrogeologic units (HGUs) for the 387 wells identified as having one or more water-level measurements representative of predevelopment (steady-state) groundwater conditions are tabulated and can be displayed interactively from a Microsoft® Excel workbook. Underground nuclear test boreholes on Pahute Mesa also are included. The workbook is designed to view a stratigraphic column interpreted from the Pahute Mesa–Oasis Valley hydrostratigraphic framework model, the mean predevelopment water-level altitude, and basic well-construction information for wells and nuclear-test boreholes in the study area. Information for an individual well can be viewed by selecting the well from a column-header dropdown list.

Appendix 4. Analysis of Hydraulic Conductivity with Depth using Wells in the Pahute Mesa–Oasis Valley Groundwater Basin, Southern Nevada

The hydraulic conductivity with depth analysis for the Pahute Mesa–Oasis Valley (PMOV) groundwater basin is contained in worksheets within a Microsoft® Excel workbook. Hydraulic-head estimates (appendix 2), well-construction information (appendix 3), and aquifer-test results (Frus and Halford, 2018) were compiled for 356 wells in the PMOV basin. The hydraulic conductivity with depth analysis translated transmissivity to hydraulic conductivity using an appropriate saturated thickness. Hydraulic conductivity and construction information for wells in the PMOV basin were binned into 400-foot intervals from the water table to the bottom of wells. The hydraulic conductivity with depth analysis was used to determine the vertical location of permeable saturated intervals. Results were plotted using a 400-ft bin interval.

Appendix 5. Analysis of Volcanic-Rock Alteration Abundance with Depth and by Hydrogeologic Unit using Wells in the Pahute Mesa–Oasis Valley Groundwater Basin, Southern Nevada

Data and analyses used to evaluate alteration abundance with depth below the water table and by hydrogeologic unit in the Pahute Mesa–Oasis Valley (PMOV) groundwater basin, southern Nevada. Data and analyses are contained in worksheets within a Microsoft® Excel workbook. Hydrogeologic and alteration information for wells are derived from the PMOV hydrostratigraphic framework model (U.S. Department of Energy, 2020a). Compiled data of hydrogeologic, alteration, and construction information for boreholes in the PMOV basin were binned into 400-foot intervals from the water table to the bottom of boreholes. Alteration data were categorized into alteration groups for plotting. Plots were generated of alteration abundance with depth using a 400-ft bin interval and alteration abundance by hydrogeologic unit.

Appendix 6. Analysis of Transmissivity by Hydrostratigraphic and Hydrogeologic Units in the Pahute Mesa–Oasis Valley Groundwater Basin, Southern Nevada

Data and analyses used to correlate transmissivity to one or more hydrostratigraphic units (HSUs) and hydrogeologic units (HGUs) in the Pahute Mesa–Oasis Valley (PMOV) groundwater basin, southern Nevada. Data and analyses are contained in worksheets within a Microsoft® Excel workbook. Hydraulic-head estimates (appendix 2), well-construction information (appendix 3), and aquifer-test results (Frus and Halford, 2018) were compiled for 356 wells in the PMOV basin. Hydrostratigraphic and hydrogeologic information for wells are derived from the PMOV hydrostratigraphic framework model (U.S. Department of Energy, 2020a). Analyses were used to correlate transmissivity to HSUs and HGUs, respectively. The methodology used to correlate transmissivity to HSUs and HGUs is described and results are summarized.

Appendix 7. Analysis of Transmissivity by Volcanic-Rock Alteration in the Pahute Mesa–Oasis Valley Groundwater Basin, Southern Nevada

Data and analyses used to compare transmissivity to one or more volcanic-rock alteration groups within the open interval of wells in the Pahute Mesa–Oasis Valley (PMOV) groundwater basin, southern Nevada. Data and analyses are contained in worksheets within a Microsoft® Excel workbook. Hydraulic-head estimates (appendix 2), well-construction information (appendix 3), and aquifer-test results (Frus and Halford, 2018) were compiled for 356 wells in the PMOV basin. Hydrostratigraphic, hydrogeologic, alteration, and lithologic information for wells are derived from the PMOV hydrostratigraphic framework model (U.S. Department of Energy, 2020a). Analyses were used to compare transmissivity to alteration code(s) in the open interval of wells. The methodology used to compare transmissivity to alteration code(s) and alteration groups in the open interval of wells is described and results are summarized.

For more information concerning the research in this report, contact the

Nevada Water Science Center
U.S. Geological Survey
2730 N. Deer Run Road
Carson City, Nevada 95819
https://www.usgs.gov/centers/nv-water

Publishing support provided by the U.S. Geological Survey
Science Publishing Network, Sacramento Publishing Service Center

ISSN 2328-0328 (online)
https://doi.org/10.3133/sir20205134